VOL. 25 NO. 3 MAY 1970
COMPLETING VOLUME 25
PUBLISHED MONTHLY

JOURNAL OF

ELECTROANALYTICAL CHEMISTRY

AND INTERFACIAL ELECTROCHEMISTRY

International Journal devoted to all Aspects of Electroanalytical Chemistry, Double Layer Studies, Electrokinetics, Colloid Stability, and Electrode Kinetics.

ELSEVIER SEQUOIA S.A.
LAUSANNE

GENERAL INFORMATION

Types of contributions

(a) Original research work not previously published in other periodicals.
(b) Reviews on recent developments in various fields.
(c) Short communications.
(d) Preliminary notes.

Languages

Papers will be published in English, French or German.

Submission of papers

Papers should be sent to one of the following Editors:
Professor J. O'M. BOCKRIS, John Harrison Laboratory of Chemistry, University of Pennsylvania, Philadelphia 4, Pa. 19104, U.S.A.
Dr. R. H. OTTEWILL, Department of Chemistry, The University, Bristol 8, England.
Dr. R. PARSONS, Department of Chemistry, The University, Bristol 8, England.
Professor C. N. REILLEY, Department of Chemistry, University of North Carolina, Chapel Hill, N.C. 27515, U.S.A.

Authors should preferably submit two copies in double-spaced typing on pages of uniform size. Legends for figures should be typed on a separate page The figures should be in a form suitable for reproduction, drawn in Indian ink on drawing paper or tracing paper, with lettering etc. in thin pencil. The sheets of drawing or tracing paper should preferably be of the same dimensions as those on which the article is typed. Photographs should be submitted as clear black and white prints on glossy paper. Standard symbols should be used in line drawings, the following are available to the printers:

All references should be given at the end of the paper. They should be numbered and the numbers should appear in the text at the appropriate places.
A summary of 50 to 200 words should be included.

Reprints

Fifty reprints will be supplied free of charge. Additional reprints (minimum 100) can be ordered at quoted prices. They must be ordered on order forms which are sent together with the proofs.

Publication

The *Journal of Electroanalytical Chemistry and Interfacial Electrochemistry* appears monthly For 1969, each volume has 3 issues and 4 volumes will appear.
Subscription price: Sfr. 316.— (U.S. $ 74.60) per year incl. postage. Additional cost for copies by air mail available on request. For subscribers in the U.S.A. and Canada, 2nd class postage paid at New York, N.Y. For advertising rates apply to the publishers.

Subscriptions

Subscriptions should be sent to:

ELSEVIER SEQUOIA S.A., P.O. Box 851, 1001 Lausanne 1, Switzerland

Detect one part per billion!

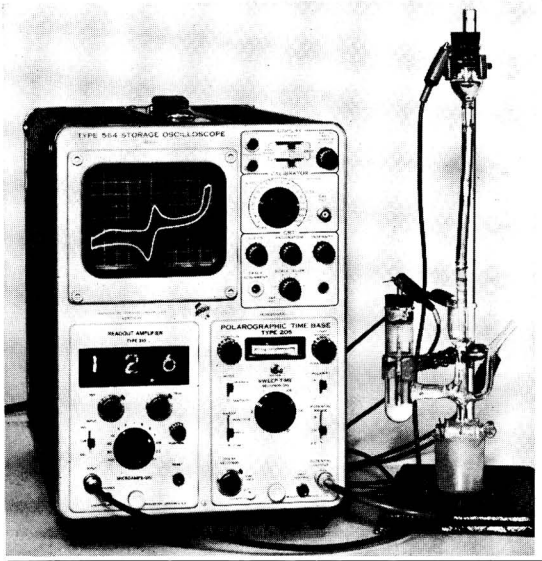

by Anodic Stripping Polarography

Anodic Stripping Polarography with Chemtrix Single-Sweep Polarographic Analyzers is capable of detecting many elements and compounds in amounts of one ppb and less. This high sensitivity is due to a combination of factors: the concentrating effect of stripping technique, characteristics of the mercury film electrode, and the fast scan capabilities of the Chemtrix Instruments. If you have a detection problem with trace elements or contaminants, anodic stripping may well be the solution.

free-new booklet

The complete story of ANODIC STRIPPING POLAROGRAPHY with detailed experiments and many references.

simple procedure for detection

1. Use wax impregnated graphite electrode coated with a thin layer of mercury.
2. Immerse electrode in cell with electrolyte.
3. Electrolyze at 1.00 volt for 10 minutes with controlled stirring.
4. Stop stirring and scan anodically to zero volts. (Leave peaks stored on oscilloscope screen as blank).
5. Add sample and repeat steps 3 and 4. Note change in peaks and relate to trace metal calibration curves.

rapid simultaneous detections

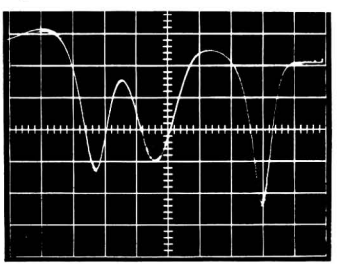

Anodic peaks in illustration are Zinc, Cadmium, and Lead at approximately 50 ppb in 1 molar KC1, stored on screen with single anodic scan.

some typical applications for anodic stripping polarography

- Trace impurities in reagents
- Trace metals in biological systems
- Water pollutants
- Lead in air (tetraethyl)
- Semiconductor trace metals

U.S. SALES PRICES F.O.B. FACTORY

CHEMTRIX polarographic analyzers

for Single-Sweep and Anodic Stripping Polarography

Model SSP-2 Three-Electrode Polarographic Analyzer . . . $3070.00

Model SSP-5 Differential System with Dual DME 3785.00

Illustrated Above:

Model SSP-3 Digital Readout Polarographic Analyzer . . . 3510.00

NEW—TYPE 804—$495 Potentiostatic Waveform Source

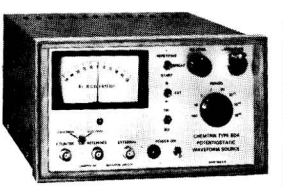

This versatile instrument is a waveform source for triangle and square waveforms, single or repetitive, with ±5 volt dc offset and up to 5 volt amplitude. It is also a potentiostat which can accept an external input and combine it with an internal dc level to provide controlled-potential output. It is both a waveform source and a potentiostat, providing controlled-potential output of its internally generated waveforms. In addition, it is

■ A Power Supply, ±5 v dc at 100 ma ■ A Controlled Potential Coulometer ■ An Integrator for Coulometric Titrations ■ An Integrator for External Signals ■ A Supply for Controlled-Current Titrations

CHEMTRIX, INC.

Instrumentation for Science

P.O. Box 725 Beaverton, Oregon 97005 (503) 648-1434

RADIATION RESEARCH *REVIEWS*

CONTENTS

Subscription price per volume of four issues:

£ 10.9.6, Dfl. 90.00 or US $ 25.00 plus postage 10s. 7d., Dfl. 4.50 or US $ 1.25.

Orders may be sent to your regular bookseller or to Elsevier Publishing Company.

Elsevier

P.O. Box 211
Amsterdam - The Netherlands

188 E

ELECTROANALYTICAL CHEMISTRY AND INTERFACIAL ELECTROCHEMISTRY
Elsevier Sequoia S.A., Lausanne – Printed in The Netherlands

REVIEW

THE ELECTRICAL DOUBLE LAYER IN MOLTEN SALTS

PART 1. THE POTENTIAL OF ZERO CHARGE

A. D. GRAVES

Nuffield Research Group in Extraction Metallurgy, Department of Metallurgy, Imperial College of Science and Technology, London, S.W.7 (England)

(Received January 17th, 1969; in final form December 4th, 1969)

INTRODUCTION

Frumkin[1] has demonstrated the existence of an empirical relationship between the potential of zero charge ($E^{M}_{q=0}$, measured against a reference electrode) of a metal (M) in contact with an electrolyte and the electronic work function (w_M) of the metal, as given by the expression,

$$E^{M}_{q=0} \approx w_M + K \tag{1}$$

where K is approximately constant at constant temperature. He therefore suggested[1] that the e.m.f. of a cell consisting of two electrodes M_1 and M_2 at their respective zero charge potentials should be equal to the contact potential ($^1\Delta^2\psi$) between them because

$$E^{1}_{q=0} - E^{2}_{q=0} \approx w_1 - w_2 = \psi_2 - \psi_1 = {}^1\Delta^2\psi \tag{2}$$

where ψ_1 and ψ_2 are the volta potentials of M_1 and M_2, respectively.

At that time (*ca.* 1930) the available $E^{M}_{q=0}$ and w_M data were mostly for solid metals and aqueous electrolyte systems and showed poor agreement with eqn. (2). It was soon realised[1] that measurements would have to be made with liquid metals before eqn. (2) could be checked reliably. This would ensure that the surface states of the metals were closely similar in both sets of measurements. Furthermore, contact potentials between liquid metals can be determined more accurately than the corresponding work functions.

The zero charge potentials were generally measured with molten electrolytes, in order that a reasonable range of liquid metals could be used. Also it was hoped that the use of a purely ionic electrolyte system such as a molten alkali halide would eliminate the dipolar effects found with aqueous electrolyte systems. These measurements[2] were made with a high temperature version of the classical capillary electrometer at one, or at most two, temperatures. Reasonably good agreement[1] was obtained with eqn. (2).

Prisekina *et al.*[3] extended these measurements over a wider temperature range in order to examine the effect of temperature on $E_{q=0}$ for a number of different metals. They discussed their results with reference to eqns. (1) and (2) and concluded that the potential of zero charge did not vary significantly with temperature. This conclusion

will be re-examined here in the course of discussing the theoretical derivation[4-6] of eqn. (1).

THEORY

Equation (1) may be derived very simply from the equation (see Appendix) used by Klein and Lange[7], Randles[8] and others to calculate real solvation energies of ions from volta potential measurements:

$$E_M^0 = w_M + E_N^0 - \frac{(\Delta G_{sub}^0(N) + \Sigma I_N + \alpha_{N^{z+}}^S)}{zF} + {}^S\Delta^M\psi^0 \tag{3}$$

where N/N^{z+} is the reference couple.

When the metal M is at its zero charge potential, and assuming that the surface potential of the solvent (s) is unaffected by the presence of the solute (see Randles[8]), eqn. (3) becomes

$$E_{q=0}^M = w_M + E_N^0 - \frac{(\Delta G_{sub}^0(N) + \Sigma I_N + \alpha_{N^{z+}}^S)}{zF} + {}^S\Delta^M\psi_{q=0}$$

$$= w_M + K' + {}^S\Delta^M\psi_{q=0} \tag{4}$$

where ${}^S\Delta^M\psi_{q=0}$ is the volta potential difference for the uncharged metal/electrolyte interphase, and

$$K' = E_N^0 - \frac{(\Delta G_{sub}^0(N) + \Sigma I_N + \alpha_{N^{z+}}^S)}{zF} = E_{q=0}^M - w_M - {}^S\Delta^M\psi_{q=0} \tag{5}$$

Equation (4) is identical to eqn. (1) for

$$K = K' + {}^S\Delta^M\psi_{q=0} \tag{6}$$

It is apparent from eqn. (5) that K' is a constant as the parameters characteristic of electrodes N and M have been separated entirely in this equation. This conclusion is confirmed by the work of several authors[4,5,9], who showed that K' is determined by the characteristics of the reference couple chosen as standard ($E^0 = 0$). Thus K is a constant if ${}^S\Delta^M\psi_{q=0}$ is a constant (or zero).

DISCUSSION

(a) *Aqueous electrolyte systems*

Novakovskii *et al.*[4], who published the first satisfactory derivation of eqn. (4)*, assumed that ${}^S\Delta^M\psi_{q=0}$ for metals in contact with aqueous electrolyte solutions was a constant equal to -0.33 V[10]. They stated that their assumption was justified by the close correspondence between the K of eqn. (1) and the constant calculated from their eqn. (15)* using this value of ${}^S\Delta^M\psi_{q=0}$. However, as pointed out above and as emphasized by Parsons[11], work function data, in particular, are insufficiently accurate for this purpose. Furthermore, if ${}^S\Delta^M\psi_{q=0}$ is a constant then eqn. (2) is strictly valid, which

* It can be demonstrated that eqn. (4) is identical to their eqn. (15)[4] by substituting their eqns. (3), (4) and (6). U_1 in their eqn. (4) is taken with a negative sign as it corresponds to the reverse process to that represented by $\alpha_{N^{z+}}^S$ in eqn. (4) of this paper.

is unlikely as this would infer that the orientation of water molecules at the metal/aqueous electrolyte interphase is independent of the metal[11,12].

Thus a more satisfactory form of eqn. (2) is

$$E^1_{q=0} - E^2_{q=0} = {}^1\Delta^2\psi + ({}^S\Delta^1\psi_{q=0} - {}^S\Delta^2\psi_{q=0}) \tag{7}$$

where ${}^S\Delta^1\psi_{q=0} - {}^S\Delta^2\psi_{q=0} \neq 0$.

Finally, using the most reliable data of Randles[8], it can be shown[1] that the volta potential difference for the uncharged mercury/non-specifically adsorbed aqueous electrolyte solution interphase is -0.26 V and not -0.33 V: if eqn. (4) is substituted into eqn. (3), then

$$E^0_M - E^M_{q=0} = \varphi^0_M = {}^S\Delta^M\psi^0 - {}^S\Delta^M\psi_{q=0} \tag{8}$$

where φ^0_M is the standard φ-potential for the M/M^{z+} couple. As φ^0_M for the standard calomel electrode is 0.47 V[13] and the standard volta potential for the same system is 0.208 V[8], then ${}^{H_2O}\Delta^{Hg}\psi_{q=0} = -0.26$ V.

Bockris and Argade[6] have adopted a slightly different approach to the derivation of eqn. (1) and stated at the outset that the volta potential difference for the uncharged metal/electrolyte solution interphase is zero. They then go on to define a quantity $\delta\chi$, which accounts for the change in the surface potentials of the metal and solution when they are brought into contact with one another. It is apparent from their arguments that $\delta\chi$ is identical with ${}^S\Delta^M\psi_{q=0}$ defined above and that the quantity which they have put equal to zero is ${}^Sg^M_{ion}$, which is the part of ${}^S\Delta^M\Phi_{q=0}$ (the galvani potential difference at the potential of zero charge) that is due to the existence of charge separation across the metal/electrolyte solution interphase[11]. Although the approach of Bockris and Argade[6] is equally valid, it does not conform to previous conventions and could cause confusion. Indeed, some confusion appears to have occurred already in this paper as $\delta\chi$ has been put equal to 0.26 V (or 0.27 V in the early part of the paper) whereas it should be -0.26 V. This changes their estimate of the surface potential of water (χ_{H_2O}) to approximately -0.3 V.

Many attempts[14] have been made to estimate χ_{H_2O}, which cannot be measured directly[11]. The value of Bockris and Argade[6] is based on a recent calculation of the enthalpy of hydration of the proton by Halliwell and Nyberg[15]. However, a negative value of χ_{H_2O} is incompatible with observations of the variation in this quantity in the presence of surface active organic molecules[14]. Thus the situation regarding the sign and magnitude of the surface potential of water remains unresolved[16].

(b) Molten alkali halide electrolyte systems

The potentials at the uncharged mercury/water interphase have been discussed in some detail as this is the only system for which quantitative information is available. Also it is necessary to have a clear idea what is meant by the terms $E_{q=0}$, ${}^S\Delta^M\psi_{q=0}$, φ^0_M, χ_S, K, etc., before using them to describe the behaviour of the liquid metal/molten salt interphase.

It is apparent from Tables 1 and 2 (Tables 3 and 4 of ref. 1) that these concepts can be applied to melts. The results in Table 1 support eqn. (2) and suggest that $({}^S\Delta^1\psi_{q=0} - {}^S\Delta^2\psi_{q=0})$ in eqn. (7) is small for the systems chosen. In Table 2 it is shown that the differences between the zero charge potentials of metals in contact with an aqueous electrolyte solution are aproximately equal to the corresponding potential

differences in molten alkali halides. It follows that these potential differences are largely independent of the electrolyte system, as predicted by eqn. (2). Therefore K in eqn. (1) must be approximately constant for the two electrolyte systems, although the actual value will be different for each.

TABLE 1

COMPARISON BETWEEN THE CONTACT POTENTIAL DIFFERENCES (*vacuo*) AND THE ZERO CHARGE POTENTIAL DIFFERENCES (IN LiCl-KCl) OF LIQUID METALS AND ALLOYS

M	*Alloy*	${}^{M}\Delta^{Alloy}\psi/V$	$(E^{M}_{q=0}-E^{Alloy}_{q=0})/V$
Sn	Sn–Te (0.15 wt.%)	−0.15	−0.18
Sn	Sn–Tl (23.8 at.%)	0.17	0.24
Sn	Sn–Cd (53.0 at.%)	0.25	0.27
Bi	Bi–Te (3.6 at.%)	−0.30	−0.25
Bi	Bi–Te (9.0 at.%)	−0.35	−0.33
Tl	Tl–Te (50.5 at.%)	−0.65	−0.67

TABLE 2

POTENTIALS OF ZERO CHARGE REFERRED TO THE POTENTIAL OF ZERO CHARGE OF LEAD IN AQUEOUS AND MOLTEN ALKALI HALIDE ELECTROLYTES

M	$(E^{M}_{q=0}-E^{Pb}_{q=0})_{aq}/V$	$(E^{M}_{q=0}-E^{Pb}_{q=0})_{melt}/V$
Te	1.25	1.06
Hg	0.46	0.47
Bi	0.29	0.23
Sn	0.19	0.31
Ga	0.04	0.13
Ag	−0.05	0.01
Tl	−0.17	−0.15
Cd	−0.25	−0.12

It also follows that the differences between the zero charge potentials of the metals are largely independent of temperature[1]. This observation has been confirmed by Prisekina *et al.*[3] (see Fig. 1) for tin, bismuth, gallium, lead, indium and thallium in a LiCl–KCl eutectic melt at temperatures from 400°–750° C using the electrocapillary method. In addition, Kuznetsov and co-workers[17] resolved an anomaly in the work of Bukun and Ukshe[18]. The latter workers measured the zero charge potential of indium at approximately 450°C and at 700°C using the capacitance method (see Part 2[19]). When these results were compared with similar data for lead, they appeared to contradict Frumkin's observation[1], *i.e.* ${}^{In}\Delta^{Pb}E^{450°C}_{q=0}\sim 0.05$ V, whereas ${}^{In}\Delta^{Pb}E^{700°C}_{q=0}=0.27$ V. Alekseeva *et al.*[17] repeated the capacitance measurements with indium and showed that ${}^{In}\Delta^{Pb}E^{700°C}_{q=0}=0.05$ V. Thus there are still no exceptions to the general rule that the differences between the zero charge potentials of the metals are practically independent of temperature.

On the basis of eqn. (2) this result is not unexpected, as it is known that the individual work functions of the metals are relatively insensitive to temperature ($\sim 5\times 10^{-5}$ V/°C)[20]. In this case it may be concluded from eqn. (7) that the differences between the volta potential differences at the uncharged metal/melt interphases are also temperature independent. Prisekina *et al.*[3] have taken this a stage further and

suggested that the individual zero charge potentials are almost independent of temperature and that the curves in Fig. 1 represent the variation of the potential of their reference electrode (Pb/2.5 mole% $PbCl_2$ + eutectic) with temperature. They stated that this follows from eqn. (1), assuming K is independent of temperature when the zero charge potential is the actual potential difference across the uncharged metal/melt interphase (*i.e.* the galvani potential difference, ${}^{S}\Delta^{M}\Phi_{q=0}$).

Apparently Prisekina *et al.*[3] have misunderstood the paper by Novakovskii

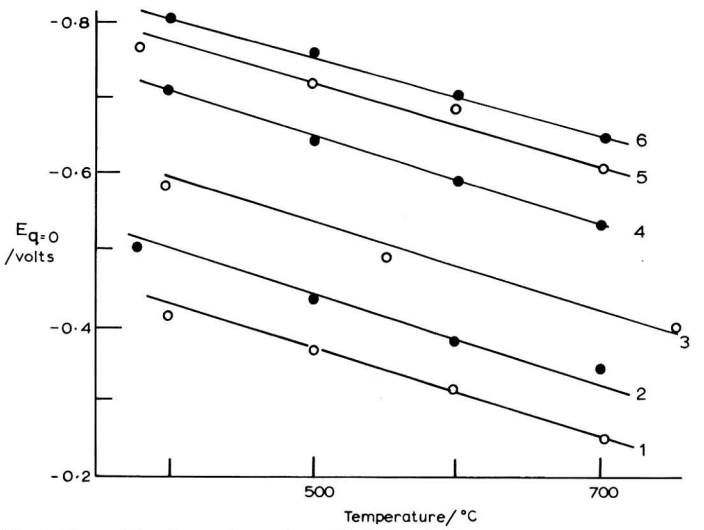

Fig. 1. Potentials of zero charge (*vs.* a Pb/2.5 mole% $PbCl_2$ + eutectic reference electrode) of several metals in a LiCl–KCl eutectic melt at temperatures in the range 400°–750°C. (1) Tin, (2) bismuth, (3) gallium, (4) lead, (5) indium, (6) thallium[3].

et al.[4], to which they refer, as it is quite clear that eqn. (1) is valid only when the zero charge potential is measured against a reference electrode. This may be shown by deriving an expression for ${}^{S}\Delta^{M}\Phi_{q=0}$ from eqn. (4) using the relationship[11]

$$ {}^{S}\Delta^{M}\Phi = {}^{S}\Delta^{M}\psi + (\chi_M - \chi_S) \tag{9} $$

where χ_M and χ_S are the surface potentials of the metal and electrolyte, respectively.

Therefore

$$ {}^{S}\Delta^{M}\Phi_{q=0} = -w_M + [E^{M}_{q=0} - K' - (\chi_M - \chi_S)] \tag{10} $$

There is no reason to suppose that the quantity in square brackets in eqn. (10) is a constant and even less reason to assume it is independent of temperature.

Nevertheless Prisekina *et al.*[3] state that the parallelism of the curves in Fig. 1 can be explained only if it is understood that the curves represent the variation of the reference electrode with temperature, whereas according to eqn. (2) the data in Fig. 1 merely confirm the observation that the differences between the work functions of the metals (*i.e.* the contact potentials) are practically independent of temperature.

CONCLUSIONS

The potential of zero charge of a metal in contact with an electrolyte is related

to the work function of the metal by the expression

$$E^{M}_{q=0} = w_M + K' + {}^{S}\Delta^{M}\psi_{q=0}$$

where K' is a constant, determined by the characteristics of the reference couple chosen as electrochemical standard and ${}^{S}\Delta^{M}\psi_{q=0}$ is the volta potential difference at the uncharged metal/electrolyte interphase.

The only available value for the latter quantity is for the mercury/aqueous electrolyte interphase and leads to an estimate for the surface potential of water. Although values of ${}^{S}\Delta^{M}\psi_{q=0}$ are not available for melts it appears that the differences between them for different metals in contact with the same melt, are small and substantially independent of temperature.

The zero charge potential data of Prisekina *et al.*[3] for tin, bismuth, gallium, lead, indium and thallium in contact with a LiCl–KCl eutectic melt at temperatures from 400°C–750°C show good agreement with eqn. (2) and support the conclusion (from work function data[20]) that the contact potentials between the metals are practically independent of temperature.

However, their assumptions that an expression similar to eqn. (1) may be used when the potential of zero charge is the actual potential difference across the metal/electrolyte interphase and that in this case K is independent of temperature, appear to be unjustified. Therefore their conclusion that the zero charge potentials are independent of temperature is unlikely to be correct.

ACKNOWLEDGEMENT

The author wishes to thank Dr. R. Parsons for helpful discussions and for communicating the derivation given in the appendix.

APPENDIX[21]

Consider the cell:

$N'|N^{z+}$ + electrolyte (s)||electrolyte(s) + $M^{z+}|M|N''$ where M and N are metals, and M^{z+} and N^{z+} are ions of charge z present in dilute solution in the electrolyte (s).

Assuming a negligible liquid junction potential, under standard conditions[11] the e.m.f. of the cell is given by

$$E^{0}_{M} - E^{0}_{N} = \Phi^{N''} - \Phi^{N'}$$

where E^{0}_{M} and E^{0}_{N} are the standard reduction potentials of the M/M^{z+} and N/N^{z+} couples and $\Phi^{N'}$ and $\Phi^{N''}$ are the galvani potentials of N′ and N″. Since N′ and N″ are the same substance, the chemical potential of electrons (μ_e^{N}) is the same for both. Therefore,

$$\Phi^{N''} - \Phi^{N'} = -\frac{1}{F}(\bar{\mu}_e^{N''} - \bar{\mu}_e^{N'})$$

where $\bar{\mu}_e^{N'}$ and $\bar{\mu}_e^{N''}$ are the electrochemical potentials of electrons in N′ and N″, and F is the Faraday.

Electrons are in equilibrium between M and N''. Thus,

$$\bar{\mu}_e^{N''} = \bar{\mu}_e^{M} = \alpha_e^{M} - \psi^{M}F$$

where α_e^{M} ($= -Fw_M$) is the electronic work function of M and ψ^{M} is the volta potential of M.

Within N, $\mu_N^N = \bar{\mu}_{N^{z+}}^N + z\bar{\mu}_e^N$ where μ_N^N is the standard free energy of formation of pure N from gaseous N^{z+} and e, *i.e.* $\mu_N^N = -(\Delta G_{sub}^0(N) + \Sigma I_N)$, where $\Delta G_{sub}^0(N)$ is the standard free energy of sublimation and ΣI_N is the sum of the ionisation potentials of N, and $\bar{\mu}_{N^{z+}}^N$ is the electrochemical potential of N^{z+} ions in N. Since N^{z+} ions are in equilibrium between N' and the electrolyte (s), then $\bar{\mu}_{N^{z+}}^N = \bar{\mu}_{N^{z+}}^S = \alpha_{N^{z+}}^S + z\psi^S F$ where $\bar{\mu}_{N^{z+}}^S$ is the electrochemical potential of N^{z+} ions in the electrolyte (s), $\alpha_{N^{z+}}^S$ is the standard real free energy of solvation of gaseous N^{z+} ions and ψ^S is the volta potential of the electrolyte (s). If these equations are combined, then the standard e.m.f. of the cell is given by:

$$E_M^0 - E_N^0 = -\frac{(\Delta G_{sub}^0(N) + \Sigma I_N + \alpha_{N^{z+}}^S)}{zF} - \frac{\alpha_e^M}{F} + (\psi^M - \psi^S)$$

$$= -\frac{(\Delta G_{sub}^0(N) + \Sigma I_N + \alpha_{N^{z+}}^S)}{zF} + w_M + {}^S\Delta^M\psi^0$$

which is eqn. (3) above.

SUMMARY

A relationship between the potential of zero charge of a metal in contact with an electrolyte and the work function of the metal is derived and discussed with the help of data for aqueous electrolyte and molten electrolyte systems.

The data for the metal/molten LiCl–KCl eutectic system due to Prisekina *et al.*[3] show that the differences between the zero charge potentials of tin, bismuth, gallium, lead, indium and thallium are independent of temperature. This result is explained in terms of the above relationship without introducing the suggestion by Prisekina *et al.*[3] that the individual zero charge potentials are independent of temperature. It is shown that this suggestion is unlikely to be correct.

REFERENCES

1 A. N. Frumkin, *Svensk Kem. Tidskr.*, 77 (1965) 300.
2 E. A. Ukshe, N. G. Bukun, D. I. Leikis and A. N. Frumkin, *Electrochim. Acta*, 9 (1964) 431.
3 T. N. Prisekina, V. A. Kuznetsov and N. P. Malyutina, *Sov. Electrochem.*, 2 (1966) 1194.
4 V. M. Novakovskii, E. A. Ukshe and A. I. Levin, *Zh. Fiz. Khim.*, 29 (1955) 1847.
5 B. Jakuszewski, *J. Chem. Phys.*, 31 (1959) 846.
6 J. O'M. Bockris and S. D. Argade, *J. Chem. Phys.*, 49 (1968) 5133.
7 O. Klein and E. Lange, *Z. Elektrochem.*, 43 (1937) 570.
8 J. E. B. Randles, *Trans. Faraday Soc.*, 52 (1956) 1573.
9 A. J. de Bethune, *J. Chem. Phys.*, 29 (1958) 616; 31 (1959) 847.
10 A. N. Frumkin, *J. Chem. Phys.*, 7 (1939) 552.
11 R. Parsons in J. O'M. Bockris (Ed.), *Modern Aspects of Electrochemistry*, Vol. 1, Butterworths, London, 1954, Chap. 3, pp. 169–171.
12 R. Parsons, *Surface Sci.*, 2 (1964) 418.

13 D. C. GRAHAME, E. M. COFFIN, J. I. CUMMINGS AND M. A. POTH, *J. Am. Chem. Soc.*, 74 (1952) 1207.
14 A. N. FRUMKIN, *Electrochim. Acta*, 2 (1960) 351.
15 H. F. HALLIWELL AND S. C. NYBERG, *Trans. Faraday Soc.*, 59 (1963) 1126.
16 B. CASE AND R. PARSONS, *Trans. Faraday Soc.*, 63 (1967) 1224.
17 R. A. ALEKSEEVA, V. A. KUZNETSOV AND T. A. OZORNINA, *Sov. Electrochem.*, 3 (1967) 1114.
18 N. G. BUKUN AND E. A. UKSHE, *J. Appl. Chem., USSR, English Transl.*, 36 (1963) 1907.
19 A. D. GRAVES AND D. INMAN, *J. Electroanal. Chem.*, 25 (1970) 357.
20 C. HERRING AND M. H. NICHOLS, *Rev. Mod. Phys.*, 21 (1949) 227.
21 R. PARSONS, private communication.

ELECTROANALYTICAL CHEMISTRY AND INTERFACIAL ELECTROCHEMISTRY
Elsevier Sequoia S.A., Lausanne – Printed in The Netherlands

REVIEW

THE ELECTRICAL DOUBLE LAYER IN MOLTEN SALTS

PART 2. THE DOUBLE-LAYER CAPACITANCE

A. D. GRAVES AND D. INMAN

Nuffield Research Group in Extraction Metallurgy, Department of Metallurgy, Imperial College of Science and Technology, London, S.W.7 (England)

(Received January 17th, 1969; in final form December 4th, 1969)

INTRODUCTION

The classical methods for characterising the electrical double layer of any metal/electrolyte system involve making measurements of the interfacial tension and the differential capacitance as a function of the applied potential. The interfacial tension/potential ("electrocapillary") curves for metal/molten electrolyte systems are similar to those obtained in other electrolytes and are discussed adequately elsewhere[2]. The capacitance/potential curves, however, differ in several important respects from those obtained in other systems and are still a source of controversy.

It was discovered[2] that capacitance/potential curves for molten electrolytes are roughly parabolic in shape with a minimum capacitance at a potential which coincides within the experimental error with the potential of the corresponding electrocapillary maximum, *i.e.* $E_{q=0}$ (see, however, refs. 31 and 32). Curves of this kind have previously been associated with the diffuse double layer in dilute aqueous electrolyte systems. However, it is unlikely that the diffuse double layer is responsible in melts, because of their high ionic strength, the high value of the minimum capacitance and its positive temperature coefficient[2,17,47]. It is more likely to be a property of the special structure of the melt at the interphase[2,22-24].

It has been suggested[2,25] that the strong correlation between anions and cations in melts produces an ordering of several layers of melt at the interphase under the influence of the electric field. In other words the excess charge on the melt side of the electrical double layer is located several ionic layers deep, the layers being alternately positively and negatively charged. It may be supposed that, when the charge on this "multilayer" is zero, the electric field strength is weakest. Hence, at the potential of zero charge the melt structure at the interphase is likely to be in its least compact condition and the associated capacitance will be a minimum. Thus the increase of capacitance with φ-potential (potentials measured relative to the potential of zero charge) is thought to be due to the melt becoming increasingly compact[2].

According to Dogonadze and Chizmadzhev[22] the increase in the minimum capacitance with temperature is due to a corresponding reduction in the correlation radius between anions and cations in the multilayer. Graves *et al.*[26] stated that this is consistent with the quasi-lattice concept of melt structure, which predicts a loss of "crystallinity" (long range order) with increase in temperature. Thus under the in-

fluence of the electric field the multilayer can become more compact in this case also. It is surprising, therefore, that the capacitance changes more rapidly with the φ-potential at high temperatures than at low[2]. However it has been observed[27,49,50] that at sufficiently large anodic or cathodic φ-potentials the capacitance increases rapidly with potential even at low temperatures. This observation is used here to explain the high temperature behaviour.

THEORIES OF THE DOUBLE LAYER

(a) *Dogonadze and Chizmadzhev*[22]

They attempted to calculate the charge distribution in the melt surface at the metal/melt interphase by means of the binary distribution functions which characterise the microstructure of the bulk melt. The expression for the charge distribution they derived, possessed an "oscillating quenching character" corresponding to the multilayer structure proposed earlier[2,25].

They were able to derive from this expression an approximate formula for the minimum capacitance (C_{min}– the minimum on the capacitance/potential curve):

$$C_{min} = \kappa^2 \lambda d^2 / 8\pi^4 \quad (1)$$

where d is the distance to the first maximum of the binary distribution function, $1/\lambda$ is the correlation radius, which characterises the dimensions of short range order in the melt ($1/\lambda > d$) and $1/\kappa$ is the Debye radius giving $C_{min} \sim 50\ \mu F\ cm^{-2}$.

Dogonadze and Chizmadzhev stressed that accurate values of C_{min} for individual melts could not be calculated from eqn. (1). Several rough approximations were used in its derivation and no account had been taken of the different sizes of anions and cations. Also no data existed for correlation radii in melts. The correlation radius used to estimate the value of C_{min} given above was for liquid caesium.

Nevertheless Dogonadze and Chizmadzhev claimed that the fact that the correlation radius for liquid caesium decreased with increase in temperature, was in agreement with the observation[2,17,47] that the capacitance of the electrical double layer in molten alkali halides increased with temperature.

It should be noted however, that on the basis of these observations[2,17,47], the expected increase of capacitance with temperature (in the range 390°–480° C) was not obtained by Heus *et al.*[28] in their recent measurements with a dropping lead electrode in a LiCl–KCl eutectic melt. Also they obtained a substantially higher value for C_{min} at 450°C ($\sim 30\ \mu F\ cm^{-2}$) than had been obtained previously[2,27,49,50] (20–25 $\mu F\ cm^{-2}$). This could be because the previous measurements[2,27,49,50] were made with stationary electrodes, which are less satisfactory for capacitance measurements than a dropping electrode. The area of a dropping electrode is better defined and the effects of electrolyte seepage are reduced[40,46]. For example, frequency dispersion of the capacitance was absent above 1 kHz in the work of Heus *et al.*[28], whereas the capacitances measured by Ukshe *et al.*[2] only became independent of frequency at about 20 kHz (electrode area $\sim 0.08\ cm^2$). In addition, the dropping electrode is less likely to be affected by the adsorption of impurities in the melt. The results of Heus *et al.*[28] will be referred to again later.

Hills and Power[29] and Palanker *et al.*[30] have shown that there is a slight decrease of capacitance with increase in temperature (highest temperature 260° C[30])

for a dropping mercury electrode in contact with molten alkali nitrate mixtures. Hills and Power[29] have suggested that this effect may be associated with the special properties of the nitrate ion. For this reason, the remainder of this paper will be concerned only with molten alkali halide systems.

(b) Sotnikov and Esin[23]

They assumed that for a charge density ε on the metal there is an equal and opposite charge density on the melt produced by anion and cation vacancies, whose concentration ($c_\pm$) is given by the Boltzmann equation:

$$c_\pm = c_0 \exp(W_\pm/kT) \tag{2}$$

where c_0 is the concentration of vacancies of the same sign in the bulk melt and $W_\pm$ is the energy gained when a vacancy is "transported" (Sotnikov and Esin's quotation marks) from the bulk to a given point in the double layer.

It is assumed also that the crystal structure of the solid is preserved to some extent in the melt and that each ion is surrounded by a rigid sphere of z ions of opposite sign. The centre of the sphere is supposed to shift relative to the central ion under the influence of the electric field in the double layer. The amount of shift may be calculated by means of the formula for the formation of induced dipoles:

$$\text{shift} = \alpha|\psi'|/q \tag{3}$$

where α is the polarisability, ψ' is the potential gradient and q is the charge on the vacancy.

At this stage it is possible to derive a function for the distribution of potential in the double layer by calculating W_+ for anions and W_- for cations and introducing Poisson's equation. The function obtained has the expected sign-alternating, damped-oscillating character and gives a value for the distance between neighbouring experimental points, which turns out to be close to the lattice parameter of the salt, *e.g.* ≈ 1 Å for NaCl and 1.5 Å for RbCl.

An expression for the double-layer capacitance (C) is obtained by integrating this potential distribution function under the appropriate boundary conditions:

$$\frac{1}{C} = \frac{1}{C_k} - \frac{4\pi\delta}{1-4\pi\delta\beta|\varepsilon|} \tag{4}$$

where $C_k = D/4\pi r$ is the capacitance of a parallel plate capacitor with a plate separation equal to the radius r of the cation, D being the dielectric constant, $\delta^2 = kT/[8\pi q^2 c_0(z-2)]$, and $\beta = 8\pi\alpha q c_0(z-1)/kT$.

As most of the available experimental evidence [2] suggests that the minimum capacitance occurs at the potential of zero charge (see, however, refs. 31 and 32) then

$$1/C_m = 1/C_k - 4\pi\delta \tag{5}$$

The concentration of vacancies of the same sign in the bulk melt was calculated from the formula:

$$c_0 = (\rho_s^{m.p.} - \rho_l^{m.p.})N/M \tag{6}$$

where $\rho_s^{m.p.}$ and $\rho_l^{m.p.}$ are the densities of the solid and liquid at the melting point, N is Avogadro's number and M is the molecular weight.

The "effective" coordination number z was calculated from the formula:

$$z = b(\rho_l / \rho_s^{\text{m.p.}}) \tag{7}$$

where ρ_l is the density of the melt at a given temperature and b, although not defined by Sotnikov and Esin, is presumably the coordination number of the solid.

A value of 2.7 was used for the dielectric constant of all the melts considered.

Values of C_m calculated from eqn. (5) are compared with the experimental values in Table 1 (reproduced from ref. 23). Also, calculated and experimental values for the temperature coefficient of C_m are compared in Table 1.

TABLE 1

COMPARISON BETWEEN THE EXPERIMENTAL* AND CALCULATED VALUES OF C_{min} AND dC_{min}/dT

Melt	$C_{min}/\mu F\ cm^{-2}$ (800° C)		$100(dC_{min}/dT)/\mu F\ cm^{-2} K^{-1}$	
	Exptl.	*Calcd.*	*Exptl.*	*Calcd.*
NaCl	40.7	40.5	13.6	3.4
KCl	28.8	29.2	3.5	1.6
RbCl	28.1	26.9	2.0	1.3
CsCl	28.0	25.8	2.6	1.6
NaBr	48.7	46.0	22.5	3.5
KBr	30.7	31.3	3.3	4.4
NaI	69.4	54.7	27.4	5.0
KI	32.5	34.8	3.3	2.2

* The experimental data are taken from the abstract of E.A. Ukshe's Ph.D. Thesis, 1964.

The calculated and experimental results are in reasonably good agreement for caesium, rubidium and potassium salts. However, for sodium salts the agreement is good only at temperatures close to the melting point. For lithium salts the agreement is only approximate.

Sotnikov and Esin concluded that with their simplified model it is only possible to calculate the dependence of the capacitance on temperature and potential (without the use of adjustable parameters) for melts with similar anion and cation radii. This is probably because, where the radii are markedly different, the vacancies of different sign are not equivalent in size and structure.

(*c*) *Bukun and Ukshe*[24]

They have adopted a physically less rigorous approach than Dogonadze and Chizmadzhev[22] or Sotnikov and Esin[23] and assumed the multilayer model at the outset. If the charged layers can be treated as the plates of an infinite series of parallel plate capacitors then the integral capacitance (C_i–which is practically the same as the differential capacitance at the potential of zero charge) of this series is given by the expression:

$$C_i = \frac{\varepsilon}{4\pi a_1} \frac{(1-\beta)}{(1-k\beta)} \tag{8}$$

where ε is the dielectric constant, a_1 is the distance between the electrode surface and a plane passing through the centres of the first layer of ions, $k = (a_1 + a_2)/a_1$, a_2 being the

distance between the first and second ionic layers, etc., (*i.e.* $a_2 = a_3 = a_4 = \ldots = a_n$ for n layers) and β is the excess charge factor.

The nature of β may be ascertained from the method used in its calculation, *i.e.*

$$\beta = [(N_A/V_{KP})^{\frac{2}{3}} - (N_A/V_P)^{\frac{2}{3}}]/(N_A/V_P)^{\frac{2}{3}} = (V_P/V_{KP})^{\frac{2}{3}} - 1 \quad (9)$$

where N_A is Avogadro's number, V_{KP} is the molar volume of the crystalline alkali halide at 0°K, and V_P is the molar volume at temperature T. Thus $(N_A/V_{KP})^{\frac{2}{3}}$ is taken to be the number of ionic positions in a unit surface of the solid and $(N_A/V_P)^{\frac{2}{3}}$ is the corresponding quantity for the melt at temperature T. Therefore β is determined by the relative number of positions available in the surface layer of the melt for the accommodation of excess charge (*i.e.* ions) at the given temperature. It appears that Bukun and Ukshe have assumed that all the available positions in the first layer of ions (called the "pre-electrode layer" by Bukun and Ukshe) are occupied. On this basis it follows that the pre-electrode layer should have a close-packed structure similar to that found in the crystalline solid (not the same structure, as there are unequal numbers of anions and cations present). Values of β calculated according to eqn. (9) are around 0.2 (see Table 2 – reproduced from ref. 24) which suggests that only about three* layers of melt at the metal/melt interphase are ordered in the manner described.

Bukun and Ukshe suggested that a_1 should be close to the average ionic radius and a_2 the average ionic diameter for each melt. Thus $a_2 \approx 2a_1$ and $k \approx 3$. It may be seen from Table 2 that k is indeed close to 3 but a_1 is not close to the average ionic radius as expected. However, in each case the value of a_1 does lie between the values for the anionic and cationic radii of the melt.

Although not clearly stated by Bukun and Ukshe, it appears that the values of a_1 and k in Table 2 (and ε) have been calculated from the experimental values of the capacitance at various temperatures. The sole justification for the model, then, is that a_1, k and ε have reasonable values (ε is within 10% of theoretical values or of experimental values calculated from refractive indices).

THE PRESENT STUDY

(*a*) *The effect of temperature*

The theories of Sotnikov and Esin[23] and Bukun and Ukshe[24] have been presented in some detail as this information is not readily available elsewhere. Also now it should be clear that little attempt has been made in any of the above theories to account for the rapid change of capacitance with potential at high temperatures.

In their review Devanathan and Tilak[33] suggested that the lead/molten alkali halide interphase was only ideally polarisable over a relatively small range of potentials at high temperatures. They stated that "adsorption pseudocapacitance" was probably contributing to the high values of capacitance obtained at the higher temperatures. Ukshe and Tomskikh[34] claimed to have eliminated this possibility by demonstrating that the doubly-integrated capacitance/potential curves coincided with the corresponding electrocapillary curves (see also ref. 35).

Graves and Inman[27] agreed that the high values of capacitance were "true"

* Equation (8) is arrived at by summing a geometric series in β, *i.e.* $1 + \beta + \beta^2 + \ldots \beta^{n-1} = (1-\beta)^{-1}$ as $n \to \infty$. When β is 0.2, the series can be approximated by the first three terms.

TABLE 2

DATA USED TO INVESTIGATE THE VALIDITY OF EQUATION (8)

Melt	*t*/°C	V_p/cm^3 mol^{-1}*	β	a_1/Å	k	$C_{calc.}$ $\mu F\,cm^{-2}$	$C_{expt.}$ $\mu F\,cm^{-2}$
LiCl	694	28.9	0.260	1.70	2.87	31.2	31.2
	713	29.1	0.265			33.2	33.2
	722	29.2	0.270			34.8	34.6
	755	29.5	0.279			38.4	38.2
	775	29.7	0.285			41.9	42.0
	800	29.9	0.291			45.3	45.5
NaCl	820	37.8	0.251	1.11	2.96	44.0	43.4
	853	38.1	0.259			47.8	47.9
	865	38.4	0.263			49.7	49.8
	890	38.8	0.272			55.4	55.2
	900	38.9	0.275			58.0	57.7
	922	39.2	0.284			65.8	65.2
	940	39.5	0.288			71.0	70.8
KCl	800	49.4	0.202	1.09	2.86	28.4	28.8
	840	50.0	0.212			29.7	30.1
	865	50.6	0.222			31.5	31.0
	880	50.9	0.226			32.3	32.0
	920	51.6	0.238			34.8	34.6
	960	52.6	0.253			39.1	39.2
RbCl	735	54.3	0.169	1.07	2.95	26.2	26.4
	770	55.0	0.181			27.5	27.5
	800	55.7	0.190			28.6	28.2
CsCl	690	61.5	0.145	1.04	2.86	25.5	25.6
	750	63.0	0.162			26.9	26.7
	800	64.1	0.174			28.6	28.0
LiBr	680	35.7	0.265	2.17	3.05	33.7	33.2
	720	36.0	0.272			38.3	38.0
	760	36.3	0.280			45.3	45.7
	805	36.8	0.291			57.5	58.2
	822	37.0	0.298			63.5	65.7
NaBr	787	44.6	0.246	1.16	3.06	47.7	47.9
	800	44.8	0.248			48.8	48.9
	820	45.3	0.256			53.2	53.2
	853	45.7	0.265			59.9	60.0
KBr	783	57.0	0.202	1.16	2.92	29.2	30.0
	800	57.5	0.210			30.6	30.7
	815	57.9	0.215			31.3	31.5
	845	58.5	0.221			32.6	32.6
	880	59.5	0.235			35.9	34.6
NaI	735	56.2	0.237	0.99	3.05	58.0	58.5
	765	56.9	0.246			63.0	62.4
	806	57.6	0.256			69.9	71.0
	825	58.0	0.262			76.1	76.2
KI	739	69.5	0.196	1.15	2.80	30.0	30.5
	759	70.0	0.201			30.6	31.1
	780	70.5	0.207			31.4	31.7
	807	71.4	0.217			33.0	32.7
	828	72.0	0.223			34.0	33.4
CsI	680	83.7	0.153	1.13	2.85	26.5	26.8
	715	84.8	0.164			27.3	27.3
	770	86.7	0.181			29.0	28.8
	800	87.7	0.190			30.2	29.9
	835	89.0	0.202			31.9	31.7

* V_p data, I. S. YAFFE AND E. R. VAN ARTSDALEN, *J. Phys. Chem.*, 60 (1956) 1125.

double-layer capacitances in the sense intended by Ukshe and Tomskikh[34] but nevertheless maintained that they were also a consequence of an electrode reaction taking place at the metal/molten electrolyte interphase. The high values are obtained because the double-layer capacitance at an interphase sustaining a reversible reaction, is given by $d(q+zF\Gamma_+)/dE$ and not by dq/dE[36] (where Γ_+ is the surface excess of the reversible ion, M^{z+}, and q is the charge on the electrode). Delahay[37] has shown theoretically that large values for the "reversible" double-layer capacitance can be attained in aqueous solution. This is confirmed by the measurements of Sluyters–Rehbach and Sluyters[38] with the Hg/Hg_2^{2+} system in aqueous perchloric acid solution. It appears that similar results can be obtained with liquid metal electrodes in molten alkali halides[27,48–50].

Graves and Inman[27] have divided their capacitance/potential plots for a lead electrode in the LiCl–KCl eutectic at 450° C (see Fig. 1) into two regions; a region

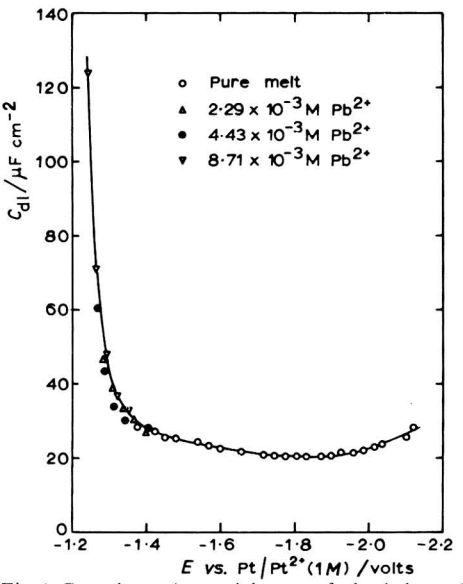

Fig. 1. Capacitance/potential curve of a lead electrode in a LiCl–KCl eutectic melt at 450°C[27].

where the capacitance is only slightly dependent on potential and a region where the capacitance varies sharply with potential. The former region has been called the "ideally polarisable" region, where the situation in the double layer may be described in terms of the theories presented above[22–24]. Graves and Inman[27] have shown that in the latter region, substantial charge transfer is taking place across the metal/melt interphase due to the reaction $Pb^{2+}+2e \rightleftharpoons Pb$. For example, at the Pb^{2+} ion concentrations given in Fig. 1 the exchange current densities are:

2.29×10^{-3} M Pb^{2+} ($E=-1.290$ V), $i_0=0.57$ A cm^{-2}

4.43×10^{-3} M Pb^{2+} ($E=-1.269$ V), $i_0=0.95$ A cm^{-2}

8.71×10^{-3} M Pb^{2+} ($E=-1.248$ V), $i_0=1.64$ A cm^{-2}

Thus, this region has been called the "ideally reversible" region, where the double-layer capacitance is given by the expression $d(q+2F\Gamma_{Pb^{2+}})/dE$. Of course, these regions are not ideally polarisable or ideally reversible in the strict sense, as in the former region small "residual" currents may be detected[28] and in the latter the exchange current densities are not equal to infinity. However, as the following discussion shows, the ideal situations are approached sufficiently closely for the present purpose.

The transition from the ideally polarisable to the ideally reversible region occurs in the case of a lead electrode at 450° C, at a φ-potential ($\varphi^{R/P}_{Pb}$) of 0.4 V, *i.e.* a potential which is about 0.4 V positive to the potential of zero charge. It would appear that $\varphi^{R/P}_{Pb}$ is the potential at which the surface excess of Pb^{2+} ions ($\Gamma_{Pb^{2+}}$) begins to have a measurable effect on the electrode capacitance.

Assuming, for example, a linear adsorption isotherm, it is possible to relate $\varphi^{R/P}_{Pb}$ to the critical surface excess $\Gamma^{c}_{Pb^{2+}}$ by means of the Nernst equation, *i.e.*

$$(\varphi^{R/P}_{Pb})_{450^\circ} = (\varphi^{0}_{Pb})_{450^\circ} + \frac{723R}{2F} \ln\left(\frac{\Gamma^{c}_{Pb^{2+}}}{\gamma_a}\right) \quad (21)$$

where $(\Gamma^{c}_{Pb^{2+}}/\gamma_a)$ is the corresponding critical surface concentration, γ_a being the adsorption coefficient. If it is further assumed that the critical surface concentration is independent of temperature, then at temperature t° C

$$(\varphi^{0}_{Pb} - \varphi^{R/P}_{Pb})_{t^\circ} = (\varphi^{0}_{Pb} - \varphi^{R/P}_{Pb})_{450^\circ} \times (t+273)/723 \quad (22)$$

or

$$(\varphi^{R/P}_{Pb})_{t^\circ} = (\varphi^{0}_{Pb})_{t^\circ} - (\varphi^{0}_{Pb} - \varphi^{R/P}_{Pb})_{450^\circ} \times (t+273)/723 \quad (23)$$

Values of φ^{0}_{Pb} calculated from the experimental $\varphi^{ref}_{Pb}(=E^{ref}_{Pb} - E^{Pb}_{q=0})/t^\circ$ data of Bukun and Ukshe[39] and Kuznetsov and co-workers[3], together with the corresponding values of $\varphi^{R/P}_{Pb}$, calculated from eqn. (23), are given in Table 3 for several different

TABLE 3

DETERMINATION OF $\varphi^{R/P}_{Pb}$ AT DIFFERENT TEMPERATURES FROM THE DATA OF BUKUN AND UKSHE[39] AND KUZNETSOV *et al.*[3]

The potentials have been calculated on the mole fraction scale and are accurate to within ±0.03 V.

$t^\circ C$	*Pb/LiCl–KCl* (1 : 1)			*Pb/LiCl–KCl eutectic*		
	$\varphi^{ref.39}_{Pb}/V$	φ^{0}_{Pb}/V	$\varphi^{R/P}_{Pb}/V$	$\varphi^{ref.3}_{Pb}/V$	φ^{0}_{Pb}/V	$\varphi^{R/P}_{Pb}/V$
450	0.70	0.81(4)	0.40	0.68	0.79(4)	0.40
600	0.64	0.77(8)	0.28	0.59	0.72(8)	0.25
700	0.59	0.74(4)	0.19	0.53	0.68(4)	0.15
800	0.55	0.71(9)	0.10	0.47	0.63(9)	0.05

temperatures. Despite the discrepancy between the two sets of φ^{ref}_{Pb} data [3,39] which may be partly associated with the use of LiCl–KCl melts of different composition, there is in each case a marked decrease of $\varphi^{R/P}_{Pb}$ with increase in temperature. If the appropriate $\varphi^{R/P}_{Pb}$ values are marked on the plots obtained by Bukun and Ukshe[39], replotted on the φ-potential scale by Graves *et al.*[26] (Fig. 2), it would appear that the change in shape of the anodic branch of these curves with increasing temperature is due primarily to the approach of the region of the capacitance/potential curve where

the electrode is behaving in an ideally reversible manner, to the potential of zero charge.

A similar process appears to be taking place in the cathodic branch of the curves in Fig. 2. The capacitances in this region are presumably associated with the

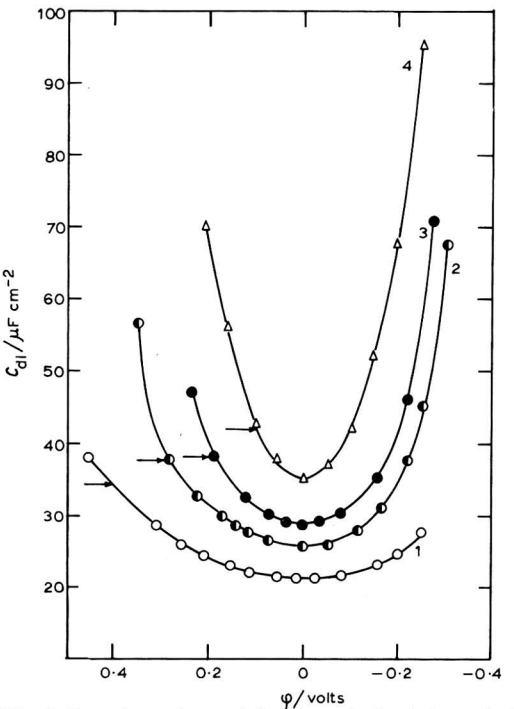

Fig. 2. Capacitance/potential curves of a lead electrode in an equimolar LiCl–KCl melt at: (1) 450°, (2) 600°, (3) 700°, (4) 800°C[26]. The approximate position of $\varphi_{Pb}^{R/P}$ is indicated on each plot by means of an arrow.

deposition of alkali metal (A) according to the reaction $A^+ + e \rightleftharpoons A(Pb)$. Although the rate of this reaction has not been measured for either potassium or lithium, it may safely be assumed that it is very rapid, *i.e.* reversible. Certainly capacitances measured at potentials more negative than −2.1 V in Fig. 1, increased rapidly with potential[27]. Usually measurements were discontinued at this point in order to avoid contaminating the lead electrode with alkali metal. Bek and Lifshits[49,50] obtained similar results with lead, cadmium and bismuth electrodes and also associated the sharp increase of capacitance in the cathodic branch with the onset of alkali metal deposition. Presumably[36] the double-layer capacitance in this region is given by the expression $d(q - F\Gamma_{A^+})/dE$, where Γ_{A^+} is the surface excess of alkali metal ions in the electrode metal. In the absence of e.m.f. data for the cell $Pb|PbCl_2$, LiCl–KCl ‖ LiCl–KCl|A(Pb) at various temperatures it is not possible to show that $\varphi_{A(Pb)}^{R/P}$ (the φ-potential at which the transition from ideally polarisable to ideally reversible behaviour occurs in the cathodic branch) has a similar temperature dependence to $\varphi_{Pb}^{R/P}$ in Table 3.

Nevertheless it seems fairly certain that the range of potentials where a lead electrode exhibits ideally polarisable behaviour, decreases with increase in tempera-

ture. Therefore, at sufficiently high temperature a lead electrode will behave in an ideally reversible manner at all potentials. It appears from the results of Ukshe, Bukun and Leikis[41] (Fig. 2) that this occurs at about 800° C for the LiCl–KCl system. However, according to the value of $\varphi_{Pb}^{R/P}$ at 800° C given in Table 3, a small range of ideally polarised behaviour should exist even at this temperature. We have recently discovered a publication[48] which supports this prediction. Bek and Lifshits[48] measured the double-layer capacitance of a lead electrode in an equimolar NaCl–KCl melt at 800° C over the potential range from lead dissolution to alkali metal deposition and showed that symmetrically placed within these limits there was a small range of potential (~0.2 V) where the capacitance was practically independent of temperature (within the experimental error). It is known[39] that the Pb/NaCl–KCl and Pb/LiCl–KCl systems give rise to similar capacitance potential curves, so a 0.2 V range of ideally polarisable behaviour is in good agreement with that expected from Table 3, assuming $\varphi_{Pb}^{R/P} \approx \varphi_{A(Pb)}^{R/P}$.

The results of Bek and Lifshits[48] are likely to be more reliable than those of Bukun and Ukshe[39], as Bek and Lifshits have allowed for the effects of the Pb/Pb^{2+} charge-transfer process on their measurements. In fact, they stated that the analysis of their results to give double-layer capacitances was strictly valid only at potentials where the limiting diffusion current for Pb^{2+} ions had been reached, *i.e.* where the surface concentration of Pb^{2+} ions was zero. Bek and Lifshits[48] had deliberately introduced small quantities of Pb^{2+} ions into their melts in order to measure charge-transfer rates, but it appears that these ions are generated even in carefully purified melts by corrosion of the lead electrode[27]. Ukshe and Bukun[40] attempted to correct their capacitance measurements for the presence of "non-equilibrium processes". However, the analysis they used was inadequate for a reversible charge-transfer system under d.c. polarisation[38,48,51,52], so their measurements are likely to be in error on this account. On the other hand the technique used by Graves *et al.*[26,27] was designed to give reliable double-layer capacitance measurements in the presence of reversible charge transfer over the whole range of potentials. The success of this process can be judged from the results in Fig. 1, where the same values of capacitance (within the experimental error) were obtained in a melt containing various Pb^{2+} ion concentrations and in the "pure" melt (containing $\sim 10^{-4}$ *M* Pb^{2+} ions) both in the ideally reversible and ideally polarised regions (only the "pure" melt results are shown in the latter region, for clarity).

In view of the above remarks it is surprising that Ukshe and Tomskikh[34] obtained such good agreement between doubly-integrated capacitance/potential curves and the corresponding electrocapillary curves. Furthermore, as pointed out by Bek and Lifshits[48], the comparison of these curves by means of Lippmann's equation[11] is not straightforward as, on account of the deposition of alkali metal, the composition of the lead electrode does not remain constant.

It was noted earlier (see the discussion of Dogonadze and Chizmadzhev's theory of the double layer) that at low temperatures (390°–480° C) Heus *et al.*[28] were unable to find any significant variation of capacitance with temperature of a lead electrode in the LiCl–KCl eutectic melt. This observation is supported by the measurements of Bek and Lifshits[48], who obtained a C_{min} value of about 25 μF cm^{-2} for the Pb/NaCl–KCl system at 800° C, a value which is typical of alkali chloride melts at *low* temperatures. The value obtained by Bukun and Ukshe[39] for the same system

was 40 μF cm^{-2}. Thus the measured[17,47] temperature dependence of the capacitance may be an artifact of the technique of measurement. The measurements at low temperatures, where the electrode has a wide range of ideally polarisable behaviour are presumably fairly reliable but at high temperatures the effect of charge transfer must be taken into account, as described above. Evidently, the measured capacitance is not necessarily equal to the double-layer capacitance just because it is independent of frequency, as stated previously[40].

An additional contribution to the measured temperature dependence of the capacitance may arise when $\varphi_{Pb}^{R/P}$ is $\leqq 0$. In this case the ideally reversible regions will overlap and the degree of overlap will increase with temperature producing an apparent increase in C_{min}. Certainly, the melts for which $\varphi_{Pb}^{R/P}$ is close to zero (LiCl and NaCl, see next section) are those with the highest temperature coefficient[2] (see Table 1).

However, as these conclusions conflict with much of the previous theoretical work[22-24], we do not wish to speculate further until the experiments of Heus *et al.*[28] and Bek and Lifshits[48] have been independently confirmed.

(*b*) *The effect of changing the melt*

The shapes of the capacitance/potential curves and the potentials of zero charge are hardly affected by changing the anionic component of the melt[41,47]. (This is not true of melts which contain fluoride ions. Melts of this kind will not be considered in detail here). However, the magnitude of the minimum capacitance (C_{min}) is affected and increases in accordance with the polarisability of the anion, *i.e.* $Cl^- < Br^- < I^-$. The increase in C_{min} is particularly marked for the sodium or lithium halide melts[41], where the sodium and lithium ionic radii are sufficiently small for the anions to be almost close-packed. According to Ukshe *et al.*[2], in this case the mutual repulsion between the anions would be expected to dominate the melt structure and hence the magnitude of the double-layer capacitance. In potassium or caesium halides the anion/cation ratio is much closer to unity, so that the cationic contribution to the melt structure becomes more important. The influence of the anion on C_{min} is correspondingly reduced[41].

The shapes of the capacitance/potential curves and the potentials of zero charge are both affected by changing the cationic component of the melt[41,47]. For example, lithium or sodium chloride melts at 800° C, are characterised by capacitance/potential curves with relatively sharp minima, high values of C_{min} and small values of φ_{Pb}^{ref}. On the other hand potassium or caesium chloride melts at the same temperature are characterised by capacitance/potential curves with relatively broad minima, low values of C_{min} and large values of φ_{Pb}^{ref} (see Table 4).

It is possible to correlate the different capacitance/potential behaviour of these two groups of melts with the potentials at which the lead/melt interphase changes from ideally polarisable to ideally reversible behaviour (see the $\varphi_{Pb}^{R/P}$ values in Table 4, which were calculated on the assumption that $\Gamma_{Pb^{2+}}^{c}$ is independent of the melt). Apparently the ideally reversible regions of the capacitance/potential curves for the lithium or sodium chloride systems overlap ($\varphi_{Pb}^{R/P} \sim 0$, and assuming that $\varphi_{A(Pb)}^{R/P}$ is also approximately zero), which would explain the sharp minima exhibited by these curves. Conversely, the small range of ideally polarisable behaviour ($\varphi_{Pb}^{R/P} \sim 0.1$ V) shown by the potassium or caesium chloride melts is consistent with the relatively

TABLE 4

DETERMINATION OF $\varphi_{Pb}^{R/P}$ AT 800°C FOR THE ALKALI CHLORIDE MELTS USING THE DATA OF UKSHE *et al.*[41]

N.B. The reference electrode used in this work had a slightly difference composition to that described above, *i.e.* 10 wt. % $PbCl_2$ + solvent melt, giving $(\varphi_{Pb}^{0} - \varphi_{Pb}^{R/P})_{450°} = 0.419$ V, *cf.* Table 1.

Melt	$\varphi_{Pb}^{ref.}/V$	φ_{Pb}^{0}/V	$\varphi_{Pb}^{R/P}/V$	$C_{min}/\mu F\,cm^{-2}$
LiCl	0.48	0.65(6)	0.03	45
NaCl	0.47	0.64(6)	0.02	43
KCl	0.60	0.77(6)	0.15	28
CsCl	0.55	0.72(6)	0.10	28

broad capacitance/potential minima associated with these systems.

The influence of the cation on the transition potential ($\varphi_{Pb}^{R/P}$) may be explained by considering the significance of the φ_{Pb}^{0} values in Table 4, on which the transition potentials depend. It was shown[42] that

$$\varphi_{M}^{0} = {}^{S}\Delta^{M}\psi^{0} - {}^{S}\Delta^{M}\psi_{q=0} \tag{10}$$

where ${}^{S}\Delta^{M}\psi^{0}$ is the standard volta potential for a metal/electrolyte system and ${}^{S}\Delta^{M}\psi_{q=0}$ is the volta potential difference across the metal/electrolyte interphase at the potential of zero charge. ${}^{S}\Delta^{M}\psi_{q=0}$ may be accounted for by the change in the surface potentials of the metal and the electrolyte, when the two phases are brought into contact with one another[1,6,11,12,14,42]. Thus the φ_{Pb}^{0} data in Table 4 depend, not only on the volta potential difference of the Pb/Pb^{2+} couple but also on the interaction between the lead electrode and the alkali halide melt. In the absence of volta potential data for molten salt systems it will be assumed, as a first approximation, that ${}^{S}\Delta^{Pb}\psi^{0}$ is independent of the melt. Therefore, ${}^{S}\Delta^{Pb}\psi_{q=0}$ is independent of the anionic component of the melt but is dependent on the cationic component; or in other words the change in the surface potentials of the lead electrode and the alkali halide electrolyte, when the two phases are brought into contact, is not affected by the anionic but only by the cationic component of the melt. As the interaction between metal and melt is presumably dependent on the surface structure of the melt (for a given metal), it appears from Table 4 that the differences in melt surface structure, which determine the different values of the minimum capacitance for lithium or sodium halide melts and potassium or caesium halide melts (see the first paragraph of this section), are also responsible for the differences in the φ_{Pb}^{0} values and hence for the shapes of the capacitance/potential curves for these groups of melts.

Some authors (*e.g.* see refs. 29 and 47) have suggested that the effect of the anion on the double-layer capacitance may be due to "adsorption". In addition, ionic specific adsorption has been proposed to account for the experimental behaviour of at least one molten salt system (Cs^{+} in LiCl–CsCl[43]). However, the phenomenon of adsorption at interphases between metals and molten salts, has not been described in an explicit way. It is obviously particularly difficult to define, when the metal dips into a melt consisting of one type of cation and one type of anion. To a first approximation in this type of system, capacitance/potential curves are symmetrical and the potentials of zero charge are apparently independent of solvent anion (except in the case of F^{-}). However, the potentials of zero charge do depend on the cationic compo-

sition of the melts. If judged on the basis of the ideas developed to explain aqueous solution behaviour, these observations would seem to mitigate against an explanation in terms of specific adsorption. Indeed, one of the aims of this paper is to show that many of the results of capacitance/potential measurements which have been obtained for molten salts can be explained in terms of non-specific structural models. However, it will probably be necessary to consider specific interactions leading to overlap between the atoms in the surface of the metal and the ions in the surface of the melt and the formation of long-lived surface complexes, in the next stage of development of this topic. This has certainly been necessary to explain the results of studies of electrode processes in molten salts[44].

The effects of melt composition on C_{min}, etc. in binary melts can generally be explained in terms of the replacement of one ionic species by another at the metal/melt interphase[2,47]. This replacement does not necessarily lead to overlap between the surface layers of metal and melt, *i.e.* the process is non-specific. Delimarskii and Kikhno[47], following suggestions by Ukshe *et al.*[41], attempted to explain the anion/cation effect on the potential of zero charge in this way, after they had confirmed that the experimental results of Ukshe *et al.*[41] were characteristic of the melts concerned, by using nickel instead of lead for the electrode metal. They suggested that the zero charge potential did not change with the type of anion, because replacement of one anion by another took place in an outer layer of the multilayer without changing the overall excess charge, *e.g.* one Cl^- ion is replaced by one I^- ion, etc. On the other hand small surface active cations such as Li^+ can penetrate into the inner layer more easily than anions can be displaced from the outer layer so in this case additional positive charge is introduced into the multilayer and the potential of zero charge becomes more positive. However, it is difficult to understand how this explanation can be applied to individual alkali halide melts without invoking specific interactions with the electrode surface, especially since anions are also highly surface active.

(*c*) *The effect of changing the electrode metal*

The effect on φ_M^0 of changing the electrode metal is shown in Table 5 using the

TABLE 5

DETERMINATION OF φ_M^0 FOR SEVERAL METALS IN THE LiCl–KCl EUTECTIC AT 450°, 600° AND 700°C USING THE DATA OF KUZNETSOV *et al.*[3]

Metal	450°C			600°C			700°C		
	$(E_M^0-E_{Pb}^0)/V$	$\varphi_M^{ref.}/V$	φ_M^0/V	$(E_M^0-E_{Pb}^0)/V$	$\varphi_M^{ref.}/V$	φ_M^0/V	$(E_M^0-E_{Pb}^0)/V$	$\varphi_M^{ref.}/V$	φ_M^0/V
In	0.266	0.74	1.12	–	0.66	–	–	0.61	–
Bi	0.431	0.47	1.01	–	0.38	–	–	0.32	–
Ga	0.221	0.57	0.90	–	0.47	–	–	0.42	–
Pb	0.000	0.68	0.79	0.000	0.59	0.73	0.000	0.53	0.68
Tl	−0.269	0.78	0.62	−0.272	0.70	0.57	−0.275	0.65	0.53
Sn	0.019	0.40	0.53	0.020	0.31	0.47	0.020	0.24	0.41

data of Kuznetsov and co-workers[3]. Experimental data for $E_{Pb}^0-E_M^0$ in the LiCl–KCl eutectic melt are only available at 450°C. The values at 700°C for thallium and tin

were taken from the standard electrode potential data compiled by Plambeck[45] for the equimolar NaCl–KCl melt, and the values at 600° C were obtained by linear interpolation. Similar data are not available for indium, bismuth and gallium to the authors' knowledge.

A decrease of φ_M^0 with increase in temperature is characteristic of both thallium and tin, which shows that in this respect these metals are similar to lead. However, the actual values of φ_M^0 at a particular temperature (*i.e.* 450° C) are different for all the metals listed in Table 5. Values of $\varphi_M^{R/P}$ have not been included because the behaviour with respect to temperature of the capacitance/potential curves for metals other than lead (in the LiCl–KCl melt) is not generally known.

The φ_M^0 data at 450° C in Table 5 can be compared with a similar set of data in Table IV of ref. 26. The latter data were calculated from the experimental results of other workers (see ref. 26 for the appropriate references) and refer to a molar e.m.f. scale. Nevertheless the results are similar to those given in Table 5 of the present publication and show the same order, with indium having the largest value of φ_M^0 and tin the smallest. The φ_M^0 series in Table IV of ref. 26 was intended to show that the electrodeposition of metals from molten alkali halide solvents generally takes place on a positively charged electrode surface. At the same time Graves *et al.*[26] suggested that there might be some correlation between the magnitude of φ_M^0 and the charge number (z) of the ion. In view of the uncertain nature of the surface potential contribution to φ_M^0 it seems that this correlation is fortuitous.

CONCLUSIONS

If the proposal[27] that the capacitance/potential curves for a lead/molten alkali halide interphase can be divided into "ideally polarisable" and "ideally reversible" regions is correct, then the observation that the potential at which the transition occurs approaches the potential of zero charge with increase in temperature (*i.e.* $\varphi_{Pb}^{R/P}$ decreases as t increases), would seem to be the most important factor governing the change in the shapes of the capacitance/potential curves with temperature.

At potentials close to the potential of zero charge (*i.e.* in the ideally polarisable region) it is possible that the temperature dependence of the capacitance can be accounted for in terms of the model proposed by Ukshe *et al.*[2] and investigated quantitatively by Dogonadze and Chizmadzhev[22], Sotnikov and Esin[23] and Bukun and Ukshe[24] (see, however, the remarks made concerning the work of Heus *et al.*[28] and Bek and Lifshits[48]).

A change in the anionic component of the melt from $Cl^- \rightarrow Br^-$ or $Cl^- \rightarrow I^-$, etc. affects only the magnitude of the double-layer capacitance, whereas a change in the cationic component from Li^+ or Na^+ to K^+ or Cs^+ affects not only the capacitance but also the shape of the capacitance/potential curve and the potential of zero charge. The change in shape of the capacitance/potential curve with the cation can be correlated with the corresponding change in the transition potential ($\varphi_{Pb}^{R/P}$), which in turn appears to depend on a change in the surface structure of the melt.

Although there are few capacitance data available for metals other than lead, the range of potentials, where, for example, a thallium or tin electrode behaves in an ideally polarisable manner appears to decrease with increase in temperature in the same way as it does for lead.

ACKNOWLEDGEMENTS

The authors wish to thank Dr. R. Parsons for helpful discussions of parts of this paper. Also we are grateful for help with the translation of publications in Russian given by Mr. A. M. Arthur.

SUMMARY

The dependence of the double-layer capacitance of the liquid metal/molten alkali halide interphase on potential and temperature is discussed. The effects of temperature, melt composition and electrode metal on the shapes of the capacitance/potential curves are explained by considering a recent suggestion[27] that these curves can be divided into ideally polarisable and ideally reversible regions. An equation is given for the temperature dependence of the potential at which the transition from ideally polarisable to ideally reversible behaviour occurs.

REFERENCES

(For refs. 1–21 see Part 1[42])

22 R. R. DOGONADZE AND YU. A. CHIZMADZHEV, *Proc. Acad. Sci., USSR, Phys. Chem. Sect. English Transl.*, 157 (1964) 778.
23 A. I. SOTNIKOV AND O. A. ESIN in *Physical Chemistry and Electrochemistry of Molten Salts and Slags* (Proceedings 3rd All-Soviet Conference, May 1966), Khimiya, Leningrad, 1968, pp. 209–214.
24 N. G. BUKUN AND E. A. UKSHE, in *Physical Chemistry and Electrochemistry of Molten Salts and Slags* (Proceedings 3rd All-Soviet Conference, May 1966), Khimiya, Leningrad, 1968, pp. 214–223.
25 O. A. ESIN, *Zh. Fiz. Khim.*, 30 (1956) 3.
26 A. D. GRAVES, G. J. HILLS AND D. INMAN, in P. DELAHAY (Ed.), *Advan. Electrochem. Electrochem. Eng.*, 4 (1966) 117.
27 A. D. GRAVES AND D. INMAN in C. B. ALCOCK (Ed.), *E.m.f. Measurements in High Temperature Systems* (Proceedings of a Symposium held by the Nuffield Research Group, Imperial College, London, April 1967), Institute of Mining and Metallurgy, London, 1968, pp. 183–197; A. D. GRAVES, Ph.D. Thesis, University of London, 1967.
28 R. H. HEUS, T. TIDWELL AND J. J. EGAN, in G. MAMANTOV (Ed.), *Molten Salts: Characterisation and Analysis*, Marcel Dekker, New York, 1969.
29 G. J. HILLS AND P. D. POWER, *Trans. Faraday Soc.*, 64 (1968) 1629; P. D. POWER, Ph.D. Thesis, University of Southampton, 1966.
30 V. SH. PALANKER, A. M. SKUNDIN AND V. S. BAGOTSKII, *Sov. Electrochem.*, 2 (1966) 592.
31 R. A. ALEKSEEVA, V. A. KUZNETSOV AND M. I. TALANOVA, *Sov. Electrochem.*, 4 (1968) 182.
32 R. A. ALEKSEEVA AND V. A. KUZNETSOV, *Sov. Electrochem.*, 4 (1968) 1214.
33 M. A. V. DEVANATHAN AND B. V. K. S. R. A. TILAK, *Chem. Rev.*, 65 (1965) 635.
34 E. A. UKSHE AND I. V. TOMSKIKH, *Proc. Acad. Sci., USSR, Phys. Chem. Sect. English Transl.*, 150 (1963) 416.
35 A. N. FRUMKIN, B. B. DAMASKIN AND YU. A. CHIZMADZHEV, *Sov. Electrochem.*, 2 (1966) 813.
36 D. M. MOHILNER, *J. Phys. Chem.*, 66 (1962) 724.
37 P. DELAHAY, *J. Phys. Chem.*, 70 (1966) 2373.
38 M. SLUYTERS-REHBACH AND J. H. SLUYTERS, *Rec. Trav. Chim.*, 83 (1963) 967.
39 N. G. BUKUN AND E. A. UKSHE, *J. Appl. Chem. USSR English Transl.*, 36 (1963) 1907.
40 E. A. UKSHE AND N. G. BUKUN, *Russ. J. Phys. Chem. English Transl.*, 37 (1963) 890.
41 E. A. UKSHE, N. G. BUKUN AND D. I. LEIKIS, *Bull. Acad. Sci. USSR, Div. Chem. Sci. English Transl.*, 1 (1963) 25.
42 A. D. GRAVES, *J. Electroanal. Chem.*, 25 (1970) 349.
43 E. A. UKSHE AND N. G. BUKUN, *Russ. J. Inorg. Chem. English Transl.*, 10 (1965) 393.
44 D. INMAN, D. G. LOVERING AND R. NARAYAN, *Trans. Faraday Soc.*, 64 (1968) 2487.

45 J. A. PLAMBECK, *J. Chem. Eng. Data*, 12 (1967) 77.
46 E. A. UKSHE, N. G. BUKUN AND D. I. LEIKIS, *Russ. J. Phys. Chem. English Transl.*, 36 (1962) 1260.
47 YU. K. DELIMARSKII AND V. S. KIKHNO, *Ukr. Khim. Zh.*, 35 (1969) 468.
48 R. YU. BEK AND A. S. LIFSHITS, *Siberian Chem. J.*, 6 (1967) 713.
49 R. YU. BEK AND A. S. LIFSHITS, *Siberian Chem. J.*, 5 (1968) 485, 489.
50 A. S. LIFSHITS AND R. YU. BEK, *Izv. Sibirsk. Otd. Akad. Nauk SSSR, Ser. Khim. Nauk*, 4(2) (1969) 161.
51 R. YU. BEK AND A. S. LIFSHITS, *Sov. Electrochem.*, 3 (1967) 658.
52 M. SLUYTERS-REHBACH AND J. H. SLUYTERS, *Rec. Trav. Chim.*, 82 (1963) 525.

ELECTROANALYTICAL CHEMISTRY AND INTERFACIAL ELECTROCHEMISTRY
Elsevier Sequoia S.A., Lausanne – Printed in The Netherlands

ELECTROCHEMICAL STUDIES OF THE EU(III)/(II) REACTION BY CONVENTIONAL AND KALOUSEK POLAROGRAPHY

W. FRANK KINARD* AND ROBERT H. PHILP, JR.
Department of Chemistry, University of South Carolina, Columbia, South Carolina 29208 (U.S.A.)
(Received December 5th, 1968)

INTRODUCTION

The Eu(III)/(II) electrochemical reaction at the dropping mercury electrode (DME) has been the subject of a large number of investigations. Comprehensive studies have been reported by Misumi and Ide[1], Vleck[2], Gierst and Cornelissen[3], and by Macero and co-workers[4]. The interest in this system stems primarily from the facts that europium is the only lanthanide that exhibits a relatively stable oxidation state of $+2$ in aqueous solution and that the E^0 value of this system is very near the point of zero charge at mercury in the absence of specific adsorption.

It has been generally found that the reduction of Eu(III) at the DME is polarographically irreversible in most supporting electrolytes except thiocyanate in which it appears diffusion controlled[3]. The cathodic wave is relatively unaffected by the nature of the supporting electrolyte.

The rate of the Eu(III) reduction in various concentrations of $NaClO_4$ has been treated theoretically and good quantitative agreement with double layer theory has been demonstrated[3].

An unstable Eu(II) intermediate of different electronic configuration from the final product has been postulated and the activation overpotential associated with the electrochemical reaction has been attributed to a shielding effect by the 5*s* and 5*p* electrons[2].

The purposes of this study were twofold. The first was to elucidate further the effect of supporting electrolyte on the reaction, particularly in view of recent data on the stability and nature of Eu(III) complexes[4,5]. The second was to employ this reaction to systematically investigate the utility of Kalousek Type I (K-I) and Type II (K-II) polarography in the investigations of systems showing variable electrode kinetics. The analytical applications and the theory of the Kalousek methods for reversible systems have recently been reviewed[6]. Europium appeared to be an excellent model system for this purpose, exhibiting behavior that ranges from totally irreversible to reversible with respect to these techniques, depending upon the supporting electrolyte.

---

* Present address: Department of Chemistry, Florida State University, Tallahassee, Florida 32306 (U.S.A.).

EXPERIMENTAL

The europium solutions were obtained from stock solution prepared by dissolving 99.9% europic oxide (Trona) in concentrated $HClO_4$. Supporting electrolytes were reagent grade sodium salts of the appropriate anions. The pH was adjusted to 2 in each case with $HClO_4$. No maximum suppressors were employed.

A standard three-electrode polarographic cell was employed with bridges consisting of agar saturated with NaCl. The isolated electrode was a gold foil about 8 cm^2 in area. The reference electrode was the saturated sodium calomel electrode (SSCE) rather than the saturated calomel electrode (SCE) as perchlorate solutions were used extensively in this study. Laitinen and Subcasky report the potential of the SSCE to be about 5 mV negative of the SCE[7]. The capillary characteristics of the DME employed were $t = 4.12$ s and $m = 2.08$ mg s^{-1} in 1 M $NaClO_4$ at -0.6 V *vs.* SSCE.

Both conventional and Kalousek polarograms were obtained using the multipurpose instrument previously described[6,8]. In the conventional mode the current recorded is that at the end of the drop life. In the K-I mode the amplitude of the square wave is 50 mV. The half period of the square wave in both K-I and K-II was 0.085 s. The curves were plotted using a Moseley-7035B X-Y recorder.

RESULTS AND DISCUSSION

Conventional polarograms

Conventional polarograms of the Eu(III) reduction in 1 M solutions of various supporting electrolytes are shown in Fig. 1. The half wave potentials were in good agreement with those values reported by Vlcek for comparable media[2]. It is noteworthy that the waves appear to fall into two distinct groups. The less negative group includes only anions that have been shown to form weak outer sphere complexes with Eu(III)[5]. Sulfate forms an inner sphere complex and it is highly likely that acetate does also by analogy with other carboxylate anions which have been shown to form inner sphere complexes[5]. This correlation also extends to the fluoride system which forms an inner sphere complex and which is reported to have an $E_{\frac{1}{2}}$ of -1.05 V *vs.* SCE[2].

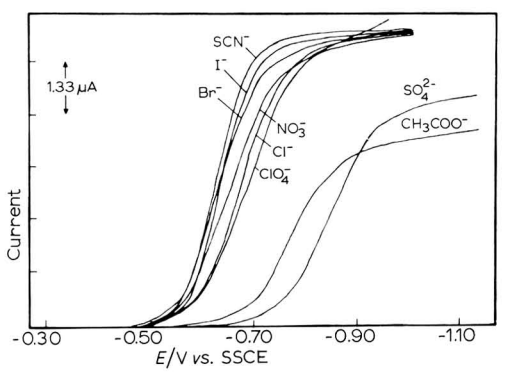

Fig. 1. Conventional polarograms of 1.75×10^{-3} M Eu(III) in 1 M concn. of various supporting electrolytes.

The temperature coefficients of half wave potentials and limiting currents were measured in a number of cases in order to test for kinetic complications. For the Cl^- and Br^- systems the temperature coefficient of the limiting current was found to be 1.6 % deg^{-1} and for the SO_4^{2-} system 1.3 % deg^{-1}, in good agreement with the theoretical estimate of 1.3 % deg^{-1} for a diffusion controlled process[9]. The temperature coefficients of the half wave potentials of the Cl^-, Br^- and SO_4^{2-} systems were of the order of 3 mV deg^{-1} again indicating absence of kinetic complications.

The polarograms of all of the outer sphere group go to essentially the same limiting current, indicating similarity of reduction mechanism within the group. The diffusion coefficient calculated from the average limiting current of the group is 8.6×10^{-6} cm^2 s^{-1} in fairly good agreement with values reported by Timmer *et al*[10]. The diffusion currents in the case of SO_4^{2-} and OAc^- are considerably smaller.

Within the group forming outer sphere complexes, the shift between the most positive and most negative is only about 50 mV and the order of half wave potentials does not appear to correlate with relative stability of the complexes. As will be shown below, with the exception of SCN^-, all of the waves are irreversible to varying degrees and no simple relation between complex stability and half wave potential is expected.

Since the reduction in the presence of SCN^- is reversible it is of interest to consider the significance of the $E_{\frac{1}{2}}$ values. The $E_{\frac{1}{2}}$ value in 1 *M* SCN^- is -0.640 V *vs.* SCE. The best value for the standard formal potential, E^0, of the Eu(III)/(II) system appears to be -0.600 to -0.605 V *vs.* SCE[3,4,10]. The correction term for ratios of $D^{\frac{1}{2}}$ values is 5 mV based on the diffusion coefficient values of Timmer *et al.*[10]. If equality of activity coefficients is assumed and difference in junction potentials neglected one can write for 1 *M* SCN^- the relation:

$$(E_{\frac{1}{2}})_c - (E_{\frac{1}{2}})_s = 0.05915 \log (K_{ox}/K_{red})$$

where K_{ox} and K_{red} are overall dissociation constants for the oxidized and reduced forms of the complex. Based on our data we estimate a ratio $(K_{ox}/K_{red}) = 0.21$ in line with the expected greater stability of the oxidized form of the complex.

Kalousek polarograms

Figures 2 and 3 show K-I and K-II polarograms in the same supporting electrolytes as Fig. 1. Among the outer sphere group the change in kinetics is readily

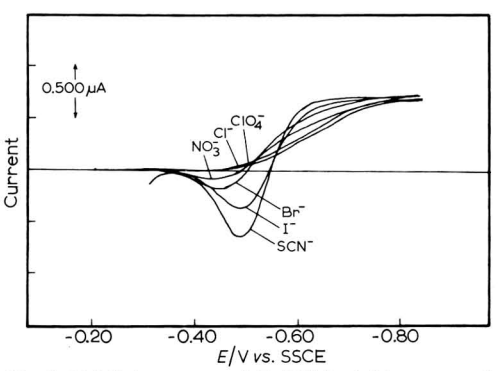

Fig. 2. K-I Polarograms of Eu(III) in 1 *M* concns. of various supporting electrolytes. Actual electrode potential is 50 mV negative of indicated value.

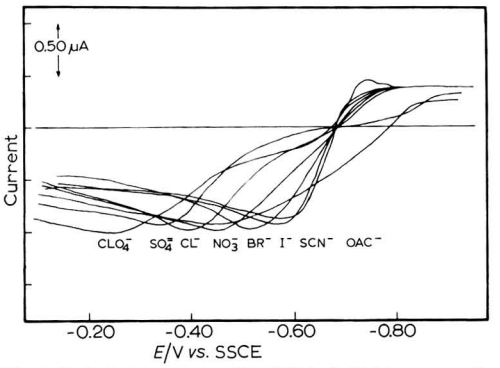

Fig. 3. K-II Polarograms of Eu(III) in 0.10 *M* concns. of various supporting electrolytes.

apparent in the K-I curves as an increase in the anodic peak current ($i_{K\text{-}I}$) and in the K-II curves as a movement toward merged anodic and cathodic branches. The reversibility increases in the order, $ClO_4^- < Cl^- < NO_3^- < Br^- < I^- < SCN^-$. With the exception of interchange of positions of SCN^- and I^- this is the order of increasing specific adsorption at the mercury electrode[11].

In the case of SCN^- the reaction has reached mass transfer control as evidenced by all classical criteria with respect to the d.c. polarograms and by the fact the K-I curve for Eu(III) is identical to the K-I curve of Tl(I) which is reversible under these conditions.

It thus appears that the change of rate is a result of increased facility toward oxidation of the Eu^{2+} and can be correlated with the decreasing positive charge at the electrode surface due to specific adsorption of anions. Complexation appears to have little effect.

Effects of added thiocyanate

The behavior of this sytem can be further elucidated by observation of Eu(II) oxidation *via* K-II curves in the presence of small concentrations of thiocyanate. Figure 4 shows the effect of added thiocyanate on K-II curves in 0.10 *M* Cl^- and Br^-.

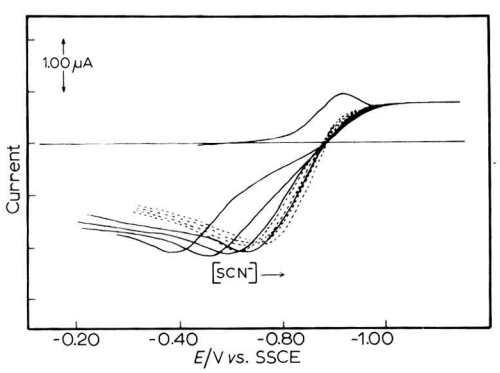

Fig. 4. Effect of added SCN^- on K-H Polarograms of Eu(III) in 0.10 *M* Cl^- (——) and Br^- (– – –). The SCN^- concn. is varied between 0 and 0.01 *M*. A conventional curve in Cl^- is shown for comparison.

The relatively greater effect in the case of chloride, which exhibits a more positive electrocapillary maximum is noteworthy. In the presence of SCN^- concentration of only 0.01 *M* both curves have taken on essentially a reversible morphology.

Effects of variation in ionic strength

Figure 5 shows a series of K-II curves of Eu(III) in various concentrations of $NaClO_4$. The similarity between these curves and the conventional current potential

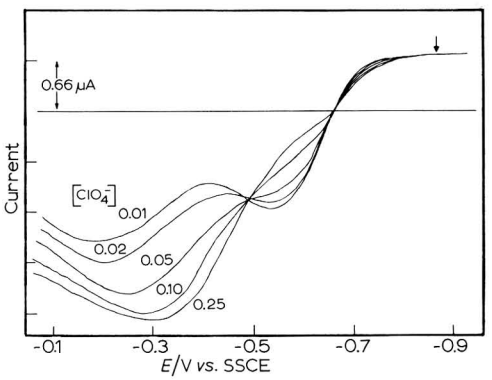

Fig. 5. K-II Polarograms of Eu(III) as a function of $NaClO_4$ concn. Auxiliary potential is indicated by arrow.

curves shown by Gierst[3] is striking. The point of convergence of the anodic branches agrees, within measurement uncertainty, with that shown by Gierst (*i.e.* −0.48 V *vs.* NCE) and corresponds to the accepted best value of the electrocapillary maximum in the absence of specific adsorption.

In perchlorate and in most other media in concentrations of supporting electrolyte less than about 0.1 *M* a sharp maximum was noted on the d.c. polarogram. Whenever a maximum was present on the conventional polarogram the anodic branch of the K-II curve was characterized by having the appearance of a double wave. As the medium was changed (*e.g.* ionic strength increased) to the point that the maximum disappeared, the inflection on the anodic K-II curve disappeared.

Vlcek attributed a double K-II wave to the formation of an unstable Eu(II) intermediate of different electronic configuration than that of the final form. In view of the strong correlation between the appearance of maximum and the inflection on the K-II curve we feel that, at least in perchlorate, its origin must be in double layer effects rather than in an unstable intermediate.

Kinetic parameters

The kinetic parameters (α, the cathodic transfer coefficient and k_{sh}, the rate constant at the standard formal potential) were calculated for the reaction in 1.0 *M* ClO_4^- by the method of Koutecky[12] as modified by Meites and Israel[13]. In making this calculation a computer program was employed and the calculation was based on 60 data points along the rising portion of the polarogram. Values of k_{sh} of 0.3×10^{-4} cm s^{-1} ($E^{0\prime} = -0.600$ V *vs.* SCE) and α of 0.7 ± 0.1 were obtained in fairly good agreement values reported in perchlorate media of[10] $k_{sh} = 2.9 \times 10^{-4}$ cm s^{-1}, $\alpha = 0.41$ and[3] $k_{sh} = 0.72 \times 10^{-4}$ cm s^{-1}, $\alpha = 0.66$. Our measured value would not be expected

to be very accurate in view of the fact that the K-II polarogram clearly shows partial overlap of anodic and cathodic waves and the method of calculation is based on assuming negligible back reaction. In fact the K-II curve provides a rapid and convenient method for determining whether the kinetics of a system may be treated by this method.

The only theoretical treatment of Kalousek polarography in cases where the rate of the electrode process has been taken into account has been that of Matsuda[14]. While this treatment for the Type I experiment refers to average current during a complete cycle and is valid only for $\Delta E \ll (RT/\alpha nF)$ the qualitative agreement between the curves in Fig. 2 and calculated curves shown by Matsuda is quite good. Based on the ratio of anodic peak current to cathodic limiting current one would estimate values of k_{sh} for the system in Br^- and I^- at around 10^{-3}–10^{-2} cm s^{-1}. A value of 1.6×10^{-3} cm s^{-1} in I^- has been reported by Randles and Somerton[15] from faradiac impedance measurements. Considerable caution must be exercised in estimating rate constants from these curves as the form of the curve depends both upon the rate constant and the transfer coefficient.

ACKNOWLEDGEMENT

The authors wish to thank R. C. Propst for assistance in instrument design and for helpful discussions.

A grant from the Faculty Research Committee of the University of South Carolina is gratefully acknowledged.

SUMMARY

The Eu(III)/(II) reaction was studied by conventional and by Type I and Type II Kalousek polarography in a number of media. Reduction waves appear to fall into two groups depending upon whether inner or outer sphere complexes are formed between Eu(III) and the anion of the supporting electrolyte.

The reversibility as evidenced by K-I and K-II curves increases in order of supporting electrolytes as $ClO_4^- < Cl^- < NO_3^- < Br^- < I^- < SCN^-$ and appears to correlate only with decreasing charge at the electrode surface due to increased specific adsorption of the anions.

The double anodic wave observed at low ionic strength in perchlorate is consistent with previous studies of the system and appears to have its origin in double layer effects rather than in an intermediate in the reduction. The utility of Type I and II Kalousek polarography in the study of irreversible processes is demonstrated.

REFERENCES

1 S. MISUMI AND Y. IDE, *Bull. Chem. Soc. Japan*, 32 (1959) 1159.
2 A. A. VLCEK, *Collection Czech. Chem. Commun.*, 24 (1959) 181.
3 L. GIERST AND P. CORNELISSEN, *Collection Czech. Chem. Commun.*, 25 (1960) 3004; L. GIERST in E. YEAGER (Ed.), *Transactions of the Symposium on Electrode Processes*, Wiley, New York, 1961.
4 D. J. MACERO, L. B. ANDERSON AND P. MALACHESKY, *J. Electroanal. Chem.*, 10 (1965) 76; D. J. MACERO, H. B. HERMAN AND A. J. DUKAT, *Anal. Chem.*, 37 (1965) 675.
5 G. R. CHOPPIN AND P. J. UNREIN, *J. Inorg. Nucl. Chem.*, 25 (1963) 387; G. R. CHOPPIN AND W. F.

STRAZIK, *Inorg. Chem.*, 4 (1965) 1250; G. R. CHOPPIN AND A. J. GRAFFEO, *Inorg. Chem.*, 4 (1965) 1254; G. R. CHOPPIN AND J. KETELS, *J. Inorg. Nucl. Chem.*, 27 (1965) 1335.
6 W. F. KINARD, R. H. PHILP AND R. C. PROPST, *Anal. Chem.*, 39 (1967) 1556.
7 H. A. LAITINEN AND W. J. SUBCASKY, *J. Am. Chem. Soc.*, 80 (1958) 2623.
8 R. C. PROPST, *U.S. At. Energy Comm. Report*, DP-903 (1964).
9 L. MEITES, *Polarographic Techniques*, Interscience, New York, 2nd edn., 1965, p. 138.
10 B. TIMMER, M. SLUYTERS-REHBACH AND J. H. SLUYTERS, *J. Electroanal. Chem.*, 14 (1967) 181.
11 D. C. GRAHAME, *Chem. Rev.*, 41 (1947) 441.
12 J. KOUTECKY, *Collection Czech. Chem. Commun.*, 18 (1953) 597.
13 L. MEITES AND Y. ISRAEL, *J. Am. Chem. Soc.*, 83 (1961) 4903.
14 H. MATSUDA, *Z. Elektrochem.*, 62 (1958) 977.
15 J. E. B. RANDLES AND K. W. SOMERTON, *Trans. Faraday Soc.*, 43 (1952) 937.

ELECTROANALYTICAL CHEMISTRY AND INTERFACIAL ELECTROCHEMISTRY
Elsevier Sequoia S.A., Lausanne – Printed in The Netherlands

POLAROGRAPHIC REDUCTION OF HEXAQUO-, ISOTHIOCYANATO- AND AZIDO-CHROMIUM(III) IONS ON A DROPPING MERCURY ELECTRODE IN AQUEOUS ACID PERCHLORATE SOLUTION

H. YAMAOKA
Chemistry Department A, Technical University of Denmark, Lyngby (Denmark)
(Received October 2nd, 1969; in revised form November 22nd, 1969)

1. INTRODUCTION

The primary object of the present investigation was to see how the rate and mechanism of the heterogeneous charge-transfer step of the overall one-electron polarographic reduction in aqueous acid perchlorate solution

$$Cr(III) + e^- \rightarrow Cr(II)$$

is affected, when one or two water molecules in $[Cr(H_2O)_6]^{3+}$ are substituted by a simple inorganic ligand X. Cr(III) thus stands for $[Cr(H_2O)_6]^{3+}$, $[Cr(H_2O)_5X]^{2+}$ or $[Cr(H_2O)_4X_2]^{+}$, while the final form of Cr(II) in aqueous acid perchlorate solution, in any case, would be $[Cr(H_2O)_6]^{2+}$ due to the substitution-lability of chromium(II) species. $X = SCN^-$ and N_3^- were tried, as the reduction of Cr(III) complexes of these ligands by Cr(II) in homogeneous solution is known[1,2], and thus can provide a basis for a comparison between rates of homogeneous and heterogeneous electron transfer.

$[Cr(H_2O)_6]^{3+}$ and some of its mono- and disubstituted derivatives in aqueous acid perchlorate solution are reduced (d.c.-) polarographically "totally irreversibly"[3,4]. The half-wave potential $E_{\frac{1}{2}\mathrm{irr}}$ of a totally irreversible d.c. polarographic wave is given approximately by[5]:

$$E_{\frac{1}{2}\mathrm{irr}} = E^0 + \frac{2.303\,RT}{\alpha nF} \log 0.886\, k_s \left(\frac{\tau}{D}\right)^{\frac{1}{2}} \qquad (2)$$

where E^0 is the standard potential of the half-cell reaction in question, k_s the heterogeneous charge-transfer rate constant at E^0, α the transfer coefficient of the forward (cathodic) reaction, τ the drop life time, D the diffusion coefficient of the depolarizer (assumed to be the same for the oxidized and reduced form), n the number of electrons transferred in the rate-determining step, and R, T and F have their usual meaning. Equation (2) implies that $E_{\frac{1}{2}\mathrm{irr}}$ for a series of compounds can be quantitatively correlated to k_s, only if the thermodynamic quantity E^0 is known for each member of the series*. This is not the case for the half-cell reactions (1), however** (*cf.* refs. 8, 40 and 7).

* A knowledge of D and α is also required. D can easily be determined from the observed value of the limiting diffusion current i_d, while α can be obtained from the d.c. polarographic log-plot, provided that the double-layer effect is either negligible or can be corrected for.

** Even for Cr^{3+}/Cr^{2+}, E^0 is not exactly known. Most text books of analytical, inorganic or physical chemistry quote the E^0-value of -0.41 V (hydrogen scale at 25°C) for Cr^{3+}/Cr^{2+} by Grube and Breitinger[6]. This value is unreliable. A recent work[4] did not make any effort to replace this value.

To overcome this difficulty, rather than to make the arbitrary assumption that E^0 is constant throughout a series of related compounds[8], a.c.[9] and Kalousek[10] polarography were applied together with conventional d.c. polarography in the present investigation. The advantage of the relaxation methods over the d.c. method is that the a.c. peak current (or wave height) and the Kalousek polarographic anodic peak current do not depend explicitly on E^0 (*cf.* ref. 11, Abb. 4 and 5)*. They depend, however, explicitly on k_s (and α). This means that when dealing with an irreversible electrode process where the backward reaction is negligible, one may for a while neglect the question of the unknown E^0 value. Comparison of the relative values of k_s for the forward reaction is feasible by measuring the a.c. wave height or the Kalousek polarographic anodic peak current for a series of related compounds**.

2. EXPERIMENTAL

2.1. *Reagents*

Doubly distilled water was used throughout. All chemicals used were of analytical grade and were not further purified.

Commercial $[Cr(H_2O)_6](ClO_4)_3$ (K.E.K.Lab., N.Y.) was used. Other Cr(III) species were prepared and separated on a Dowex 50 W cation exchange resin in the hydrogen form[12-15] and identified by their visible and u.v. adsorption spectra (Fig. 1). The SCN^- : Cr and N_3^- : Cr ratios were determined analytically[12-15] and found to be 1.00 ± 0.02 for $[Cr(H_2O)_5NCS]^{2+}$, 2.00 ± 0.04 for *cis*- and *trans*-$[Cr(H_2O)_4(NCS)_2]^+$, 1.00 ± 0.03 for $[Cr(H_2O)_5N_3]^{2+}$ and 2.10 ± 0.05 for *trans*-$[Cr(H_2O)_4(N_3)_2]^+$.

All chromium(III) stock solutions prepared by the use of the ion-exchange technique were stored in a refrigerator at about $-5°C$ in the dark, where the aquation process as well as possible photochemical effects[7] are suppressed. Spectroscopic control could not reveal any appreciable change in composition of the stock solutions after storage for half a year.

2.2. *Apparatus*

For the d.c. measurements, a Radiometer Polariter PO 4 was used. To increase the accuracy of the logarithmic plots, the potential scale was expanded to $5\ mV\ cm^{-1}$ by means of a calibrated potential scale expander, based on the operational amplifier principle.

Circuit diagrams for the a.c. and Kalousek polarographic attachments are shown in Figs. 2 and 3. A detailed description of the former is given elsewhere[16]. The device was not equipped with a phase-sensitive rectifier and thus responds to an overall a.c. current. Simple faradaic impedance measurements[9,17] were carried out after a slight modification of the circuit of Fig. 2. The functional feature of the Kalousek polarographic attachement corresponds to the "circuit III" of ref. 18, p. 479. All

---

* In Matsuda's treatment[11], only the oxidized form of the reactants is assumed to be initially present in the solution (*cf.* ref. 28). This matches with the experimental condition of the present work.

** Matsuda's treatment[11] does not take into account the specific and non-specific adsorption of the reactants. Therefore, the statement above is only qualitative in such a case. In respect to the limited resolution power of the measuring device used in the present work, it is not profitable to employ more rigorous treatments (*cf.* ref. 42).

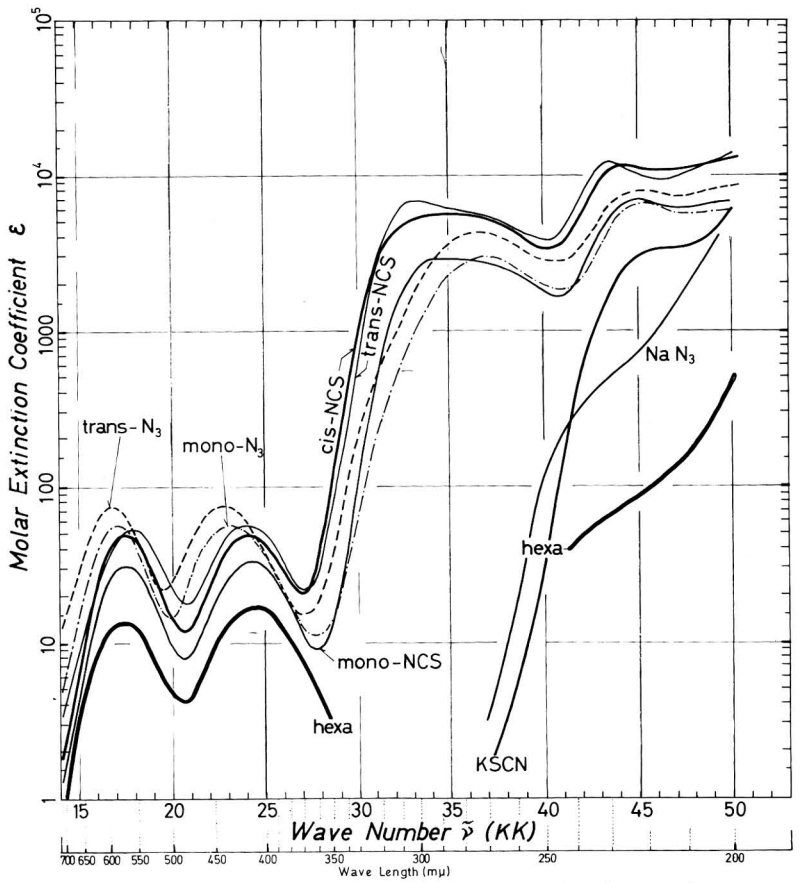

Fig. 1. Spectra of chromium(III) species and alkali pseudohalides in aq. soln. at room temp.

	Visible	*U.v.*
hexa	$[Cr(H_2O_6]^{3+}$ alone	in 0.020 *M* $HClO_4$ + 0.480 *M* $NaClO_4$
mono-NCS	$[Cr(H_2O)_5NCS]^{2+}$ in 1 *M* $HClO_4$	in 0.01 *M* $HClO_4$
trans-NCS	*trans*-$[Cr(H_2O)_4(NCS)_2]^+$ in 0.1 *M* $HClO_4$	in 0.001 *M* $HClO_4$
cis-NCS	*cis*-$[Cr(H_2O)_4(NCS)_2]^+$ in 0.1 *M* $HClO_4$	in 0.001 *M* $HClO_4$
mono-N_3	$[Cr(H_2O)_5N_3]^{2+}$ in 1 *M* $HClO_4$	in 0.04 *M* $HClO_4$
trans-N_3	*trans*-$[Cr(H_2O)_4(N_3)_2]^+$ in 0.1 *M* $HClO_4$	in 0.004 *M* $HClO_4$
KNCS	—	KNCS alone
NaN_3	—	NaN_3 alone
$NaClO_4$	—	very weak absorption in the u.v. range

polarograms were recorded with the minimum damping available (response time 2.25 s for 99 % of full scale deflection) and those shown are plots of points halfway between the maximum and the minimum on the rising part of each current oscillation, caused by the periodical drop growth and fall[19].

An ordinary thermometer capillary, Radiometer B 405 was used. In an aqueous N_2-saturated solution, 0.020 *M* and 0.480 *M* with respect to $HClO_4$ and $NaClO_4$, and

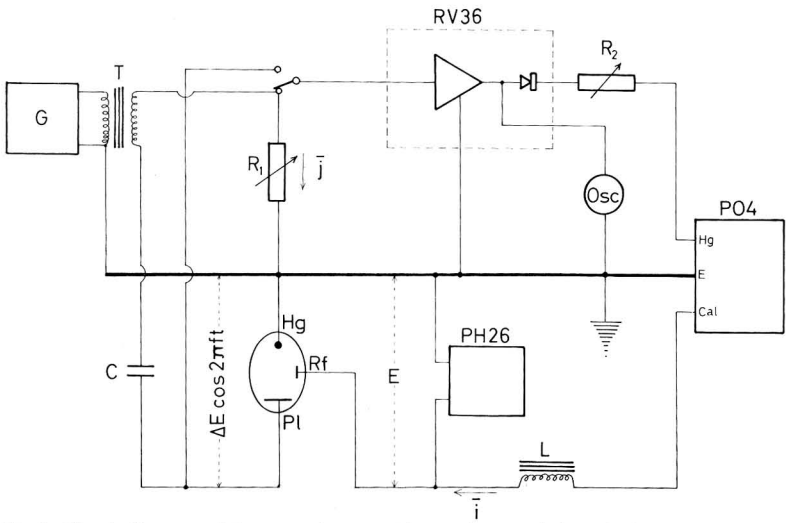

Fig. 2. Circuit diagram of the a.c. polarographic attachment: (G) audio-frequency generator, (T) step-down transformer, (R) series resistors (10 ~ 100 Ω), (C) d.c. blocking capacitor (2000 μF), (RV36) Radiometer a.c. millivoltmeter with external d.c. and a.c. output terminals, (R_2) series resistor (~ 3 MΩ), (Osc) oscilloscope, (PO4) conventional d.c. polarograph (recorder), (L) a.c. blocking choke coil (1 kΩ, 100 H), (PH26) Radiometer pH-meter (d.c. millivoltmeter), (Hg) dropping mercury electrode, (Rf) reference electrode, (Pl) mercury pool electrode, (E) d.c. cell voltage, ($\Delta E \cos 2\pi ft$) a.c. cell voltage, (i) d.c. polarographic current, (j) a.c. polarographic current.

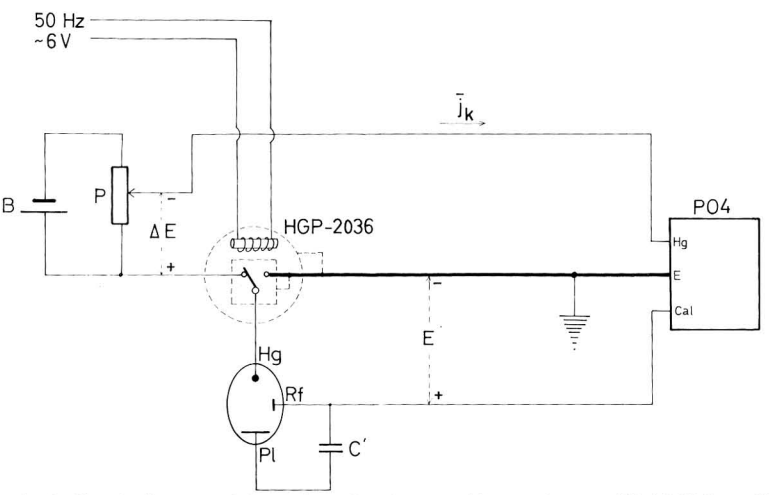

Fig. 3. Circuit diagram of the Kalousek polarographic attachment: (B) 1.5 V dry cell, (P) potentiometer, (HGP-2036) Clare mercury wetted relay (break-before-make type), (C') shunt capacitor (4000 μF), (ΔE) square wave voltage amplitude, (j_k) Kalousek polarographic current; the other symbols are defined as in Fig. 2.

using a potential of −0.600 V *vs.* SCE and an effective Hg-column height of 39.6 cm (corrected for back-pressure), the mercury flow rate m and the drop life time τ were found to be 2.550 mg s^{-1} and 4.06 s respectively. No artificial drop life or blanking timer was used.

An all-glass H-shaped electrolysis cell was used. Nitrogen was purified for O_2 by BTS Katalysator (BASF, Ludwigshafen). A saturated calomel electrode with mercury surface area of about 7 cm^2 was used as reference electrode. Towards the end of a drop life time, the ohmic resistances between the DME and the reference electrode or the mercury pool electrode (surface area about 12 cm^2) were typically 600 and 90 Ω, respectively, of which that of the capillary was 31 Ω. The d.c. potential scale E was corrected for the ohmic drop including that of the blocking choke L in Fig. 2.

All polarographic measurements were carried out at 25.0 ± 0.1°C and an ionic strength $\mu = 0.50$. Test solutions except for those of $[Cr(H_2O)_6]^{3+}$ were prepared immediately before use. As a tenfold increase in $[H^+]$ for a constant μ and [Cr(III)] did not change the d.c. polarographic waves, no particular effort was taken to keep the acidities constant. No maximum suppressor was added unless stated. Measurements usually lasted for several hours during which only a negligible amount of aquation could have taken place[7].

3. RESULTS

3.1. *D.c. polarographic measurements*

The d.c. polarograms of the chromium(III) compounds are shown in Figs. 4, a and 5, a. The polarogram of thallium(I) ion is also shown as a typical example of a one-electron reversible electrode reaction[20,21]. Drop life time (natural) is shown as a function of the applied d.c. potential at a fixed mercury column height (see Figs. 4, b and 5, b).

Substitution of water ligand molecules by SCN^- caused shifts of the (irreversible) half-wave potential $E_{\frac{1}{2}irr}$ in a positive direction, increasing in the order: $[Cr(H_2O)_6]^{3+} < [Cr(H_2O)_5NCS]^{2+} <$ *trans*-$[Cr(H_2O)_4(NCS)_2]^+ <$ *cis*-$[Cr(H_2O)_4(NCS)_2]^+$. The d.c. polarograms of $[Cr(H_2O)_5N_3]^{2+}$ and *trans*-$[Cr(H_2O)_4(N_3)_2]^+$ were both virtually the same as those of $[Cr(H_2O)_6]^{3+}$.

The limiting diffusion current i_d for a given chromium(III) concentration was about the same for all chromium(III) species studied, the diffusion coefficients were all about 1×10^{-5} cm^2 s^{-1}. Plots of i_d *versus* the square root of the corrected Hg-column height gave straight lines through the origin, showing that no slow chemical reaction precedes the heterogeneous charge-transfer reaction.

A remarkable d.c. polarographic maximum was observed with $0.5 \sim 1$ m*M* *cis*-$[Cr(H_2O)_4(NCS)_2]^+$. This might be attributed to a polarographic maximum of the first kind[18], since addition of a trace of a surface active substance (1×10^{-5} % Triton X-100) removed it almost completely. On the corresponding a.c. polarogram this was reflected in some 18 % decrease of the wave height (not shown in Fig. 4, b).

3.2. *A.c. polarographic measurements*

For the isothiocyanato-chromium(III) species, a shift in the summit potential E_s is observed, corresponding to the change of $E_{\frac{1}{2}irr}$ (*cf.* Fig. 4, a and b). The a.c. wave height $(j)_s$ increases in the order: $[Cr(H_2O)_5NCS]^{2+} <$ *trans*-$[Cr(H_2O)_4(NCS)_2]^+ <$ *cis*-$[Cr(H_2O)_4(NCS)_2]^+ \ll Tl^+$. The a.c. polarograms of the azido-chromium(III) species were both virtually the same as that of $[Cr(H_2O)_6]^{3+}$ (Fig. 5, b).

Within experimental accuracy, no a.c. base current depression[9] was detected in the whole d.c. potential range and in the frequency range between 40 and 160 Hz.

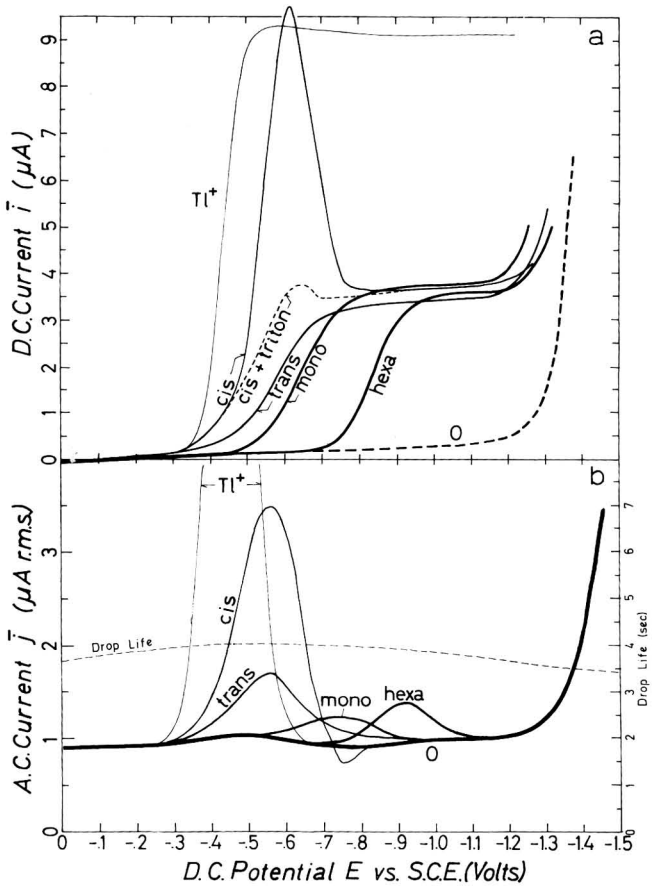

Fig. 4. D.c. (a) and a.c. (b) polarograms of isothiocyanato-chromium(III) species.

0	0.020 *M* $HClO_4$ + 0.480 *M* $NaClO_4$
hexa	1.00 m*M* $[Cr(H_2O)_6]^3$ + 0.020 *M* $HClO_4$ + 0.480 *M* $NaClO_4$
mono	1.00 m*M* $[Cr(H_2O)_5NCS]^{2+}$ + 0.094 *M* $HClO_4$ + 0.406 *M* $NaClO_4$
trans	1.00 m*M* *trans*-$[Cr(H_2O)_4(NCS)_2]^+$ + 0.042 *M* $HClO_4$ + 0.458 *M* $NaClO_4$
cis	1.00 m*M* *cis*-$[Cr(H_2O)_4(NCS)_2]^+$ + 0.027 *M* $HClO_4$ + 0.473 *M* $NaClO_4$
cis + Triton	as above + 1×10^{-5}% Triton X-100
Tl	1.00 m*M* $TlNO_3$ + 0.020 *M* $HClO_4$ + 0.480 *M* $NaClO_4$

Measured at a constant mercury column height $h_{corr} = 39.6$ cm; $\Delta E = 10$ mV r.m.s.; $f = 40$ Hz; 25°C; nitrogen-satd.; drop life time measured with the supporting electrolyte 0 alone.

Preliminary faradaic impedance measurements indicated that $(j)_s$ was mainly of a resistive nature (except for Tl^+). The a.c. waves for all chromium(III) species were therefore not typical "tensammetric waves"[9].

3.3. *Kalousek polarographic measurements*

None of the chromium(III) species studied gave a Kalousek polarographic anodic peak current $(j_k)_p$, while Tl^+ did, as expected (Fig. 6).

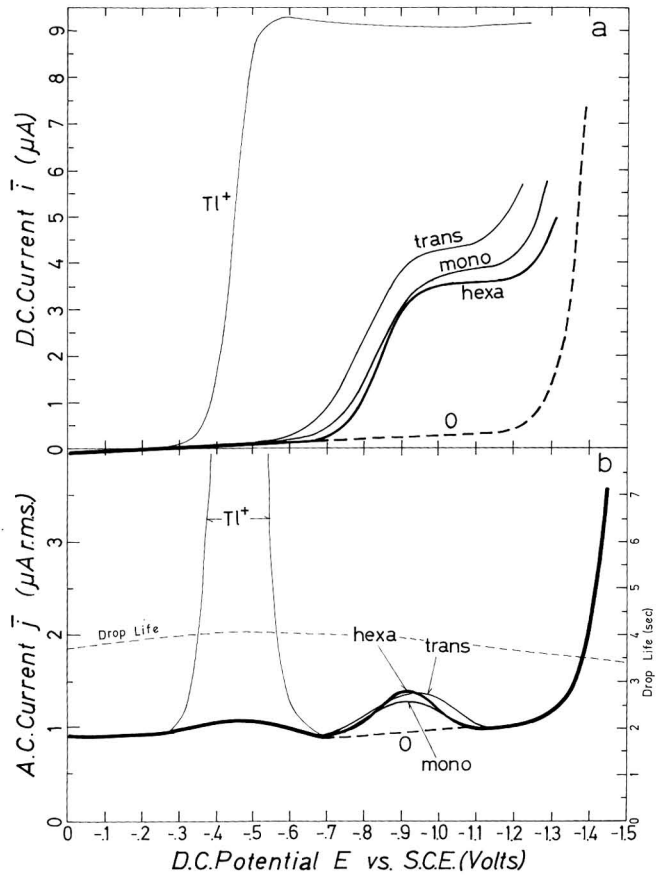

Fig. 5. D.c. (a) and a.c. (b) polarograms of azido-chromium(III) species.

0	see Fig. 4, a and b
hexa	
mono	1.00 m*M* $[Cr(H_2O)_5N_3]^{2+}$ + 0.180 *M* $HClO_4$ + 0.320 *M* $NaClO_4$
trans	1.00 m*M* *trans*-$[Cr(H_2O)_4(N_3)_2]^+$ + 0.090 *M* $HClO_4$ + 0.410 *M* $NaClO_4$

Otherwise same working conditions as in Fig. 4, a and b.

4. FURTHER TREATMENT OF RESULTS

4.1. *D.c. polarograms*

Literature values of the outer Helmholtz layer potential ϕ_2 on mercury in perchlorate solutions are shown in Fig. 7. The ϕ_2-values of Asada *et al.*[22] in the presence of 1 m*M* Ga^{3+} in 0.4 *M* $NaClO_4$ are nearly the same as those of Parsons and Passeron[4], calculated from the data of Wroblowa *et al.*[23]. These ϕ_2-values will be used for the double-layer corrections, calculated below. The calculations by the present author for 0.3 and 1 *M* $NaClO_4$ agree with those of Elliott and Buchanan[24] on the data of ref. 23, but, for 0.1 *M* $NaClO_4$, they differ from those of Asada *et al.*[22], presumably due to the interference of the 1 m*M* Ga^{3+}.

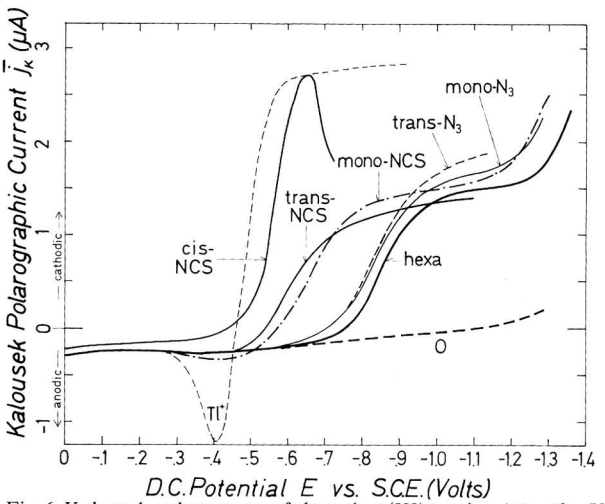

Fig. 6. Kalousek polarograms of chromium(III) species. $\Delta E = 10$ mV; $f = 50$ Hz; otherwise same conditions as in the preceding diagrams.

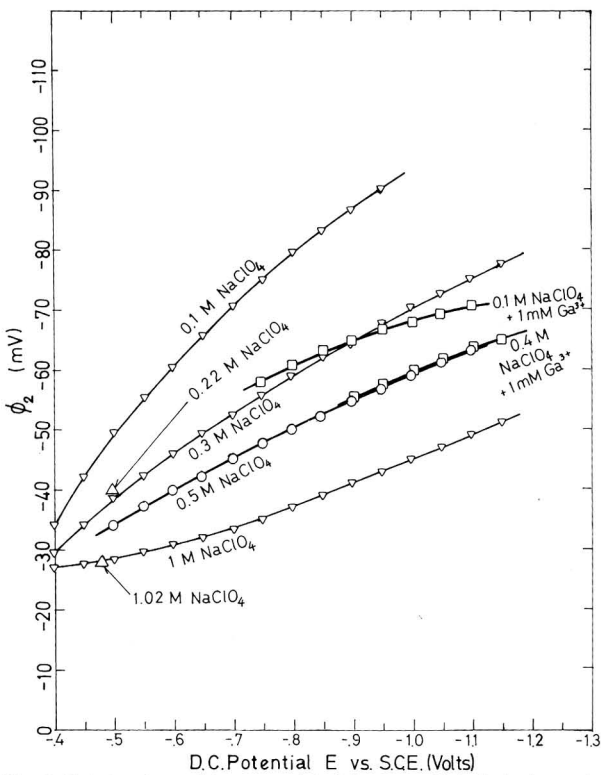

Fig. 7. Existing data of the potential of the outer Helmholtz layer ϕ_2 on mercury in aq. sodium perchlorate solns: (□) exptl. values of Asada *et al.*[22], (○) calcd. values of Parsons and Passeron based on data of Wroblowa *et al.*[23], (△) calculation of Elliott and Buchanan from the same source, (▽) calculation of present author from the same source.

D.c. polarograms recorded at low scanning rates were plotted to fit the Oldham and Parry[25] formulae for a totally irreversible d.c. polarographic wave, taking into account the movement of the solution caused by the expansion of the mercury drop:

$$E_{\frac{1}{2}\mathrm{irr}} - E = \frac{0.0592}{\alpha n} \log \left\{ \frac{\chi(5.5-\chi)}{5(1-\chi)} \right\} \text{ (in volts at 25°C)} \tag{3}$$

α is the cathodic transfer coefficient, uncorrected for the double-layer effect, n is 1 for a one-electron process and χ is the ratio between the (averaged) current i at potential E and the (averaged) limiting diffusion current i_d. Differentiation gives the Tafel-slope b:

$$b = -\frac{0.0592}{\alpha n} = \partial E / \partial \log \left\{ \frac{\chi(5.5-\chi)}{5(1-\chi)} \right\} \tag{4}$$

b' and α', uncorrected for the spherical expansion of the mercury drop is given by:

$$b' = -\frac{0.0592}{\alpha' n} = \partial E / \partial \{\log i/(i_d - i)\} \tag{5}$$

The relation between d.c. current density i and d.c. potential E for a first-order electrode process involving a single rate-determining step for which the backward reaction can be neglected, is:

$$i = i_t^0 \exp \left\{ \frac{(\alpha_t n - z)F}{RT} \phi_2 \right\} \exp \left\{ -\frac{\alpha_t n F}{RT} (E - E^0) \right\} \tag{6}$$

where i_t^0 is the (true) exchange current density corrected for ϕ_2 at the equilibrium potential E^0, and z the average value of the charge of the depolarizer in the bulk of the solution[22,26]. Equation (6) is valid in the absence of specific adsorption of the depolarizer. Taking the natural logarithm of both sides of eqn. (6) and replacing ln i by the mass-transfer corrected term of eqn. (3) gives:

$$\log \left\{ \frac{\chi(5.5-\chi)}{5(1-\chi)} \right\} + \frac{zF}{2.303\,RT} \phi_2 = \log i_t^0 + \frac{\alpha_t n F}{2.303\,RT} E^0 - \frac{\alpha_t n F}{2.303\,RT} (E - \phi_2) \tag{7}$$

from which the Tafel-slope b_t corrected for ϕ_2 is found to be:

$$b_t = -\frac{0.0592}{\alpha_t n} = \partial (E - \phi_2) / \partial \left[\log \left\{ \frac{\chi(5.5-\chi)}{5(1-\chi)} \right\} + \frac{z\phi_2}{0.0592} \right] \tag{8}$$

Results of calculated b_t-values, using the ϕ_2-values of Fig. 7, are shown in Fig. 8 for all chromium(III) species studied, except for *cis*-$[Cr(H_2O)_4(NCS)_2]^+$. In Table 1, α, α' and α_t, determined graphically from eqns. (4), (5) and (8), are summarized. Deviations from linearity were not detected over a reasonably wide d.c. potential range, contrary to the observations of Elving and Zemel[3] and of Parsons and Passeron[4].

Owing to surface tension effects, the surface area of the mercury drop towards the end of a drop life decreases by some 3% when the d.c. potential is changed from -0.5 to -1.0 V *vs.* SCE at a constant Hg-column height. However, this factor which is not included in eqns. (4), (5) and (8) has only a negligible influence on the log-plots.

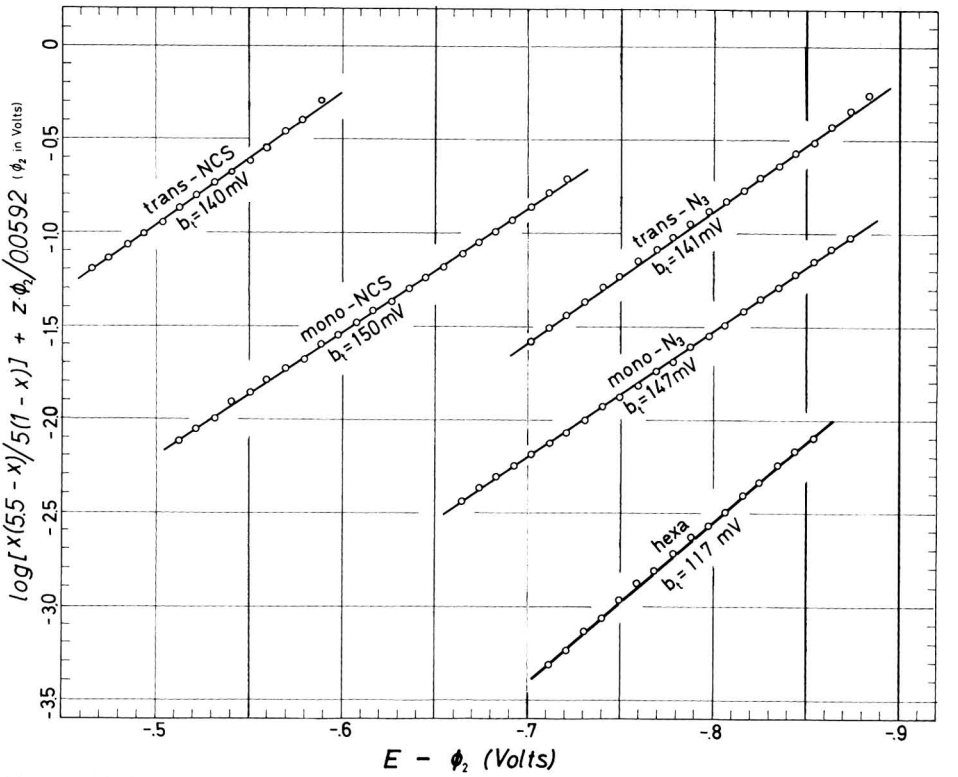

Fig. 8. Tafel-plots corrected for the outer Helmholtz layer potential ϕ_2. See working conditions in Figs. 4 and 5, a. $z = +3$ for hexa, $z = +2$ for mono- and $z = +1$ for trans-di. See also footnote in Table 1.

TABLE 1

TAFEL-SLOPES AND TRANSFER COEFFICIENTS OF THE CATHODIC REDUCTION OF CHROMIUM(III) SPECIES ON DME IN AQUEOUS ACID PERCHLORATE SOLUTION

Cf. experimental conditions in Figs. 4,a and 5,a; also see Fig. 8

Depolarizer	*Both ϕ_2- and Hg-expansion-uncorrected*		*ϕ_2-Uncorrected; Hg-expansion-corrected*		*Both ϕ_2- and Hg-expansion-corrected*	
	$-b'/mV$	α'	$-b/mV$	α	$-b_t/mV$	α_t
$[Cr(H_2O)_6]^{3+}$	90	0.65	95	0.62	117	0.51
$[Cr(H_2O)_5NCS]^{2+}$	117	0.51	128	0.46	150[a]	0.39[a]
trans-$[Cr(H_2O)_4(NCS)_2]^{+}$	117	0.51	126	0.47	140[a]	0.42[a]
$[Cr(H_2O)_5N_3]^{2+}$	118	0.50	123	0.48	147[a]	0.40[a]
trans-$[Cr(H_2O)_4(N_3)_2]^{+}$	129	0.46	133	0.45	141[a]	0.42[a]

[a] Justification for applying the same double-layer correction for the isothiocyanato- and azido-chromium-(III) species as for $[Cr(H_2O)_6]^{3+}$ is not quite established since they might undergo specific adsorption on the mercury surface (*cf.* Discussion). Table 1 and Fig. 8 are shown rather for the sake of completeness to indicate the results of all calculations according to the respective formula.

4.2. *A.c. polarograms*

Since the apparatus had no phase-sensitive rectifier, and the contribution of a.c. base current was not negligible, a direct comparison of the experimental data with Matsuda's diagram (Abb. 5, ref. 11) is not profitable. Also, the blocking effect of the choke coil L may be insufficient at the frequency $f = 40$ Hz, when compared with the high impedance of the cell in which irreversible electrode reactions take place. It can, however, be assumed that the observed trend in the a.c. wave height is correct.

An estimation of the reversibility of electrode reactions was proposed by Senda *et al.*[27]:

$$K' = n \cdot K \cdot \tau^{\frac{1}{2}} = (j)_s/i_d \tag{9}$$

K' is a semi-quantitative measure of the reversibility for a series of electrode reactions when the a.c. wave height $(j)_s$ is measured at a relatively low frequency (*e.g.* commercial line frequency). K is a constant which depends on the characteristics of the apparatus. Table 2 shows the calculated values of K'.

TABLE 2

SEMI-QUANTITATIVE MEASURE K' OF THE REVERSIBILITY OF THE CATHODIC REDUCTION OF CHROMIUM(III) SPECIES ACCORDING TO SENDA *et al.*[27]

Cf. experimental conditions in Figs. 4, a and b, and 5, a and b.

Depolarizer	*D.c. limiting current* $i_d/\mu A$	*A.c. peak current* $(j)_s/\mu A$ *r.m.s.*	$K' = (j)_s/i_d$	*Literature value* $k_s/cm\ s^{-1}$
$[Cr(H_2O_6]^{3+}$	3.2	0.43	0.14	$10^{-5.15}$ (Parsons and Passeron[4])
$[Cr(H_2O)_5NCS]^{2+}$	3.3	0.33	0.10	—
trans-$[Cr(H_2O)_4(N_3)_2]^+$	3.7	0.34	0.10	—
trans-$[Cr(H_2O)_4(NCS)_2]^+$	3.0	0.71	0.24	—
cis-$[Cr(H_2O)_4(NCS)_2]^+$	3.3	2.5	0.76	—
Tl^+	9.1	11.7	1.29	1.2 (Barker *et al.*[20])

The apparent higher $(j)_s$ of $[Cr(H_2O)_6]^{3+}$ compared to $[Cr(H_2O)_5NCS]^{2+}$ might be corrected for by a higher depolarizer enrichment at the ϕ_2 potential plane for the former, because of its higher positive charge and the more negative value of E_s. The corrected $(j)_s$ would presumably be about the same for $[Cr(H_2O)_6]^{3+}$ and $[Cr(H_2O)_5NCS]^{2+}$. The same correction, however, would not change the order of reversibility among $[Cr(H_2O)_5NCS]^{2+}$, *trans*- and *cis*-$[Cr(H_2O)_4(NCS)_2]^+$.

Equation (9) was derived, using a reversible electrode process as a reference[27]. Consequently it is not valid when k_s is small compared with the applied frequency f. It has been shown recently[28,29], that a finite, measurable a.c. polarographic wave, independent of k_s is in fact expected for utterly irreversible electrode processes. Comparison of the observed $(j)_s$-values in the present investigation with calculated data for the high frequency limit[29] suggests that the $(j)_s$-values of $[Cr(H_2O)_6]^{3+}$, $[Cr(H_2O)_5NCS]^{2+}$, $[Cr(H_2O)_5N_3]^{2+}$ and *trans*-$[Cr(H_2O)_4(N_3)_2]^+$ might be close to this limit, while the $(j)_s$-values of *trans*-$[Cr(H_2O)_4(NCS)_2]^+$ and especially of *cis*-$[Cr(H_2O)_4(NCS)_2]^+$ are far from this limit.

The a.c. measurements then indicate that the heterogeneous rate constant k_s for the reduction (the forward reaction) of the chromium(III) species increases in the order: $[Cr(H_2O)_6]^{3+} \simeq [Cr(H_2O)_5NCS]^{2+} \simeq [Cr(H_2O)_5N_3]^{2+} \simeq$ *trans*-$[Cr(H_2O)_4(N_3)_2]^{+} <$ *trans*-$[Cr(H_2O)_4(NCS)_2]^{+} <$ *cis*-$[Cr(H_2O)_4(NCS)_2]^{+}$, while the results do not justify a more detailed kinetic analysis.

4.3. *Kalousek polarograms*

The Kalousek polarographic current j_k for a sufficiently small amplitude ΔE of superimposed square wave voltage is given by[11]:

$$j_k = \tfrac{1}{2}(i - j_1) \tag{10}$$

where i is the conventional d.c. polarographic current and j_1 the a.c. current components resulting from the superimposed square wave voltage ΔE.

In the Kalousek polarograms recorded, the values of the parameters f (square wave frequency) = 50 Hz, and $\tau = 4$ s were chosen, while the results of the d.c. polarographic measurements justify putting $D \simeq 1 \times 10^{-5}$ cm^2 s^{-1}, and $\alpha \simeq 0.5$ for all chromium(III). The parameter values are then identical with Matsuda's numerical values[11], and as they are the only quantities determining the curve characteristics of the j_1 *vs.* E plots, a comparison of the data with Matsuda's diagram (Abb. 4, ref. 11) could predict the order of magnitude of k_s. As, however, Kalousek polarographic anodic peak currents are entirely absent for all chromium(III) species studied, the k_s-values for the forward reaction can not exceed 1×10^{-3} cm s^{-1}*.

The d.c. potential range in which the Kalousek anodic peaks either appeared or were expected to appear, is apparently very close to the e.c.m. (*cf.* drop life time curve); double-layer corrections were not considered in this section.

5. DISCUSSION

The results show that the azido-chromium(III) species and the hexaquo-chromium(III) ion behave almost identically, regardless of the polarographic technique applied. However, for the isothiocyanato-chromium(III) species, a pronounced increase in k_s is observed. To account for this and for the observed trend in the various isothiocyanato-chromium(III) species, the following mechanism is proposed:

(I) The isothiocyanato-chromium(III) species are first specifically adsorbed with the sulphur end attached to the mercury electrode surface (Fig. 9, a).

(II) After a reorganization[30,31] of the ligand and solvent sphere, the electron is transferred from the electrode to chromium(III) *via* the thiocyanate bridge (Fig. 9, b and c).

(III) The chromium(II), the primary product of the electrode process, is desorbed from the electrode surface, possibly with a change of coordination number from 6 to 5. It then undergoes a ligand substitution outside the Helmholtz layer and is transformed to $(Cr(H_2O)_6]^{2+}$ (Fig. 9, d).

(IV) The nitrogen end of the coordinated N_3^--ligand has a weaker affinity to

* The $(j_k)_p$-value observed for Tl^+ (see Fig. 6) is apparently too small compared with the literature value of $k_s = 1.2$ cm s^{-1} (*cf.* ref. 20). The discrepancy was due to an appreciable series ohmic resistance of the capillary and the electrolyte (see Section 2.2).

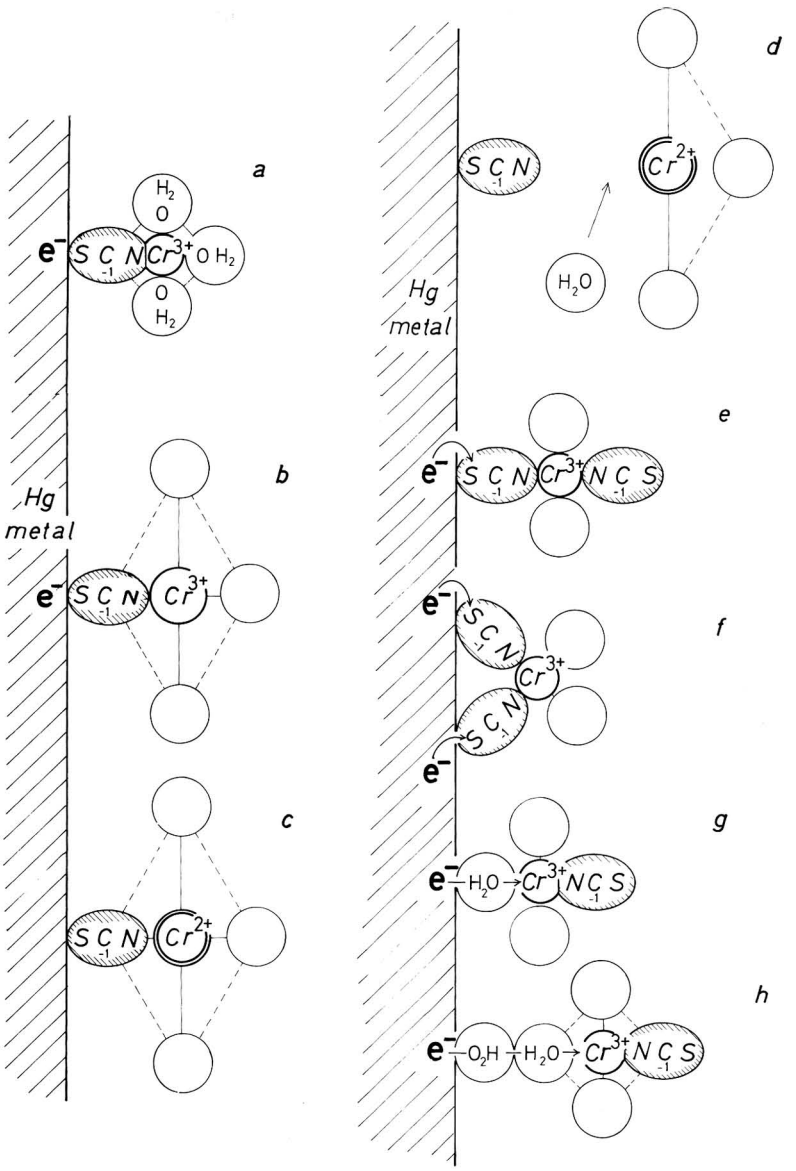

Fig. 9. Hypothetical model of the electrode process of the isothiocyanato-chromium(III) species on the mercury electrode surface: (a) Specific adsorption of $[Cr(H_2O)_5NCS]^{2+}$ with its sulphur end attached to the mercury surface, (b) configurational reorganization of the depolarizer ion prior to electron transfer (bond-stretching as example), (c) formation of the primary product of the electrode process, (d) desorption of the primary product in a 5-coordinated form and its aquation outside the Helmholtz layer, (e) *trans*-$[Cr(H_2O)_4(NCS)_2]^+$, single-bridged specific adsorption, (f) *cis*-$[Cr(H_2O)_4(NCS)_2]^+$, double-bridged specific adsorption, (g) $[Cr(H_2O)_5NCS]^{2+}$ at the inner Helmholtz plane: water-bridged, (h) $[Cr(H_2O)_5NCS]^{2+}$ at the outer Helmholtz plane: no specific adsorption.

the mercury surface than the sulphur end of the SCN^--ligand. The inner-sphere mechanism of step (II) is therefore not so effective for the azido-chromium(III) species*.

Many halide or pseudo-halide anions are known to be capillary-active on the mercury surface, and their ability to undergo specific adsorption on mercury is estimated to increase in the order: $Cl^- < Br^- < NCS^- < I^- < S^{2-}$ [32,33]. Apparently no data are available for N_3^-*. The possibility of specific adsorption of the isothiocyanate ligand with its sulphur end attached to the mercury surface has been purely hypothetically suggested[34] in connection with the anodic oxidation of $[Cr(H_2O)_6]^{2+}$ on the mercury surface in the presence of free thiocyanate anions. Also, the conduction effect of the ligand bridge has been suggested to account partly for the increased rate constant of homogeneous inner-sphere reactions[35] as well as for reactions of the hydrated electron[36].

The model has features in common with that proposed recently by Watanabe *et al.*[37] for the redox system $[Cr(H_2O)_5Br]^{2+}/[Cr(H_2O)_6]^{2+}$ on a DME in the presence of Br^-. Also, the reverse of the steps Fig. 9, a, b, c and d corresponds to the mechanism suggested recently by Ulrich and Anson[38] for the anodic oxidation of $[Cr(H_2O)_6]^{2+}$ on a DME in the presence of Cl^-, Br^- and I^-**.

The probability of *trans*-$[Cr(H_2O)_4(NCS)_2]^+$ being specifically adsorbed to the mercury surface through one of its two thiocyanate ligands is approximately twice as large as that of $[Cr(H_2O)_5NCS]^{2+}$ if the thermal agitation of the solvent is the same (Fig. 9, e). It would therefore be natural to observe an increase in the rate compared with $[Cr(H_2O)_5NCS]^{2+}$. *cis*-$[Cr(H_2O)_4(NCS)_2]^+$ might be thought capable of being adsorbed simultaneously by its two sulphur ends, thus providing a double bridged transition state (Fig. 9, f)***. An analogous example of this is known in the homogeneous redox-kinetics[14].

Adsorption states different from that of Fig. 9, a are illustrated in Fig. 9, g and h. The situation h would probably give rise to faradaic impedance spectra of the

---

* Shortly after the submission of the present work, the author had access to some unpublished N_3^--adsorption data by Dr. R. Parsons, Bristol (personal communication from Dr. Parsons, and a quotation in ref. 43). N_3^- was found to be adsorbed on Hg to about the same extent as Br^-. However, at -1.0 V *vs.* SCE the absorption is negligibly small[43]. This potential is in the range where the a.c. polarographic waves of the azido-chromium(III) species appear (*cf.* Fig. 5, b).

Watanabe *et al.*[37] reported the half-wave potential of -0.29 V for 0.2 m*M* $CrBr^{2+}$ in 2 *M* $HClO_4$ in the absence of free Br^-. It is remarkable that coordinated Br^- causes such a drastic positive shift of $E_{\frac{1}{2}}$, whereas N_3^- does not change $E_{\frac{1}{2}}$ appreciably. This suggests that the adsorbability of the uncoordinated anions does not alone account for the observed trend in the kinetic behaviour of the substituted Cr(III) complexes. The adsorbability of the anions may not be retained uninfluenced when coordinated to the central metal ion.

The present author thanks Dr. Parsons and Professor Anson for the information.

** An essential difference between the working conditions of the present work and theirs is the negligible amount of the uncoordinated ligand in the supporting electrolyte. In the presence of an appreciable amount of the free ligand, the overall reversibility of the redox-system might increase. This may, however, be due mainly to the enhancement of the backward reaction (anodic oxidation) which is a second-order reaction in $[Cr^{2+}]$ and θ_x (surface coverage of uncoordinated ligand X on Hg). The forward reaction should therefore necessarily proceed on the uncovered sites $(1-\theta_x)$ and consequently not be affected by the presence of the adsorbed X. The primary object of the present work was, as stated, to treat the forward reaction proceeding on the mercury surface free from adsorbed ligand X.

*** This agrees with a model suggested in a private communication from Professor Anson, California Inst. Techn., Passadena, to whom the present author is indebted for access to unpublished material.

normal Randles' circuit as is expected for $[Cr(H_2O)_6]^{3+}$. The situation g seems rather unlikely since the oxygen end of the hydrated water molecules is not available for direct interaction with the mercury surface[39].

The difference observed in the polarographic behaviour of the isothiocyanato- and azido-chromium(III) species seems to disagree with the prediction[8,40] that the position of the lowest energy *d–d* band of a series of transition metal compounds is closely correlated with their electrochemical charge transfer rate constant (*cf.* Fig. 1). The observed spectra of the chromium(III) species in the ultraviolet range did not differ essentially from each other, except for $[Cr(H_2O)_6]^{3+}$. This fact also makes a correlation between the charge-transfer spectra[41] and kinetic parameters difficult.

ACKNOWLEDGEMENT

The author wishes to express his thanks to mag. scient. J. Ulstrup of this institute for innumerable advices and criticism.

SUMMARY

Results are reported for the irreversible electrochemical reduction of Cr(III) to Cr(II) at a DME in aqueous acid perchlorate medium, investigated by d.c., a.c. and Kalousek polarography. The rate constant of the forward reaction has been found to increase in the order: $[Cr(H_2O)_6]^{3+} \simeq [Cr(H_2O)_5NCS]^{2+} \simeq [Cr(H_2O)_5N_3]^{2+} \simeq$ *trans*-$[Cr(H_2O)_4(N_3)_2]^+ <$ *trans*-$[Cr(H_2O)_4(NCS)_2]^+ <$ *cis*-$[Cr(H_2O)_4(NCS)_2]^+$. No clear correlation was observed between the rate constant of the forward reaction and the electronic spectrum of a given species, and it was concluded that the electrochemical reduction of Cr(III) is not necessarily governed by the same factors as the homogeneous reduction by Cr(II). For the reduction of the isothiocyanato complexes, a mechanism is suggested involving a bridged transition state in which the sulphur end points towards the mercury surface.

REFERENCES

1 D. L. BALL AND E. L. KING, *J. Am. Chem. Soc.*, 80 (1958) 1091.
2 A. ANDERSON AND N. A. BONNER, *J. Am. Chem. Soc.*, 76 (1954) 3826.
3 P. J. ELVING AND B. ZEMEL, *Can. J. Chem.*, 37 (1959) 247.
4 R. PARSONS AND E. PASSERON, *J. Electroanal. Chem.*, 12 (1966) 524.
5 R. BRDIČKA, *Collection Czech. Chem. Commun.*, 19 (1954) Suppl. II, 41.
6 G. GRUBE AND G. BREITINGER, *Z. Elektrochem.*, 33 (1927) 112.
7 F. BASOLO AND R. G. PEARSON, *Mechanisms of Inorganic Reactions*, J. Wiley, New York, 2nd edn. 1967.
8 A. A. VLČEK, *Electrochim. Acta*, 13 (1968) 1063.
9 B. BREYER AND H. H. BAUER, *Alternating Current Polarography and Tensammetry*, Interscience Publishers, New York, 1963.
10 M. KALOUSEK, *Collection Czech. Chem. Commun.*, 13 (1948) 105.
11 H. MATSUDA, *Z. Elektrochem.*, 62 (1958) 977.
12 E. L. KING AND E. B. DISMUKES, *J. Am. Chem. Soc.*, 74 (1952) 1674.
13 J. T. HOUGEN, K. SCHUG AND E. L. KING, *J. Am. Chem. Soc.*, 79 (1957) 519.
14 R. SNELLGROVE AND E. L. KING, *J. Am. Chem. Soc.*, 84 (1962) 4609.
15 T. W. SWADDLE AND E. L. KING, *Inorg. Chem.*, 3 (1964) 234.
16 H. YAMAOKA, *Acta Chem. Scand.*, 21 (1967) 2559.
17 H. H. BAUER AND P. J. ELVING, *Anal. Chem.*, 30 (1958) 334.

18 J. HEYROVSKÝ AND J. KŮTA, *Principles of Polarography*, Academic Press, New York, 1966.
19 L. MEITES, *Polarographic Techniques*, Interscience Publishers, New York, 2nd edn., 1965, p. 200.
20 G. C. BARKER, R. L. FAIRCLOTH AND A. W. GARDNER, *Nature*, 181 (1958) 247.
21 M. SLUYTERS-REHBACH, B. TIMMER AND J. H. SLUYTERS, *Rec. Trav. Chim.*, 82 (1963) 553.
22 K. ASADA, P. DELAHAY AND A. K. SUNDARAM, *J. Am. Chem. Soc.*, 83 (1961) 3396.
23 H. WROBLOWA, Z. KOVAC AND J. O'M. BOCKRIS, *Trans. Faraday Soc.*, 61 (1965) 1523.
24 D. ELLIOTT AND G. S. BUCHANAN, *Anal. Chem.*, 39 (1967) 1245.
25 K. B. OLDHAM AND E. P. PARRY, *Anal. Chem.*, 40 (1968) 65.
26 P. DELAHAY, *Double Layer and Electrode Kinetics*, Interscience Publishers, New York, 1965, p. 158.
27 M. SENDA, M. SENDA AND I. TACHI, *J. Electrochem. Soc. Japan*, 27 (1959) 83.
28 B. TIMMER, M. SLUYTERS-REHBACH AND J. H. SLUYTERS, *J. Electroanal. Chem.*, 14 (1967) 169, 181.
29 D. E. SMITH AND T. G. MCCORD, *Anal. Chem.*, 40 (1968) 476.
30 R. A. MARCUS in E. YEAGER (Ed.), *Transactions of the Symposium on Electrode Processes*, J. Wiley, New York, 1961, p. 239.
31 R. A. MARCUS, *Electrochim Acta*, 13 (1968) 995.
32 N. K. ADAM, *The Physics and Chemistry of Surfaces*, Oxford University Press London, 3rd edn., 1941.
33 D. C. GRAHAME, *Chem. Rev.*, 41 (1947) 441.
34 N. SUTIN, *Electrochim. Acta*, 13 (1968) 1175.
35 H. TAUBE, *J. Chem. Educ.*, 45 (1968) 452.
36 M. ANBAR, *Quart. Rev. London*, 22 (1968) 578.
37 I. WATANABE, E. ITABASHI AND S. IKEDA, *Inorg. Chem.*, 7 (1968) 1920.
38 J. J. ULRICH AND F. C. ANSON, *Inorg. Chem.*, 8 (1969) 195.
39 H. GERISCHER, *Angew. Chem.*, 68 (1956) 20.
40 A. A. VLČEK, *Discussions Faraday Soc.*, 26 (1958) 164.
41 H. L. SCHLÄFER, *Z. Phys. Chem., N.F.*, 3 (1955) 222; 263.
42 M. SLUYTERS-REHBACH, B. TIMMER AND J. H. SLUYTERS, *J. Electroanal. Chem.*, 19 (1968) 305 and references cited therein.
43 Z. KOWALSKI AND F. C. ANSON, *J. Electrochem. Soc.*, 116 (1969) 1208.

ELECTROANALYTICAL CHEMISTRY AND INTERFACIAL ELECTROCHEMISTRY
Elsevier Sequoia S.A., Lausanne – Printed in The Netherlands

POLAROGRAPHY OF OLEFIN–MERCURY(II) ACETATE ADDITION COMPOUNDS

B. FLEET AND R. D. JEE

Chemistry Department, Imperial College of Science and Technology, London, S.W.7. (Great Britain)

(Received November 25th, 1969)

The polarography of organo-mercury(II) compounds of the type RHgX has been widely studied due to their importance as pharmaceuticals and fungicides. Many of the papers published are analytical in nature with little or no mechanistic details[1-14]. Although the mechanism of reduction has been extensively studied[15-33] during the past twenty years, the literature still contains many conflicting statements concerning reversibility and adsorption effects.

Olefins react with mercury(II) acetate in methanol to give compounds of the type RCH(OMe)–CH(HgOAc)R′, according to the equation:

$$RCH{=}CHR' + Hg(OAc)_2 + MeOH \rightarrow RCH(OMe){-}CH(HgOAc)R' + H^+$$

Although the chemical properties of these compounds have been comprehensively reviewed by Chatt[34], there are virtually no studies of the mechanism of the electroreduction. As a consequence the present investigation was carried out.

Electrochemical reduction of organo-mercury(II) compounds can be traced to the work of Kraus[35], who electrolysed liquid ammonia solutions of alkyl mercury-(II) halides and found that the product $RHg^{\bullet}$ dimerized to R_2Hg at room temperature. Sullam[36] in an investigation of ethene mercury(II) salts observed that the organic mercury differed polarographically from that of inorganic mercury. In the work of Costa[15] which has been largely overlooked, various alkyl mercury(II) salts were examined. Two polarographic waves were observed, which from the wave shape were concluded to be irreversible,

$$R{-}Hg^+ + e \rightarrow R{-}Hg^{\bullet}$$

$$R{-}Hg^{\bullet} + H^+ + e \rightarrow R{-}H + Hg$$

Vojir[16,17] and Benesch and Benesch[18,19] studied the reduction of phenyl mercury(II) salts. The little quoted work of Vojir observed the first wave to be reversible from a.c. oscillopolarographic measurements. Benesch and Benesch, however, whose work is generally quoted in analytical papers which refer to the reduction mechanism, considered the first wave irreversible as a consequence of its shape and $E_{\frac{1}{2}}$–pH dependence above pH 7. The half-wave potential of the second wave was found to show a marked pH dependence up to approximately pH 8, though it was independent of pH above this value. Hush and Oldham[24] studied a large range of compounds and from the wave shape concluded the first wave to be reversible; the wave was also independent of pH. In very alkaline solutions αn values indicated reversibility for the second wave. Butin *et al.*[28] point out that the Heyrovský-Ilkovic

equation does not apply to a system where dimerization of the product occurs, but is described by the equation due to Hanus[37]. Using this equation he considers the first wave to be reversible.

Morris *et al.*[38] used cyclic voltammetry to study the tetraphenylstibonium ion ($Ph_4Sb^+ --- Hg + e \rightarrow Ph_3Sb + PhHg^\bullet$) using a sweep rate of 0.05 Hz, but observed no anodic peak. However, Chantal and Etienne[31] observe an anodic peak corresponding to the oxidation of the pyridyl-3-mercury radical, but only at fast scan rates (37 V s^{-1}), indicating a lifetime of only a few hundreths of a second for the radical. Dessy *et al.*[26] who considered the first wave to be electrochemically irreversible also observed an anodic current and assigned it to the reaction, $X^- + Hg \rightarrow HgX + e$.

Prewaves to the first wave have been observed and ascribed to adsorption of the radical[19,31,32]. Broman and Murray[25], however, reached a different conclusion in a chronopotentiometric study of phenylmercury(II) nitrate. They showed that both the product and reactant were adsorbed, although the adsorption of the reactant was slow. From their experimental evidence they assigned the prewave to the adsorption of reactant.

EXPERIMENTAL

Apparatus

A Radelkis polarograph type OH-102 (Metrimpex, Hungary) and a Kalousek cell with a saturated calomel electrode (SCE) as reference was used for recording the polarograms. The capillary constants measured at the potential of the SCE in 0.1 *M* potassium chloride solution were $m = 1.65$ mg s^{-1}, $t = 3.34$ s at $h = 55$ cm.

Cyclic voltammograms were obtained on a "Chemtrix" polarograph (Chemtrix Inc., Beavertron, Oregon, U.S.A.). The instrument was used in its three electrode mode, the working electrode was a hanging mercury drop electrode (HMDE) type E410 (Metrohm, Ltd., Switzerland), the counter electrode a silver wire, while a SCE was used as the reference.

Microcoulometric measurements were carried out in a H-type cell[39]. Controlled potential coulometry for *n* values (number of electrons consumed per molecule) and isolation of products were carried out at a mercury pool electrode (area 10 cm^2). A solid state potentiostat[40] and integrator based on a voltage to frequency converter[41] constructed from a GEC circuit[42] was used. The output pulses were counted on a Harwell 2117B scaler.

Materials

With the exception of 2,5-dimethyl-1,5-hexadiene, the compounds (Table 2) were used without further purification. The latter was of "practical" quality and redistilled before use. Samples of ethene and propene were provided by I.C.I. Plastics Division.

Buffers

pH 2.1, sulphuric acid; pH 3.65, formic acid/sodium formate; pH 4–7, acetic acid/sodium acetate; pH 7–9 phosphate; pH 9–10.1, borate; pH 11–12.5, phosphate and pH 12.9, sodium hydroxide. Where possible the buffer concentration in the solutions polarographed was 0.1 *M*.

Preparation of olefin–mercury(II) acetate compounds

Stock solutions 10^{-1} or 10^{-2} *M* were prepared by weighing out stoichiometric quantities of olefin and mercury(II) acetate (nitrate) and dissolving in methanol, finally diluting with methanol to the required volume. The solutions were allowed to stand for the time indicated in Table 2 before use to allow the olefin and mercury(II) salt to react. In the case of 4-methyl-1-pentene, N-vinylcarbazole and 2,5-dimethyl-1,5-hexadiene, the addition compounds were isolated and found polarographically identical to the stock solutions.

Polarograms were recorded in a 50% methanol medium, the depolariser concentration being 2×10^{-4} *M*. The solution was deaerated for 5 min before the polarogram was recorded.

RESULTS AND DISCUSSION

All the compounds except the 2,5-dimethyl-1,5-hexadiene derivative showed a similar d.c. polarographic behaviour to those of other organo-mercury(II) compounds. The compounds exhibit two waves over most of the pH scale (Fig. 1). At

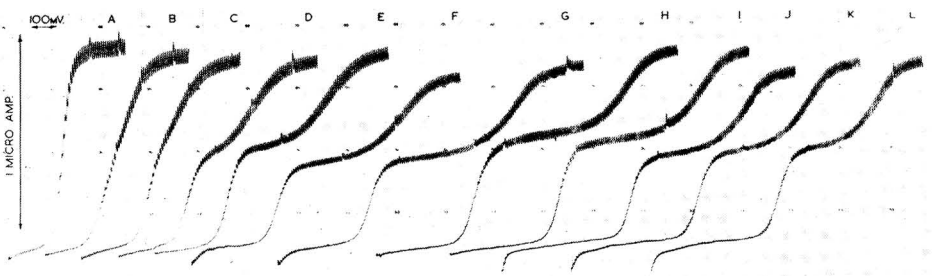

Fig. 1. pH dependence of allyl alcohol/mercury(II) acetate, 2×10^{-4} *M* 50% methanol, 0.002% Triton X100 plus buffer medium. Starting potential 0.0 V. pH: (A) 1.5, (B) 3.65, (C) 4.48, (D) 5.56, (E) 6.52, (F) 7.50, (G) 8.54, (H) 9.55, (I) 10.1, (J) 11.4, (K) 12.25, (L) 12.9.

low pH values, derivatives of some of the olefins, allyl alcohol, vinyl acetate, α-methylstyrene, N-vinyl-2-pyrrolidone, give a single 2-electron wave and in the case of the α-methylstyrene derivative a single wave again at high pH values, but two waves at intermediate pH's. Comparison of wave heights with benzaldehyde ($n=1$) and benzil ($n=2$) indicate that both waves are 1-electron. The first wave generally shows a small prewave, while the second wave normally exhibits a large maximum; both are eliminated by Triton X100. Mercury reservoir height dependence studies show both waves to be diffusion controlled. The 2,5-dimethyl-1,5-hexadiene derivative differed from the other compounds at pH 12.9 in that the second reduction step gave rise to two 1-electron waves.

The stability of the compounds varies with the olefin, in acid medium (pH 1.5) only the compounds from allyl alcohol, crotyl alcohol and 4-methyl-1-pentene are stable. The least stable compounds are those obtained from vinyl ethers. The addition of iodide, bromide, etc., which form strong complexes with mercury(II) also decompose the compounds at acid pH values where they are normally stable.

The stable reduction products isolated[18,27] in the overall reduction process of

organo-mercury(II) compounds were the dimer and the hydrocarbon. Coulometric evidence has been presented only for the tetraphenylstibonium ion[38]. Microcoulometry using a DME gives an n value of 1.97 ∓ 0.10 for the overall reduction of 4-methyl-1-pentene/mercury(II) acetate; polarograms recorded during the electrolysis showed that both waves decreased equally. Electrolysis at a potential on top of the first wave also caused both waves to decrease equally, indicating rapid deactivation of the intermediate species. Controlled potential coulometry at a mercury pool confirmed that the reduction occurred in two 1-electron steps (Table 1). In the case of N-vinylcarbazole/mercury(II) acetate the reduction products, R_2Hg and RH, were isolated and identified by C–H–N-analysis. Dimer: C, 55.2% (55.5%); H, 3.94% (4.35%); N, 4.85% (4.32%). Final product: C, 83.7% (80.0%); H 5.63% (6.71%); N, 7.38% (6.22%). Theoretical values in brackets.

TABLE 1

n VALUES AS DETERMINED BY CONTROLLED POTENTIAL COULOMETRY AT A MERCURY POOL ELECTRODE

Olefin	*pH*	*First wave*	*Both waves*
4-methyl-1-pentene	12.9	0.99	2.02
4-methyl-1-pentene	9.5	1.03	1.94
4-methyl-1-pentene	5.6	—	1.99
N-vinylcarbazole	12.9	1.05	1.95
N-vinyl-2-pyrrolidone	12.9	—	2.01
vinyl acetate	12.9	1.08	1.96
2,5-dimethyl-1,5-hexadiene	12.9	—	3.98

pH dependence of the first wave

pH plots show the half-wave potential of the first wave ($E'_{\frac{1}{2}}$) to be dependent on pH (Fig. 2 and Table 2). Close examination shows small irregularities in the pH dependence, and can be correlated with a change in buffer composition. Increasing the buffer concentration causes a negative shift in $E'_{\frac{1}{2}}$.

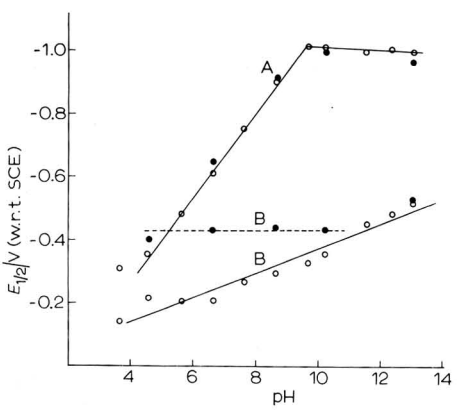

Fig. 2. pH dependence of 4-methyl-1-pentene/mercury(II) acetate, 2×10^{-4} M. (A) Second wave. (B) First wave: (○) 50% methanol, 0.002% Triton X100 plus buffer medium; (●) as above plus 0.1 M potassium bromide.

As earlier workers[15,18,22,24,28] had observed, the addition of complexing anions (*e.g.* thiocyanate, chloride, bromide and iodide) was found to cause a negative shift in $E'_{\frac{1}{2}}$ proportional to their complexing affinity for mercury. The anions had no effect on the half-wave potential of the second wave. The effects of acetate, bromide and hydroxide were investigated in detail for 4-methyl-1-pentene/mercury(II) acetate derivative. A supporting electrolyte of negligible complexing properties, i.e. sodium nitrate, was chosen and known quantities of deformable anion added, the overall concentration of sodium nitrate and sodium salt of the anion being kept constant (0.1 *M*). From plots of $\log_{10}$[anion] against $E'_{\frac{1}{2}}$ (Fig. 3) the species in solution would appear to be RHgOAc, RHgBr and RHgOH. The value of the stability constants being approximately: $K_{OAc}=2.1\times10^{3}$ l mol^{-1}, $K_{Br}=4.4\times10^{7}$ l mol^{-1} and $K_{OH}=1.5\times10^{8}$ l mol^{-1}. In a similar study, Butin *et al.*[28] give stability constants for the formation of RHgBr and $RHgBr_2$ for a number of compounds. In our opinion, however, their experimental data gives no indication that the $RHgBr_2$ species is formed.

The apparent pH dependence of the first wave can therefore be explained in terms of complexation with the buffer components. A pH dependence carried out in the presence of a large excess of bromide should therefore give a pH independent system, this is in fact obtained, except at high pH values (Fig. 2) where RHgOH will be preferentially formed. The work of Benesch and Benesch[18] and that of Hush and Oldham[24] was carried out in a buffer plus halide medium, thus the pH dependence observed by these workers is easily explained. Chantal and Etienne[31] observed for pyridyl-3-mercury(II) acetate and thienyl-2-mercury(II) chloride a similar pH dependence though no explanation was given.

pH dependence of the second wave

Over the pH range 3–9 the second wave undergoes a considerable shift in

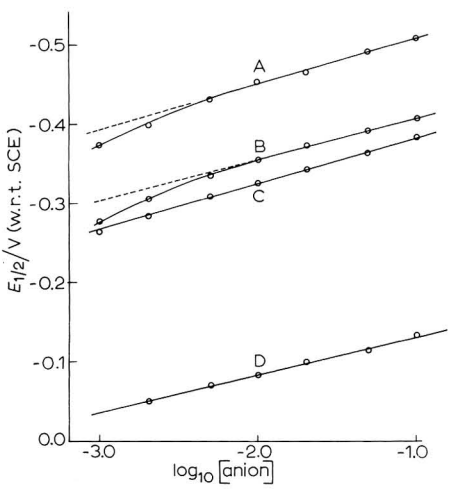

Fig. 3. Dependence of $E'_{\frac{1}{2}}$ for 4-methyl-1-pentene/mercury(II) acetate 2×10^{-4} *M*, on the concn. of added complexing ion: 50% methanol, 0.002% Triton X100 medium, supporting electrolyte $NaNO_3$ + Na-[anion] = 0.1 *M*. (A) Hydroxide (diffusion wave), slope = 60 mV/$\log_{10}[OH^-]$; (B) hydroxide (adsorption wave), slope = 53.5 mV/$\log_{10}[OH^-]$; (C) bromide, slope = 57 mV/$\log_{10}[Br^-]$; (D) acetate, slope = 51 mV/$\log_{10}[OAc^-]$.

TABLE 2

POLAROGRAPHIC CHARACTERISTICS OF OLEFIN–MERCURY(II) ACETATE ADDITION COMPOUNDS, MEASURED IN A 50% METHANOL, 0.002% TRITON X100 MEDIUM

Depolariser concentration, $2 \cdot 10^{-4}$ M; i = total height of both waves

Olefin	*pH* 5.56			*pH* 9.55			*pH* 12.9			*Time of formation/min*
	$E'_{\frac{1}{2}}/V$	$E''_{\frac{1}{2}}/V$	$i/\mu A$	$E'_{\frac{1}{2}}/V$	$E''_{\frac{1}{2}}/V$	$i/\mu A$	$E'_{\frac{1}{2}}/V$	$E''_{\frac{1}{2}}/V$	$i/\mu A$	
allyl acetate	−0.27	−0.65	0.94	−0.39	−1.09	0.98	−0.60	−0.99	0.98	1500
allylacetone	−0.27	−0.43	0.95	−0.37	−0.73	0.98	−0.59	−0.70	0.98	2
allyl alcohol	−0.28	−0.56	0.98	−0.41	−1.02	1.00	−0.58	−0.98	1.04	180
crotyl alcohol	−0.21	−0.33	0.91	−0.33	−0.65	0.95	−0.51	−0.63	0.98	1500
cyclohexene	−0.16	−0.43	1.02	−0.28	−0.80	1.03	−0.48	−0.77	0.94	180
2,5-dimethyl-1,5-hexadiene	−0.15	−0.22		−0.28	−0.92		−0.45	−0.65, −0.95		60
ethene	−0.26	−0.54		−0.34	−1.00		−0.52	−0.95		< 1
4-methyl-1-pentene	−0.20	−0.46	0.97	−0.31	−0.99	1.03	−0.50	−0.98	1.01	60
α-methylstyrene	−0.14	−0.20	0.96	−0.28	−0.51	1.00	−0.47		0.99	40
propene	−0.23	−0.41		−0.35	−0.90		−0.53	−0.87		< 1
styrene	−0.17	−0.40	0.82	−0.30	−0.73	0.91	−0.49	−0.71	0.84	180
vinyl acetate	−0.26		1.06	−0.38	−0.88	1.13	−0.56	−0.86	1.05	2
vinyl-n-butyl ether	−0.26	−0.35		−0.38	−0.91	0.91	−0.58	−0.88	0.97	2
vinyl-iso-butyl ether	−0.26	−0.36		−0.39	−0.92	0.96	−0.58	−0.89	0.94	2
N-vinylcarbazole	−0.11	−0.62	0.93	−0.27	−0.84	0.90	−0.45	−0.84	0.93	2
vinyl-2-chloroethyl ether	−0.26	−0.37		−0.39	−0.92	1.01	−0.58	−0.89	1.01	2
N-vinyl-2-pyrrolidone	−0.23	−0.33	0.90	−0.37	−0.73	1.00	−0.53	−0.69	0.95	10

potential (Fig. 2), the shift corresponding to approximately 140 mV/pH. This is considerably greater than the theoretical value of 58 mV/pH expected for the involvement of a single proton required by the overall reduction process. Changing the maximum suppressor from Triton X100 to methyl cellulose was without effect. The large $E''_{\frac{1}{2}}$ shift with pH would suggest the existence of a second pH dependent step such as a deactivation process. The pH dependence was, however, unaltered by reducing the temperature to 0°C, indicating either that the shift in $E''_{\frac{1}{2}}$ is not due to a side reaction or that the side reaction is too fast for a 25°C decrease in temperature to have an effect.

Above pH 9 the second wave becomes independent of pH, indicating that at these pH values electron transfer occurs before protonation.

$$RHg^{\bullet} + e \rightarrow RHg^{\bullet -} + H^{+} \rightarrow RH + Hg$$

Reversibility of the polarographic steps

Cyclic voltammetry at a HMDE shows the reversibility of the first step at all pH values but not that of the second step. The anodic peak can easily be shown not to be due to the reaction $X^{-} + Hg \rightarrow HgX + e$ (X = halide) as indicated by Dessy *et al.*[26] by using a nitrate medium and the mercury(II) nitrate addition compound of the olefin. The oscillopolarographic investigation of phenyl mercury(II) acetate by Vojir[16] and Chantal and Etienne[31] only showed an anodic peak when a streaming mercury electrode was used. In the case of the DME or HMDE a layer of dimer was formed, inhibiting further reactions. The reduction products from olefin-mercury(II) compounds are relatively more soluble and inhibition effects are generally not observed.

Hush and Oldham[24] from αn measurements found that when the anion of RHgX had a stronger affinity for mercury than that of the supporting electrolyte, then the first step was irreversible. Cyclic voltammograms of 4-methyl-1-pentene/mercury(II) acetate derivative in the presence of small quantities of iodide show the first step split into two (Fig. 4a). Presumably two different species are being reduced, RHg(buffer) and RHgI. On oxidation of the radical, only enough iodide to complex with a small proportion of RHg^{+} will be present. At slower scan rates (Fig. 4b) a large proportion of the radical will be lost by dimerization and consequently all the oxidised radical will be complexed by the iodide. In the presence of large quantities of added complexing anion single cathodic and anodic peaks are observed.

Adsorption and dimerization effects

Prewaves to the first reduction step were observed for nearly all the compounds, with the resolution of the prewave increasing as the pH is raised. In a sodium hydroxide medium, the 4-methyl-1-pentene/mercury(II) acetate derivative gives a well developed prewave ($E_{\frac{1}{2}}(ads) - E_{\frac{1}{2}}(dif) = 120$ mV) which is independent of concentration above 1×10^{-4} *M*. The wave height is directly proportional to the corrected mercury reservoir height. From drop time curves (Fig. 5) it can be seen that the prewave is due to the adsorption of the radical. Compounds which did not exhibit a separate adsorption wave showed evidence of adsorption from *i–t* curves recorded near the foot of the first wave.

On increasing the sweep rate (v) cyclic voltammograms showed a rapid

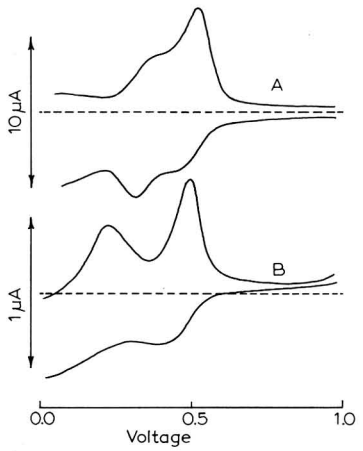

Fig. 4. Cyclic voltammograms of 4-methyl-1-pentene/mercury(II) acetate 2×10^{-4} *M*, in the presence of 1×10^{-4} *M* sodium iodide: 50% methanol, pH 9.55 medium, HMDE. Scan rate: (A) 1 V s^{-1}; (B) 100 mV s^{-1}.

increase in the ratio of anodic to cathodic peak heights, but at faster scan rates a limiting value was reached. The cathodic peak height is directly proportional to $v^{\frac{1}{2}}$ indicating a diffusion controlled process. The height of the anodic peak shows a rapid initial increase due to the combined effects of adsorption and dimerization. At higher scan rates the rectilinear relationship between i_a and $v^{\frac{1}{2}}$ is due to the fact that under these conditions little of the radical is lost and the rate of adsorption is too slow to have any effect. As the scan rate is decreased the anodic peak gradually disappears. From these measurements the half life of the adsorbed radical was found to be about 5 s.

If the HMDE is allowed to remain in contact with the organo-mercury(II) solution at zero applied volts for a short period before the scan is started, then the cyclic voltammogram shows the presence of an additional cathodic peak at more positive potentials than the main peak (Fig. 6a). The height of this peak increases with the time of standing, reaching a limiting value after about 15 min. This peak has been assigned to the adsorption of the reactant[25]. Using a DME, however, where the time interval is very short no peak is observed. The slowness of adsorption makes it highly unlikely that the d.c. polarographic prewave is due to adsorption of the reactant as claimed by Broman and Murray[25].

Repetitive scan cyclic voltammetry at a HMDE shows that the adsorbed radical is much more stable than the free radical in solution. After the first scan the cathodic peak shows a marked decrease in size while the anodic peak remains unaltered (Fig. 6a). This is easily explained if it is assumed that the unadsorbed radical undergoes rapid dimerization. Only the adsorbed radical formed during the first scan will be oxidised and take part in subsequent scans. As the depolariser concentration is reduced the equilibrium ratio of i_a/i_c increases indicating a greater proportion of the radical is adsorbed.

When a Pt electrode is used no indication of an anodic peak is found thus indicating the influence of adsorption on the stability of the radical. With a glassy

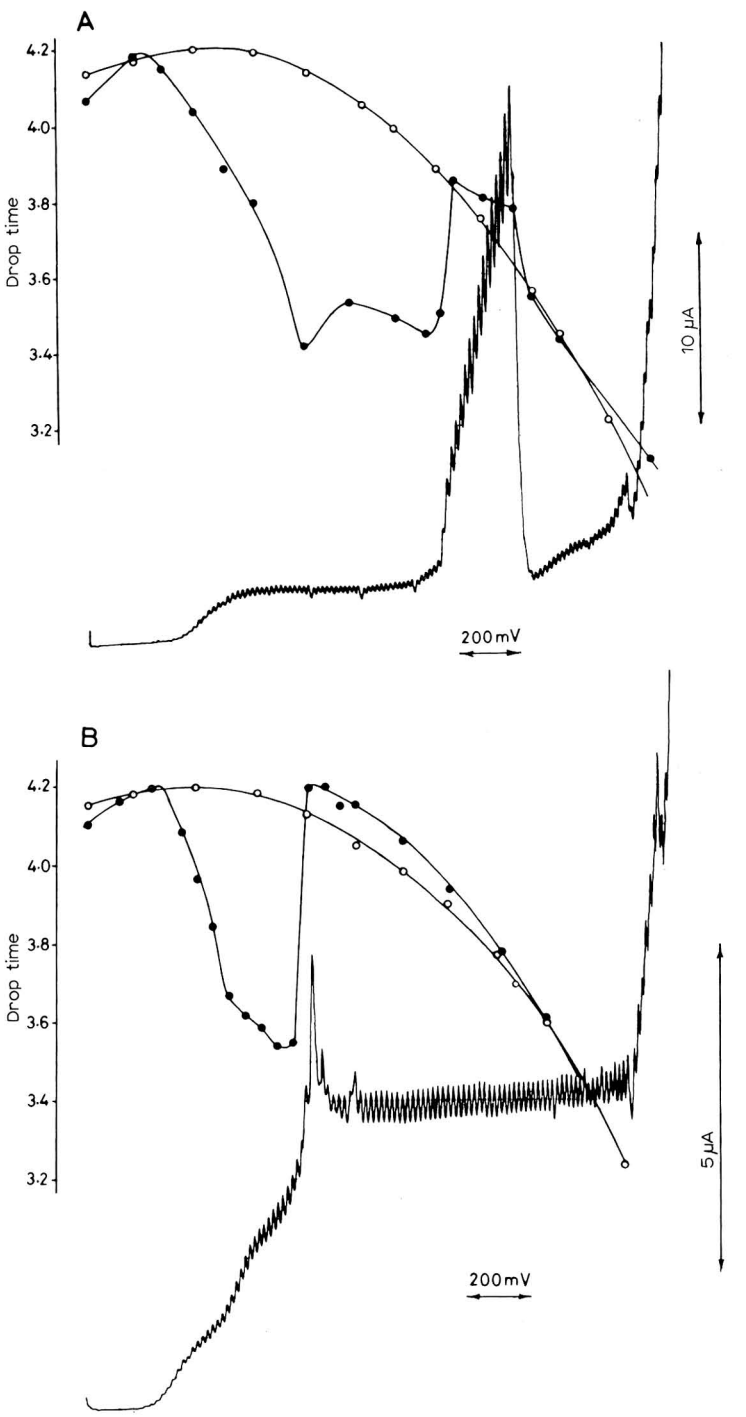

Fig. 5. Drop time curves measured in a 0.1 *M* sodium nitrate methanol medium. Starting potential 0.0 V. (A) 4-Methyl-1-pentene/mercury(II) acetate 5×10^{-4} *M*, (B) α-methylstyrene/mercury(II) acetate 5×10^{-4} *M*.

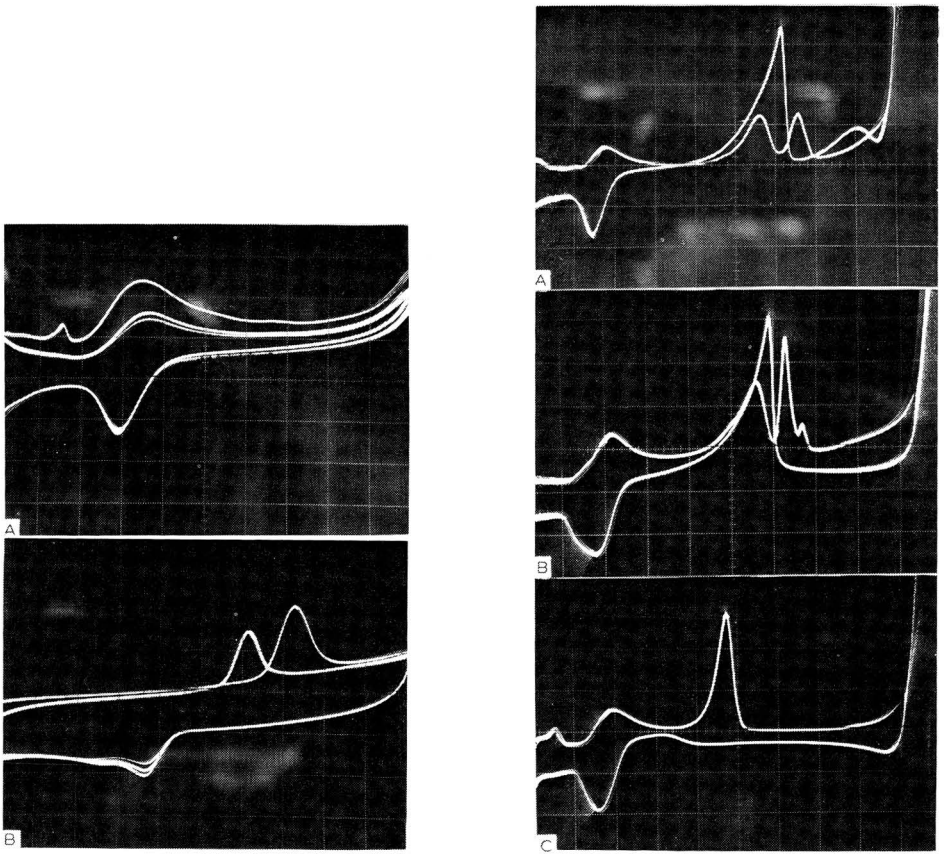

Fig. 6. (A) Repetitive scan cyclic voltammetry of 4-methyl-1-pentene/mercury(II) acetate 1×10^{-4} *M*. Recorded in a 50% methanol, pH 9.55 medium at a HMDE. Scan rate 0.5 V s^{-1}, 1 volt scan, starting potential 0.0 V, sensitivity 0.5 μA div^{-1}. (B) Repetitive scan cyclic voltammetry of 4-methyl-1-pentene/mercury(II) acetate 2×10^{-4} *M*. Recorded in a 50% methanol, pH 9.55 medium at a glassy carbon electrode. Scan rate 0.5 V s^{-1}, 1 volt scan, starting potential 0.5 V.

Fig. 7. Cyclic voltammograms in methanol containing 0.1 *M* sodium nitrate at a HMDE. Scan rate 200 mV s^{-1}, 2 volt scan, starting potential 0.0 V, sensitivity 0.5 μA div^{-1}. (A) 4-methyl-1-pentene/mercury(II) acetate 1×10^{-4} *M*, (B) vinyl acetate/mercury(II) acetate 1×10^{-4} *M*, (C) N-vinyl-2-pyrrolidone/mercury(II) 1×10^{-4} *M*.

carbon electrode the cathodic peak shifts to more positive potentials after the first scan; an anodic peak is also observed, but there is a considerable separation between the cathodic and anodic peaks indicating marked irreversibility (Fig. 6b). The shift in potential of the cathodic peak is connected with the adsorption of the reactant. The longer the delay before the voltage scan starts the more negative and ill defined is the cathodic peak. It is interesting to note that at the mercury electrode the relative positions of the peak due to the adsorption of the reactant and the main reduction peak are at variance with the Brdicka theory[43], while at the glassy carbon electrode (system highly irreversible) the relative positions fit in with the normal Brdicka interpretation.

Cyclic voltammograms in methanol containing 0.1 *M* sodium nitrate show some unexpected phenomena associated with the second cathodic step (Fig. 7), only the derivatives from crotyl alcohol, cyclohexene, α-methylstyrene, N-vinylcarbazole and N-vinyl-2-pyrrolidone do not give to any marked extent the large inverted peak on the positive going sweep. The exact form of the peaks varies from compound to compound and can be observed on a DME or HMDE. The sharpness of the peaks obtained on the negative going sweep suggests adsorption and/or capacitive effects and this is consistent with the droptime/voltage curves (Fig. 5). The inverted peaks can be eliminated by the addition of Triton X100, however, it is not clear how these peaks arise though they are undoubtedly connected with adsorption of the radical species.

An overall reduction scheme for this type of compound is shown in Fig. 8.

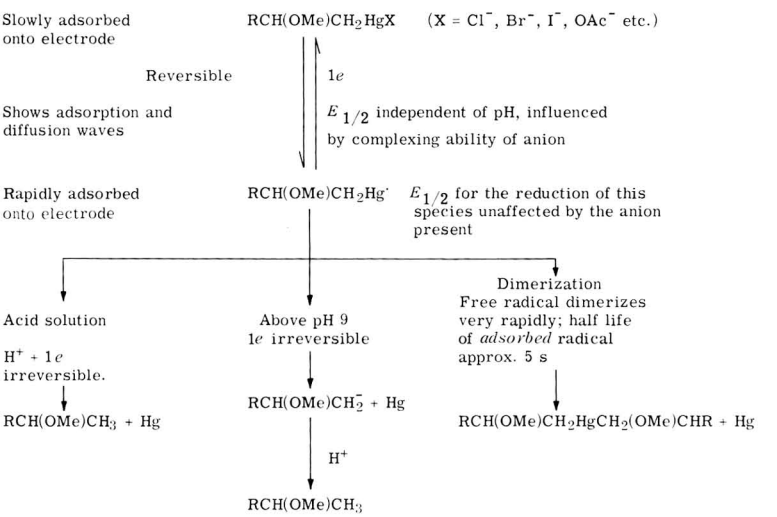

Fig. 8. Overall reduction scheme for olefin/mercury(II) derivatives.

ACKNOWLEDGEMENT

One of us (R.D.J.) would like to thank the Science Research Council for the award of a Research Studentship.

SUMMARY

A wide range of olefin–mercury(II) acetate addition compounds were polarographically examined and found to exhibit two 1-electron waves over most of the pH scale. The first wave represents the reversible formation of a radical species RHg· which is adsorbed on the electrode surface, often giving rise to a separate adsorption wave. The adsorbed radical which has a half life of approximately 5 s is considerably more stable than the free radical in solution and is some two orders of magnitude more stable than that obtained from other organo-mercury(II) compounds which have been examined by other workers. The second wave which is irreversible corresponds to the reduction of the radical to RH.

REFERENCES

1 J. E. PAGE AND J. G. WALLER, *Analyst*, 74 (1949) 292.
2 T. KAJIMURA AND S. JAMAMOTO, *Japan Analyst*, 4 (1955) 152
3 S. USAMI, *Japan Analyst*, 5 (1956) 499.
4 M. KOTAKEMORI AND H. HANDA, *Ann. Report Takamine Lab.*, 8 (1957) 231.
5 N. SHIROTA, M. KOTAKEMORI AND H. HANDA, *Ann. Rep. Takamine Lab.*, 9 (1957) 198.
6 P. CASEY, J. J. CARROLL AND N. R. STALICA, *Proc. Penn. Acad. Sci.*, 32 (1958) 63.
7 N. Z. BRUJA, *Rev. Chim. Bucharest*, 9 (1958) 685.
8 P. CASEY AND W. WAGNER, *Proc. Penn. Acad. Sci.*, 36 (1962) 281.
9 V. D. BEZUGLYI, Y. P. PONOMAREV AND V. N. DMITRIEV, *J. Anal. Chem. USSR, English Transl.*, 19 (1964) 817.
10 H. SATO AND M. SHIMAMINE, *Eisei Shikensho Hohoku*, 83 (1965) 59.
11 V. D. BEZUGLYI AND Y. P. PONOMAREV, *J. Anal. Chem. USSR, English Transl.*, 20 (1965) 1274.
12 T. M. HOPES, *J. Assoc. Offic. Agr. Chemists*, 49 (1966) 840.
13 G. S. PORTES, *J. Pharm. Pharmacol.*, 20 (Suppl.) (1968) 43.
14 B. FLEET AND R. D. JEE, *Talanta*, 16 (1969) 1561.
15 G. COSTA, *Ann. Chim. (Rome)*, 38 (1948) 655.
16 V. VOJIR, *Collection Czech. Chem. Commun.*, 16 (1951) 488.
17 V. VOJIR, *Chem. Listy*, 46 (1952) 129.
18 R. BENESCH AND R. E. BENESCH, *J. Am. Chem. Soc.*, 73 (1951) 3391.
19 R. BENESCH AND R. E. BENESCH, *J. Phys. Chem.*, 56 (1952) 648.
20 W. L. WUGGATZER AND J. M. CROSS, *J. Am. Pharm. Assoc.*, 41 (1952) 80.
21 M. L. O'DONNEL AND C. W. KREKE, *J. Am. Pharm. Assoc.*, 48 (1959) 268.
22 J. HAMAMOTO AND N. KOTAKEMORI, *Nippon Nogeikagaku Kaishi*, 35 (1961) 48.
23 M. L. O'DONNEL, A. SCHWARZKOPF AND C. W. KREKE, *J. Pharm. Sci.*, 52 (1963) 659.
24 N. S. HUSH AND K. B. OLDHAM, *J. Electroanal. Chem.*, 6 (1963) 34.
25 R. F. BROMAN AND R. W. MURRAY, *Anal. Chem.*, 37 (1965) 1408.
26 R. E. DESSY, W. KITCHING, T. PSARRAS, R. SALINGER, A. CHEN AND T. CHIVERS, *J. Am. Chem. Soc.*, 88 (1966) 460.
27 K. YOSAHIDA AND S. TSUTSUMI, *J. Org. Chem.*, 32 (1967) 468.
28 K. P. BUTIN, I. P. BELETSKAYA, A. N. RYABTSEV AND O. A. REUTOV, *Elektrokhimiya*, 3 (1967) 1318.
29 K. P. BUTIN, A. N. RYABTSEV, V. S. PETROSYAN, I. P. BELETSKAYA AND O. A. REUTOV, *Dokl. Akad. Nauk SSSR*, 183 (1968) 1328.
30 K. P. BUTIN, A. N. RYABTSEV, I. P. BELETSKAYA AND O. A. REUTOV, *Zh. Org. Khim.*, 4 (1968) 934.
31 D. CHANTAL AND L. ETIENNE, *Bull. Soc. Chim. France*, 5 (1968) 2228.
32 D. CHANTAL AND L. ETIENNE, *Bull. Soc. Chim. France*, 5 (1968) 2233.
33 K. P. BUTIN, A. N. KASHIN, I. P. BELETSKAYA AND O. A. REUTOV, *J. Organometal. Chem.*, 16 (1969) 27.
34 J. CHATT, *Chem. Rev.*, 48 (1951) 7.
35 C. A. KRAUS, *J. Am. Chem. Soc.*, 35 (1913) 1732.
36 C. SULLAM, *Atti Ist. Veneto Sci. Lettere Anti Classe Sci. Mat. Nat.*, 95 (1937–8) 221.
37 V. HANUS, *Chem. Zvesti*, 8 (1954) 702.
38 M. D. MORRIS, P. S. MC. KINNEY AND E. C. WOODBURY, *J. Electroanal. Chem.*, 10 (1965) 85.
39 B. FLEET AND P. ZUMAN, *Collection Czech. Chem. Commun.*, 32 (1967) 2066.
40 G. PHILLIPS AND G. W. C. MILNER, *Analyst*, 94 (1969–9) 833.
41 A. J. BARD AND E. SOLON, *Anal. Chem.*, 34 (1962) 1181.
42 *General Electric Company U.S.A. Transistor Manual*, 7th edn., 1964, p. 346.
43 R. BRDICKA, *Z. Elektrochem.*, 48 (1942) 278.

ELECTROANALYTICAL CHEMISTRY AND INTERFACIAL ELECTROCHEMISTRY
Elsevier Sequoia S.A., Lausanne – Printed in The Netherlands

POTENTIAL SWEEP VOLTAMMETRY OF METAL DEPOSITION AND DISSOLUTION

PART I. THEORETICAL ANALYSIS

N. WHITE AND F. LAWSON
Department of Chemical Engineering, Monash University, Clayton, Victoria (Australia)
(Received December 16th, 1969)

INTRODUCTION

Most of the theoretical and practical investigations of electrode processes using linear sweep voltammetry have been concerned with those processes where the reduced (R) and oxidized (O) species are soluble in the solution or electrode phase. Metals which are deposited into an amalgam fall into this category. However, if amalgam formation does not occur or if a suitable electrode is chosen, the metal deposits as a separate phase. Similar considerations hold for the investigations into the stripping of metals.

At room temperature, a platinum electrode is sometimes used as an inert electrode. Delahay and Berzins[1] first solved the boundary value problem for metal deposition by a linear scan voltage sweep. Nicholson[2,3] has studied, by voltammetric means, the stripping into an initially quiescent solution of both bulk deposits and submonolayer deposits of various metals from a platinum electrode. In these investigations, the activity of the submonolayer deposit was assumed to be equal to the fractional coverage. It is generally held that platinum does not alloy with the deposited metal and that once the inert electrode has been covered by a monolayer, the activity of the deposit is unity. The results obtained by Schmidt and Gygax[4], Breiter[5], Astley[6] and others have cast serious doubts on this assumption particularly for the case of deposition from aqueous solutions. The most consistently successful voltammetric work has been that of Mamantov and Manning and their coworkers[7–9] who used platinum and other electrodes in fused salt solutions. Kawamura[10] has also used this technique to measure the diffusivity of Ag^+ in alkali nitrate melts. However, voltammetric studies of metal deposition at a carbon paste electrode[11] did not produce peak currents which compared at all well with the theoretical values. Michael-Krebs and Roe[12] have produced an activity model for the stripping of silver by cyclic voltammetry.

When using cyclic voltammetry to investigate the commonly encountered problem, both O and R soluble, one needs to account for sphericity effects, kinetic control, uncompensated cell resistance and the shape of the anodic branch when the scan is reversed. Similar factors have to be considered when the voltammetry of metal deposition and dissolution is considered. Boundary value solutions for these situations are given.

THEORETICAL ANALYSIS

The diffusion equation has to be solved for either the spherical case or the planar case.

For the spherical case

$$\frac{\partial c_0}{\partial t} = D_0\left(\frac{\partial^2 c_0}{\partial r^2} + \frac{2}{r}\frac{\partial c_0}{\partial r}\right) \tag{1}$$

with the following boundary conditions

(a) $t = 0, \quad c_0 = c_0^* \quad \text{for} \quad r > r_0$
(b) $t \geqq 0, \quad c_0 \rightarrow c_0^* \quad \text{as} \quad r \rightarrow \infty$
(c) $t \geqq 0, \quad c_0/a(t) = \exp \lambda(E - E_0)$ at $r = r_0$,

where $a(t)$ is the activity of the deposited metal, and for the planar case

$$\frac{\partial c_0}{\partial t} = D_0 \frac{\partial^2 c_0}{\partial x^2} \tag{1a}$$

with the following boundary conditions

(a) $t = 0, \quad c_0 = c_0^* \quad \text{for} \quad x > 0$
(b) $t \geqq 0, \quad c_0 \rightarrow c_0^* \quad \text{as} \quad x \rightarrow \infty$
(c) $t \geqq 0, \quad c_0/a(t) = \exp \lambda(E - E_0)$ at $x = 0$.

Where kinetic control of the electrode reaction must be accounted for, for a planar electrode

$$D_0 \frac{\partial c_0}{\partial x} = k_f c_0 - k_b a(t) \tag{2}$$

and the effect of applied potential on the forward and reverse rate constants is

$$k_f = k_s \exp -\alpha\lambda(E - E_0) \tag{3}$$
$$k_b = k_s \exp (1 - \alpha)\lambda(E - E_0) \tag{3a}$$

where k_s is the standard rate constant and α is the transfer coefficient.

It is also assumed that the number of electrons transferred in the activation step is the same as that involved in the stoichiometric equation. The symbols used have their usual meaning, but here λ is used for the quantity nF/RT.

The applied potential (exciting function) takes the form

$$E = E_i - vt, \quad 0 < t \leqq t_\lambda, \tag{4}$$

for the cathodic region, and when the cathodic scan is reversed, the exciting function becomes

$$E = E_i - 2vt_\lambda + vt \quad \text{for} \quad t_\lambda < t \leqq 2t_\lambda \tag{4a}$$

where t_λ is the switching time and v is the voltage sweep rate.

Ultimately, a solution for current is required, so Faraday's Law is used in the following manner

$$i = nFAD_0\left(\frac{\partial c_0}{\partial r}\right)_{r = r_0} \tag{5}$$

for a spherical electrode and

$$i = nFAD_0 \left(\frac{\partial c_0}{\partial x} \right)_{x=0} \tag{5a}$$

at the planar electrode.

Solutions to the boundary value problems are in terms of the dimensionless current parameter I, defined by

$$I = i/[nFAc_0^*(D_0\lambda v)^{\frac{1}{2}}]$$

and the dimensionless voltage parameter V, defined by

$$V = (nF/RT)\, vt\ .$$

These quantities include all the variables which may possibly be altered in any one experiment, including the temperature. The need to include the temperature variation arises from the different temperature used in the experimental work (−48°C) and the temperature for which such results are usually tabulated (25°C). The frequently used practice of plotting $\alpha(nF/RT)vt$ as a voltage parameter rather than $(nF/RT)vt$ in the kinetic control situation, whilst allowing the results to be graphed or tabulated in compact form, is not a good one because α is generally an unknown.

1. *Reversible deposition of a metal at an inert spherical electrode*

For this situation, the activity of the deposited metal will be assumed to be constant and equal to a^*. Then by using Laplace transforms, it is possible to show

$$\begin{aligned} \bar{\imath} = nFAD_0\{&(c_0^*/r_0 s) - (a^*/r_0)\mathrm{L}\ \exp\ \lambda(E-E_0) \\ &+ (s/D_0)^{\frac{1}{2}}[(c_0^*/s) - a^*\mathrm{L}\ \exp\ \lambda(E-E_0)]\}\ . \end{aligned} \tag{6}$$

It is seen that the inverse of the term containing $(s/D_0)^{\frac{1}{2}}$ is in fact the solution at a planar electrode as given by Delahay and Berzins[1]. This solution will be represented by $I(V) = 2\pi^{-\frac{1}{2}} F(\lambda vt)^{\frac{1}{2}}$ where F is Dawson's integral, namely

$$F(x) = \mathrm{e}^{-x^2} \int_0^x \mathrm{e}^{y^2}\, \mathrm{d}y\ .$$

Hence on back transforming, the current may be represented by

$$i_T = i_{PL} + i_s$$

where

$$i_{PL} = nFAc_0^* D_0 (\lambda v)^{\frac{1}{2}} 2\pi^{-\frac{1}{2}} F(\lambda vt)^{\frac{1}{2}} \tag{7}$$

and

$$i_s = nFAc_0^*(D_0/r_0)(1 - \exp(-\lambda vt)) \tag{8}$$

An alternative form for expressing the planar current which was found to be quite useful, is by converting the planar contribution of eqn. (6) into a Volterra integral of the form

$$\int_0^y \frac{\chi(z)}{(y-z)^{\frac{1}{2}}}\, \mathrm{d}z = 1 - \mathrm{e}^{-y} \tag{9}$$

where $\pi^{\frac{1}{2}}\, \chi(y) = I(V)$, and $y = V$.

2. *Anodic stripping following the cathodic scan*

The analysis is identical to case 1 above. Inspection of eqn. (6) shows that the spherical contribution becomes

$$i_s = nFAc_0^*(D_0/r_0)\{1-\exp\ -\lambda v(2t_\lambda - t)\} \tag{10}$$

whereas the planar contribution now involves the back transformation of the function $s^{\frac{1}{2}}L \exp \lambda(E-E_i)$. Care must be taken with the evaluation of the transform for the anodic response, as the boundary conditions at the commencement of the anodic branch have been altered by the cathodic branch which has preceeded it. Further details are given elsewhere[13], but letting

$$\tau = t - t_\lambda, \quad V = \lambda v t, \quad W = \lambda v \tau\ ,$$

the dimensionless planar current becomes

$$I(V) = 2\pi^{-\frac{1}{2}}[F(\sqrt{V}) - F(\sqrt{W})] - \exp(-\lambda v t_\lambda) \exp W \operatorname{erf}\sqrt{W}\ . \tag{11}$$

An alternative solution for the planar anodic case can be obtained from eqn. (9) by the evaluation of the integral

$$\int_0^y \frac{\chi(z)}{(y-z)^{\frac{1}{2}}}\,dz = 1 - \exp[-2vt_\lambda + y] \tag{12}$$

for $\lambda v t_\lambda < y \leqq 2\lambda v t_\lambda$.

3. *The effect of uncompensated cell resistance*

The effect of uncompensated cell resistance Ru is to reduce the applied cell voltage by an amount $i(t)Ru$. Thus

$$E - i(t)Ru = E_i - vt\ .$$

Considering only planar electrodes, eqn. (9) becomes

$$\int_0^y \frac{\chi(z)}{(y-z)^{\frac{1}{2}}}\,dz = 1 - \exp[RH \cdot \chi(y) - y]$$

where $RH = Ru\lambda nFAc_0^*(\lambda v D_0 \pi)^{\frac{1}{2}}$, as suggested by Nicholson[14].

4. *Solution to kinetically controlled metal deposition and dissolution under sweep conditions for a planar electrode*

Nicholson[14] has treated the problem of

$$O + ne \underset{k_b}{\overset{k_f}{\rightleftharpoons}} R$$

and by analogy, boundary condition (c) is used with the assumption of constant activity, *i.e.* $a(t) = a^*$ for all values of t. By letting

$$k_i = k_s \exp\ -\alpha\lambda(E_i - E_0)$$

and following the analysis of Delahay[15], one arrives at the Volterra integral

$$\chi(y) = e^{y-u}(1 - e^{-y/\alpha}) - e^{y-u}\int_0^y \frac{\chi(z)}{(y-z)^{\frac{1}{2}}}\,dz \tag{14}$$

where $k_i/(\pi D_0 \beta)^{\frac{1}{2}} = e^{-u}$.

The dimensionless current and voltage functions are related to these variables by

$$I(V) = \sqrt{\pi\alpha}\chi(y)$$
$$V \quad = y/\alpha\,.$$

5. *Submonolayer deposition under sweep conditions*

Again considering only planar electrodes, the boundary value problem is the same as in the previous case with exception of boundary condition (c) which now becomes

$$\text{(c)} \quad t \geqq 0 \quad \frac{\mathrm{d}a}{\mathrm{d}t} = \frac{1}{ms}\frac{\mathrm{d}m}{\mathrm{d}t} \quad \text{at} \quad x = 0$$

where m is the number of moles of the species deposited; ms is the number of moles required to be deposited to form a monolayer.

The assumption is that the activity is proportional to the fractional coverage of the electrode surface. Faraday's Law for this case leads to

$$\frac{1}{ms}\frac{\mathrm{d}m}{\mathrm{d}t} = \frac{AD_0}{ms}\left(\frac{\partial c}{\partial x}\right)_{x=0}$$

For the solution of this boundary problem, the variables listed below are necessary:

$$y \;= \lambda v t$$
$$\frac{a}{a^*} = \phi(y)$$
$$H \;= \frac{m^*}{Ac_0^*}\left(\frac{\lambda v}{\pi D_0}\right)^{\frac{1}{2}}$$

where $m^* = msa^*$.

Since it is current which is required, one introduces $\psi(y)$, where

$$\psi(y) = H\,\mathrm{d}\phi/\mathrm{d}y\,,$$

and it may readily be shown that

$$i = nFAc_0^*(D_0\lambda v\pi)^{\frac{1}{2}}\psi(y)$$

and therefore

$$I(V) = \pi^{\frac{1}{2}}\psi(y)\,.$$

Following the analysis of Nicholson[2] (up to the author's eqn. (9) only) one arrives at the transform equation

$$L\{\pi^{-\frac{1}{2}}\phi(y)\mathrm{e}^{-y}\} - (\pi s)^{-\frac{1}{2}} + Hs^{-\frac{1}{2}}\,L\{\mathrm{d}\phi(y)/\mathrm{d}y\} = 0 \tag{15}$$

from which the Volterra integral

$$\psi(y) = 2\pi^{-1}F(\sqrt{y}) - (\mathrm{e}^{-y}/H\pi)\int_0^y \psi(z)[\mathrm{e}^{y-z}(y-z)^{-\frac{1}{2}} - 2\mathrm{e}^{y-z}F(y-z)^{\frac{1}{2}}]\mathrm{d}z \tag{16}$$

is obtained.

6. *Stripping a submonolayer deposit*

Though the results obtained for this section are not required for the analysis of the experimental work to be given, it is contended that the solution published by Nicholson[2] for this particular case is incorrect. This is discussed in detail elsewhere[13]. By a method similar to the one above but now with an applied potential which varies according to the relationship

$$E = E_i + vt ,$$

it is possible to show that

$$\psi(y) = -e^y \pi^{-\frac{1}{2}} \operatorname{erf} \sqrt{y} + (e^y/H\pi) \int_0^y \psi(z)[e^{-(y-z)}(y-z)^{-\frac{1}{2}} + \pi^{\frac{1}{2}} \operatorname{erf}(y-z)^{\frac{1}{2}}]\,dz \qquad (17)$$

The parameter $-\psi(y)/H$ is equivalent to Nicholson's $-\psi'(y)$, and the final shape of the curves for the former parameter are noticeably different to those in Nicholson's Fig. 1. Nicholson also gives (eqn. (27)) the equation for the stripping of a bulk metal into a quiescent solution and the result in terms of the parameter used here is

$$I(V) = -\operatorname{erf} V^{\frac{1}{2}} \exp V \qquad (18)$$

The planar solutions of cases (1) and (2) are plotted in Fig. 1 for two different switching potentials. The effect of uncompensated cell resistance on the planar reversible response is shown in Fig. 2 for different values of the resistance parameter RH. Only one representative result is plotted for the kinetic control situation, namely $u = 1.0$, and is given in Fig. 3 (graphs for other values of u, however, are available). Submonolayer deposition is plotted in Fig. 4 for different values of the initial coverage parameter H. Some details of the plotting technique are given at the end of the next section.

DISCUSSION OF THEORY

The usual assumption made for the value of the activity of the deposited metal is that it is always unity. The analysis presented above suggests that the less restrictive assumption, namely that the activity be constant and equal to its initial value (or reach a constant value before the concentration of the ion is altered to any large extent) leads to the same result. The usual experimental procedure in voltammetry is to commence the sweep at a potential well anodic of the standard potential. If this is the case, then the reverse scan will continue on to potentials anodic of the potential at which, theoretically, the current began to flow. For this reason, the anodic curve has been calculated and plotted beyond the starting point of the cathodic branch. In practice the anodic curve does not continue on indefinitely but rapidly drops down to zero when the deposit is depleted.

Interesting comparisons can be made for the situations where one has reversible depositition and dissolution of the metal and no uncompensated cell resistance. Taking eqn. (16), letting $H \to \infty$ and making the appropriate substitution will give the solution for the deposition at constant activity, eqn. (7) ($H \to \infty$ therefore represents conditions under which a monolayer deposit behaves as a constant activity deposit).

Before making the next comparison, it should be made clear, that, experimentally, when stripping is carried out the cell is open circuited to allow the concentration gradient to be zero throughout the cell, or, the electrode is transferred to a different cell. Thus the boundary conditions which hold for stripping into a quiescent solution

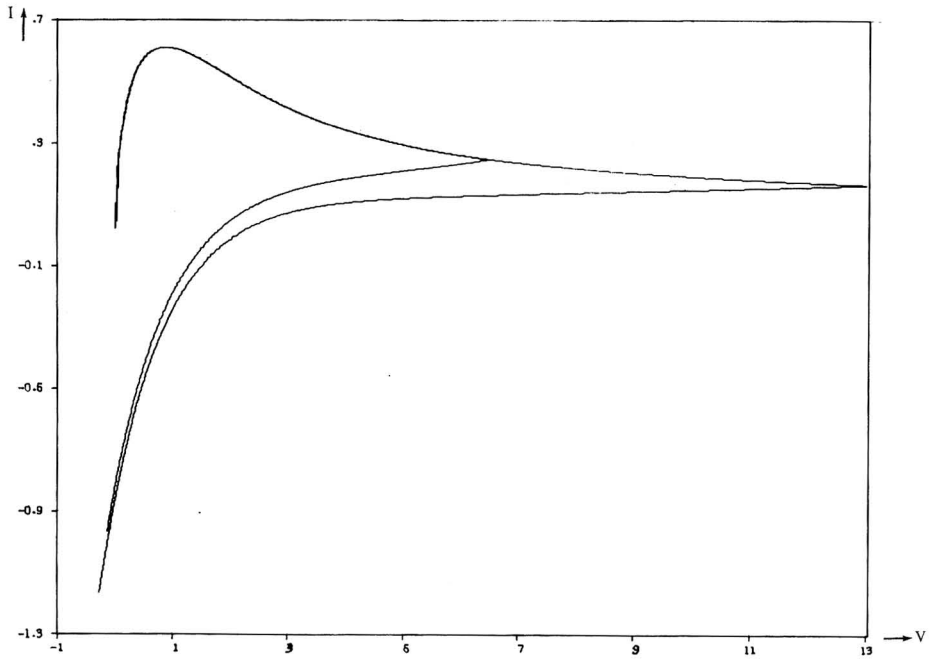

Fig. 1. Current parameter I *vs.* voltage parameter V for reversible metal deposition, for two different switching potentials.

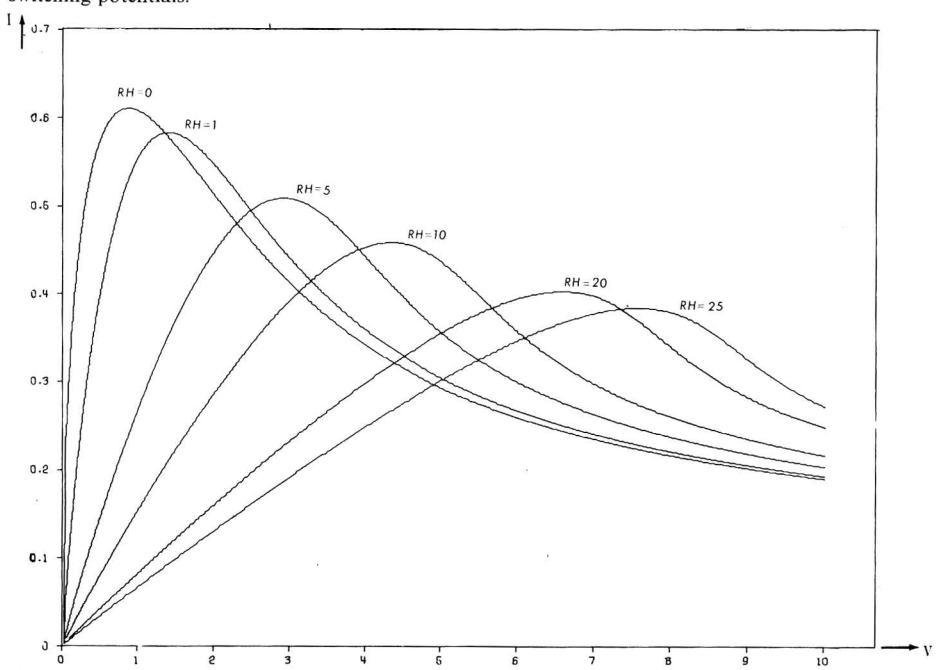

Fig. 2. Effect of uncompensated cell resistance of the reversible deposition of a metal, for various values of the resistance parameter RH.

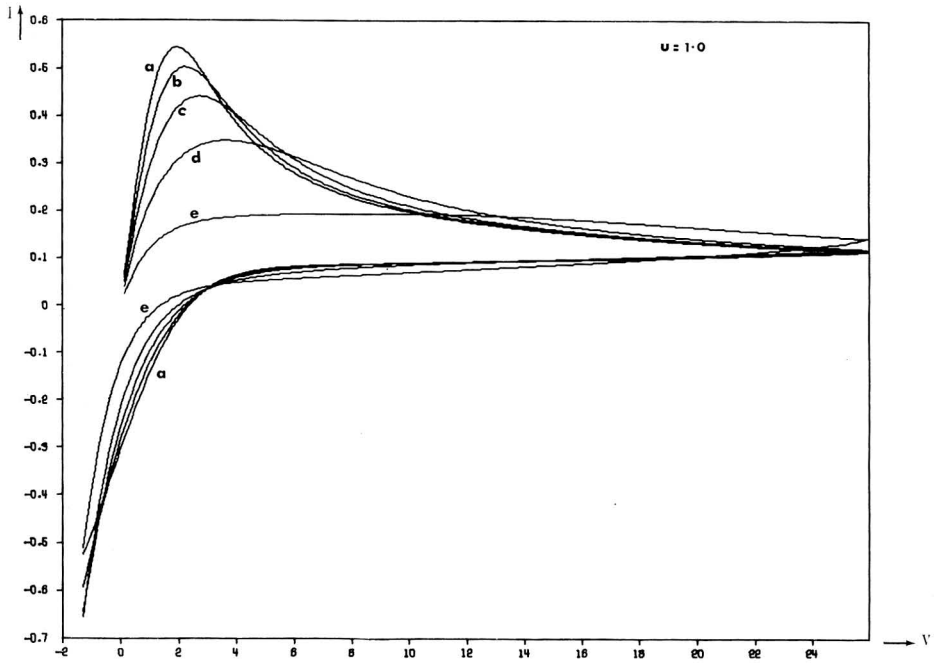

Fig. 3. Effect of kinetic control of the deposition of a metal, for $u = 1.0$ and for values of α: (a) 0.9, (b) 0.7, (c) 0.5, (d) 0.3, (e) 0.1.

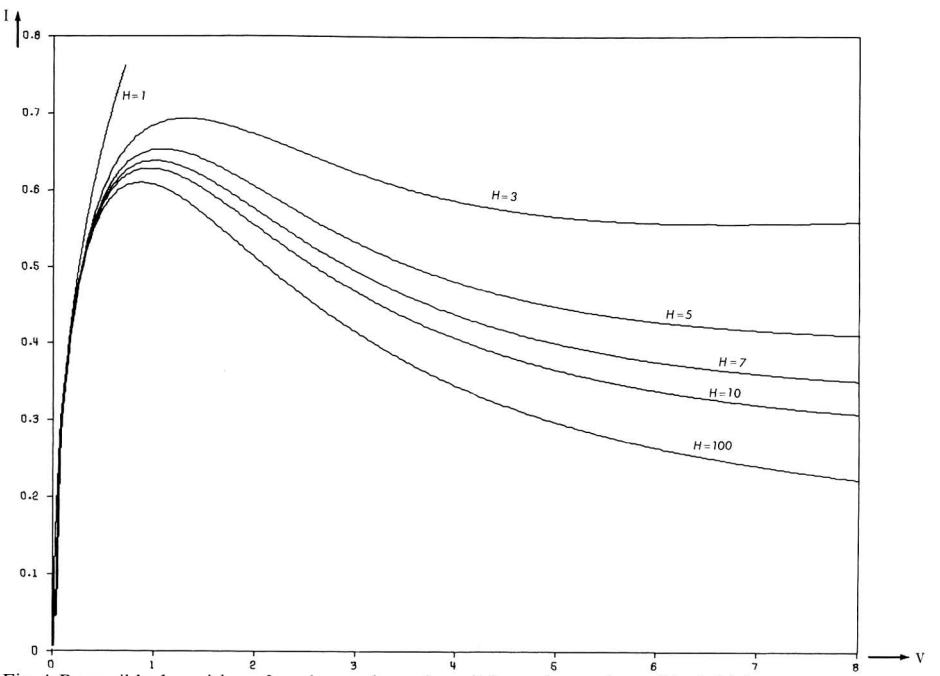

Fig. 4. Reversible deposition of a submonolayer deposit for various values of the initial coverage parameter H.

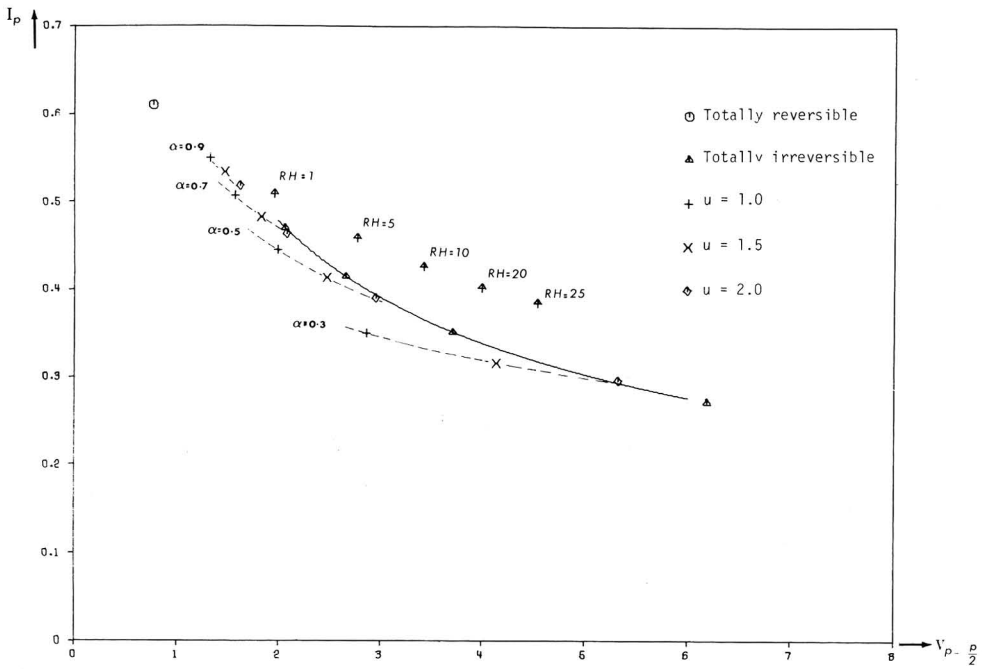

Fig. 5. Peak current *vs.* peak minus half peak voltage parameter, showing the effect on metal deposition of kinetic control and uncompensated cell resistance.

are different to those which hold for an anodic scan which has been preceeded by a cathodic scan. Equations (17) and (10) become identical when the switching time (t_λ) is zero, that is when no cathodic sweep has occurred or the effects of the cathodic sweep have been eliminated. The two stripping equations, eqns. (17) and (18) become identical when $H \rightarrow \infty$, as might be expected from what has been said earlier.

Taking eqn. (14) and allowing either u to be large and/or α to be small, with the result that

$$e^{y-u}(1-e^{-y/\alpha}) \simeq e^{y-u}$$

one arrives at the equation given by Delahay[15] for the situation where the electrode reaction is irreversible (the fate and nature of the reduced species is not important). Numerically when u is about seven, the two solutions (eqn. (14) and Delahay's eqn. 15) differ by less than 1% for values of α less than about 0.7.

It is also evident the spherical contributions for both cases 1 and 2 are identical to those obtained where the reduced species is soluble in the solution and are independent of the sweep rate. At the cathodic peak potential, the spherical current contribution for metal deposition is 57.3% of its limiting value, whereas for the case where the reduced species is soluble (in either the solution or the electrode) the spherical current contribution is 75.2% of its limiting value[17].

Recently, Roffia and Lavacchielli[16] solved the boundary value problem for an irreversible charge transfer with uncompensated cell resistance. No extension of their work was carried out here. The difficulty arising with uncompensated cell resistance

is that it alters the shape of the current–potential curves in much the same way as the kinetic effect. A convenient method for distinguishing between the two effects is to examine the functional relationship between the peak current (i_p) and the value of the peak potential minus the half-peak potential ($E_p - E_{p/2}$, which will now be designated as $E_{p-p/2}$) for different sweep rates. The latter quantity is a "shape factor" directly obtainable from the current–potential response, and its use was first suggested by Mamantov and his coworkers[7]. It is more useful for studying metal deposition than either the peak or half peak potential because it eliminates the necessity of measuring potentials with respect to a fictitious initial potential.

Figure 5 shows a plot of the current parameter I_p against the voltage shift parameter $V_{p-p/2}$, for different values of u, α, and the resistance parameter RH. The full curve shown is the locus $I_p^2 = 0.4565/V_{p-p/2}$ (with values of α of 0.9, 0.7, 0.5, 0.3 marked off such that $I_p = 0.4958\alpha^{\frac{1}{2}}$) which can be obtained from the irreversible charge transfer solutions given by Nicholson and Shain[17].

The Volterra integrals of eqns. (9), (12), (14), (16) and (17) and the non-linear Volterra integral of eqn. (13) have been solved by Nicholson's[14] method. The numerical and explicit solutions (eqns. (7) and (9), and eqns. (11) and (12)) did not differ by more than 1% when the increment for calculating the former was 0.01. Figures 1–5 were plotted by a Calcomp Digital Plotter from data generated on a CDC 3200 computer (further details on the methods for solution evaluation are available on request).

The experimental verification of some of these solutions is presented in the second part of this communication.

ACKNOWLEDGEMENT

One of us (N.W.) is grateful to Monash University for the provision of a Monash Research Grant.

SUMMARY

Solutions are presented for the voltammetric deposition and dissolution of a metal onto or from a solid electrode, accounting for the effects of sphericity, kinetic control of the charge transfer and uncompensated cell resistance. Numerical and explicit solutions have been derived for reversible deposition and dissolution. It is suggested that the effect of kinetic control of the charge transfer can be differentiated from the effect of uncompensated cell resistance by examining the variation of the peak current and peak minus half peak potential for different experimental conditions, such as the voltage sweep rate.

REFERENCES

1 P. DELAHAY AND T. BERZINS, *J. Am. Chem. Soc.*, 75 (1953) 555.
2 M. M. NICHOLSON, *J. Am. Chem. Soc.*, 79 (1957) 7.
3 M. M. NICHOLSON, *Anal. Chem.*, 32 (1960) 1058.
4 E. SCHMIDT AND H. R. GYGAX, *J. Electroanal. Chem.*, 12 (1966) 300; 13 (1967) 378; 14 (1967) 126.
5 M. W. BREITER, *J. Electrochem. Soc.*, 114 (1967) 1125.
6 D. J. ASTLEY, J. A. HARRISON AND H. R. THIRSK, *J. Electroanal. Chem.*, 19 (1968) 325.
7 G. MAMANTOV, D. L. MANNING AND J. M. DALE, *J. Electroanal. Chem.*, 9 (1965) 253.

8 G. MAMANTOV, J. M. STRONG AND F. R. CLAYTON, JNR., *Anal. Chem.*, 40 (1968) 488.
9 D. L. MANNING, *J. Electroanal. Chem.*, 7 (1964) 302.
10 K. KAWAMURA, *Electrochim. Acta*, 12 (1967) 1233.
11 T. KITAGAWA, *Chem. Abstr.*, 65 (1966) 16495; 66 (1967) 110, 946.
12 W. MICHAEL-KREBS AND P. K. ROE, *J. Electrochem. Soc.*, 114 (1967) 892.
13 N. WHITE, *Ph. D. Thesis*, 1969, Monash University, Victoria, Australia.
14 R. S. NICHOLSON, *Anal. Chem.*, 37 (1965) 667.
15 P. DELAHAY, *J. Am. Chem. Soc.*, 75 (1963) 1190.
16 S. ROFFIA AND M. LAVACCHIELLI, *J. Electroanal. Chem.*, 22 (1969) 117.
17 R. S. NICHOLSON AND I. SHAIN, *Anal. Chem.*, 36 (1964) 706.

ELECTROANALYTICAL CHEMISTRY AND INTERFACIAL ELECTROCHEMISTRY
Elsevier Sequoia S.A., Lausanne – Printed in The Netherlands

UNTERSUCHUNGEN ZUR ANODISCHEN OXIDATION VON AMMONIAK AN PLATIN-ELEKTRODEN*

H. GERISCHER UND A. MAUERER
Institut für Physikalische Chemie, Technische Hochschule, München (D.B.R.)
(Eingegangen am 1. Dezember, 1969)

1. EINLEITUNG

Die Autoren, die bisher das Problem der anodischen Oxidation von Ammoniak bearbeitet haben, stimmen lediglich in Bezug auf die Gesamtreaktion überein[1-9]. Danach läuft diese in basischen Elektrolyten nach der Bruttogleichung

$$2\,NH_3 + 6\,OH^- \rightarrow N_2 + 6\,H_2O + 6\,e^- \qquad (1)$$

mit praktisch 100%iger Ausbeute ab.

Erhebliche Unklarheit herrscht jedoch über den Mechanismus, der zu dieser Bruttoreaktion führt. Ebenso sind die bei längerer Versuchsdauer an den bisher verwendeten Elektroden auftretenden Vergiftungserscheinungen noch ungeklärt.

In den angegebenen Arbeiten wird als Reaktionsmechanismus ausnahmslos die sukzessive Dehydrierung des Ammoniakmoleküls mit gleichzeitiger Oxidation des freiwerdenden Wasserstoffs angenommen:

$$NH_{3\,aq} \rightarrow NH_{3\,ad} \qquad (2a)$$
$$NH_{3\,ad} + OH^- \rightarrow NH_{2\,ad} + H_2O + e^- \qquad (2b)$$
$$NH_{2\,ad} + OH^- \rightarrow NH_{ad} + H_2O + e^- \qquad (2c)$$
$$NH_{ad} + OH^- \rightarrow N_{ad} + H_2O + e^- \qquad (2d)$$
$$N_{ad} + N_{ad} \rightarrow N_{2ad} \qquad (2e)$$
$$N_{2ad} \rightarrow N_{2\,aq} \qquad (2f)$$

Den letzten Schritt in der vorgeschlagenen Reaktionskette bildet stets die Rekombination zweier an der Elektrodenoberfläche adsorbierter Stickstoffatome N_{ad} zu einem adsorbierten Stickstoffmolekül $N_{2\,ad}$, das dann in die Elektrolytlösung übertritt. Von verschiedenen Autoren[2,4] wird dieser Rekombinationsschritt Gl. (2e) als geschwindigkeitsbestimmend für die Gesamtreaktion betrachtet. Gegen diesen Ablauf spricht die Tatsache, dass Stickstoff in Nitridform sehr fest an der Oberfläche von Übergangsmetallen haftet, was auch für die Bindung an das Pt gilt[10,11]. Das Experiment wird dies noch beweisen. Die Rekombination adsorbierter N-Atome und die nachfolgende Desorption als N_2 sollten daher extrem langsam ablaufen, sehr viel

* Auszug aus der von der Fakultät für Allgemeine Wissenschaften der Technischen Hochschule München genehmigten Dissertation des Dipl.-Ing. A. Mauerer.
Tag der Promotion: 29.4.1969

langsamer als man in der elektrochemischen Oxidation von Ammoniak findet. Wir werden deshalb einen anderen Mechanismus vorschlagen, in dem die Entstehung von adsorbierten N-Atomen nicht enthalten ist und somit diese Schwierigkeit entfällt.

2. EXPERIMENTELLES

In sämtlichen Versuchen wurde der Brennstoff Ammoniak direkt im Elektrolyten gelöst. Da eine Oxidation des Ammoniaks im sauren Milieu praktisch nicht möglich ist[4], wurden ausschliesslich basische Elektrolyte, nämlich KOH-Lösungen verschiedener Konzentrationen verwendet. Anscheinend reagiert in der Oxidationsreaktion nicht das in Säuren hauptsächlich vorhandene NH_4^+-Ion, sondern das in basischen Lösungen dominierende NH_3-Molekül.

Als Messelektroden wurden hauptsächlich platinierte Platin-Draht-Elektroden (Pt/Pt-Elektroden) verwendet, wie sie bereits Spahrbier und Wolf[2] beschrieben haben. Als Bezugselektroden wurden Quecksilberoxid-Elektroden (Hg/HgO-Elektroden) benützt. Wenn nicht anders angegeben, beziehen sich alle Potentiale jedoch auf eine Wasserstoff-Elektrode in derselben Lösung, in der die Messung durchgeführt wurde, bei einem Wasserstoffpartialdruck $p_{H_2}=1$ atm (bezeichnet durch U_H). Die Elektrolytlösung wurde vor jeder Messreihe etwa 2 Stunden lang mit nachgereinigtem Stickstoff gespüllt, um eventuell störenden Sauerstoff zu entfernen. Teilweise wurde diese Spülung auch während der Messungen fortgesetzt.

3. ERGEBNISSE

3.1. *Das Ruhepotential*

Das Ruhepotential, das sich in einer $1M$ KOH + $1M$ NH_3-Lösung an einer Pt/Pt-Elektrode einstellt, liegt bei etwa +420 mV und ist innerhalb einer Streubreite von etwa 20 mV reproduzierbar. Es kann also auf keinen Fall durch die mit Sicherheit irreversible[3,12] Bruttoreaktion Gl. (1) bestimmt sein, denn für diese liegt das errechnete theoretische Normalpotential bei etwa 92 mV. Die Abhängigkeit des gefundenen Ruhepotentials von der NH_3-Konzentration ist in Abb. 1 dargestellt. Wie sich aus

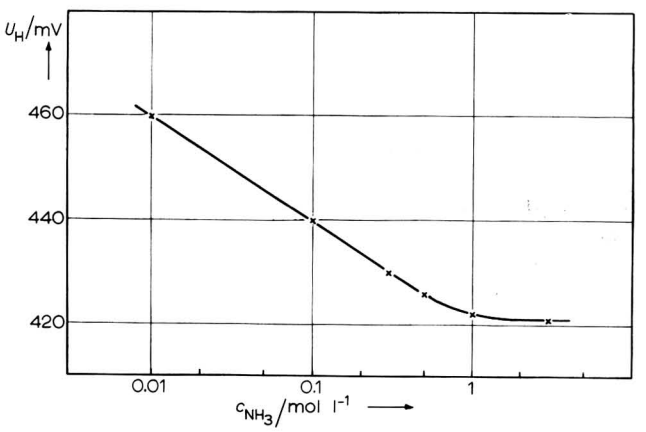

Abb. 1. Abhängigkeit des Ruhepotentials von der Ammoniak-Konzentration. Pt/Pt-Elektrode in $1M$ KOH + NH_3-Lösung.

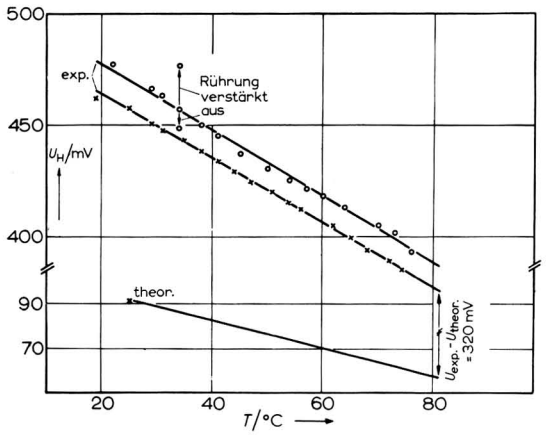

Abb. 2. Abhängigkeit des Ruhepotentials einer Pt/Pt-Elektrode von der Temperatur der Elektrolytlösung. Massstab zwischen theoretischer Kurve und den experimentell ermittelten Werten unterbrochen. (×) 1*M* KOH + 1*M* NH_3, (○) 1*M* KOH + 0.1*M* NH_3.

Abb. 2 erkennen lässt, wird der Unterschied zwischen dem experimentellen und dem theoretischen Wert mit steigender Temperatur geringer. Trotzdem besteht auch bei höherer Temperatur immer noch eine Differenz von einigen 100 mV.

Bemerkenswert ist, dass das Ruhepotential bei Rührung des Elektrolyten ansteigt, wie in Abb. 2 für einen Messpunkt eingezeichnet. Bei ruhendem Elektrolyten fällt es wieder auf den ursprünglichen Wert zurück. Nachdem oxidierende Stoffe im Elektrolyten als Ursache für dieses Verhalten ausgeschlossen werden konnten, bleibt nur eine Belegung der Elektrode mit Zwischenprodukten aus der potentialbestimmenden Elektrodenreaktion als Ursache dafür übrig. Durch Rührung werden diese Produkte schneller von der Elektrodenoberfläche in das Lösungsinnere abtransportiert und das Potential stellt sich den veränderten Konzentrationsverhältnissen entsprechend positiver ein.

Als ein mögliches Zwischenprodukt kommt vor allem Wasserstoff aus einer Spaltungsreaktion des Ammoniaks in Betracht. Die aus einer solchen katalytischen Spaltung resultierende H_2-Konzentration vor der Elektrode kann zwar nur sehr gering sein, weil das Gleichgewicht der Ammoniak-Spaltung fast vollständig auf der Seite des undissoziierten NH_3-Moleküls liegt. Für diese Annahme spricht aber, dass schon ein geringer Zusatz von H_2 zum Elektrolyten das Potential in negativer Richtung ändert. Da aber sicher noch andere Durchtrittsreaktionen neben denen der Wasserstoff-Oxidation gleichzeitig an der Elektrode ablaufen, ist das gemessene Ruhepotential sicher ein Mischpotential, das nur zum Teil durch die Wasserstoffkonzentration bestimmt wird. Genauere Aussagen über die einzelnen beteiligten Reaktionen lassen sich zur Zeit nicht machen.

3.2. *Periodische Strom–Spannungs-Kurven (i–U-Kurven)*

Die von Will und Knorr[13] entwickelte potentiostatische Dreieckspannungsmethode ist schon vielfach für die Untersuchung der anodischen Oxidation von Brennstoffen benutzt worden[14–20].

In Abb. 3 ist das Verhalten einer Pt-/Pt-Elektrode bei Anwendung der potentiostatischen Dreieck-Spannungsmethode in KOH ohne und mit NH_3 gegenübergestellt. In Abb. 4 lässt sich die Entwicklung des ersten Strommaximums Ox-1 für die Ammoniakoxidation aus dem ersten Peak für die Sauerstoffadsorption besonders gut verfolgen.

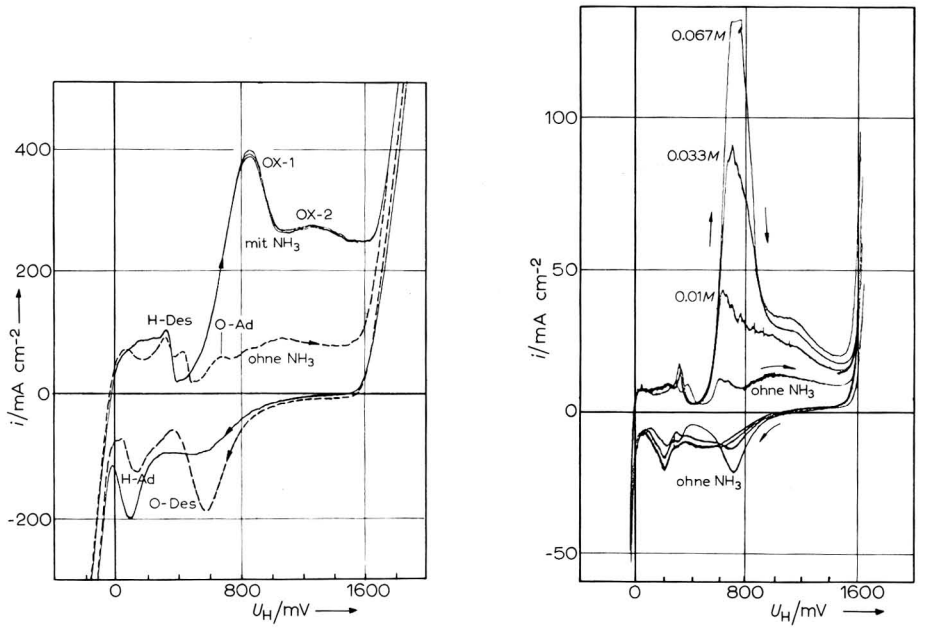

Abb. 3. Periodische i–U-Kurve an einer Pt/Pt-Elektrode in 1M KOH bzw. 1M KOH + 1M NH_3. Spannungsgeschwindigkeit 400 mV s^{-1}, 25°C.

Abb. 4. Periodische Strom–Spannungs-Kurven an einer Pt/Pt-Elektrode in 1M KOH bei Zugabe von kleinsten Mengen Ammoniaks. (Die Entwicklung des Oxidationsmaximums für NH_3 aus dem Maximum O-Ad der Grundkurve ist deutlich zu erkennen). Spannungsgeschwindigkeit 38 mV s^{-1}, 25°C.

Bei einer NH_3-Konzentration von etwa 1–3 Mol l^{-1} erreichen beide Oxidationspeaks Ox-1 und Ox-2 ihren Höchstwert und fallen mit weiter zunehmender Konzentration wieder langsam ab. Gleichzeitig verschieben sie sich etwas in anodischer Richtung.

Die kathodische Sauerstoff-Desorption bei etwa 600 mV ist nach der Zugabe von NH_3 stark gehemmt. Sie wird in den Potentialbereich der Wasserstoff-Adsorption bei 100 mV verschoben und bewirkt eine scheinbare Verstärkung des H-Adsorptionspeaks.

Wegen dieser verzögerten O-Desorption erscheint im kathodischen Durchlauf auch kein anodischer Strom für die Oxidation von NH_3. Die bis zu Potentialen von etwa 300 mV reichende starke Sauerstoffbelegung der Elektrode behindert offenbar die Oxidation des Ammoniaks: Auch im anodischen Durchlauf fallen die NH_3-Oxidation und damit die Maxima Ox-1 und Ox-2 fast vollständig aus, wenn im vorhergehenden kathodischen Durchlauf schon vor dem H-Ad-peak, z.B. bei 400 mV, wieder auf anodischen Potentialvorschub geschaltet wird.

Die Anwesenheit von NH_3 im Elektrolyten behindert aber nicht nur die O-Desorption sondern auch die H_2- und O_2-Entwicklung in den kathodischen und anodischen Umkehrpunkten der *i–U*-Kurven.

In den "quasistationären" *i–U*-Kurven, d.h. bei sehr langsamem Durchlauf, erscheint das Maximum Ox-1 ganz besonders deutlich, weil die übrigen Peaks, die zum grössten Teil Adsorptions- und Desorptionsvorgänge repräsentieren, wegen des langsamen Spannungsvorschubs fast vollständig verschwinden (Abb. 5). Bemerkenswert ist, dass der Oxidationsstrom sofort abfällt, wenn der Spannungsvorschub im Bereich dieses Maximums gestoppt oder umgekehrt wird. Das besagt, dass auch bei sehr niederiger Spannungsgeschwindigkeit das Gleichgewicht im Maximum noch nicht eingestellt ist. In der Diskussion wird auf diesen Punkt nochmals zurückgegriffen werden. Interessant ist in diesem Zusammenhang ein Vergleich der periodischen *i–U*-Kurven an Platin-Elektroden für Ammoniak und verschiedene andere Brennstoffe. Aus der Zusammenstellung von Kutschker und Vielstich[21] und aus ähnlichen Arbeiten anderer Autoren[14,22–25] ersieht man, dass für die verschiedenen untersuchten Brennstoffe (z.B. Methanol, Äthanol, Ameisensäure, Essigsäure,

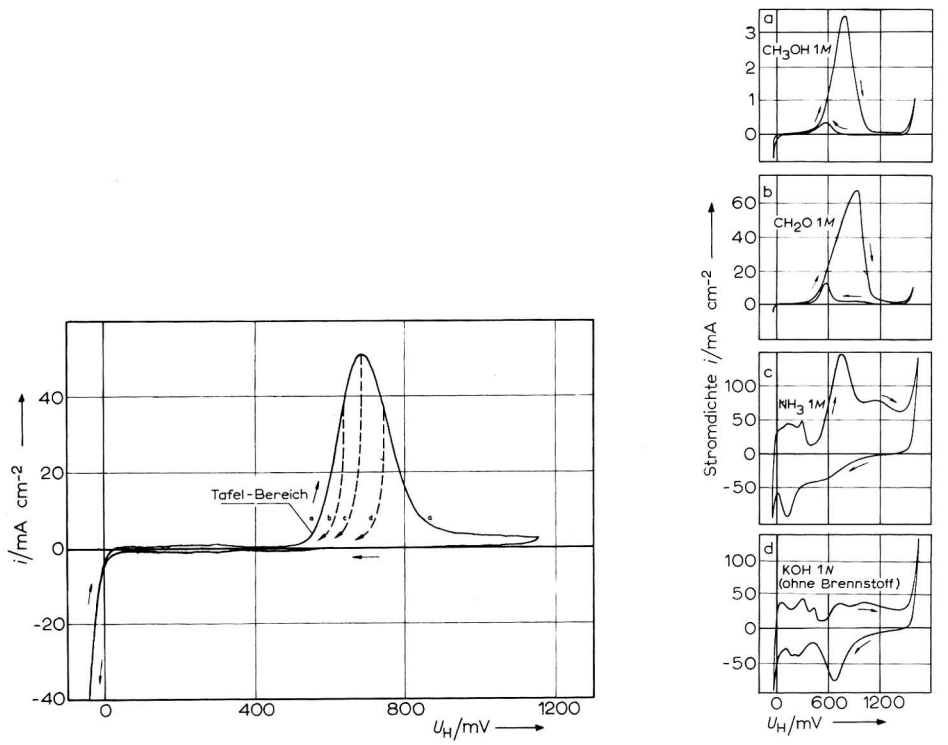

Abb. 5. Quasistationäre Strom–Spannungs-Kurve an einer Pt/Pt-Elektrode in 1*M* KOH + 1*M* NH_3, 25°C, Spannungsgeschwindigkeit 1 mV s^{-1}. (a) Kurve vollständig durchfahren. (b, c, d) Spannungsvorschub bereits vorzeitig im Maximum Ox-1 umgekehrt; Steiler Abfall des Oxidationsstromes im Umkehrpunkt!

Abb. 6. Periodische Strom–Spannungs-Kurven an Pt/Pt-Elektroden in 1*m* KOH bei Zusatz verschiedener Brennstoffe. Spannungsgeschwindigkeit 50 mV s^{-1}, 25°C. (a, b) nach Vielstich.

Formaldehyd, Acetaldehyd) sowohl im Sauren als auch im Basischen die anodischen Oxidationsmaxima alle bei demselben Potential auftreten, nämlich dort, wo in der Grundkurve ohne Brennstoff die beiden Sauerstoff-Adsorptionsmaxima liegen (Abb. 6). Das spricht eindeutig dafür, dass adsorbierte OH-Radikale an der Oxidationsreaktion der angegebenen Brennstoffe beteiligt sind. Diese OH-Radikale entstehen in einer vom Brennstoff unabhängigen vorgelagerten elektrochemischen Reaktion, wahrscheinlich einer oxidativen Adsorption von OH^--Ionen an der Elektrodenoberfläche nach der Reaktionsgleichung

$$OH^-_{aq} \rightleftharpoons OH^{(\delta-)}_{ad} + (1-\delta)e^- \qquad (3)$$

mit $0 \leqq \delta \leqq 1$.

Entsprechende Ergebnisse beweisen die Beteiligung von OH_{ad}-Radikalen auch bei der Ammoniak-Oxidation. Wie bereits in den Abb. 3 und 4 dargestellt, gehen an der Pt-Elektrode die beiden anodischen Maxima der Ammoniak-Oxidation eindeutig aus den Maxima für die Sauerstoff-Adsorption hervor. Auch an einer Gold-Elektrode setzt die Oxidation von Ammoniak erst beim Potential der Sauerstoff-Adsorption ein, d.h. bei etwa 1200–1300 mV. Dass überhaupt eine Oxidbelegung an Platin-Elektroden in Anwesenheit von Ammoniak entsteht, konnte von Conway und Mitarb.[26] nachgewiesen werden.

Beim Vergleich der Strom–Spannungs-Kurven für die angegebenen organischen Brennstoffe und Ammoniak fällt noch ein wesentlicher Unterschied auf: Bei allen organischen Brennstoffen entsteht im kathodischen Rücklauf der *i–U*-Kurven nach der fast vollständigen Desorption des Sauerstoffs ein schwaches aber deutliches anodisches Oxidationsmaximum (vgl. Abb. 6a, b).

Für Ammoniak ist dies nicht der Fall, weil die die NH_3-Oxidation behindernde vollständige Sauerstoff-Belegung unter dem Einfluss von NH_3 erst bei etwa 100 mV desorbiert. Bewiesen wird dieser Einfluss von Ammoniak auf die Sauerstoffbelegung z.B. dadurch, dass auch die Oxidation von Methanol an Platin-Elektroden durch Zugabe von Ammoniak zum Elektrolyten gehemmt wird. In der Strom–Spannungs-Kurve der Methanol-Oxidation verschwindet nach Zusatz von geringen Mengen Ammoniaks nicht nur der im kathodischen Durchlauf erscheinende schwache Oxidationspeak, sondern auch das anodische Oxidationsmaximum wird ziemlich abgeschwächt.

3.3. *Potentiostatische Strom–Zeit-Kurven*

Wie bereits Spahrbier und Wolf[2] gezeigt haben, fällt nach sprunghaftem Übergang vom Ruhepotential zu einem vorgegebenen konstanten anodischen Potential der Oxidationsstrom anfänglich sehr rasch, später langsamer ab. Nach einigen Stunden Belastung fliessen nur noch wenige Prozent des Anfangsstromes, d.h. die Elektrodenoberfläche wird entweder durch Reaktionsprodukte der Ammoniak-Oxidation ("self-passivation") oder durch gleichzeitig gebildete Oberflächenoxide vergiftet. Dass es sich tatsächlich um einen solchen Effekt handelt und nicht um eine blosse Diffusionshemmung, wird dadurch bewiesen, dass dieser Abfall des Stromes durch Rührung nicht beeinflusst werden kann.

Durch kurzzeitiges Abschalten der anodischen Belastung für einige Minuten lässt sich diese Blockierung fast vollständig wieder rückgängig machen. Das Potential der Elektrode strebt während dieser Reaktivierungspause dem ursprünglichen

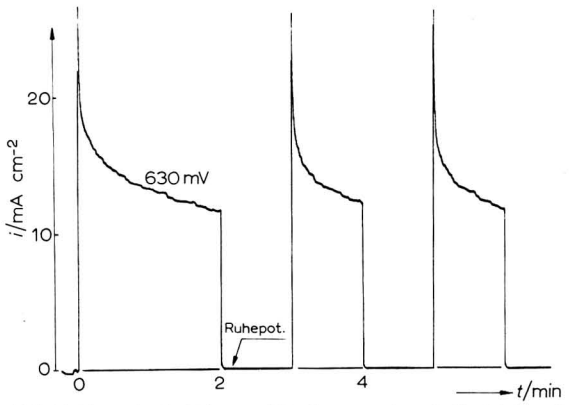

Abb. 7. Abwechselnde Be- und Entlastung einer Pt/Pt-Elektrode in 1*M* KOH + 1*M* NH_3 bei 25°C. Ruhepotential bei Beginn der Messung + 440 mV.

Ruhepotential zu und kommt ihm umso näher, je länger diese Pause ausgedehnt wird und je kürzer die vorangegangene Belastung war. In Abb. 7 ist eine Reihe solcher aufeinanderfolgender Belastungen mit dazwischenliegendem Erholungsintervall dargestellt. Ein noch besserer Reaktivierungseffekt kann durch kurzzeitige kathodische Polarisierung bzw. Wasserstoff-Entwicklung erzielt werden.

Eine solche Reaktivierung der erschöpften Platin-Elektrode lässt sich mit der sog. "Ausschaltaktivierung" bzw. der "kathodischen Stromaktivierung" zur Auflösung von Passivschichten vergleichen, die sich vielfach an Elektrodenoberflächen bilden[27]. Die Funktion des Reduktionsmittels übernimmt in diesem Falle der Brennstoff Ammoniak.

Durch Erhöhung der Temperatur kann die Anfangsstromdichte in der Belastungsphase wesentlich gesteigert werden (bei konstanter Überspannung!), doch fällt der Strom dann auch rascher ab. Derselbe Effekt kann durch Erhöhung der KOH-Konzentration erzielt werden. Dagegen zeigt sich bei der Erhöhung der Ammoniak-Konzentration eine Steigerung des Anfangsstromes verbunden mit einem langsameren Abfall. Neben der soeben beschriebenen schnell eintretenden Blockierung der Elektrode findet auch noch eine langsame irreversible Vergiftung der Elektrodenoberfläche statt, die nicht durch Ausschalten oder kathodische Belastung beseitigt werden kann. Diese Vergiftung macht sich dadurch bemerkbar, dass bei der in Abb. 7 dargestellten pulsierenden Belastung der Elektrode der über die Zeiteinheit gemittelte Strom langsam absinkt. Auch durch Variation der Belastungs- und Erholungsintervalle von einigen Stunden bis herab zu wenigen msec oder durch Temperaturerhöhung kann dieser Abfall der Aktivität bei lange andauernden Experimenten nicht ausgeschlossen werden.

Durch ein analytisches Verfahren konnte nachgewiesen werden, dass diese langsam eintretende Vergiftung durch atomar an der Elektrodenoberfläche adsorbierten Stickstoff verursacht wird. Für diesen Nachweis wurde eine zylindrische Elektrode aus platiniertem Platinblech von etwa 50 cm^2 Oberfläche verwendet. Zunächst wurde an dieser Elektrode im potentiostatischen Verfahren solange Ammoniak oxidiert, bis die Elektrode nahezu inaktiv war. Die danach auf der Elektrodenoberfläche vorhandenen Reaktionsprodukte konnten dann durch induktives Auf-

heizen der Elektrode auf etwa 400–600°C unter Schutzgas von der Oberfläche abgelöst und im Gaschromatografen analysiert werden. Es zeigte sich, dass maximal eine monoatomare Schicht N_{ad} auf der Elektrodenoberfläche adsorbiert wird, wenn man ein Verhältnis effektive/geometrische Oberfläche von etwa 1000 zugrundelegt. Die gleichzeitig gefundenen Spuren an Wasserstoff und, bei sehr stark anodischer Polarisierung auch von Sauerstoff, konnten gegenüber Stickstoff vernachlässigt werden.

4. DISKUSSION DER ERGEBNISSE UND VORSCHLAG EINES REAKTIONSMECHANISMUS

Die wichtigsten experimentellen Ergebnisse für die Erstellung eines Reaktionsmechanismus sind:

1. Die NH_3-Oxidation läuft nur unter Beteiligung von an der Elektrodenoberfläche adsorbierten OH-Radikalen ab.

2. Die bei der Oxidation eintretende Desaktivierung der Elektrode erfolgt

(*a*) durch einen schnellen Passivierungsvorgang, der aber durch kathodische Polarisation wieder aufgehoben werden kann,

(*b*) durch eine langsame, völlig irreversible Belegung der Elektrodenoberfläche mit adsorbiertem Stickstoff N_{ad}.

Der einfachste mit der ersten Feststellung zu vereinbarende Reaktionsmechanismus ist eine sukzessive Dehydrierung des Ammoniakmoleküls nach Gl. (2), wie z.b. von Spahrbier und Wolf[2] vorgeschlagen, jedoch unter Beteiligung von adsorbierten OH-Radikalen an mindestens einem Schritt. Diese Reaktionskette kann jedoch nicht mit der Rekombination zweier adsorbierter Stickstoffatome enden. Dieser letzte Schritt läuft offenbar, im Gegensatz zu den Annahmen verschiedener Autoren, sehr langsam ab. So mussten für die Analyse im Gaschromatografen 400–600°C angewendet werden, um den nach langer Belastung an der Elektrode adsorbierten Stickstoff ablösen zu können. Bei Zimmertemperatur ist dies auch unter Vakuum nicht möglich. Aus diesem Grunde kann die sogenannte Ausschaltaktivierung der Elektrode, wie sie bei den potentiostatischen Strom–Zeit-Kurven angewendet wurde, keinesfalls auf einer Rekombination atomar adsorbierten Stickstoffs beruhen.

Wesentlich näher liegt die Vermutung, dass die schnelle Inaktivierung der Elektrode durch eine Blockierung der NH_3-Adsorption infolge zu starker Belegung der Oberfläche mit adsorbiertem Sauerstoff verursacht wird. Die zunächst beim Ruhepotential nur mit adsorbiertem Ammoniak belegte Elektrode bedeckt sich nach dem Umschalten auf das Messpotential, bei dem die Ammoniak-Oxidation abläuft, in sehr kurzer Zeit mit OH-Radikalen. Es ist wahrscheinlich, dass diese OH-Radikale zunächst an bereits mit NH_3 belegten Adsorptionsplätzen hinzutreten. Die geometrischen Verhältnisse erlauben ohne Schwierigkeiten die gleichzeitige Adsorption eines NH_3-Moleküls und eines OH-Radikals pro Oberflächenatom des Pt-Gitters, wie man anhand eines Kalottenmodelles feststellen kann. In der folgenden Konkurrenz um frei werdende Adsorptionsplätze kann die OH^--Adsorption die weitere NH_3-Adsorption umso mehr zurückdrängen, je positiver das Potential ist. Das erklärt das rasche Absinken des Oxidationsstromes.

Bei kontinuierlichem Potentialvorschub spielen sich demnach folgende Prozesse ab: Zunächst erhöht sich die Zahl der Oberflächenplätze, die aufgrund ihrer Belegung mit adsorbierten OH-Radikalen für eine Oxidationsreaktion mit Ammoniak

geeignet sind, mit dem ansteigenden Potential. Dies führt zu einer ständigen Erhöhung des Ammoniak-Oxidationsstromes. Gleichzeitig verändert sich mit dem wachsenden Potential aber auch die Zahl der blockierten Plätze durch ausschliessliche Belegung mit OH_{ad}. Diese beiden gegenläufigen Effekte bewirken die Ausbildung des Maximums Ox-1.

Dieser Reaktionsablauf kann ausserdem erklären, dass die potentiostatischen Strom–Zeit-Kurven umso schneller abfallen, je grösser der Potentialsprung und die KOH-Konzentration bei konstanter NH_3-Konzentration sind. Jedoch geht diese Blockierung je nach dem angelegten Elektrodenpotential nur bis zu einem bestimmten Ausmass.

Das erkennt man daran, dass der Strom bei festgehaltener Spannung bis auf einen sehr kleinen Wert abfällt, aber sofort wieder ansteigt, wenn die Spannung positiver gemacht wird. Das zeigt Abb. 8 für das Wiedereinschalten eines kontinuierlichen Spannungsvorschubs.

Wir möchten für diese Adsorptionsphänomene, welche mit der Oxidationsreaktion einhergehen, folgende Deutung geben: Anscheinend besteht zwischen den verschiedenen möglichen Adsorptions-Zuständen der Pt-Oberfläche ein potentialabhängiges Gleichgewicht. Bei niedrigem Potential, etwa im Bereich des Ruhepotentials, herrscht die Belegung der Pt-Oberfläche mit NH_3-Molekülen vor. Da die Bindung des NH_3-Moleküls an ein Pt-Atom durch ein freies Elektronen-Paar erfolgt und die H-Atome benachbarter NH_3-Moleküle stark abstossend aufeinander wirken, kann angenommen werden, dass in diesem Zustand jedes Pt-Atom nur mit einem NH_3-Molekül besetzt ist.

Mit steigendem anodischen Potential werden dann sowohl an unbesetzten wie auch an bereits mit NH_3 belegten Pt-Atomen OH^--Ionen adsorbiert. Diese Adsorption ist mit einer zumindest partiellen Entladung zu OH-Radikalen verbunden und deshalb wesentlich stärker vom Potential beeinflusst als die NH_3-Adsorption. Die dehydrierende Oxidation der adsorbierten NH_3-Moleküle zu NH_x-Radikalen erfolgt durch diese adsorbierten OH-Radikale.

Mit weiter ansteigendem Elektrodenpotential werden die durch die Oxidation

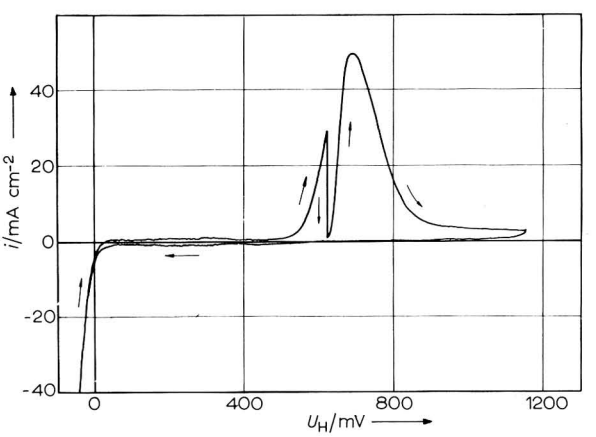

Abb. 8. Quasistationäre Strom–Spannungs-Kurve nach Abb. 5. Spannungsvorschub im Anstieg zum Maximum Ox-1 für 2 s unterbrochen.

freiwerdenden Plätze vermehrt mit OH^- anstatt mit NH_3 belegt, so dass schliesslich an jedem Pt-Atom mindestens zwei OH-Radikale bzw. ein oder mehrere O-Atome adsorbiert sind[28]. Das verhindert schliesslich die Oxidation von NH_3 weitgehend.

Ein kritischer Punkt im Reaktionsablauf ist die Entstehung der N–N-Bindung aus den Oxidationsprodukten des Ammoniaks. Da adsorbierte N-Atome dazu offenbar besonders schlecht fähig sind, weil ihre Chemisorptionsbindung an die Pt-Oberfläche zu stark ist[10,11] liegt die Annahme nahe, dass die N–N-Bindung durch Rekombination zweier NH_x-Radikale ($x = 2, 1$) in einem früheren Stadium geschlossen wird. Demnach führt die völlig Dehydrierung des NH_3-Moleküls ohne Rekombination in einer Zwischenstufe zur dauerhaften Blockierung der Oberfläche infolge Nitridbildung. Die lange Zeit, welche bis zu der irreversiblen Inaktivierung vergeht, zeigt, dass es sich hierbei nur um eine anteilmässig sehr untergeordnete Nebenreaktion handeln kann. In der Hauptreaktion entsteht aus den zwei Radikalen NH_x ein Zwischenprodukt N_2H_y ($2 \leqq y \leqq 4$). Solche Produkte werden sehr glatt bis zu N_2 oxidiert, wie man von der Hydrazin-Oxidation weiss.

Für eine solche frühzeitige Bildung der N–N-Bindung sprechen auch die neueren Untersuchungen zur Ammoniak-Synthese von Schmidt[29] und Brill und Mitarb.[30]. In diesen Arbeiten wurde festgestellt, dass der einleitende Schritt für die Ammoniak-Synthese aus gasförmigem Stickstoff und Wasserstoff an Eisen-Katalysatoren eine nichtdissoziative Adsorption des Stickstoffmoleküls ist. Die Bindung zwischen den beiden Stickstoffatomen wird erst gelöst, nachdem bereits ein oder mehrere Wasserstoffatome an das adsorbierte Stickstoffmolekül angelagert sind. In unserem System verläuft die Reaktion zwar in umgekehrter Richtung; die Teilreaktionen sollten trotzdem analog ablaufen. Ein ähnliches Ergebnis wurde auch von Fogel und Mitarb.[31] für die NH_3-Spaltung in der Gasphase gefunden. Diese Vorstellungen lassen sich in dem folgenden Reaktionsschema zusammenfassen (Abb. 9):

$$OH^-_{aq} \longrightarrow OH^{(\delta-)}_{ad} + (1-\delta)e^- \qquad (3)$$

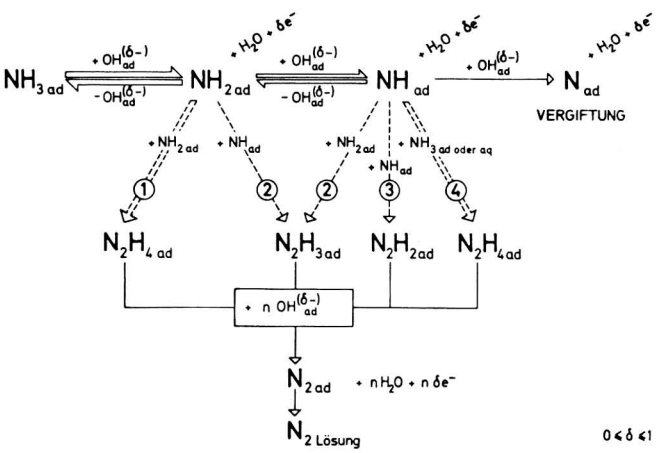

Abb. 9. Reaktionsschema zur Oxidation von Ammoniak an der Platin-Elektrode.

Die ausgezogenen Pfeile zeigen elektrochemische, d.h. potentialabhängige Prozesse an, die gestrichelten Pfeile stellen chemische Reaktionen dar. Die elektrochemischen Reaktionen sind so formuliert, dass partielle Ladungsübergänge im Adsorptionszustand zugelassen bleiben. Das gilt auch für die einzelnen Oxidationsschritte des Ammoniaks und ist z.B. für den ersten Schritt in folgender Weise ausgedrückt:

$$NH_{3\,ad} + OH_{ad}^{(\delta-)} \rightleftharpoons NH_{2\,ad} + H_2O + \delta e^- \qquad (4)$$

Die sonstigen potentialabhängigen Oxidationsschritte sind in gleicher Weise zu verstehen, wobei δ mit dem angelegten Potential variieren dürfte. Bei dem Reaktionsmechanismus ist auch die Möglichkeit in Betracht gezogen, dass der Reaktionspartner für die Ausbildung der N–N-Bindung an einem adsorbierten Radikal auch ein NH_3-Molekül aus der Lösung sein könnte (Reaktionsweg 4).

Der Reaktionsweg, der zum adsorbierten N-Atom führt, ist in unserem Schema nicht durch einen Rekombinationsschritt fortgesetzt. Er stellt in diesem Schema die irreversible Inaktivierung dar. Wir glauben zu dieser Annahme berechtigt zu sein, da die Desorption von adsorbierten N-Atomen offensichtlich erst bei sehr viel höheren Temperaturen messbar wird. Wegen der mit starker Polarität der Bindung gekoppelten Wechselwirkung im adsorbierten Zustand der Reaktionspartner und der Inhomogenität der verwendeten Pt-Oberfläche scheint es uns nicht sinnvoll, detaillierte kinetische Gleichungen aufzustellen. Man kann von einem solchen Modell nicht mehr verlangen, als dass es die beobachteten Messergebnisse qualitativ befriedigend wiedergibt.

Trägt man den Stromverlauf im Anstiegsbereich des NH_3-Oxidationsmaximums (vgl. Abb. 5) bei sehr langsamer Spannungsänderung logarithmisch gegen das Potential auf, so erhält man eine Gerade (Tafel-Gerade). Die Neigung dieser Geraden erwies sich in unseren Versuchen als stark temperaturabhängig, im Gegensatz zu den Befunden anderer Autoren[3,4]. Bei 0°C findet man Werte zwischen 80 und 110 mV/Dekade, was etwa $3RT/2F$–$2RT/F$ entspricht. Mit zunehmender Temperatur fällt diese Steigung ab und erreicht bei etwa 80°C einen Wert von 35 mV/Dekade $\approx RT/2F$.

Aus diesen Neigungen der Tafel-Geraden kann man folgende Schlüsse ziehen:

Bei Annahme einfachster Kinetik wäre eine Steigung $RT/2F$ entweder für den Reaktionsweg 1 mit der Rekombination von zwei $NH_{2\,ad}$ als geschwindigkeitsbestimmendem Schritt oder den Reaktionsweg 4 mit der Rekombination zwischen NH_{ad} und NH_3 als langsamstem Schritt zu erwarten. Für den ersten Weg spricht eine Beobachtung bei der Photolyse des Ammoniaks. Schindler und Mitarb.[32] konnten dabei feststellen, dass bevorzugt NH_2-Radikale gebildet werden. Die energetisch gleichfalls mögliche Spaltung zu NH und H_2 findet nicht statt. Allerdings sind solche Stabilitätsbetrachtungen nicht ohne weiteres auf den adsorbierten Zustand zu übertragen.

Eine Vergrösserung des Neigungsfaktors bis maximal $RT/\alpha F$ ($\alpha < 1$) würde sich ergeben, wenn der erste Oxidationsschrit zu $NH_{2\,ad}$ geschwindigkeitsbestimmend würde. Die Befunde deuten auf eine solche Verlagerung des geschwindigkeitsbestimmenden Schrittes zu einem Reaktionsschritt am Anfang der Folge mit sinkender Temperatur hin. Eine genauere Analyse erscheint jedoch auch hier angesichts der Komplexität der Reaktionsmöglichkeiten und der Inhomogenität der Elektroden-

oberfläche nicht als sinnvoll. Für ein prinzipielles Verständnis des Reaktionsablaufs reichen diese Befunde aber aus.

ZUSAMMENFASSUNG

Die elektrochemische Oxidation des Ammoniak in stark alkalischer Lösung wurde an platinierten Platin-Elektroden untersucht. Aufgrund der gefundenen Messergebnisse und der Analyse der Reaktionsprodukte wird ein Reaktionsmechanismus vorgeschlagen, bei dem die Oxidation des NH_3-Moleküls im adsorbierten Zustand durch gleichzeitig adsorbierte OH-Radikale erfolgt. Aus den als Zwischenprodukten entstehenden NH_x-Radikalen ($x=2$ oder 1) enstehen durch Rekombination N_2H_y-Moleküle ($y=4$ oder 2) bzw. Radikale ($y=3$), welche sehr rasch zu N_2 oxidiert werden. In einer Nebenreaktion entstehende N-Atome bleiben dagegen auf der Oberfläche chemisorbiert und bewirken die beobachtete irreversible Inaktivierung der Elektrode.

SUMMARY

The electrochemical oxidation of ammonia has been studied at platinized platinum electrodes in strongly alkaline solution. As a result of electrochemical studies and of analytical investigation of the products, a reaction mechanism is proposed in which the oxidation of NH_3-molecules occurs by OH-radicals which are simultaneously adsorbed at the same surface sites. The intermediate products are NH_x-radicals ($x=2$ or 1) which form N_2H_y-molecules ($y=4$ or 2) or an N_2H_3-radical by recombination. These products can easily be oxidized to form molecular nitrogen. N-atoms are produced only very slowly in a parallel reaction. They are so strongly chemisorbed on the surface that no recombination is possible, but their production causes the irreversible inactivation of the catalytic electrode as observed after some longer period of time.

DANK

Der Deutschen Forschungsgemeinschaft und der Firma Varta A.G. sind wir für die Förderung dieser Arbeit sehr zu Dank verpflichtet.

LITERATUR

1 W. VIELSTICH, *Brennstoffelemente*, Verl. Chemie GmbH Weinheim/Bergstrasse, 1965, S. 277.
2 D. SPAHRBIER UND G. WOLF, *Z. Naturforsch.*, 19a (1964) 614.
3 A. R. DESPIĆ, D. M. DRAŽIĆ UND P. M. RAKIN, *Electrochim. Acta*, 11 (1966) 997.
4 H. G. OSWIN UND M. SALOMON, *Can. J. Chem.*, 41 (1963) 1686.
5 R. A. WYNVEEN, Symposium Am. Chem. Soc., Chicago, 1961, B. 49.
6 E. MÜLLER UND F. SPITZER, *Z. Elektrochem.*, 11 (1905) 917.
7 R. A. WYNVEEN in C. G. YOUNG (Ed.), *Fuel Cells*, Vol. II, Reinhold Publishing Co. New York, Chapman and Hall Ltd., London, 1963, p. 153.
8 I. MAY, VARTA-EDU, unveröffentlicht.
9 T. KATAN UND R. J. GALIOTTO, *J. Electrochem. Soc.*, 110 (1963) 1022.
10 K. D. RENDULIC UND Z. KNORR, *Surface Sci.*, 7 (1967) 205.
11 J. F. MULSON UND E. W. MÜLLER, *J. Chem. Phys.*, 38 (1963) 2615.
12 W. VIELSTICH, *Brennstoffelemente*, Verl. Chemie GmbH Weinheim/Bergstrasse, 1965, S. 111.

13 F. G. WILL UND C. A. KNORR, *Z. Elektrochem.*, 64 (1960) 258, 270.
14 S. GILMAN UND M. W. BREITER, *J. Electrochem. Soc.*, 109 (1962) 622, 1099.
15 M. W. BREITER, *Electrochim. Acta*, 8 (1963) 973.
16 V. S. BAGOTZKY UND YU. B. VASILYEV, *Electrochim. Acta*, 9 (1964) 869.
17 J. GINER, *Electrochim. Acta*, 9 (1964) 63.
18 S. GILMAN, *J. Phys. Chem.*, 68 (1964) 70.
19 R. P. BUCK UND L. R. GRIFFITH, *J. Electrochem. Soc.*, 109 (1962) 1005.
20 D. R. RHODES, *Electrochim. Acta*, 9 (1964) 36.
21 A. KUTSCHKER UND W. VIELSTICH, *Electrochim. Acta*, 8 (1963) 985.
22 M. W. BREITER, *Electrochim. Acta*, 8 (1963) 447, 457.
23 W. VIELSTICH, *Brennstoffelemente*, Verl. Chemie GmbH Weinheim/Bergstrasse, 1965, S. 76 ff.
24 P. R. JOHNSON UND A. T. KUHN, *J. Electrochem. Soc.*, 112 (1965) 599.
25 D. R. RHODES UND E. F. STEIGELMANN, *J. Electrochem. Soc.*, 112 (1965) 16.
26 B. E. CONWAY, N. MARINCIC, D. GILROY UND E. RUDD, *J. Electrochem. Soc.*, 113 (1966) 1144.
27 K. J. VETTER, *Elektrochemische Kinetik*, Springer-Verlag, Berlin, 1961, S. 628.
28 T. BIEGLER UND R. WOODS, *J. Electroanal. Chem.*, 20 (1969) 73.
29 W. A. SCHMIDT, *Angew. Chem.*, 80 (1968) 151.
30 R. BRILL, E.-L. RICHTER UND E. RUCH, *Angew. Chem.*, 79 (1967) 905.
31 JA. M. FOGEL', B. T. NADIKTO, V. F. RIBALKO, R. P. SLABOSPITSKII, I. E. KOROBCHANSKAJA UND V. I. SHVACHKO, *J. Cat.*, 4 (1965) 153.
32 R. N. SCHINDLER, U. SCHURATH UND P. TIEDEMANN, Vortrag anlässlich der Bunsentagung, 1968, Augsburg.

ELECTROANALYTICAL CHEMISTRY AND INTERFACIAL ELECTROCHEMISTRY
Elsevier Sequoia S.A., Lausanne – Printed in The Netherlands

THE ELECTROCHEMICAL OXIDATION OF THE DIPHOSPHATE ESTER OF 2-METHYLNAPHTHOHYDROQUINONE

EUGENE P. MEIER AND JAMES Q. CHAMBERS*
Department of Chemistry, University of Colorado, Boulder, Colo. 80302 (U.S.A.)
(Received July 7th, 1969)

The electrochemical oxidation in aqueous media of the diphosphate ester of 2-methyl-1,4-naphthohydroquinone (Synkavit) is characterized in this paper using the techniques of cyclic, single-sweep, and ring-disc electrode voltammetry. Evidence is presented which shows that the oxidation proceeds *via* dephosphorylation of the one-electron intermediate over the entire pH range. The rate of approach to equilibrium for this reaction is pH dependent, decreasing as the pH increases. The mechanism suggested here appears to have some generality in describing oxidation of hydroquinone derivatives in aqueous solution.

Previous work in the general area of electrochemical oxidation of aromatic hydroxy compounds is reviewed by Adams[1] and Weinberg and Weinberg[2]. The results reported here amplify and extend the mechanistic conclusions of previous work on the anodic oxidation of quinol phosphates[3]. In this paper the time scale of the electrochemical experiments is extended by a factor of 10^3 over the previous work[3]. Specific adsorption of Synkavit occurs in acidic solutions and this aspect of the oxidation process has been reported previously[4].

The chemical oxidation of quinol phosphates with a variety of oxidizing agents has been studied by a number of workers[5-15]. A complete review is not appropriate here. Loss of the phosphate substituent was monitored by trapping with an alcohol to form the alkyl phosphate or by observing the formation of condensed phosphates, generally with the conclusion that a metaphosphate (PO_3^-) intermediate was involved. Isotopic labeling experiments indicate that the oxidation proceeds by two different pathways, P–O and C–O bond fission. The pathway of biological interest involves fission of the P–O bond in an unimolecular step to produce the metaphosphate species. In aqueous solution (pH 4)[8] or N,N-dimethylformamide[9], 30% P–O bond fission was shown to occur. Radical anions of the semiquinone phosphates have been detected by electron spin resonance (ESR) in basic solutions[11].

EXPERIMENTAL

Experimental details, including instrumentation, procedures, and chemical analysis of Synkavit have been described elsewhere[3,4,16]. Carbon paste electrodes were used throughout this investigation since well defined oxidation waves were not obtained with platinum electrodes.

* Present address: Department of Chemistry, University of Tennessee, Knoxville, Tenn. 37916.

All data reported here are the average of at least two and usually three separate measurements on newly prepared carbon paste surfaces. At slow sweep rates (less than 0.2 V s^{-1}) precision was excellent, ± 2–3 mV on peak potential data and better than $\pm 2\%$ on current function data. At fast sweep rates the reproducibility decreased because background currents become more difficult to reproduce. At these sweep rates the peak potential and current function data are good to *ca.* 5–10 mV and ± 5–10%, respectively. In the most basic solutions (pH 12) estimation of the background currents is especially difficult.

All solutions contained 0.5 *M* $NaClO_4$ as the supporting electrolyte and 0.02 *M* acetic, phosphoric, and boric acid as the buffer components. All peak potential data are given *vs.* an aqueous SCE.

RESULTS

Product identification

The anodic oxidation of Synkavit (abbreviated PQP in the equations below) in aqueous solutions is an irreversible two-electron process over the entire pH range investigated in this study: 1 *M* H_2SO_4 to pH 12. The corresponding quinone, 2-methyl-1,4-naphthoquinone (Q), and inorganic or pyrophosphate[5,13] are the overall products of the oxidation (eqn. 1).

$$PQP \rightarrow Q + 2[P] + 2e^- \qquad (1)$$

Identification of the quinone was made by cyclic voltammetry and electron spin resonance studies on electrolysis solutions. Cyclic voltammograms of Synkavit (Fig. 1) exhibit an oxidation wave at a potential *ca.* 0.5 V more positive than the

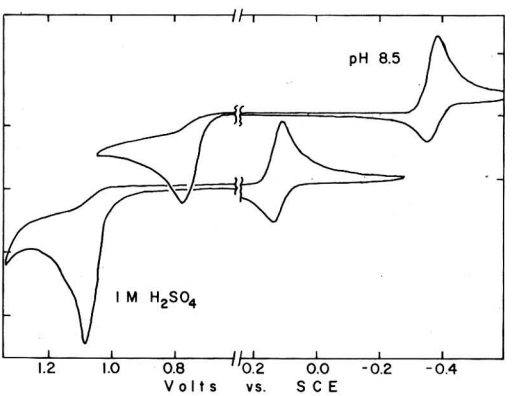

Fig. 1. Cyclic voltammograms of 0.72×10^{-3} *M* Synkavit in 1 *M* H_2SO_4 and pH 8.5. Sweep rate: 0.06 V s^{-1}; electrode area: 0.724 cm^2; 0.1 mA per ordinate division.

oxidation wave of the monophosphate[3] and waves due to the quinone redox couple on the reverse and subsequent cycle. No evidence of a reduction wave due to an intermediate species is detected at sweep rates up to 500 V s^{-1}. Cyclic voltammograms of authentic samples of the quinone are essentially identical to the product waves which are observed as a result of the Synkavit oxidation. An e.s.r. spectrum of $Q^{\cdot -}$ is

easily generated from neutral or basic solutions of Synkavit *after* electrolysis at a platinum anode. This behavior is analogous to that of the monophosphate derivative[3].

No attempt was made to determine the extent of P–O or C–O bond fission in the oxidation process, but mechanistic evidence presented below indicates that the oxidation is proceeding, at least in part, by P–O bond scission and generation of kinetically important metaphosphate species.

Coulometry at controlled potential gave an n-value of 2 (1.9 ± 0.1) from pH 1.9 to 11.0.

pH Dependence

Although the main oxidation wave is irreversible, a considerable amount of information can be obtained from the pH dependence of the peak voltammetry parameters. Table 1 presents some of these data. In acidic solutions (*e.g.* pH 1.9) the diffusion portion of the main oxidation wave is characterized by a relatively large current function (units: A cm^{-2} M^{-1} $V^{-\frac{1}{2}}$ $s^{\frac{1}{2}}$) and a narrow peak width: $i_p/AC\sqrt{v} \approx 2$, $E_p - E_{p/2} = 23$ mV. In this pH region the oxidation process is complicated by specific adsorption of Synkavit which masks the diffusion wave at low concentrations and fast sweep rates[4]. However, at high concentrations and slow sweep rates, the peak voltammetry parameters can be determined accurately. As the pH increases, the current function decreases and the wave broadens. This behavior is shown in Figs. 2 and 3. At pH 7.08 a single, broad oxidation wave is evident in the cyclic voltammograms, the current function is *ca.* 1.2 A cm^{-2} M^{-1} $V^{-\frac{1}{2}}$ $s^{\frac{1}{2}}$ and the peak width is *ca.* 45 mV. At pH greater than 7, the oxidation wave splits into two overlapping waves (Fig. 2) and the current function and peak width become independent of pH.

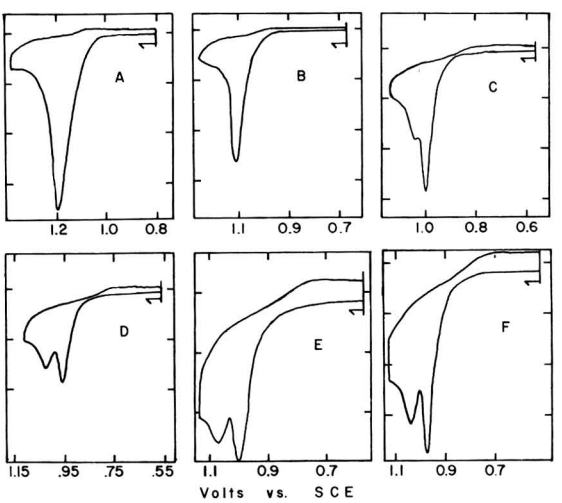

Fig. 2. Cyclic voltammograms of Synkavit in aqueous solution at fast sweep rates. (A) pH 1.90, 0.86×10^{-3} M Synkavit, 118 V s^{-1}, and 2.0 mA per ordinate division; (B) pH 3.60, 1.00×10^{-3} M Synkavit, 119 V s^{-1}, and 2.0 mA per ordinate division; (C) pH 6.40, 0.98×10^{-3} M Synkavit, 121 V s^{-1}, and 1.0 mA per ordinate division; (D) pH 8.10, 1.01×10^{-3} M Synkavit, 109 V s^{-1}, and 1.0 mA per ordinate division; (E) pH 9,40, 0.87×10^{-3} M Synkavit, 128 V s^{-1}, and 0.4 mA per ordinate division; (F) pH 10.20, 1.02×10^{-3} M Synkavit, 118 V s^{-1}, and 0.4 mA per ordinate division.

TABLE 1

PEAK VOLTAMMETRY PARAMETERS IN AQUEOUS SOLUTION

Solution/ pH ± 0.05	*Sweep Rate/V s^{-1}*	*$E_{p/2}$/ V vs. SCE*	*$E_p - E_{p/2}$/ mV*	*$i_p/AC\sqrt{v}$ / A cm^{-2} M^{-1} V$^{-\frac{1}{2}}$ s$^{\frac{1}{2}}$*	*$(\partial E_{p/2}/\partial \log v)_{pH}$/ mV*	*Concn./ mM l^{-1}*
1 *M* H_2SO_4	0.004	1.030	32	1.53	24	0.72
	0.03	1.045	37	1.67		
	0.06	1.052	38	1.73		
	0.10	1.054	41	1.74		
	1.20	1.098	42	2.51		0.67
	12.0	1.122	56	3.45		
	120	1.196	98	10.6		
1.90	0.004	0.990	23	1.88	24	0.49
	0.03	0.991	23	2.17		
	0.06	1.014	22	2.28		
	0.10	1.009	24	2.30		
	1.20	1.038	30	2.07		0.66
	12.0	1.063	30	2.53		
	120	1.128	44	7.67		
4.43	0.03	0.889	29	1.68	22	0.55
	0.06	0.889	30	1.61		
	0.10	0.889	35	1.61		
4.42	1.20	0.920	37	1.57		0.67
	12.0	0.966	49	2.06		
	120	1.032	42	4.07		
6.50	0.004	0.740	40	1.28	23	0.50
	0.03	0.754	43	1.27		
	0.06	0.762	46	1.22		
	0.10	0.764	48	1.20		
6.58	1.20	0.808	77	1.07		0.68
	12.0	0.892	34	1.50		
	120	0.946	33	2.78		
7.00	0.004	0.738	39	1.22	25	0.51
	0.03	0.761	44	1.19		
	0.06	0.765	47	1.14		
	0.10	0.780	50	1.11		
7.35	1.20	0.786	76	0.63		0.66
	12.0	0.868	42	1.10		
	120	0.923	27	1.82		
9.62	0.004	0.702	38	1.19	36	0.49
	0.03	0.734	43	1.12		
	0.06	0.745	49	1.09		
	0.10	0.749	49	1.01		
9.45	1.20	0.797	68	0.80		0.66
	12.0	0.832	70	0.64		
	120	0.905	50	0.47		
11.72	0.004	0.709	38	1.27	50	0.49
	0.03	0.725	44	1.20		
	0.06	0.748	53	1.16		
	0.10	0.739	48	1.16		

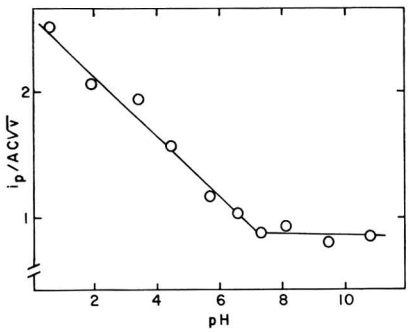

Fig. 3. Variation of current function with pH. Sweep rate: 1.20 V s^{-1}; electrode area: 0.113 cm^2; concn.: $(0.67 \pm 0.01) \times 10^{-3}$ *M*.

The dependence of the current function on pH is paralleled by the plots of $E_{p/2}$ *vs.* pH. In the acidic region, the half-peak potential ($E_{p/2}$) becomes negative by 40–55 mV per pH unit, depending on the sweep rate. Above pH 7, $E_{p/2}$ is independent of pH. The inflection points in these graphs correspond very well with the p*K* data on Synkavit, $pK_3 \approx pK_4 \approx 6.6_5$[4].

Although the current function changes markedly with pH (and sweep rate) the chronoamperometric constant ($it^{\frac{1}{2}}/AC$) is approximately constant over the entire pH range when the working electrode potential is stepped beyond all oxidation waves. Diffusion coefficients calculated from the Cottrell equation assuming a two-electron process are given in Table 2 as a function of pH. The observed diffusion coefficient

TABLE 2

DIFFUSION COEFFICIENT OF SYNKAVIT IN 0.5 *M* $NaClO_4$

Solution/ $pH \pm 0.05$	$D^{\frac{1}{2}}$/ *cm* $s^{-\frac{1}{2}}$
1.90	2.45×10^{-3}
3.85	2.31
4.43	2.24
5.81	2.32
6.50	2.09
6.75	2.03
7.00	2.08
7.85	2.02
9.62	2.10
11.72	1.80

varies with pH in accord with the p*K* values. The data indicate that diffusion coefficients of the neutral, dianion, and tetraanion species are *ca.* 6.0, 5.3, and 4.3×10^{-6} cm^2 s^{-1}, respectively.

Sweep rate dependence

In acidic solution the general shape of the peak voltammogram is independent of sweep rate after allowance is made for specific adsorption of electroactive species.

One relatively narrow oxidation wave is observed at sweep rates up to 500 V s^{-1}. The value of $E_{p/2}$ shifts to more positive potentials by 22 mV per decade increase in the sweep rate. This parameter is pH dependent, changing to *ca.* 50 mV per decade increase in the sweep rate in basic solutions.

In basic solutions the relative heights of the two waves which are observed are dependent on the sweep rate. This behavior is shown in Fig. 4. At slow sweep rates

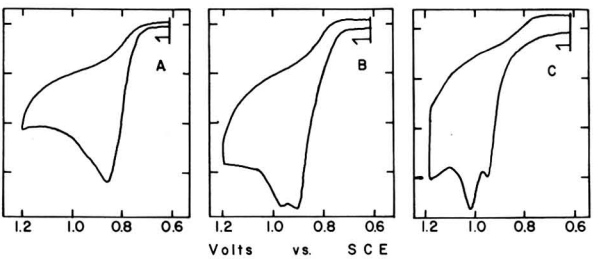

Fig. 4. Variation of peak voltammograms of 1.13×10^{-3} *M* Synkavit with sweep rate at pH 9.80. (A) 1.20 V s^{-1}, 0.04 mA per ordinate division; (B) 12.0 V s^{-1}, 0.10 mA per ordinate division; (C) 120 V s^{-1}, 0.40 mA per ordinate division.

the first wave dominates the composite wave and as the sweep rate increases, the contribution of the second wave becomes larger. This behavior is indicative of an e.c.e. mechanism. At high concentrations ($>1 \times 10^{-3}$ *M*) the current function for the overall oxidation wave decreases with sweep rate to *ca.* 0.6. Selected peak voltammetry parameters are given in Table 1 as a function of sweep rate.

Concentration dependence

The peak voltammograms are dependent on concentration at all pH values. In acid solutions the marked concentration dependence is a result of specific adsorption of the Synkavit molecule. In basic solutions there is also evidence of adsorption effects although these effects are not as striking as those in acid solution and only show up at low concentrations (*i.e.* $< 0.5 \times 10^{-3}$ *M*). At these concentrations the current function for the *initial* oxidation wave increases by *ca.* 50% at fast sweep rates and the wave tends to sharpen somewhat. Careful chronocoulometry experiments in basic solutions did not indicate adsorption of the electroactive species[4], $\Gamma_{ads} < 0.1 \times 10^{-10}$ mole cm^{-2}. As the pH increases, background correction becomes more of a problem since the Synkavit oxidation potential is independent of pH and the solvent decomposition potential shifts to negative potentials. At the low concentrations where adsorption effects appear, estimation of the peak currents is especially difficult. However participation of adsorbed species is indicated in view of the evidence that the quinone product is adsorbed at the electrode/solution interface as a result of the Synkavit oxidation[4]. At fast sweep rates the current function of the quinone reduction wave in the Synkavit cyclic voltammograms increases markedly. This behavior is not observed in the cyclic voltammograms of identical solutions prepared with Q instead of Synkavit. In the discussion which follows these tentative adsorption effects at high pH are ignored and emphasis is placed on elucidation of the chemical reactions coupled to the electron transfer steps from the data at relatively high concentration.

MECHANISTIC IMPLICATIONS

The cyclic and peak voltammetry data suggest that this oxidation process fits into the general scheme of an e.c.e. mechanism (eqn. 2).

$$\left.\begin{array}{ll} A \rightleftharpoons B + e^- & E_1 \\ B \underset{k_{-1}}{\overset{k_1}{\rightleftharpoons}} C & \\ C \rightleftharpoons D + e & E_2 \end{array}\right\} \quad E_2 \ll E_1 \tag{2}$$

E.c.e. mechanisms have been treated for cyclic voltammetry by Nicholson and Shain[17] who considered the simplest case in which the chemical reaction between the electron transfer steps is totally irreversible ($k_{-1}=0$) and disproportionation of species B or C is neglected. However, in general, electron transfer between species B and C and variation of the rates k_1 and k_{-1} with solution conditions (*i.e.* pH) will complicate the electrochemical behavior. Hawley and Feldberg[18] have taken into account the coproportionation reaction between B and C for the case of potentiostatic chronoamperometry and Mastragostino *et al.*[19] have considered the effect of disproportionation as well as "quasi-reversibility" of the chemical step. The latter workers elaborated on their treatment to take into account the variations with solution pH in the case where the coupled chemical reactions are proton transfers. In addition to these possibilities, the system reported here possesses several features which further hinder definition of the mechanistic pathways. These are as follows:

1. Adsorption effects are definitely present in acidic regions and perhaps at low concentrations in basic media.

2. Not only are proton transfers coupled to the oxidation process, but loss of phosphate is indicated as an intermediate step. This conclusion is supported by ring-disc electrode experiments and experiments involving novel addition of species which react with intermediates in the oxidation process. These are reported below.

3. At fast sweep rates the process becomes electrochemically irreversible.

4. The e.c.e. mechanism is followed by a very fast chemical reaction so that the oxidation scheme becomes an e.c.e.c. process.

Acidic solutions

In acidic solution the peak voltammetry parameters indicate that the oxidation is proceeding by a reversible two-electron transfer followed by an irreversible chemical step which is fast on the time scale of the electrochemical experiment, (eqn. 3).

$$PQP \overset{-2e^-}{\rightleftharpoons} [\quad] \xrightarrow[k_f]{\text{fast}} \text{products} \tag{3}$$

To apply the treatment of Nicholson and Shain[20] for this case to the data, the following criteria must be met (for $n=2$):

$$\frac{i_p}{AC\sqrt{v}} = 298(2)^{\frac{3}{2}}D^{\frac{1}{2}} = 2.1 \text{ A cm}^{-2}\, M^{-1}\, V^{-\frac{1}{2}}\, s^{\frac{1}{2}} \text{ (pH 1.9)}, \tag{4}$$

$$E_p - E_{p/2} = 48/2 = 24 \text{ mV} \tag{5}$$

and

$$dE_{p/2}/d \log v = 29.5/2 = 15 \text{ mV}. \tag{6}$$

Inspection of Table 1 shows that the experimental data are in agreement with the first two criteria at slow sweep rates, while not with the third. Of the three criteria the dependence of $E_{p/2}$ on sweep rate is the most likely to be affected by adsorption of Synkavit since data are used over a wide range of sweep rates to determine the slope. The reversible two-electron step in eqn. (3) involves a fast chemical equilibrium and is expanded below.

The wave shape in the most acidic range (*e.g.* pH 1.9) is roughly constant over a wide range of sweep rates after approximate allowance is made for the adsorption postwave. Although slow electron transfer probably has shifted the wave somewhat, an approximate limit on k_f in eqn. (3) can be determined from the lack of a reverse reduction wave corresponding to a reversible two-electron product and Fig. 11 of ref. 20. The result is that k_f must be greater than 5×10^3 s^{-1}.

Neutral solutions

In the pH region 4–7 the oxidation wave has broadened considerably although the current function is still that of a two-electron transfer. Ring-disc electrode experiments at pH 7.08 indicate the presence of an electroactive intermediate which is reduced at potentials more negative than *ca.* 0.3 V. A typical result is shown in Fig. 5. This curve was obtained by potentiostating the ring at 0.0 V and sweeping

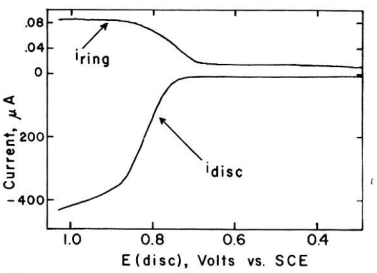

Fig. 5. Ring-disc electrode voltammogram of 0.68×10^{-3} *M* Synkavit at pH 7.1. Rotation rate: 398 rad s^{-1}; ring potential: 0.0 V *vs.* SCE.

the disc potential through the Synkavit oxidation wave. This potential is more positive than the reduction of Q by at least 0.2 V at this pH. Although a rather wide gap carbon paste ring-disc electrode was used[3], a small reproducible ring current is evident. The kinetic collection efficiency (i_{ring}/i_{disc}) increases as the rotation rate increases. This ring current is not observed if the ring potential is greater than *ca.* 0.3 V. A likely possibility for the origin of the ring current which fits the e.c.e. character of the process is reduction of the radical ion of the monophosphate species (QP·).

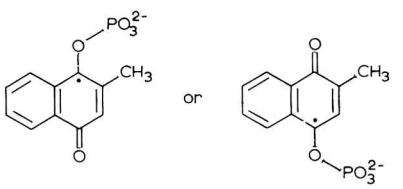

This species can be generated from the monophosphate derivative in neutral solutions and detected by ring-disc voltammetry under identical conditions at the same potential[3].

Schematically the e.c.e. process can be written as follows:

$$PQP \underset{+e^-}{\overset{-e^-}{\rightleftharpoons}} PQP\cdot \tag{7}$$

$$PQP\cdot \underset{k_{-1}}{\overset{k_1}{\rightleftharpoons}} QP\cdot + [P] \tag{8}$$

$$QP\cdot \xrightarrow[\text{fast}]{-e^-} QP^+ \rightarrow Q + [P] \tag{9}$$

This scheme is consistent with the peak voltammetry parameters if the chemical step (eqn. 8) is pH dependent and irreversible on the time scale of the electrochemical experiment. For these conditions and reversible electron transfer the following diagnostic criteria should be met[19]:

$$\frac{i_p}{AC\sqrt{v}} = (2)(298)(1)^{\frac{3}{2}}D^{\frac{1}{2}} = 1.2 \text{ A cm}^{-2} M^{-1} \text{ V}^{-\frac{1}{2}} \text{ s}^{\frac{1}{2}} \tag{10}$$

$$E_p - E_{p/2} = 48/1 \text{ mV} \tag{11}$$

and

$$\frac{dE_{p/2}}{d \log v} = 30 \text{ mV} \tag{12}$$

The current function (eqn. 10) is simply twice the current function for a reversible one-electron transfer coupled with a fast follow-up reaction, Case VI of ref. 20. Similarly the peak width and sweep rate dependence (eqns. 11 and 12) are given by the criteria for this case. Inspection of Table 1 reveals that agreement is good for the first two criteria at slow sweep rates in neutral and basic solutions. The poor agreement for the latter criterion (eqn. 12) is probably due to manifestation of slow electron transfer and incipient adsorption(?) effects which appear at very fast sweep rates.

The slope of the $E_{p/2}$ *vs.* pH curve in acidic solutions is also in agreement with the scheme presented in eqns. (7)–(9). The value of $(\partial E_{p/2}/\partial \text{pH})_v$ is dependent on sweep rate, changing from roughly 55 mV at slow sweep rates to 35 mV at fast sweep rates. This behavior is characteristic of an e.c.e. process in which the rate at which the chemical step approaches equilibrium is pH dependent[19]. In Fig. 6 the slopes are graphed as a function of sweep rate. The solid line was estimated from Fig. 11 of ref. 19 and has been adjusted by shifting the x-axis to give the best fit. Although there are problems with this analysis, the trend is in the proper direction.

Basic solutions

In basic media the e.c.e. character of the oxidation process is clearly evident.

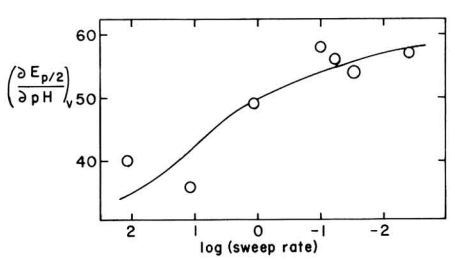

Fig. 6. Variation of $(\partial E_{p/2}/\partial \text{pH})_v$ with sweep rate in acidic solution.

At fast sweep rates two irreversible oxidation waves are present which are assigned to successive one-electron transfers (eqn. 13).

$$PQP \xrightarrow{-e^-} PQP\cdot \xrightarrow{-e^-} [PQP_{ox}] \xrightarrow{\text{fast}} \text{products} \qquad (13)$$

At slow sweep rates the oxidation proceeds *via* loss of phosphate from the PQP· species. Under these conditions eqns. (10) and (11) should be satisfied as is shown in Table 1. At fast sweep rates the peak width increases (at high concentrations) and $E_{p/2}$ increases *ca.* 50 mV per decade increase in the sweep rate. These parameters are indicative of slow electron transfer in which case the current function should decrease to a value between 0.44 to 0.51 A cm^{-2} M^{-1} $V^{-\frac{1}{2}}$ $s^{\frac{1}{2}}$ for transfer coefficients between 0.5 and 0.7. The trend is in this direction.

The presence of a reversible or "quasi-reversible" dephosphorylation of an one-electron intermediate in the oxidation process is supported by experiments in which solutions of both Synkavit and the corresponding monophosphate ester (QP) are oxidized at a carbon paste electrode. Oxidation of QP precedes the Synkavit oxidation by *ca.* 0.5 V so that peak voltammetry parameters of the Synkavit wave can be obtained in the presence of the products of the PQ oxidation. Since the oxidation pathways overlap, this affords a novel method of determining the effect of potential intermediates on the Synkavit oxidation. Typical cyclic voltammograms are shown in Fig. 7. In the presence of PQ and its oxidation products the current function of the PQP wave decreases and the wave is split into two waves. This is very similar to the behavior observed at fast sweep rates in basic solutions. This behavior is interpreted below as resulting from an increase in the equilibrium concentration of a one-electron intermediate in the oxidation process, PQP·.

This effect is observed at all pH values. At pH 1.9 addition of PQ decreases the specific adsorption of Synkavit and a small additional oxidation wave (not the ad-

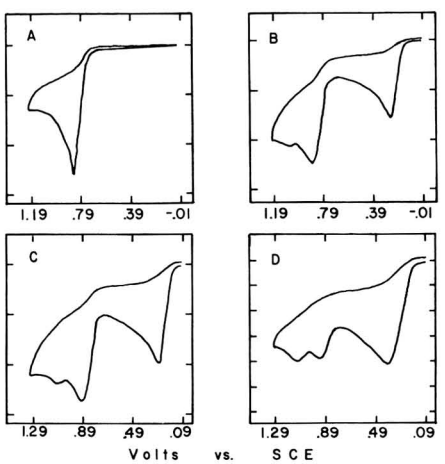

Fig. 7. Cyclic voltammograms of 0.70×10^{-3} *M* Synkavit in the presence of the monophosphate ester (PQ) at pH 7.08. Sweep rate: 0.245 V s^{-1}. (A) 0.02 mA per ordinate division; (B) 0.51×10^{-3} *M* PQ, 0.02 mA per ordinate division; (C) 0.70×10^{-3} *M* PQ, 0.02 mA per ordinate division; (D) 1.76×10^{-3} *M* PQ, 0.04 mA per ordinate division.

sorption postwave) is evident at fast sweep rates. The additional wave becomes more prominent as the pH increases until at pH 7 the behavior shown in Fig. 7 is observed. In neutral solutions, addition of QP drastically alters some features of the Synkavit wave as well as splitting it into two waves. The peak width increases considerably and the value of $E_{p/2}$ becomes markedly dependent on sweep rate. Evidently, the PQ oxidation products have changed the electron transfer rates of the Synkavit oxidation.

DISCUSSION

The results can be rationalized simply by an ECE oxidation scheme in which the rate of the backward reaction of the chemical step decreases as the pH is increased. Several reactions meet this requirement, two are given in eqns. (14) and (15).

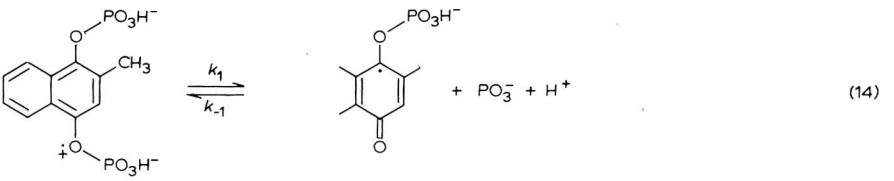

or

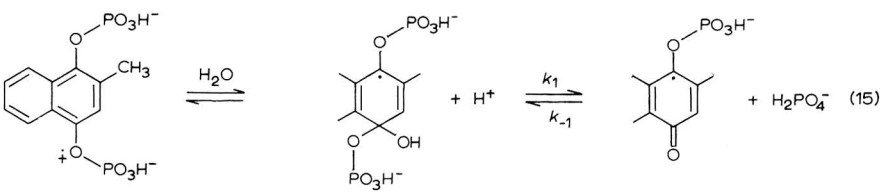

Both of these hypothetical reactions involve rapid dephosphorylations whose backward rate is potentially dependent on pH, decreasing as the pH is increased. These electrochemical experiments of course cannot give information regarding structures of intermediates or distribution between these reaction paths. Equation (14) involves loss of metaphosphate which would react rapidly to form orthophosphate. Equation (15) is similar to the reaction proposed by Dürckheimer and Cohen[10] to explain the C–O bond fission route. Oxidation products of the monophosphate would drive both reactions to the left in accord with the results observed for the cyclic voltammograms of PQP/PQ mixtures.

Both reactions are interesting and deserve brief comment. Since orthophosphate is a poor phosphorylating agent, it would be surprising if the backward rate in eqn. (15) were fast on the time scale of the electrochemical experiment. Furthermore, the concentration of QP· generated from QP would not be large enough (especially in acid solutions) to explain the effect of the added monophosphate species. Therefore eqn. (14) is the more likely possibility for the reversible dephosphorylation step. Metaphosphate generated from the monophosphate

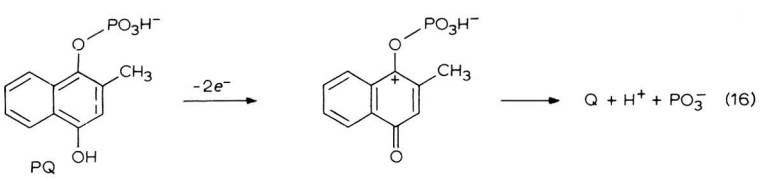

could readily phosphorylate the QP·species. The metaphosphate species is believed to be a product of the hydrolysis of anions of phosphate esters although definite proof of its existence is not available[21]. However it is a highly reactive species under these conditions, reacting before losing information about its precursor[22]. The kinetic role for metaphosphate suggested by these results would imply that it is longer lived than this. Thus eqn. (14) is an oversimplification of the situation. However it is difficult to conceive of a phosphorylating agent other than metaphosphate which would reversibly phosphorylate QP· in this system. In concentrated $NaClO_4$, bromine oxidation of Synkavit results in trace amounts of pyrophosphate which is indicative of metaphosphate intermediate[13].

These mechanistic implications illustrate the importance of the one-electron intermediate in determining the pH dependence of the electrode process. The variation with pH of the rate of approach to equilibrium of eqn. (8) determines the kinetic characteristics of the electrode process. This result appears to have some generality for oxidation of hydroquinone and phenol derivatives in aqueous media. Other phosphate, sulfate[23], and carboxylate[24] derivatives of hydroquinones seem to fit into the same pattern. These results will be reported elsewhere.

Finally, these results again emphasize that schemes devised to account for biological phosphorylations based on oxidation of C–O–P linkages[25] should consider the critical role of the one-electron intermediate oxidation state in neutral solutions.

ACKNOWLEDGEMENT

Helpful discussions with Dr. Brian R. Eggins are hereby acknowledged. This work was supported by the Research Corporation and the National Institutes of Health, Grant No. GM14815.

SUMMARY

The electrochemical oxidation of the diphosphate ester of 2-methyl-1,4-naphthohydroquinone (Synkavit) has been studied in aqueous solution at carbon paste electrodes. The oxidation process is complicated by adsorption phenomena, coupled chemical reactions, and slow electron transfer. Details of the mechanistic pathways have been deduced from peak voltammetry and rotating ring-disc electrode experiments. Over the entire pH range, the oxidation proceeds *via* a reversible or "quasi-reversible" dephosphorylation of a one-electron intermediate. The rate at which this reaction comes to equilibrium is pH dependent, decreasing as the pH is increased. This scheme appears to have some generality in describing the anodic oxidation pathways of hydroquinone derivatives.

REFERENCES

1 R. N. ADAMS, *Electrochemistry at Solid Electrodes*, Marcel Dekker, Inc., New York, 1969, p. 363.
2 N. L. WEINBERG AND H. R. WEINBERG, *Chem. Rev.*, 68 (1968) 449.
3 C. A. CHAMBERS AND J. Q. CHAMBERS, *J. Am. Chem. Soc.*, 88 (1966) 2922.
4 E. P. MEIER AND J. Q. CHAMBERS, *Anal. Chem.*, 41 (1969) 914.
5 V. M. CLARK, D. W. HUTCHINSON, G. W. KIRBY AND A. TODD, *J. Chem. Soc.*, (1961) 715.

6 TH. WIELAND AND F. PATTERMAN, *Chem. Ber.*, 92 (1959) 2917.
7 B. R. EGGINS, Ph.D. Thesis, Univ. of Warwick, England, 1968.
8 A. LAPIDOT AND D. SAMUEL, *Biochim. Biophys. Acta*, 65 (1962) 164.
9 A. LAPIDOT AND D. SAMUEL, *J. Am. Chem. Soc.*, 86 (1964) 1886.
10 W. DÜRCKHEIMER AND L. A. COHEN, *Biochem.*, 3 (1964) 1948.
11 B. T. ALLEN AND A. BOND, *J. Phys. Chem.*, 68 (1964) 2439.
12 G. E. TOMASI, J. W. HAMILTON AND R. D. DALLAM, *Federation Proc.*, 21 (1962) 53.
13 G. E. TOMASI AND R. D. DALLAM, *J. Biol. Chem.*, 239 (1964) 1604.
14 J. S. COHEN AND A. LAPIDOT, *J. Chem. Soc.* (C), (1967) 1210.
15 P.-S. SONG AND T. A. MOORE, *J. Am. Chem. Soc.*, 90 (1968) 6507.
16 J. Q. CHAMBERS, A. D. NORMAN, M. R. BICKELL AND S. H. CADLE, *J. Am. Chem. Soc.*, 90 (1968) 6056.
17 R. S. NICHOLSON AND I. SHAIN, *Anal. Chem.*, 37 (1965) 178.
18 M. D. HAWLEY AND S. W. FELDBERG, *J. Phys. Chem.*, 70 (1966) 3459.
19 M. MASTRAGOSTINO, L. NADJO AND J. M. SAVEANT, *Electrochim. Acta*, 13 (1968) 721.
20 R. S. NICHOLSON AND I. SHAIN, *Anal. Chem.*, 36 (1964) 706.
21 J. R. COX AND O. B. RAMSAY, *Chem. Rev.*, 64 (1964) 317.
22 C. A. BUNTON, *J. Chem. Educ.*, 45 (1968) 21; C. A. BUNTON, E. J. FENDLER AND J. H. FENDLER, *J. Am. Chem. Soc.*, 89 (1967) 1221.
23 C.-S. LIAO, Masters Thesis, Univ. of Colorado, 1968.
24 B. R. EGGINS, personal communication.
25 V. M. CLARK AND D. W. HUTCHINSON, *Progr. Org. Chem.*, 7 (1968) 103.

ELECTROANALYTICAL CHEMISTRY AND INTERFACIAL ELECTROCHEMISTRY
Elsevier Sequoia S.A., Lausanne – Printed in The Netherlands

THE ELECTROCHEMISTRY OF POLYNUCLEAR HYDROCARBONS IN THE MOLTEN SALT SYSTEM $AlCl_3$–NaCl–KCl

M. FLEISCHMANN AND D. PLETCHER
Department of Chemistry, The University, Southampton (England)
(Received November 6th 1969; in revised form January 2nd, 1970)

While the electrochemistry of organic compounds has been studied in a wide range of protonic and aprotic solvents, relatively little is known of the electrochemistry or, indeed, the chemistry of organic molecules in molten salt media. This communication reports the electrochemical behaviour of a series of polynuclear hydrocarbons in a low melting point molten salt system: aluminium trichloride plus sodium chloride and potassium chloride. A similar salt mixture has been the medium for some elegant, novel chemistry reported by Sundermeyer[1,2].

EXPERIMENTAL

The sodium and potassium chlorides were B.D.H. AnalaR Reagent grade while the aluminium trichloride was supplied by Fluka Chemicals. The mixture used was 50 mole% aluminium trichloride, 36 mole% sodium chloride and 14 mole% potassium chloride; it has a melting point of approximately 120°C. This study was carried out in a furnace thermostatted at 150 ± 5°C. The chlorides were weighed out and ground together to a fine powder in a dry box. After melting, aluminium powder was added (to remove trace iron which colours the melt) and the solution was stirred overnight with a dry nitrogen and dry hydrogen chloride mixture. The aluminium powder was then allowed to settle and the molten salt was decanted into the cell.

The electrochemical cell consisted of a carbon (pyrolytic graphite) working electrode, an aluminium secondary electrode and the reference electrode which was an aluminium wire dipping into the melt. The reference electrode was separated from the working electrode by a Luggin capillary. The cell also had a gas inlet which allowed nitrogen stirring during runs.

The electrochemical data was obtained using a Chemical Electronics potentiostat and pulse generator together with standard recording equipment.

RESULTS AND DISCUSSION

At a pyrolytic graphite working electrode, the potential range is -0.4 to $+2.4$ V *versus* the aluminium wire reference electrode. At potentials more negative than -0.4 V, rising current–time transients may be observed and an aluminium deposit appears on the electrode surface. The range to anodic potentials is limited by chlorine evolution. At a platinum electrode the anodic limit is $+2.0$ V since the platinum electrode oxidises to give platinum chloride.

TABLE 1

	$E_{p/2}/V$	*Ratio of wave heights*		$E_{p/2}/V$	*Ratio of wave heights*
benzene	2.09	–	chrysene	1.34	1
naphthalene	1.57	–		1.78	2
anthracene	1.24	1		2.10	4
	1.72	1	pyrene	1.19	1
	1.90	1		1.79	2
	2.30	2		2.03	4
phenanthrene	1.43	1	diphenylan-	1.25	1
	1.84	1	thracene	1.75	2
chlorobenzene	2.48	–		2.20	4
			biphenyl	1.66	1
				2.03	1

In Table 1, the oxidation potentials are reported for a selection of aromatic hydrocarbons and chlorobenzene; the data were obtained at a potential sweep rate of 0.1 V s^{-1}. The large polynuclear hydrocarbons show a series of electron transfers while the simple hydrocarbons show a single wave. At this sweep rate, pyrene, anthracene and diphenylanthracene give peaks on the reverse sweep showing the initial products of the first electron transfer to have some stability, although it is clear from the peak size that they are not completely stable. Furthermore, these peaks occur at a potential close to that expected if the oxidation was electrochemically reversible. The other hydrocarbons, with the exception of benzene, show reverse peaks at slightly higher sweep rates. In no case was there any evidence for reduction of the aromatic hydrocarbon.

Figure 1 shows cyclic voltammograms run at 0.1 V s^{-1} between 0.3 and 2.7 V for the molten salt and the molten salt + naphthalene. The other hydrocarbons,

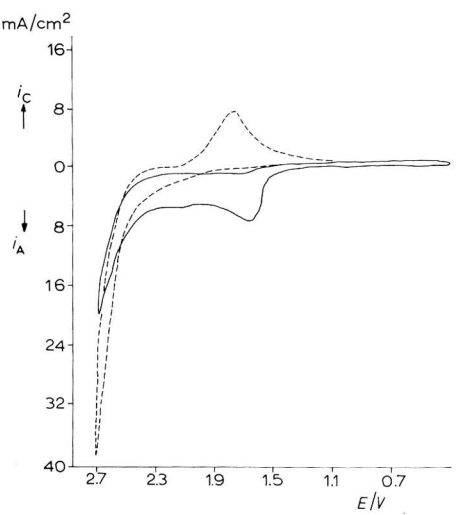

Fig. 1. (------) Cyclic voltammogram of the $AlCl_3$–NaCl–KCl melt between +0.3 and +2.7 V; (——) cyclic voltammogram after addition of naphthalene to the melt.

however, behave in a similar manner. In the presence of the aromatic species there is a considerable reduction in the chlorine evolution current indicating adsorption on the electrode surface of the product from the oxidation of the hydrocarbon. Moreover, the peak, which is observed on the reverse sweep in the melt alone at $E_{p/2} = 1.93$ V and which must be due to the reduction of free or adsorbed chlorine, is missing showing that the chlorine reacts chemically with the hydrocarbon under the electrolysis conditions.

Making the assumption that the potentials for chlorine evolution and aluminium deposition are not both greatly different in the molten salt medium from their potentials in aqueous solution, it is possible to estimate that the aluminium wire reference electrode has a potential of approximately -1.2 V *versus* an aqueous NHE. Then it can be seen that the hydrocarbons, anthracene, diphenylanthracene, chrysene, pyrene and phenanthrene are oxidised at potentials very close to zero *versus* the NHE and that benzene is oxidised at less than $+1.0$ V. These oxidation potentials are much more negative than in any common solvent. However, similar behaviour is presumably observed in the work reported by Wisdom[3] on the electrochemical oxidation of the liquid complexes formed by mixing the aromatic hydrocarbon with hydrogen chloride and aluminium trichloride in the ratio 4 : 1 : 1, since polymerisation of the hydrocarbon was observed at the anode. That is, the hydrocarbons including benzene must oxidise at more negative potentials than chlorine evolution.

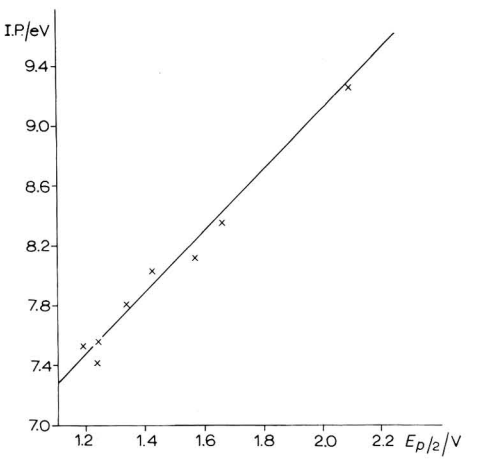

Fig. 2. Plot of ionisation potential *versus* half peak potential for a series of aromatic hydrocarbons in $AlCl_3$–NaCl–KCl melt.

Figure 2 shows a plot of $E_{p/2}$ *versus* ionisation potential for the series of aromatic hydrocarbons; within the errors in the measurement of the ionisation potentials, I.P., the plot is linear. Such plots have been reported for other solvents[4,5] and they show the importance of the gas phase ionisation potential and in turn, the energy of the highest filled molecular orbital, in determining the oxidation potential of organic compounds. In the simplest case, *i.e.* reversible electrode reactions and no complexing of $\varnothing H$ or $\varnothing H^{\bullet +}$, these plots may be explained in terms of a thermodynamic cycle which leads to the equation

$$-FE = \Delta G_{ox} = \text{I.P.} + \Delta G_{sol}^{\varnothing H^{\bullet +}} - \Delta G_{sol}^{\varnothing H} + \text{const.}$$

where ΔG_{ox} and ΔG_{sol} are free energies of the oxidation reaction and of solvation, respectively, and the constant refers the equation to a reference electrode. In this simple case, the plot will have a slope of 1. However, it can be seen from Fig. 2 that in the case under discussion the linear plot has a slope, $dI.P./dE_{p/2} = 2$.

The very negative potentials at which the oxidations of aromatic hydrocarbons take place in the melt can be explained by two factors. Firstly, there is the possibility of formation of a π-complex between the hydrocarbon and aluminium trichloride. The formation of such a complex will have the result of removing the degeneracy of the highest filled molecular orbitals of the parent hydrocarbon and if the geometry of the complex is such that one of these orbitals increases in energy, the ionisation potential of the complex will be lower than that of the parent hydrocarbon. The formation of such a complex will thus have the effect of assisting the oxidation and the oxidation will take place at less positive potentials. Such complexes have been discussed elsewhere[4] although it should be remembered that the conditions in the melt are somewhat different from those in typical Friedel–Crafts reactions. Secondly, the oxidations may be assisted by the formation of a complex between the initial product of the electrode reaction $\varnothing H^{\bullet +}$ and the anion $AlCl_4^-$. Such complexes are related to normal Friedel–Crafts intermediates and the cyclic voltammetry indicates that the first oxidation product has considerably greater stability in the melt than in common solvents. Thus, the electrode reaction in the molten salt system is more accurately described by the thermodynamic cycle:

$$\begin{array}{ccccc}
[\varnothing H \rightarrow AlCl_3]_{sol} & \xrightarrow{-\Delta G_{sol}^{comp}} & [\varnothing H \rightarrow AlCl_3]_{gas} & \xrightarrow{I.P.'} & [\varnothing H^{\bullet +} - AlCl_3]_{gas} + e \\
\downarrow \Delta G_{ox} & & & & \downarrow \Delta G_{sol}^{comp^+} \\
\varnothing H^{\bullet +} AlCl_4 & \xleftarrow{\Delta G_{ion\ pair}} & [\varnothing H^{\bullet +}]_{sol} + AlCl_3 & \xleftarrow{-\Delta G_{comp^+}} & [\varnothing H^{\bullet +} - AlCl_3]_{sol}
\end{array}$$

which leads to the equation:

$$-FE_{p/2} = \Delta G_{ox} = -\Delta G_{sol}^{comp} + I.P.' + \Delta G_{sol}^{comp^+} - \Delta G_{comp^+} + \Delta G_{ion\ pair} + \text{const.}$$

assuming both types of complexing to be important and that the electrode reactions are reversible. With the exception of benzene, the electrode reactions are clearly almost reversible and, furthermore, any slight irreversibility can only have the effect of making the half peak potentials less negative and so lead to an underestimation of the importance of complex formation. If the ion pair formation between $\varnothing H^{\bullet +}$ and $AlCl_4^-$ is the sole contributor to the shift in half peak potentials the simple equation[7] with the extra term, $\Delta G_{ion\ pair}$, is sufficient.

The unusual slope of the I.P. *versus* $E_{p/2}$ graph must be due to an increase in complex formation ($\varnothing H \rightarrow AlCl_3$ and/or $\varnothing H^{\bullet +} AlCl_4^-$) with increasing ionisation potential of the parent hydrocarbon. In the case of complex formation between the hydrocarbon and aluminium trichloride it is certainly possible to envisage that the degree of distortion of the molecular orbitals diagram and thus the change in effective ionisation potential (I.P.–I.P.') is dependent on the ionisation potential of the parent hydrocarbon. On the other hand, a direct correlation between the degree of ion pair formation between $\varnothing H^{\bullet +}$ and $AlCl_4^-$ and the ionisation potential of $\varnothing H$ is more difficult to explain. However, the degree of ion pair formation will increase with

decreasing size of the cation radical and the smallest cation radicals are certainly derived from the hydrocarbons with the highest ionisation potentials

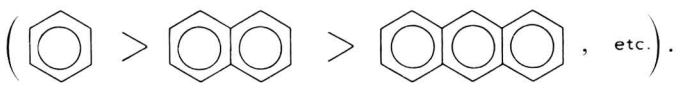

Controlled potential electrolyses were carried out on the plateau of the benzene oxidation wave (+2.25 V) so as to ascertain whether chlorinated hydrocarbons or polyphenyl polymers[3] could be isolated. In fact the major product was carbon (current yield >70%) which formed a coherent deposit on the anode and no chlorobenzene or biphenyl could be isolated. Chlorobenzene was ruled out as a reaction intermediate since its oxidation potential was more positive than the potential of the electrolysis. Thus, the likely mechanism for the formation of carbon is a polymerisation reaction followed by further oxidation until no carbon–hydrogen bonds remain. However, the oxidative behaviour of benzene is probably not typical of the other hydrocarbons where stable cation radicals are formed and more than one oxidation wave is observed. It seems likely that the products of the electrode reactions will be organic in nature, especially at low potentials. The particular melt studied is very low in free chloride ion and the formation of chlorinated products would be more likely in a melt containing free chloride ion, *i.e.* the Lewis base.

SUMMARY

Cyclic voltammetric data are reported for a series of aromatic hydrocarbons in a molten salt medium: aluminium trichloride + sodium chloride + potassium chloride. The electro-oxidations are shown to take place at unusually negative potentials and the reasons are discussed.

REFERENCES

1 W. SUNDERMEYER, *Angew. Chem. Intern. Ed. Engl.*, 4 (1965) 222.
2 W. SUNDERMEYER AND W. VERBECK, *Angew. Chem. Intern. Ed. Engl.*, 5 (1966) 1.
3 N. E. WISDOM, Proceedings of New York meeting of the Electrochem. Soc., May 1969, p. 338.
4 G. A. OLAH AND M. W. MEYER, *Friedel–Crafts and Related Reactions*, Interscience, New York, 1963.
5 E. S. PYSH AND N. C. YANG, *J. Am. Chem. Soc.*, 85 (1963) 2124.
6 M. E. PEOVER, *Electroanal. Chem.*, 2 (1967) 1.
7 M. FLEISCHMANN AND D. PLETCHER, *Roy. Inst. Chem. (London) Reviews*, (1969) 87.

ELECTROANALYTICAL CHEMISTRY AND INTERFACIAL ELECTROCHEMISTRY
Elsevier Sequoia S.A., Lausanne – Printed in The Netherlands

THE ANODIC OXIDATION OF CYCLOHEXENE–CHLORIDE ION MIXTURES IN ACETONITRILE

G. FAITA*, M. FLEISCHMANN AND D. PLETCHER
Department of Chemistry, The University, Southampton (England)

(Received November 6th, 1969; in revised form January 2nd, 1970)

As early as 1898, Haber[1], showed that the product of an electrode reaction, the reduction of nitrobenzene, was dependent on the potential of the electrode

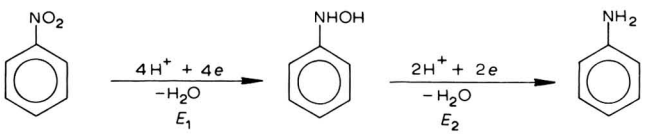

and during the last seventy years this principle has been extended to a wide range of electrode reactions. In all these cases, the variation in product is due to the further oxidation or reduction of the intermediate or product produced at the potential E_1, when the potential is changed to E_2. However, in this paper it will be shown that when two species are mixed in suitable concentrations, a variation in products with potential can be brought about by an actual change in the electrode reaction. Thus, at low potentials, the anodic oxidation of a mixture of chloride ion and cyclohexene in acetonitrile leads to products from the oxidation of chloride ions. On the other hand, at high potentials, the products arise from the oxidation of cyclohexene, provided the bulk concentration of chloride ion is such that, through its reaction with the cyclohexenyl carbonium ions diffusing away from the electrode, no chloride ion is able to reach the electrode surface.

EXPERIMENTAL

The acetonitrile was obtained from Koch Light Ltd. and purified as described by O'Donnell *et al.*[2]. The base electrolyte in all experiments was tetraethylammonium tetrafluoroborate (0.3 *M*) which was prepared from Eastman Kodak tetraethylammonium bromide and B.D.H. sodium tetrafluoroborate by precipitation from aqueous solution, followed by multiple recrystallisations from water and drying in a vacuum oven at 80°C. The chloride ion was introduced as Eastman Kodak tetraethylammonium chloride. Cyclohexene was B.D.H. reagent grade while the organic chemicals required for product analysis were prepared by standard techniques.

The three electrode cell consisted of platinum working and secondary electrodes separated by a glass frit and the reference electrode which was $Ag/10^{-2}\ M\ Ag^+$

* N.A.T.O. Research Fellow, on leave from the Instituto di Electrochimica and Metallurgia, Università di Milano.

in the base electrolyte and which was separated from the working electrode by a Luggin capillary and tap. Current–potential curves were obtained using a rotating disc electrode while during preparative runs the working electrode was a platinum sheet. A Chemical Electronics valve potentiostat was used throughout the work.

Product identification and quantitative analysis were carried out on a Pye 104 vapour phase chromatograph.

RESULTS AND DISCUSSION

Steady state current–potential curves were obtained for the oxidation of chloride ion and cyclohexene in acetonitrile. The chloride to chlorine electrode reaction occurred with a half-wave potential of +0.75 V while the half-wave potential for the oxidation of cyclohexene was +2.05. When current–potential curves were run for mixtures of chloride ion and cyclohexene there was a diffusion plateau between +0.9 and +1.5 V and this potential range will be referred to as the "low potential region". Potentials at which the cyclohexene oxidises will be referred to as the "high potential region".

Cyclic voltammograms were run for the chloride ion between 0 and +1.2 V in the absence of cyclohexene, and the peak for the oxidation of chloride ion appeared at $E_{p/2} = +0.70$ V. A peak on the reverse sweep at $E_{p/2} = +0.60$ V for the reduction of chlorine to chloride showed that chlorine does not react with the solvent. However, the addition of a concentration of cyclohexene equal to that of the chloride ion was sufficient to remove the reverse peak even at a sweep rate of 30 V s^{-1} so that the chlorine–cyclohexene reaction is clearly rapid in this solvent.

On the other hand, cyclic voltammograms run on a solution of cyclohexene alone showed only an oxidation peak in the sweep to positive potentials, with no peak on the reverse sweep even at high sweep rates. Thus the oxidation of cyclohexene is completely irreversible. The oxidation of an olefin to a carbonium ion and a proton has been reported elsewhere[4]

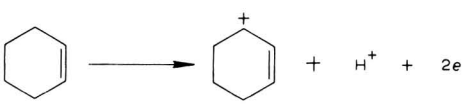

and products are expected to arise from reaction between the carbonium ion and the solvent or between the carbonium ion and further olefin. In the case of propylene, high yields of N-allylacetamide can be obtained after addition of water[4].

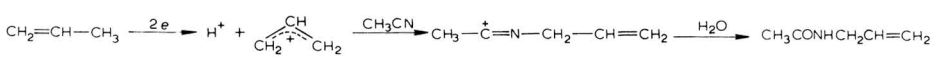

However, in the case of cyclohexene it was not possible to isolate products from the reaction between the cyclohexenyl carbonium ion and the solvent unless water was present during the electrolysis. Then, for example, during an electrolysis at +2.1 V of cyclohexene in acetonitrile containing 1% water, a current yield of 13% for N-cyclohexenyl acetamide was obtained. However, a quantitative yield of proton was obtained during the electrolysis of cyclohexene in dry acetonitrile, supporting the

initial formation of a cyclohexenyl carbonium ion. The cyclic voltammetry suggests the lifetime of this species to be very short. The addition of chloride ion does not affect the cyclic voltammetry of cyclohexene.

Electrolysis at low potential

Controlled potential electrolyses were carried out on a mixture of 0.1 *M* cyclohexene and 0.1 *M* chloride ion in acetonitrile at three potentials, 0.7, 0.9 and 1.2 V, and in each case the products isolated, after addition of water, were N-2-chlorocyclohexylacetamide with a current yield of $>80\%$ and dichlorocyclohexane with a current yield of 5%. These products and yields are almost identical to those found for the chemical reaction between chlorine and cyclohexene in acetonitrile[3]. Clearly the mechanism of the electrode reaction is

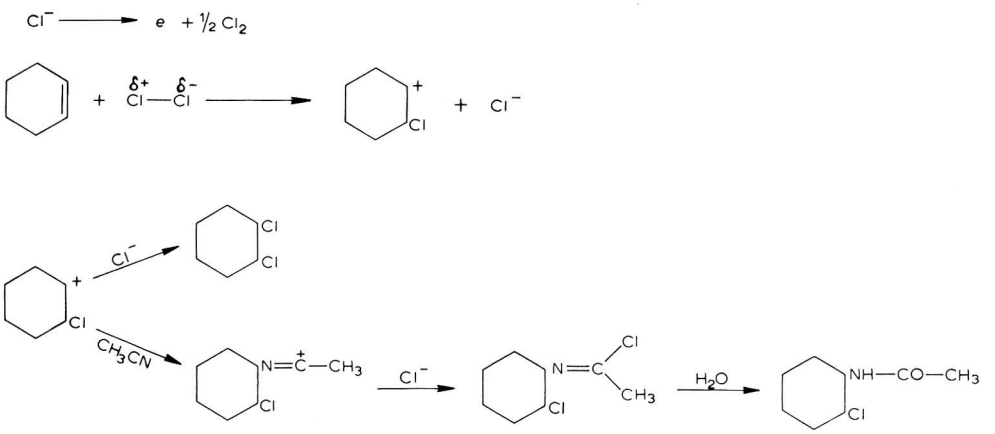

No 3-chlorocyclohexene is formed at these potentials.

Electrolysis at high potentials

Controlled potential electrolyses were carried out at +2.1 V on solutions containing different chloride ion to cyclohexene ratios. In each case, the only product which was positively identified was 3-chlorocyclohexene which will arise through the reactions

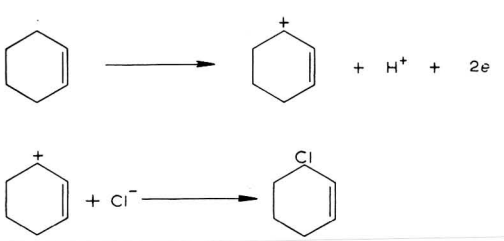

The yields of 3-chlorocyclohexene are shown in Table 1. The maximum yield is to be expected when the ratio of chloride ion to cyclohexene in the bulk of the solution is such that the flux of chloride ion to the electrode surface exactly balances the flux

TABLE 1

Ratio ⬡ : Cl^-	*Coulombs passed*	*Current yield of 3-chlorocyclohexene*
2 : 1	65	40
	185	16
	250	10
1 : 1	52	45
	173	32
	315	20
1 : 2	222	9

of cyclohexenyl carbonium ions away from the electrode. Some reaction of the cyclohexenyl carbonium with the environment (as in the absence of chloride ion) will always occur since the cyclic voltammetry in the absence of chloride ion showed the reaction to be rapid. However, this reaction will be minimised if cyclohexene is not in large excess. On the other hand, if the chloride ion is in excess, products (*i.e.* N-2-chlorocyclohexylacetamide and dichlorohexane) are formed by the reaction which takes place at low potentials. Experimentally it was found that the best yield of 3-chlorocyclohexene was obtained when the ratio cyclohexene : chloride ion was about 1 : 1.

Furthermore, the current yield of 3-chlorocyclohexene will be affected by the absolute concentration of the cyclohexene and the chloride ion as well as the ratio of the concentrations of the species. Under the electrolysis conditions, the reaction of the cyclohexenyl carbonium ion with the solvent will compete with the formation of 3-chlorocyclohexene. As the rate of the competing reaction is given by $K_1[\text{cyclo-}C_6H_9^+][CH_3CN]$ it can be seen that it is effectively "first order" with respect to cyclohexene. However, the rate of formation of 3-chlorocyclohexene is given by $K_2[\text{cyclo-}C_6H_9^+][Cl^-]$ and this reaction is effectively "second order" since the chloride ion to cyclohexene concentration ratio is fixed in the bulk of the solution. It can be concluded that the second order reaction, *i.e.* the formation of 3-chlorocyclohexene, is affected to a greater extent by an increase in the absolute concentrations; thus a high current efficiency for the formation of the desired product is favoured by the use of concentrated solutions.

It is shown in Table 1 that the current yield of 3-chlorocyclohexene decreases with duration of the electrolysis and this may largely be attributed to depletion of the chloride ion with the consequent growing importance of reaction between the cyclohexenyl carbonium ion and the solvent. The passage of 100 C was sufficient to remove 15–50% of the chloride ion on the scale on which these electrolyses were carried out. However, the decrease in yield of 3-chlorocyclohexene may also, in part, be attributed to the fact that it is itself slowly oxidised at 2.1 V; the half-wave potential for the oxidation of 3-chlorocyclohexene is 2.25 V and the electrode reaction is probably[5]

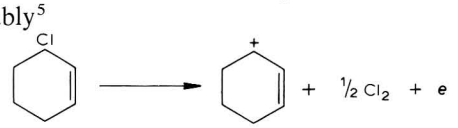

Certainly the oxidation of 3-chlorocyclohexene will be the major factor for the low yield ($< 5\%$) of this product when the electrolysis was carried out at $+2.7$ V, a potential where its oxidation will be rapid.

Therefore, it is to be concluded that the best current yield of 3-chlorocyclohexene will be obtained at low conversions using a solution where the cyclohexene and chloride ion are present at high concentration and in a ratio of approximately 1:1; the anode potential should be controlled in the range $+1.9$ to $+2.2$ V *versus* the Ag/Ag^+ reference electrode.

SUMMARY

It has been shown that when a solution contains a mixture of two species, the electrolysis product can vary with potential due to an actual change in the electrode reaction. Thus, in the example considered, the anodic oxidation of a mixture of chloride ion and cyclohexene in acetonitrile, the product at low potentials is N-2-chlorocyclohexylacetamide formed *via* the discharge of the chloride ion while the product at high potentials is 3-chlorocyclohexene formed *via* the discharge of cyclohexene. In order to obtain a maximum yield of the product formed at high potential it is necessary to vary the concentrations of the species in the bulk so that the flux of the reacting species in the diffusion layer is exactly balanced.

REFERENCES

1 F. HABER, *Z. Elektrochem.*, 4 (1898) 506.
2 J. F. O'DONNELL, J. T. AYRES AND C. K. MANN, *Anal. Chem.*, 37 (1965) 1162.
3 T. L. CAIRNS, P. J. GRAHAM, P. L. BARRICK AND R. S. SCHREIBER, *J. Org. Chem.*, 17 (1952) 751.
4 M. FLEISCHMANN AND D. PLETCHER, *Tetrahedron Letters*, (1968) 6255; also unpublished results.
5 A. K. HOFFMAN AND L. L. MILLER, *J. Am. Chem. Soc.*, 89 (1967) 593.

ELECTROANALYTICAL CHEMISTRY AND INTERFACIAL ELECTROCHEMISTRY
Elsevier Sequoia S.A., Lausanne – Printed in The Netherlands

ZUR THEORIE DER STATIONÄREN STROM–SPANNUNGSKURVEN VON REDOX-ELEKTRODENREAKTIONEN IN HYDRODYNAMISCHER VOLTAMMETRIE

V. SCHLEICHENDE KUGELSTRÖMUNGEN

HIROAKI MATSUDA
Government Chemical Industrial Research Institute, Tokyo, Hon-machi, Shibuya-ku, Tokyo (Japan)
(Eingegangen am 28. August, 1969)

EINLEITUNG

Zur Erweiterung der polarographischen Analysenmethode zur automatischen Daueranalyse haben in den letzten Jahren Štráfelda und Kimla[1] eine in die Rohrströmung eingetauchte kugelförmige Platin-Elektrode als Indikatorelektrode benützt. Später haben sie[2] ferner die Benützung der Quecksilbertropfelektrode an der dünnwandigen Spitzkapillare von etwa 100 μm Aussendurchmesser berichtet, die in eine Parallelströmung mit kleiner Reynoldsscher Zahl eingetaucht worden ist. In den letzten Jahren hat Takemori[3] im unseren Laboratorium die Anwendbarkeit der letzteren Elektrode als Sensor in der Chromatopolarographie versucht und fruchtbare Ergebnisse erhalten.

Das Problem der Stofftransportvorgänge, die nur durch konvektive Diffusion in schleichender Kugelumströmung begrenzt werden, ist bereits von Lewitsch[4] aufgelöst worden. Später hat Kimla[5] unter Berücksichtigung von Einfluss der Krümmung der Kugel das Lewitschsche Ergebnis verbessert. Trotzdem ist bisher keine theoretische Behandlung für den Fall durchgeführt worden, bei dem die Stromstärke durch beide Geschwindigkeiten der konvektiven Diffusion und der Elektrodenreaktion bedingt wird.

In der vorliegenden Arbeit wollen wir daher, mit Rücksicht auf sowohl die Geschwindigkeiten der konvektiven Diffusion als auch der Kinetik, die theoretischen Ausdrücke der stationären Strom–spannungskurven für die Redox-Elektrodenreaktionen ohne und mit einer vorgelagerten chemischen Reaktion ableiten, die auf der Oberfläche der in schleichende Parallelströmung eingetauchten Kugelelektrode verlaufen. Weiterhin sollen die erhaltenen Ergebnisse auf die Quecksilbertropfelektrode an der dünnwandigen Spitzkapillare angewandt werden.

STATIONÄRE STROM–SPANNUNGSKURVEN BEI ABWESENHEIT DER CHEMISCHEN KOMPLIKATION IN DER LÖSUNG

Abbildung 1 zeigt das System der Koordinaten und der Zeichen für die Kugelumströmung, die hier behandelt werden soll.

Bei der schleichenden Strömung verändert sich die Strömungsgeschwindigkeit langsam mit dem Abstand von der Oberfläche des Körpers, so dass dabei in der Nähe der Oberfläche keine hydrodynamische Grenzschicht entsteht. Demgegenüber tritt

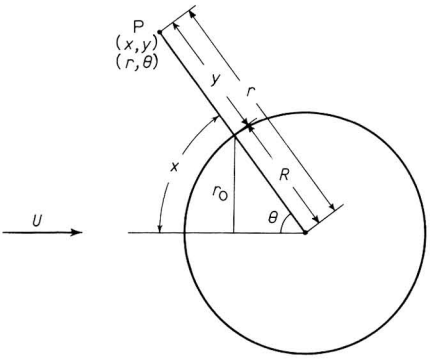

Abb. 1. Koordinatensystem und Zeichen für die Kugelumströmung.

die Ungleichmässigkeit der Konzentrationsverteilung des Depolarisators nur in der Nähe der Elektrodenoberfläche auf, weil infolge der kleinen Werte der Diffusionskoeffizienten die Pecletsche Zahl sehr gross ist[4]. Wir können darum als erste Approximation annehmen, dass die Geschwindigkeitskomponente der Strömung längs der Kugeloberfläche innerhalb der Diffusionsschicht in Verhältnis zum Abstand von der Oberfläche steht. Unter dieser Annahme gilt folgende Beziehung zwischen der Konzentration des Depolarisators auf der Elektrodenoberfläche und dem entspechenden Konzentrationsgradient, die in der früheren Arbeit[6] für die laminare rotationssymmetrische Strömung abgeleitet worden ist:

$$(c_j)_{y=0} = c_j^0 - \frac{(\frac{1}{3})^{\frac{1}{3}}}{\Gamma(\frac{2}{3})} D_j^{-\frac{2}{3}} \mu^{\frac{1}{3}} \int_0^x \frac{f_j(x_1) r_0(x_1) \mathrm{d}x_1}{\left[\int_{x_1}^x r_0(x_2)^{\frac{3}{2}} \tau(x_2)^{\frac{1}{2}} \mathrm{d}x_2\right]^{\frac{2}{3}}} \tag{1}$$

mit

$$f_j(x) = D_j(\partial c_j/\partial y)_{y=0} \,. \tag{2}$$

Hierbei bedeuten:

x = Abstand, gemessen längs der Meridiankurve des Rotationskörpers von dem Vorderstaupunkt

y = Abstand, gemessen längs der Normale von der Oberfläche des Rotationskörpers

$r_0(x)$ = Abstand des Punktes auf der Oberfläche des Rotationskörpers von der Rotationsachse

μ = innere Reibung der Lösung

$\tau(x)$ = Wandschubspannung

$(c_j)_{y=0}$, c_j^0 = Konzentration des Depolarisators S_j auf der Elektrodenoberfläche bzw. im Innern der Lösung

D_j = Diffusionskoeffizient des Depolarisators S_j

Zunächst möge das System der Kugelkoordinaten (r, θ) eingeführt werden. Für die Kugel erhalten wir dabei

$$\left.\begin{aligned} x &= R\theta, \; y = r - R \\ r_0 &= R \sin\theta \end{aligned}\right\} \tag{3}$$

wobei R den Halbmesser der Kugel bedeutet. Nach Stokes ergibt sich für die Geschwindigkeitskomponente u_θ längs der Kugeloberfläche die Formel[7]:

$$u_\theta = U\left\{1-\tfrac{3}{4}\left(\frac{R}{r}\right) - \tfrac{1}{4}\left(\frac{R}{r}\right)^3\right\}\sin\theta \tag{4}$$

wobei U die Geschwindigkeit der Parallelströmung ist. Daher erhalten wir für die Wandschubspannung

$$\tau = \mu\left(\frac{\partial u_\theta}{\partial r}\right)_{r=R} = \tfrac{3}{2}\mu\left(\frac{U}{R}\right)\sin\theta \tag{5}$$

Nach Einsetzen der Gln. (3) und (5) in Gl. (1) und Durchführung der Integration erhalten wir für die Oberflächenkonzentration des Stoffes S_j auf der Kugeloberfläche

$$(c_j)_{r=R} = c_j^0 - \frac{2}{3^{\frac{2}{3}}\Gamma(\frac{2}{3})}U^{-\frac{1}{3}}D_j^{-\frac{2}{3}}R^{\frac{2}{3}}\times \int_0^\theta \frac{f_j(\theta_1)\sin\theta_1\,\mathrm{d}\theta_1}{[(\theta-\frac{1}{2}\sin 2\theta)-(\theta_1-\frac{1}{2}\sin 2\theta_1)]^{\frac{2}{3}}} \tag{6}$$

Für die einfache Redox-Elektrodenreaktion, dargestellt durch

$$S_o + ne \rightleftarrows S_r \tag{7}$$

(S_o, S_r = oxydierter bzw. reduzierter Depolarisator, n = Zahl der Elektronen, die bei der Elektrodenreaktion aufgenommen bzw. abgegeben werden), lässt sich die Durchtrittsstromdichte i mit f_j folgendermassen zusammenfügen:

$$i = nFf_o = -nFf_r \tag{8}$$

Andererseits kann die Durchtrittsstromdichte nach der üblichen Theorie der Elektrodenkinetik ausgedrückt werden durch[8]

$$i = nFk_0\left\{(c_o)_{r=R}\exp\left[-\frac{\alpha nF}{RT}(E-E^0)\right] - (c_r)_{r=R}\exp\left[\frac{(1-\alpha)nF}{RT}(E-E^0)\right]\right\} \tag{9}$$

Hierbei bedeuten:

E = Potential der Kugelelektrode, gemessen gegen eine Bezugselektrode
E^0 = Normalpotential der Elektrodenreaktion (7), gemessen gegen eine Bezugselektrode
α = kathodischer Durchtrittsfaktor
k_0 = Geschwindigkeitskonstante der Elektrodenreaktion (7) beim entsprechenden Normalpotential

Nach Einsetzen der Gln. (6) und (8) in Gl. (9) und kurzen Umformungen erhalten wir die Volterrasche Integralgleichung zweiter Art

$$\varphi(\theta;\lambda) = \frac{2^{\frac{1}{3}}\Gamma(\frac{1}{3})}{3}\lambda\left\{1 - \frac{3(\frac{2}{3})^{\frac{2}{3}}}{\Gamma(\frac{1}{3})\Gamma(\frac{2}{3})}\times \int_0^\theta \frac{\varphi(\theta_1;\lambda)\sin\theta_1\,\mathrm{d}\theta_1}{[(\theta-\frac{1}{2}\sin 2\theta)-(\theta_1-\frac{1}{2}\sin 2\theta_1)]^{\frac{2}{3}}}\right\} \tag{10}$$

mit

$$\varphi(\theta;\lambda) = \frac{2^{\frac{1}{3}}\Gamma(\frac{1}{3})}{3} U^{-\frac{1}{3}} R^{\frac{2}{3}} \left(\frac{D_o^{\frac{2}{3}} c_o^0}{1+e^{\zeta}} - \frac{D_r^{\frac{2}{3}} c_r^0}{1+e^{-\zeta}} \right)^{-1} (i/nF) \tag{11}$$

$$\lambda = U^{-\frac{1}{3}} R^{\frac{2}{3}} (k_o/D^{\frac{2}{3}}) [e^{-\alpha\zeta} + e^{(1-\alpha)\zeta}] \tag{12}$$

$$D = (D_o)^{1-\alpha} (D_r)^{\alpha} \tag{13}$$

$$\zeta = \frac{nF}{RT} (E - E^r_{\frac{1}{2}}) \tag{14}$$

$$E^r_{\frac{1}{2}} = E^0 - \frac{RT}{nF} \ln \left(\frac{D_o}{D_r} \right)^{\frac{2}{3}} \tag{15}$$

Zunächst wollen wir die Integralgleichung (10) in die zur numerischen Auflösung geeignete Form transformieren. Ersetzen wir θ in Gl. (10) durch θ_2, multiplizieren dann die beiden Seiten mit

$$\frac{2 \sin^2 \theta_2}{[(\theta - \frac{1}{2}\sin 2\theta) - (\theta_2 - \frac{1}{2}\sin 2\theta_2)]^{\frac{1}{3}}}$$

und integrieren in Bezug auf θ_2 von Null bis θ, so erhalten wir

$$\frac{(\frac{2}{3})^{\frac{1}{3}}}{[2^{\frac{1}{3}}\Gamma(\frac{1}{3})/3]\lambda} \int_0^{\theta} \frac{\varphi(\theta_2;\lambda) \sin^2 \theta_2 \, d\theta_2}{[(\theta - \frac{1}{2}\sin 2\theta) - (\theta_2 - \frac{1}{2}\sin 2\theta_2)]^{\frac{1}{3}}}$$

$$= \tfrac{3}{4}(\tfrac{2}{3})^{\frac{1}{3}} (\theta - \tfrac{1}{2}\sin 2\theta)^{\frac{2}{3}} - \int_0^{\theta} \varphi(\theta_1;\lambda) \sin\theta_1 \, d\theta_1$$

nach Durchführung der gleichen Rechnung, wie in der Mitteilung III[9] angegeben worden ist. Differentiation der obigen Gleichung in Bezug auf θ liefert nach kurzer Rechnung mit partieller Integration

$$\varphi(\theta;\lambda) = \frac{[2^{\frac{1}{3}}\Gamma(\frac{1}{3})/3]\lambda}{1+[2^{\frac{1}{3}}\Gamma(\frac{1}{3})/3]\lambda} (\tfrac{2}{3})^{\frac{1}{3}} \frac{\sin\theta}{(\theta - \frac{1}{2}\sin 2\theta)^{\frac{1}{3}}} +$$

$$- \frac{(\frac{2}{3})^{\frac{1}{3}}}{[2^{\frac{1}{3}}\Gamma(\frac{1}{3})/3]\lambda} \sin\theta \int_0^{\theta} \frac{\frac{d\varphi(\theta_2;\lambda)}{d(\theta_2 - \frac{1}{2}\sin 2\theta_2)} d(\theta_2 - \tfrac{1}{2}\sin 2\theta_2)}{[(\theta - \frac{1}{2}\sin 2\theta) - (\theta_2 - \frac{1}{2}\sin 2\theta_2)]^{\frac{1}{3}}} \tag{16}$$

wobei die Beziehung:

$$\lim_{\theta \to 0} \varphi(\theta;\lambda) = \frac{[2^{\frac{1}{3}}\Gamma(\frac{1}{3})/3]\lambda}{1+[2^{\frac{1}{3}}\Gamma(\frac{1}{3})/3]\lambda} \tag{17}$$

benützt worden ist, deren Gültigkeit im Anhang bestätigt wird.

Zur numerischen Integration der Gl. (16) dividieren wir die θ-Achse in N gleiche Intervalle von Länge $\Delta\theta$ und ersetzen die Ableitung, $d\varphi(\theta_2;\lambda)/d(\theta_2 - \frac{1}{2}\sin 2\theta_2)$, in einzelnem Intervall $\Delta\theta$ durch den Ausdruck

$$\frac{d\varphi(\theta_2;\lambda)}{d(\theta_2 - \frac{1}{2}\sin 2\theta_2)} = \frac{\varphi(p\Delta\theta;\lambda) - \varphi([p-1]\Delta\theta;\lambda)}{\Delta\theta - \sin\Delta\theta \cos(2p-1)\Delta\theta}$$

für $(p-1)\Delta\theta \leqq \theta_2 \leqq p\Delta\theta$. Wir erhalten dabei nach Durchführung der Integration

$$\varphi(N\Delta\theta;\lambda) = \frac{[2^{\frac{1}{3}}\Gamma(\frac{1}{3})/3]\lambda}{1+[2^{\frac{1}{3}}\Gamma(\frac{1}{3})/3]\lambda}(\tfrac{2}{3})^{\frac{1}{3}}\frac{\sin N\Delta\theta}{(N\Delta\theta-\frac{1}{2}\sin 2N\Delta\theta)^{\frac{1}{3}}}$$

$$-\frac{(\frac{3}{2})^{\frac{2}{3}}}{[2^{\frac{1}{3}}\Gamma(\frac{1}{3})/3]\lambda}\sin N\Delta\theta\sum_{p=1}^{N}\{\varphi(p\Delta\theta;\lambda)-\varphi([p-1]\Delta\theta;\lambda)\}H(N,p),$$

mit

$$H(N,p) = \frac{\{(N-p+1)\Delta\theta-\sin(N-p+1)\Delta\theta\cos(N+p-1)\Delta\theta\}^{\frac{2}{3}}-\{(N-p)\Delta\theta-\sin(N-p)\Delta\theta\cos(N+p)\Delta\theta\}^{\frac{2}{3}}}{\Delta\theta-\sin\Delta\theta\cos(2p-1)\Delta\theta} \quad (18)$$

Es folgt aus der obigen Gleichung nach kurzer Umformung

$$\varphi(N\Delta\theta;\lambda) = \frac{(\frac{2}{3})^{\frac{1}{3}}\sin N\Delta\theta}{(N\Delta\theta-\sin N\Delta\theta\cos N\Delta\theta)^{\frac{1}{3}}}+\frac{(\frac{3}{2})^{\frac{2}{3}}}{[2^{\frac{1}{3}}\Gamma(\frac{1}{3})/3]\lambda}\sin N\Delta\theta\left\{H(N,1)+\sum_{p=1}^{N-1}\varphi(p\Delta\theta;\lambda)[H(N,p+1)-H(N,p)]\right\}$$

$$1+\frac{(\frac{3}{2})^{\frac{2}{3}}}{[2^{\frac{1}{3}}\Gamma(\frac{1}{3})/3]\lambda}\sin N\Delta\theta H(N,N)$$

$$(N=1,2,3,\ldots,M) \quad (19)$$

wobei M (=ganze Zahl) gleich $\pi/\Delta\theta$ ist. Mit Hilfe der Gl. (19) können wir daher die Werte der Funktion $\varphi(\theta;\lambda)$ nacheinander ermitteln. Für eine Reihe der Werte von λ sind die numerischen Berechnungen mit Hilfe der Rechenmaschine "FACOM 270-30" durchgeführt worden, wobei $M=100$ (also $\Delta\theta=\pi/100$) gesetzt worden ist*. Als Beispiele sind die Verläufe der Funktion $\varphi(\theta;\lambda)$ in Abhängigkeit von θ für einige Werte von λ in Abb. 2 wiedergegeben.

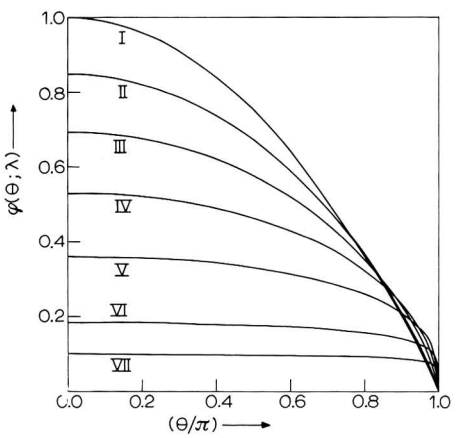

Abb. 2. Verläufe der Funktion $\varphi(\theta;\lambda)$ in Abhängigkeit von θ für einige Werte von λ. (I) $\lambda=\infty$, (II) 5.0, (III) 2.0, (IV) 1.0, (V) 0.5, (VI) 0.2, (VII) 0.1.

* Die Genauigkeit der numerischen Rechnungen ist selbstverständlich abhängig von der Grösse von $\Delta\theta$. Darum sind ferner die numerischen Berechnungen mit $M=200$ ($\Delta\theta=\pi/200$) für einige Werte von λ durchgeführt worden. Die Ergebnisse stehen in Übereinstimmung mit den entsprechenden Werten bei $M=100$ innerhalb der maximalen Fehlergrenze von etwa 0.0005 im Bereich $0\leqq\theta\leqq(19/20)$. Dies zeigt, dass die Genauigkeit der vorliegenden Rechnungen mit $M=100$ befriedigend ist.

Unter Berücksichtigung der Gl. (11) erhalten wir daher für die Verteilung der Stromdichte auf der Elektrodenoberfläche

$$i = \frac{3}{2^{\frac{1}{3}}\Gamma(\frac{1}{3})} nF\left(\frac{D_o^{\frac{2}{3}} c_o^0}{1+e^{\zeta}} - \frac{D_r^{\frac{2}{3}} c_r^0}{1+e^{-\zeta}}\right) U^{\frac{1}{3}} R^{-\frac{2}{3}} \varphi(\theta;\lambda) \tag{20}$$

Bei $\zeta \to -\infty$ und $\zeta \to +\infty$ nähert sich die Stromdichte i der entsprechenden maximalen Stromdichte, d.h. der kathodischen bzw. anodischen Diffusionsgrenzstromdichte, i_d^c bzw. i_d^a. Da $\lambda \to \infty$ bei $\zeta \to \pm\infty$, so folgt unmittelbar aus Gl. (16)

$$\varphi(\theta;\lambda\to\infty) = (\tfrac{2}{3})^{\frac{1}{3}} \frac{\sin\theta}{(\theta - \frac{1}{2}\sin 2\theta)^{\frac{1}{3}}}$$

Daraus erhalten wir für die Diffusionsgrenzstromdichten

$$i_d^c = [3^{\frac{2}{3}}/\Gamma(\tfrac{1}{3})] nF D_o^{\frac{2}{3}} c_o^0 U^{\frac{1}{3}} R^{-\frac{2}{3}} \frac{\sin\theta}{(\theta - \frac{1}{2}\sin 2\theta)^{\frac{1}{3}}} \tag{21}$$

$$i_d^a = -[3^{\frac{2}{3}}/\Gamma(\tfrac{1}{3})] nF D_r^{\frac{2}{3}} c_r^0 U^{\frac{1}{3}} R^{-\frac{2}{3}} \frac{\sin\theta}{(\theta - \frac{1}{2}\sin 2\theta)^{\frac{1}{3}}} \tag{22}$$

Diese Ausdrücke sind bereits von Lewitsch[4] abgeleitet und diskutiert worden.

Die Gesamtstromstärke I kann durch Integration der Stromdichte über die gesamte Oberfläche der Kugelelektrode ermittelt werden. Wir erhalten unter Berücksichtigung, dass $(3\pi)^{\frac{5}{3}}/[2\Gamma(\frac{1}{3})] = 7.85$ ist,

$$I = 2\pi R^2 \int_0^{\pi} i \sin\theta \, d\theta$$

$$= \left(\frac{I_d^c}{1+e^{\zeta}} + \frac{I_d^a}{1+e^{-\zeta}}\right) \Phi(\lambda) \tag{23}$$

mit

$$I_d^c = 7.85\, nF c_o^0 D_o^{\frac{2}{3}} U^{\frac{1}{3}} R^{\frac{4}{3}} \tag{24}$$

$$I_d^a = -7.85\, nF c_r^0 D_r^{\frac{2}{3}} U^{\frac{1}{3}} R^{\frac{4}{3}} \tag{25}$$

$$\Phi(\lambda) = 2^{\frac{5}{2}}(3\pi)^{-\frac{2}{3}} \int_0^{\pi} \varphi(\theta;\lambda) \sin\theta \, d\theta \tag{26}$$

Hierbei bedeuten I_d^c und I_d^a die kathodische bzw. anodische Diffusionsgrenzstromstärke, da sie durch Integration der Gln. (21) bzw. (22) über die gesamte Oberfläche der Kugelelektrode abgeleitet werden können. Die Werte der Funktion $\Phi(\lambda)$ in Abhängigkeit von λ sind dadurch berechnet worden, mit Hilfe der Simpsonsche $\frac{1}{3}$-Regel angegebene Integration durchzuführen. Die Ergebnisse sind in Tab. 1 wiedergegeben. Glücklicherweise kann der Verlauf der Funktion $\Phi(\lambda)$ in Abhängigkeit von λ innerhalb der maximalen Fehlergrenze von ± 0.0045 durch folgende einfache Formel approximiert werden:

$$\Phi(\lambda) = \lambda/(0.600 + \lambda) \tag{27}$$

Infolgedessen erhalten wir nach kurzer Umformung

$$I = \left(\frac{I_d^c}{1+e^{\zeta}} + \frac{I_d^a}{1+e^{-\zeta}}\right) \frac{(k_0/D^{\frac{2}{3}}) U^{-\frac{1}{3}} R^{\frac{2}{3}} [e^{-\alpha\zeta} + e^{(1-\alpha)\zeta}]}{A + (k_0/D^{\frac{2}{3}}) U^{-\frac{1}{3}} R^{\frac{2}{3}} [e^{-\alpha\zeta} + e^{(1-\alpha)\zeta}]} \tag{28}$$

TABELLE 1

VERLAUF DER FUNKTION $\Phi(\lambda)$ IN ABHÄNGIGKEIT VON λ

λ	$\Phi(\lambda)$	λ	$\Phi(\lambda)$	λ	$\Phi(\lambda)$
0.00	0.0000	1.4	0.7034	8	0.9331
0.02	0.0311	1.6	0.7311	9	0.9402
0.05	0.0744	1.8	0.7541	10	0.9458
0.10	0.1391	2.0	0.7735	15	0.9633
0.15	0.1956	2.2	0.7901	20	0.9723
0.2	0.2455	2.4	0.8045	25	0.9777
0.3	0.3294	2.6	0.8170	30	0.9814
0.4	0.3970	2.8	0.8280	40	0.9860
0.5	0.4526	3.0	0.8378	50	0.9888
0.6	0.4991	3.5	0.8580	60	0.9906
0.7	0.5384	4.0	0.8737	80	0.9929
0.8	0.5722	4.5	0.8863	100	0.9943
0.9	0.6014	5.0	0.8966	200	0.9972
1.0	0.6270	6	0.9125		
1.2	0.6695	7	0.9242	∞	1.0000

mit $A = 0.600$.

Diese ist die zu erhaltende Formel für die stationären Strom–spannungskurven. Gleichung (28) ist ganz gleich in der Form, wie diejenigen für die Strom–spannungskurven in der Polarographie[10] und der hydrodynamischen Voltammetrie[6,9,11]. Daher gelten hier die gleichen Diskussionen für die kinetische Analyse der Strom-spannungskurven.

GRENZSTROMSTÄRKEN UND STATIONÄRE STROM–SPANNUNGSKURVEN BEI ANWESENHEIT DER VORGELAGERTEN CHEMISCHEN REAKTION VON ERSTER ORDNUNG

Als Beispiel der Elektrodenreaktion mit einer vorgelagerten chemischen Reaktion von erster Ordnung sollen folgende Vorgänge behandelt werden:

$$S_x \rightleftarrows S_o \quad \text{(homogene chemische Reaktion)} \tag{29}$$

$$S_o + ne \rightleftarrows S_r \quad \text{(Durchtrittsreaktion)} \tag{7}$$

Wir wollen hier annehmen, dass die vorgelagerte Reaktion sehr schnell verläuft und also die Reaktionsschicht grössenordnungsgemäss dünner als die Diffusionsschicht ist. Unter dieser Voraussetzung kann das Randwertproblem für den durch Gln. (29) und (7) angegebenen Reaktionsmechanismus durch das ganz gleiche Rechnungsverfahren aufgelöst werden, wie in den früheren Arbeiten[6,11] benützt worden ist. Unter Berücksichtigung der Gln. (6) und (8) erhalten wir daher für die Oberflächenkonzentration des Stoffes S_o

$$(c_o)_{r=R} = \frac{1}{1+K}\left\{c^0 - \frac{(i/nF)}{\lambda_1 D_{xo}^{\frac{1}{3}}} - \frac{2}{3^{\frac{2}{3}}\Gamma(\frac{1}{3})} U^{-\frac{1}{3}} D_{xo}^{-\frac{2}{3}} R^{\frac{2}{3}} \times \right.$$

$$\left. \int_0^{\theta} \frac{(i/nF)\sin\theta_1 \,\mathrm{d}\theta_1}{[(\theta - \frac{1}{2}\sin 2\theta) - (\theta_1 - \frac{1}{2}\sin 2\theta_1)]^{\frac{2}{3}}}\right\} \tag{30}$$

mit

$$\lambda_1 = (D_{xo}/D_x)(D_o/D_x)^{\frac{1}{2}}[k(1+K)]^{\frac{1}{2}}/K \tag{31}$$

$$D_{xo} = (KD_x + D_o)/(1+K) \tag{32}$$

$$K = c_x^0/c_o^0 \tag{33}$$

$$c^0 = c_o^0 + c_x^0 \tag{34}$$

Hierbei bedeuten:

c_x^0 = Konzentration des Stoffes S_x im Innern der Lösung

D_x = Diffusionskoeffizient des Stoffes S_x

k, K = Reaktionsgeschwindigkeits- bzw. Gleichgewichtskonstante der vorgelagerten Reaktion (29)

Die Oberflächenkonzentration des Stoffes S_r lässt sich andererseits durch Gl. (6) mit Gl. (8) angeben. Wenn man also die Ausdrücke der Oberflächenkonzentrationen von S_o und S_r in Gl. (9) einsetzt und dann als neuen Parameter

$$\lambda' = U^{-\frac{1}{3}} R^{\frac{2}{3}} \frac{1+e^{\zeta'}}{\{[k_0'/(D')^{\frac{2}{3}}]e^{-\alpha\zeta'}\}^{-1} + \{\lambda_1 D_{xo}^{\frac{1}{2}}\}^{-1}} \tag{35}$$

mit

$$k_o' = k_o/(1+K)^{1-\alpha} \tag{36}$$

$$D' = D_{xo}^{1-\alpha} D_r^{\alpha} \tag{37}$$

$$\zeta' = (nF/RT)[E-(E_{\frac{1}{2}}^r)'] \tag{38}$$

$$(E_{\frac{1}{2}}^r)' = E^0 - (RT/nF)\ln(1+K) - (RT/nF)\ln(D_{xo}/D_r)^{\frac{2}{3}} \tag{39}$$

und als neue Funktion

$$\varphi(\theta;\lambda') = \frac{2^{\frac{1}{3}}\Gamma(\frac{1}{3})}{3} U^{-\frac{1}{3}} R^{\frac{2}{3}} \left\{\frac{D_{xo}^{\frac{2}{3}} c_o^0}{1+e^{\zeta'}} - \frac{D_r^{\frac{2}{3}} c_r^0}{1+e^{-\zeta'}}\right\}^{-1} (i/nF) \tag{40}$$

in die erhaltene Gleichung einführt, so erhält man nach kurzer Umformung die Integralgleichung (10) mit dem Parameter λ' statt λ. Daraus folgt unmittelbar für die Stromdichte

$$i = \frac{3}{2^{\frac{1}{3}}\Gamma(\frac{1}{3})} nF \left\{\frac{D_{xo}^{\frac{2}{3}} c^0}{1+e^{\zeta'}} - \frac{D_r^{\frac{2}{3}} c_r^0}{1+e^{-\zeta'}}\right\} U^{\frac{1}{3}} R^{-\frac{2}{3}} \varphi(\theta;\lambda') \tag{41}$$

wobei die Verläufe der Funktion $\varphi(\theta;\lambda')$ in Abhängigkeit von θ für einige Werte von λ' aus Abb. 2 ersehen werden können.

Die kathodischen und anodischen Grenzstromdichten lassen sich durch Einsetzen von $\zeta' \to -\infty$ bzw. $\zeta' \to +\infty$ in Gl. (41) ermitteln. Daraus ergibt sich für die kathodische Grenzstromdichte

$$i_l^c = \frac{3}{2^{\frac{1}{3}}\Gamma(\frac{1}{3})} nFD_{xo}^{\frac{2}{3}} c^0 U^{\frac{1}{3}} R^{-\frac{2}{3}} \varphi(\theta; U^{-\frac{1}{3}} R^{\frac{2}{3}} \lambda_1 D_{xo}^{\frac{1}{3}}) \tag{42}$$

Andererseits lässt sich die anodische Grenzstromdichte durch Gl. (22) angeben.

Die Gesamtstromstärke I kann durch Integration der Stromdichte über die gesamte Elektrodenoberfläche ermittelt werden. Benützen wir also die Näherungsformel (27), so erhalten wir nach kurzer Umformung für die kathodischen und ano-

dischen Grenzstromstärken, I_l^c bzw. I_l^a, und die stationäre Stromspannungskurve

$$I_l^c = I_d^c \frac{(D_{xo}/D_x)(D_o/D_x)^{\frac{1}{2}}[k(1+K)]^{\frac{1}{2}}/K}{AU^{\frac{1}{3}}R^{-\frac{2}{3}}D_{xo}^{\frac{1}{6}}+(D_{xo}/D_x)(D_o/D_x)^{\frac{1}{2}}[k(1+K)]^{\frac{1}{2}}/K} \tag{43}$$

$$I_l^a = I_l^a$$

$$I = \left\{\frac{I_d^c}{1+e^{\zeta'}} + \frac{I_d^a}{1+e^{-\zeta'}}\right\} \times \frac{[k_0'/(D')^{\frac{2}{3}}]U^{-\frac{1}{3}}R^{\frac{2}{3}}[e^{-\alpha\zeta'}+e^{(1-\alpha)\zeta'}]}{A+[k_0'/(D')^{\frac{2}{3}}]U^{-\frac{1}{3}}R^{\frac{2}{3}}[(I_d^c/I_l^c)e^{-\alpha\zeta'}+e^{(1-\alpha)\zeta'}]} \tag{44}$$

mit $A = 0.600$, wobei I_d^c und I_d^a die kathodische bzw. anodische Diffusionsgrenzstromstärke bedeuten. Die kathodische Diffusionsgrenzstromstärke lässt sich folgendermassen ausdrücken:

$$I_d^c = 7.85\, nFc^0 D_{xo}^{\frac{2}{3}} U^{\frac{1}{3}} R^{\frac{4}{3}} \tag{45}$$

und die anodische wird andererseits durch Gl. (25) wiedergegeben.

Gleichungen (43) und (44) sind, mit Ausnahme der numerischen Faktoren, gleich den entsprechenden Gleichungen für die Elektrodenreaktionen mit vorgelagerten Reaktionen in der Polarographie[12] und in der hydrodynamischen Voltammetrie[6,9,11]. Für die kinetische Analyse der Gln. (43) und (44) gelten daher analoge Diskussionen, wie in denselben Arbeiten durchgeführt worden sind.

ANWENDUNG DER OBIGEN ERGEBNISSE AUF DIE IN DER SCHLEICHENDEN PARALLELSTRÖMUNG WACHSENDE QUECKSILBERTROPFELEKTRODE

Kimla und Štráfelda[2] haben theoretisch und experimentell gezeigt, dass sich die Diffusionsgrenzstromstärke an der Quecksilbertropfelektrode, die von der Strömung mit der Stokesschen Geschwindigkeit umflossen wird, in erster Approximation in gleicher Weise verhält, wie an einer stationären festen Kugelelektrode. Infolgedessen gelten auch für die umflossenen Quecksilbertropfelektrode alle Gleichungen, die in den vorangehenden Abschnitten abgeleitet worden sind, wenn man

$$R = (3mt/4\pi d)^{\frac{1}{3}} \tag{46}$$

einsetzt. Hierbei bedeuten:

d = spezifisches Gewicht des Quecksilbers
m = Zuflussgeschwindigkeit des Quecksilbers aus der Kapillare
t = Zeit nach Beginn der Lebensdauer eines Tropfens

Zur Registrierung der Strom–spannungskurven an der Quecksilbertropfelektrode stehen gegenwärtig zwei Methoden zur Verfügung. Bei der ersten Methode wird die Stromstärke an einer bestimmten Zeit t_1 nach Beginn des Tropfenwachstums, z.B., an der Zeit unmittelbar vor dem Abfall des Tropfens, gemessen. Dabei können wir daher für die Ausdrücke der Grenzstromstärken und der Strom–spannungskurven Gln. (24), (25), (28), (43) und (44) mit $R = (3mt_1/4\pi d)^{\frac{1}{3}}$ benützen.

Bei der zweiten Methode, die heute weitgehend benützt ist, messen wir die über die Tropfzeit gemittelte Stromstärke. Als Beispiel soll hier die Strom–spannungskurve bei Abwesenheit der vorgelagerten Reaktion behandelt werden. Unter Berück-

sichtigung, dass hier R und λ abhängig von t sind, ergibt sich aus Gl. (23) für den gemittelten Wert der Stromstärke

$$\bar{I} = \frac{1}{t_2}\int_0^{t_2} I\,\mathrm{d}t$$

$$= \left(\frac{\bar{I}_\mathrm{d}^\mathrm{c}}{1+\mathrm{e}^{\zeta}} + \frac{\bar{I}_\mathrm{d}^\mathrm{a}}{1+\mathrm{e}^{-\zeta}}\right)\bar{\Phi}(\lambda(t_2)) \tag{47}$$

mit

$$\bar{I}_\mathrm{d}^\mathrm{c} = (\tfrac{9}{13})7.85\, nFc_\mathrm{o}^0 D_\mathrm{o}^{\frac{2}{3}} U^{\frac{1}{3}}[R(t_2)]^{\frac{4}{3}} \tag{48}$$

$$\bar{I}_\mathrm{d}^\mathrm{a} = -(\tfrac{9}{13})7.85\, nFc_\mathrm{r}^0 D_\mathrm{r}^{\frac{2}{3}} U^{\frac{1}{3}}[R(t_2)]^{\frac{4}{3}} \tag{49}$$

$$\bar{\Phi}(\lambda(t_2)) = (\tfrac{13}{9})\frac{1}{[R(t_2)]^{\frac{4}{3}} t_2}\int_0^{t_2} \Phi(\lambda(t))[R(t)]^{\frac{4}{3}}\,\mathrm{d}t \tag{50}$$

Hierbei bedeuten:

t_2 = Tropfzeit

$\bar{I}_\mathrm{d}^\mathrm{c}$, $\bar{I}_\mathrm{d}^\mathrm{a}$ = über die Tropfzeit gemittelte kathodische bzw. anodische Diffusionsgrenzstromstärken

$R(t_2)$, $\lambda(t_2)$ = entsprechende Werte an $t = t_2$.

Wenn man hier die Näherungsformel (27) für $\Phi(\lambda)$, so lässt sich Gl. (50), nach Umformung der Integrationsvariable unter Berücksichtigung der Gln. (12) und (46), transformieren in

$$\bar{\Phi}(\lambda(t_2)) = \tfrac{13}{2}[\lambda(t_2)]^{-13/2}\int_0^{\lambda(t_2)} \frac{\lambda^{13/2}\,\mathrm{d}\lambda}{0.6+\lambda}$$

Die obige Integration kann leicht durchgeführt werden. Es folgt

$$\bar{\Phi}(\lambda(t_2)) = 1 + \sum_{N=1}^{6}(-1)^N\left(\frac{13}{13-2N}\right)\left[\frac{0.6}{\lambda(t_2)}\right]^N - 13\left[\frac{0.6}{\lambda(t_2)}\right]^{13/2}\tan^{-1}\left[\frac{\lambda(t_2)}{0.6}\right]^{\frac{1}{2}} \tag{51}$$

Die Werte der Funktion $\bar{\Phi}(\lambda(t_2))$ in Abhängigkeit von $\lambda(t_2)$ sind numerisch ausgerechnet worden. Die Ergebnisse lassen sich glücklicherweise innerhalb der maximalen Fehlergrenze von etwa ± 0.001 durch folgende einfache Formel approximieren:

$$\bar{\Phi}(\lambda(t_2)) = \frac{\lambda(t_2)}{0.700+\lambda(t_2)} \tag{52}$$

Einsetzen der Gl. (52) in Gl. (47) liefert

$$\bar{I} = \left(\frac{\bar{I}_\mathrm{d}^\mathrm{c}}{1+\mathrm{e}^{\zeta}} + \frac{\bar{I}_\mathrm{d}^\mathrm{a}}{1+\mathrm{e}^{-\zeta}}\right)\frac{(k_0/D^{\frac{2}{3}})U^{-\frac{1}{3}}[R(t_2)]^{\frac{2}{3}}[\mathrm{e}^{-\alpha\zeta}+\mathrm{e}^{(1-\alpha)\zeta}]}{A+(k_0/D^{\frac{2}{3}})U^{-\frac{1}{3}}[R(t_2)]^{\frac{2}{3}}[\mathrm{e}^{-\alpha\zeta}+\mathrm{e}^{(1-\alpha)\zeta}]} \tag{53}$$

mit $A = 0.700$.

Wie aus dem Vergleich der Gl. (53) mit Gl. (28) zu ersehen ist, lässt sich der obige Ausdruck unmittelbar aus Gl. (28) ableiten, wenn man $\bar{I}_\mathrm{d}^\mathrm{c}$, $\bar{I}_\mathrm{d}^\mathrm{a}$, $R(t_2)$ und $A = 0.700$ statt I_d^c, I_d^a, R bzw. $A = 0.600$ einsetzt. Für die Elektrodenreaktionen mit der vorgelagerten Reaktion können wir deshalb durch Anwendung der gleichen Substitution auf Gln. (43) und (44) die Ausdrücke der Grenzstromstärke und der Strom–spannungskurve erhalten.

ANHANG

In der Nähe von $\theta=0$ gelten die Beziehungen:

$$\sin\theta \sim \theta, \quad (\theta-\tfrac{1}{2}\sin 2\theta) \sim \tfrac{2}{3}\theta^3$$

Daraus ergibt sich Gl. (10) zu

$$\varphi(\theta;\lambda) = \frac{2^{\frac{1}{3}}\Gamma(\frac{1}{3})}{3}\lambda\left\{1 - \frac{3}{\Gamma(\frac{1}{3})\Gamma(\frac{2}{3})}\int_0^{\theta}\frac{\varphi(\theta_1;\lambda)\theta_1 \mathrm{d}\theta_1}{(\theta^3-\theta_1^3)^{\frac{2}{3}}}\right\}$$

Diese Integralgleichung kann leicht in exakter Weise aufgelöst werden. Unter Annahme, dass $\varphi(\theta;\lambda)$ unabhängig von θ ist, erhalten wir nach Durchführung der angegebenen Integration

$$\varphi(\theta;\lambda) = \frac{[2^{\frac{1}{3}}\Gamma(\frac{1}{3})/3]\lambda}{1+[2^{\frac{1}{3}}\Gamma(\frac{1}{3})/3]\lambda}$$

Da die obige Gleichung nicht θ enthält, so gilt sie als Lösung der Integralgleichung im Bereich $\theta \to 0$.

Frl. C. Nishihara möchte ich an dieser Stelle für die numerischen Berechnungen mit Hilfe der Rechenmaschine "FACOM 270-30" herzlich danken.

ZUSAMMENFASSUNG

Unter Berücksichtigung der beiden Geschwindigkeiten der konvektiven Diffusion und der Kinetik werden die Redox-Elektrodenreaktionen ohne und mit einer vorgelagerten chemischen Reaktion theoretisch behandelt, die auf der Oberfläche der in schleichende Parallelströmung eingetauchten Kugelelektrode verlaufen. Es werden dabei die einfachen Näherungsformeln für die stationären Strom–spannungskurven und die kinetisch bedingten Grenzstromstärken abgeleitet. Ferner werden die Ergebnisse auf die Quecksilbertropfelektrode angewandt, welche an der dünnwandigen Spitzkapillare in der schleichenden Parallelströmung wächst.

SUMMARY

Redox-electrode reactions without and with a preceding chemical reaction proceeding on the surface of a spherical electrode immersed in a creeping parallel flow are theoretically treated, considering both rates of convective diffusion and kinetic processes. Simple approximate formulae are derived for the stationary current–voltage curves and the kinetically controlled limiting currents. Furthermore, the results obtained are applied on the dropping mercury electrode, which grows at a thin walled capillary in the creeping parallel flow.

LITERATUR

1 F. Šträfelda, *Collection Czech. Chem. Commun.*, 25 (1960) 862; F. Šträfelda und A. Kimla, *ibid.* 28 (1963) 1516.
2 A. Kimla und F. Šträfelda, *Collection Czech. Chem. Commun.*, 29 (1964) 2913.

3 Y. TAKEMORI, Vorgetragen auf den polarographischen Diskussionstagungen in Osaka am 3. November 1967 und in Hiroshima am 9. Oktober 1968.
4 V. G. LEWITSCH, *Physicochemical Hydrodynamics*, Prentice-Hall, Englewood Cliffs, N. J., 1962, p. 80.
5 A. KIMLA, *Collection Czech. Chem. Commun.*, 28 (1963) 2696; 29 (1964) 1956.
6 H. MATSUDA, *J. Electroanal. Chem.*, 15 (1967) 109.
7 Z. B. L. ROSENHEAD (Ed.), *Laminar Boundary Layers*, Oxford University Press, London, 1963, p. 170.
8 K. J. VETTER, *Elektrochemische Kinetik*, Springer-Verlag, Berlin-Gottingen-Heidelberg, 1961, S. 102.
9 H. MATSUDA, *J. Electroanal. Chem.*, 21 (1969) 433.
10 H. MATSUDA UND Y. AYABE, *Bull. Chem. Soc. Japan*, 28 (1955) 422.
11 H. MATSUDA, *J. Electroanal. Chem.*, 15 (1967) 325.
12 H. MATSUDA UND Y. AYABE, *Bull. Chem. Soc. Japan*, 29 (1956) 134.

ELECTROANALYTICAL CHEMISTRY AND INTERFACIAL ELECTROCHEMISTRY
Elsevier Sequoia S.A., Lausanne – Printed in The Netherlands

A STUDY OF THE ELECTROCHEMICAL BEHAVIOUR OF PERRHENATE ION IN AQUEOUS SOLUTION

D. W. LETCHER, T. J. CARDWELL AND R. J. MAGEE
Department of Chemistry, La Trobe University, Bundoora, Victoria 3083 (Australia)
(Received December 5th, 1969)

INTRODUCTION

The reduction of perrhenate ion in aqueous solution has been the subject of numerous papers in the last few years and many authors have calculated a value of n from the Ilkovic equation in order to determine the valence change corresponding to the reduction wave. Values of n varying from 1 to 10 have been reported for the first wave in aqueous solutions of different supporting electrolytes but at this time it is generally accepted that the first reduction wave in acid solution corresponds to a valence change of three electrons. Whether this is correct or not it still leaves unresolved the question of how many electrons are involved in the rate determining step. Shropshire[1,2] has presented evidence that (at the mercury electrode) the rate determining step involves one electron, and hence proceeds *via* a Re(VI) state in sulphuric acid solution. Demkin and Sinyakova[3], and Toul *et al.*[4] have obtained evidence of an intermediate Re(V) state, and as evidence is freely available to indicate the stability of a Re(V) state[5,6] it was decided to reinvestigate the reduction waves of Re(VII) in acid solution. This paper reports the nature of the reduction wave of Re(VII) in acid solution (4 M $HClO_4$), details of the a.c. reduction waves in this medium (not previously reported) and additional evidence that the reduction of perrhenate ion in perchloric acid proceeds *via* an intermediate Re(V) state.

EXPERIMENTAL

Rhenium as $KReO_4$ (Alfa Inorganics, Beverly, Mass.) was used without further purification. Reagent grade chemicals were used throughout and the perchloric acid used was prepurified by electrolysis using a Tacussel model PRT20-2A potentiostat.

A.c. and d.c. polarograms were obtained using a Metrohm model E261 R Polarecord with a.c. modulator E393 and drop time controller E354. Amperometric and coulometric studies were undertaken using the Tacussel potentiostat. Potential sweep chronoamperometry and cyclic voltammetry were undertaken using the Radiometer PO4 polariter in conjunction with the Metrohm I.R. compensator.

RESULTS AND DISCUSSION

In neutral solutions of KCl, LiCl and CsCl, waves were obtained which were for the most part distorted by the presence of a maximum. In 2 M KCl at low concen-

trations of the depolarizer (0.02 m*M*), a well-formed wave was obtained that did not have its plateau parallel to the residual current curve. Further investigation showed that in 2 *M* KCl solutions the inception of the H^+ discharge wave occurred at progressively more positive potentials as the concentration of the depolarizer was reduced, a phenomenon reported by Demkin and Sinyakova[3] in HCl solutions. In solutions that were more concentrated (0.02–0.14 m*M*) better plateaux were developed, although these were distorted by the presence of a maximum. It was found that the presence of Triton-X-100 affected the height of the wave and that 0.005% T-X-100 obliterated the wave completely in all media tested. The behaviour in LiCl and CsCl was similar to KCl, except that the maximum was more strongly developed. Potassium sulphate, potassium nitrate, sodium perchlorate and tetra-n-butylammonium iodide were tried but no useful waves could be obtained in these media.

In acidic solutions ($HClO_4$, H_2SO_4, H_2SO_4–K_2SO_4 and HCl), good waves were obtained at 25°C as already reported[7–9]. All of these waves were distorted however in as much as the plateau of the wave was not parallel to the residual current curve.

In 4 *M* perchloric acid this difficulty was overcome by raising the temperature to 50°C. At this temperature well developed waves were obtained that were suitable for analysis. Munze[10] has shown that the reduction product of Re(VII) is adsorbed on mercury and the effect that an adsorbed product has on the d.c. polarogram is described by Vlcek[11]. The waves that were obtained in acid solutions all exhibited behaviour that was in agreement with the predictions of Vlcek for a reduction that led to an adsorbed product. Rulfs and Elving[9] have already suggested that the reduction wave of perrhenate ion in 4 *M* perchloric acid solution may be an adsorption wave. As the slope of the plateau changes with temperature it is difficult to measure $E_{\frac{1}{2}}$ values or limiting current values to test this hypothesis. Using a.c. polarography we were able to determine the change of peak current with temperature and the change in summit potential with temperature (Table 1). In 4 *M* perchloric acid solution: (*a*) the change of summit potential with temperature did indicate a negative temperature

TABLE 1

Temp./°C	*Concn.* = 0.08 *mM*		*Concn.* = 0.04 *mM*	
	Peak curr. $I_p/\mu A$	*Summit pot.* E_s/V	*Peak curr.* $I_p/\mu A$	*Summit pot.* E_s/V
25	0.108	−0.522	0.050	−0.530
35	0.133	−0.536	0.063	−0.530
40	0.146	−0.546	0.069	−0.534
45	0.161	−0.544	0.078	−0.534
50	0.176	−0.550	0.092	−0.536

coefficient over the range 6.3°–50°C, although the change was in fact quite small; (*b*) the wave was obliterated by very small concentrations of surface active agents; (*c*) the plateau of the wave obtained at 6.3°C was more nearly parallel to the residual current curve than was the case at 25°C.

Most of these comparisons were made using rapid d.c. or rapid a.c. polaro-

grams. In these cases, where the drop time is small (0.2 s), adsorption does not have time to produce its greatest effect, hence the lack of parallelism is not as marked as at lower rates of polarization. At concentrations of 0.04 mM and below the plateau of the reduction wave in 4M perchloric acid is parallel to the residual current curve at a temperature of 50°C even at slow rates of polarization (as in normal d.c. polarography). If the concentration is reduced below 0.01 mM the plateau is not well developed even at 50°C, due to the early inception of the H^+ discharge. It is contended that these results indicate that both perrhenate ion and its reduction product are adsorbed on the mercury drop but that the perrhenate ion is more strongly adsorbed. The changes in the electrical double layer can be graphically illustrated by viewing the changes taking place in the base current of the a.c. polarograms as the temperature changes (Fig. 1).

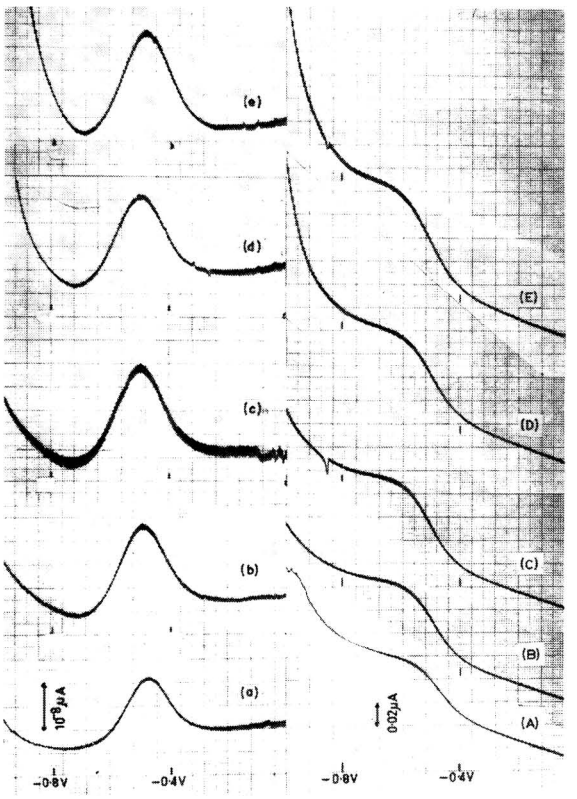

Fig. 1. A.c. polarograms at various temps. (a) (A) 6.3°C, (b) (B) 20°C, (c) (C) 25°C, (d) (D) 40°C, (e) (E) 50°C. Concn. of $KReO_4$ = 0.12 mM; supporting electrolyte is 4 M $HClO_4$.

The normal d.c. polarogram was analysed by taking a plot* of $E_{d.e.}$ *vs.* log $[2\cdot(3-x)/5(x-1)]$ at 50°C (Fig. 2) using the method of Oldham and Parry[12]. The "log plot" so obtained is curved, apparently due to the adsorption of the perrhenate ion

* x is ratio of the instantaneous current at time t and potential E to the current that would flow at the same time t and a very much more negative potential.

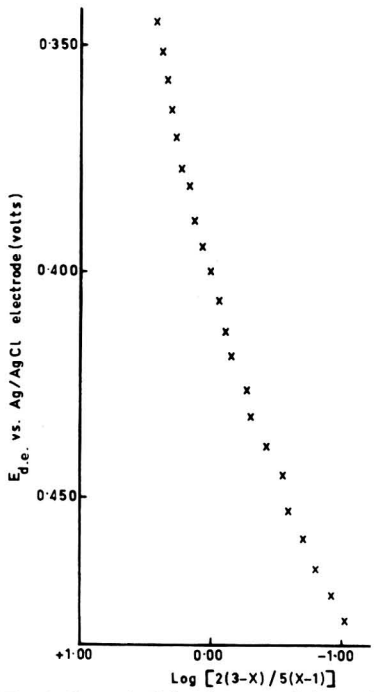

Fig. 2. "Log plot" for the normal d.c. polarogram at 50°C.

on the mercury drop. The various explanations for this type of behaviour that were considered were: (*a*) a change in the concentration of one of the substances involved in the electrochemical reduction or a rapid subsequent chemical reaction; (*b*) the presence of two coupled electrochemical reactions that have very different α values. This could cause one reduction that is slower at the foot of the wave to be more rapid at the top of the wave. Berzins and Delahay[13] examined this behaviour and the "log plots" obtained by these workers do not resemble the "log plots" reported here (Fig. 2); (*c*) the presence of a coupled chemical reduction. Feldberg[14] has examined this type of electrochemical behaviour and reports that pertechnetate ion undergoes a coupled chemical reaction in alkaline solution.

The most likely explanation for this curved "log plot" is (*a*) above, *i.e.* the concentration of oxidant at the drop surface, c_o^0, has been raised to a larger value than that predicted for a purely diffusional process. This difference between the actual and the predicted values of c_o^0 will be greatest at the foot of the wave with the actual value approaching the predicted value asymptotically as the plateau of the wave is approached. Thus the curved "log plot" should approach asymptotically the straight line that would be obtained if c_o^0 were not being artifically increased due to adsorption. If this interpretation of the behaviour is correct one would expect that, as the drop time is decreased (so that the time for adsorption is minimized and c_o^0 will be closer to the value determined by diffusion alone), the slopes of the "log plot" near the top and bottom of the wave should be more nearly coincident. A "log plot" was constructed from a polarogram using a drop time of 0.2 s and the curvature of the "log plot" was greatly reduced, Fig. 3. The values of αn_a reported here were therefore calculated from

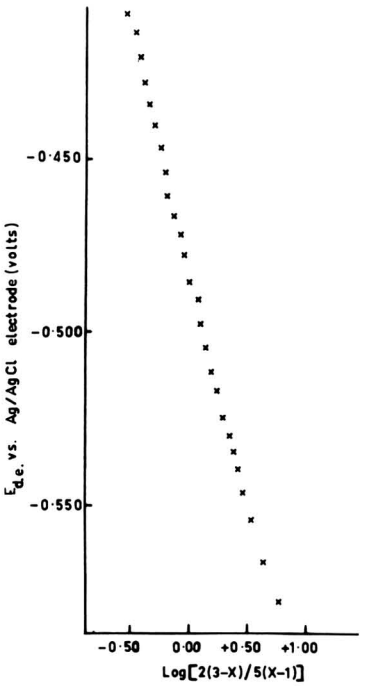

Fig. 3. "Log plot" for the d.c. polarogram using a drop time of 0.2 s.

the points occurring on the top half of the normal d.c. polarogram, *i.e.* from values of the log term equal to zero to those points where the log term assumes its most positive values. The slope of the "log plot" was obtained by carrying out a regression analysis on the points so obtained by means of a sub-routine available to users of the I.C.L. computer 1901A. The values so obtained are recorded in Table 2 along with other pertinent data.

TABLE 2

Concentration of $KReO_4 = 0.04$ mM; temperature = 50°C

	αn_a	*Std. dev.*	*Correlation coefficient*	$E_{\frac{1}{2}}/V$ *vs. Ag/AgCl*
1	0.85	0.002	0.995	−0.447
2	0.84	0.002	0.996	−0.449
3	0.85	0.004	0.987	−0.446
4	0.85	0.003	0.989	−0.440

Ag/AgCl electrode was used with a 1 M LiCl salt bridge.

Attempts to obtain confirmatory evidence with regard to the number of electrons involved in the rate determining step by means of coulometry at 50°C (mercury pool cathode) failed as have all similar attempts at 25°C in the past due to the inception of a continuous process. Our findings obtained by means of chronoamperometry in 4 M $HClO_4$ were identical in form with those obtained by Demkin and Sinyakova

in 2 *M* HCl. Potential sweep chronoamperometry at 25°C and 50°C failed due to the early inception of the H^+ discharge.

A.c. polarography in 4 *M* $HClO_4$ led to the formation of very well defined peaks most suitable for the analytical determination of ReO_4^-. This is in marked contrast to the a.c. peaks obtained by Munze in alkaline media. The peak height was dependent on the concentration of $HClO_4$ between 0.01 and 2 *M*. The height of the peak reached its maximum at approximately 2 *M* and no alteration in height could be discerned in 4 *M* $HClO_4$; however, polarograms were taken in 4 *M* $HClO_4$ in

TABLE 3

Concn. $c/mmol\ l^{-1}$	*Temp.* = 25 ± 0.1°C				*Temp.* = 50 ± 0.1°C			
	Peak Curr /μA	I_p/C	E_s/V	*Width at half height/mV*	*Peak Curr* /μA	I_p/C	E_s/V	*Width at half height/mV*
0.04	0.060	1.50	−0.508	168	0.073	1.82	−0.548	168
0.08	0.112	1.40	−0.504	173	0.185	2.31	−0.537	186
0.12	0.158	1.32	−0.501	163	0.275	2.29	−0.542	186
0.16	0.211	1.32	−0.501	180	0.376	2.34	−0.536	184
0.32	0.455	1.42	−0.494	170	0.860	2.67	−0.544	188
0.64	0.965	1.50	−0.518	176	1.623	2.53	−0.552	191

order to compare the result of a.c. and d.c. investigations and to compare these results with the results of previous authors in this medium. The peaks in the a.c. polarogram were symmetric and the parameters associated with these waves are listed in Table 3.

CONCLUSION

The evidence presented here indicates the likelihood of the rate determining step in the electroreduction of ReO_4^- involving a two-electron reduction to Re(V). This conclusion is reached on the basis of the αn_a values in conjunction with the evidence of the a.c. waves, indicating by their symmetrical nature an α value near 0.5.

ACKNOWLEDGEMENT

The authors wish to thank the Preston Institute of Technology, Preston, Victoria 3072, for making available the electrochemical apparatus and the computer time.

REFERENCES

1 J. A. SHROPSHIRE, *J. Electroanal. Chem.*, 9 (1965) 90.
2 J. A. SHROPSHIRE, *J. Electroanal. Chem.*, 16 (1968) 275.
3 A. M. DEMKIN AND S. I. SINYAKOVA, *Electrokhimya*, 3 (1967) 1175.
4 J. TOUL, N. G. IGNAT'EVA AND V. M. PESHKOVA, *Zh. Analit. Khim.*, 19 (1964) 224.
5 H. SPITZY, R. J. MAGEE AND C. L. WILSON, *Mikrochim. Acta*, 3–4 (1957) 354.
6 S. TRIBALAT, *Compt. Rend.*, 220 (1945) 881; 222 (1946) 1388.
7 J. J. LINGANE, *J. Am. Chem. Soc.*, 64 (1942) 1001.

8 R. J. MAGEE, I. A. P. SCOTT AND C. L. WILSON, *Talanta*, 2 (1959) 376.
9 C. L. RULFS AND P. J. ELVING, *J. Am. Chem. Soc.*, 73 (1951) 3284.
10 R. MUNZE, *Z. Physik. Chem. (Leipzig)*, 226 (1964) 415.
11 A. A. VLCEK, *Progress in Inorganic Chemistry*, Vol. 5, Interscience, New York, 1963, p. 221.
12 K. B. OLDHAM AND E. P. PARRY, *Anal. Chem.*, 40 (1968) 65.
13 T. BERZINS AND P. DELAHAY, *J. Am. Chem. Soc.*, 75 (1953) 5716.
14 S. FELDBERG, *J. Phys. Chem.*, 73 (1969) 1238.

ELECTROANALYTICAL CHEMISTRY AND INTERFACIAL ELECTROCHEMISTRY
Elsevier Sequoia S.A., Lausanne – Printed in The Netherlands

THE SILVER–SILVER PERCHLORATE REFERENCE ELECTRODE IN PROPYLENE CARBONATE

E. KIROWA-EISNER AND E. GILEADI
Institute of Chemistry, Tel-Aviv University, Ramat-Aviv (Israel)
(Received November 22nd, 1969)

INTRODUCTION

Propylene carbonate (PC) has attracted increasing attention in recent years as a non-aqueous solvent in electrochemistry[1], particularly in the field of high energy-density batteries[2]. Two reference electrodes suitable for this solvent have been developed: the $Li/LiClO_4$ electrode[3,4] and the Tl(Hg)/TlCl/LiCl electrode[5,6]. Both act reversibly and yield reproducible values of the potential, when carefully prepared. They are, however, very sensitive to traces of oxygen, rather incovenient to prepare, and difficult to store. For these reasons, it was decided to search further for a suitable reference electrode in PC, which will be easy to prepare and store.

The Cu/Cu^{2+} electrode cannot be used because cuprous ions are formed spontaneously in a reaction between metallic copper and cupric ions. A white precipitate formed and the potential was unstable. The Ni/Ni^{2+} system was found to be characterized by a very slow response, reaching a steady state potential only after an extended period of time. The $Ag/AgCl/Cl^-$ secondary electrode was rejected because the solubility of AgCl in PC is greatly increased in the presence of Cl^- ions, due to complex formation[7].

The $Ag/AgClO_4$ reference electrode was found to be very suitable. It is easily prepared, has a sufficiently high exchange current density and consequently has a quick response. It was found to be stable over a period of several weeks and could be easily stored. The preparation and some characteristics of this electrode will be described below. Very recently, the use of this type of reference electrode (Ag/Ag^+ (0.05 *M*), $NaClO_4$ (0.5 *M*)) was reported[8]. However, no details of its performance were given.

EXPERIMENTAL

Reagents

Propylene carbonate (Jefferson Chemical Company) was purified by distillation at a pressure of 1 torr in an adiabatic fractional distillation column[9]. High purity of the solvent was essential for satisfactory operation of the reference electrode. The electrolytes used, $LiClO_4$ and $AgClO_4$ (B.D.H.), were dried at a pressure of 1 torr at 100° and 50°C, respectively, for 24 h. A 0.5 *M* $AgClO_4$ stock solution was prepared and used.

Electrodes

The structure of the reference electrode is shown in Fig. 1. A Teflon tube was fitted at the top with a Teflon cup, and a silver wire was inserted through the cup. At the bottom, the tube was plugged with a "thirsty glass" rod (Corning, type 7930 glass). This arrangement provides for effective separation between the solution inside the

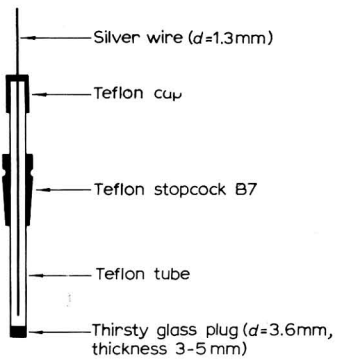

Fig. 1. Structure of the reference electrode.

tube and the solution in the rest of the cell while, at the same time, giving rise to a relatively low electrical resistance (in the range of 5–10 kΩ for a rod thickness of 3–5 mm).

When a new electrode is constructed, the "thirsty glass" plug must be equilibrated with the solution for about one hour before use. It was not found necessary to protect the reference electrode from light.

For polarization measurements, a silver wire wrapped tightly with a Teflon tape and inserted directly into the cell was used. All silver wires employed for the construction of electrodes were abraded with a fine emery paper, degreased in acetone, washed several times with triple distilled water and dried at 50°C for one hour.

Measurements

Electrode potentials for the determination of Nernst plots were measured with an expanded scale pH-meter (Radiometer type PHM 25 SE). Current–potential measurements at low overpotentials were performed galvanostically. A set of batteries and suitable resistors served as the source of current and the potential was measured on an electrometer (Keithley model 610 B). The constant current was passed between two similar silver wires immersed in the solution and the potential was measured with respect to a reference electrode (*cf.* Fig. 1).

RESULTS

Thermodynamic behavior

Nernst plots of potential *vs.* log c_{Ag^+} are shown in Fig. 2 for 0.2 *M* and 1.0 *M* concentration of the supporting electrolyte and in Fig. 3, in the absence of supporting electrolyte. The potential was measured between a silver wire indicator electrode dipping directly into the solution and a reference electrode as shown in Fig. 1. The concentration of silver ions was changed by adding known amounts of the stock solution of $AgClO_4$ in PC. At least two indicator electrodes were used in each experiment.

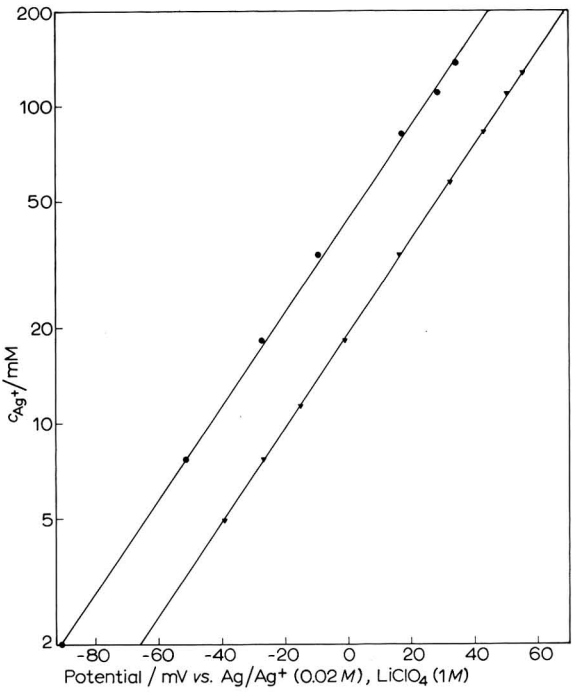

Fig. 2. Nernst plot for the Ag/Ag^+ couple at 25° C. Supporting electrolyte $LiClO_4$, (●) 0.2, (▼) 1 *M*.

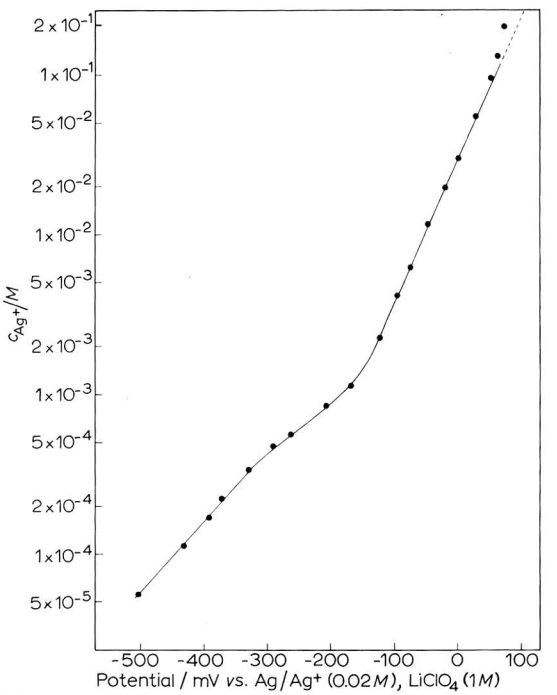

Fig. 3. Nernst plot for the Ag/Ag^+ couple at 25° C in the absence of supporting electrolyte.

At concentrations of silver ion above a few mM the bias potential between the two indicator electrodes was always less then 1 mV, and the electrodes responded rapidly, reaching equilibrium in a few seconds. At lower concentration of Ag^+ in the presence of supporting electrolyte, the bias potential increased to 10 mV or more and the electrode potential approached its equilibrium value rather slowly. In the absence of supporting electrolyte it was possible to obtain fairly reproducible results (5 mV) down to a concentration of 5×10^{-5} M Ag^+, but the points deviated markedly from linearity in this range. In the concentration range of silver ions of 2 mM–0.1 M the Nernst slope was found to be 67 mV in 0.2 M supporting electrolyte, 65 mV in 1.0 M supporting electrolyte and 110 mV in the absence of supporting electrolyte.

Kinetic behavior

Microspolarization tests showed a linear current–potential relationship in the vicinity of the equilibrium potential. Figures 4, a and b show the results obtained

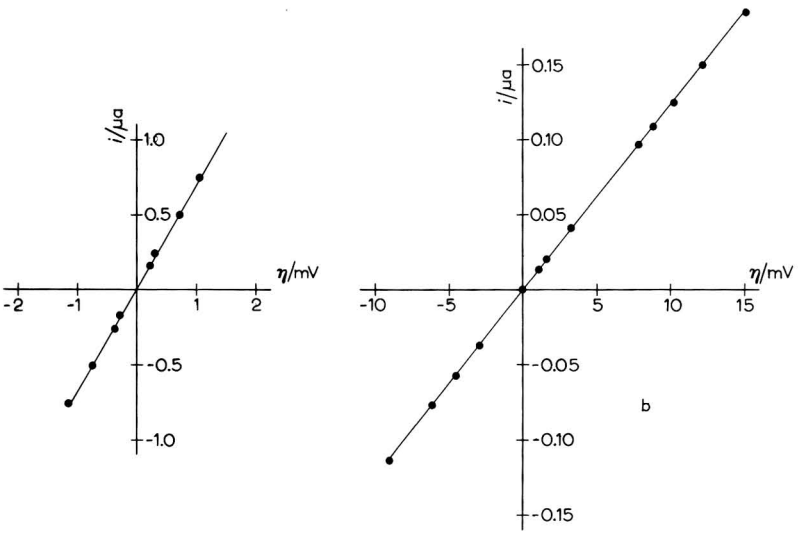

Fig. 4. Micropolarization tests for the Ag/Ag^+ couple at 25° C. (a) In the absence of supporting electrolyte, (b) with 0.1 M $LiClO_4$.

for a 20 mM solution of Ag^+ in the presence and absence of supporting electrolyte, respectively. The exchange current densities calculated from these experiments are 2×10^{-5} and 2.5×10^{-7} A cm^{-2}, respectively, nearly two orders of magnitude higher in the absence of $LiClO_4$.

Bias potential

Twenty reference electrodes of the type shown in Fig. 1 (20 mM $AgClO_4$; 0.2 M or 1.0 M $LiClO_4$) were immersed in 0.2 M and 1.0 M solutions of $LiClO_4$, respectively, and the potential differences between pairs of these electrodes were measured periodically for several days. The potential between any two electrodes usually differed by less than 0.5 mV although in a few cases a bias potential as high as 1 mV was observed. Similar reproducibility was reported for the Li/Li^+ electrode[3].

In the case of a Tl(Hg)/TlCl(satd.)LiCl electrode a higher reproducibility was found[5], probably due to the use of a liquid amalgam electrode.

Effect of water

Small amounts of water were added to a cell containing a 20 mM solution of $AgClO_4$ in PC and the potential between a silver wire dipping into the cell and a reference electrode (which contained no water) was measured. The results are given in Table 1 below. The effect of water on the long-term stability of the solution was not tested.

TABLE 1

EFFECT OF WATER CONTENT ON THE POTENTIAL OF Ag/Ag^+ (2×10^{-2} M) IN PC

$c_{H_2O}/(p.p.m.)$	0	0.5	2.0	9.0	39	90	165	240
$\Delta E/mV$	0	−0.1	−0.3	−0.35	−0.8	−1.5	−3.0	−4.0

DISCUSSION

Although linear plots of potential *vs.* log c_{Ag^+} have been observed over two decades of concentration (*cf.* Figs. 2 and 3), the slopes deviate markedly from the theoretical Nernst slope of 2.3 RT/F, even in the presence of an excess of supporting electrolyte. The liquid junction potential was minimized by having a large excess of supporting electrolyte in the reference electrode compartment. Its variation with the concentration of silver ions is probably small. The deviations from the Nernst slope are, therefore, mainly attributed to the variation in activity coefficient, γ_{Ag^+}.

To test the consistency of the results, the effect of concentration of supporting electrolyte on the potential was determined at constant silver ion concentration

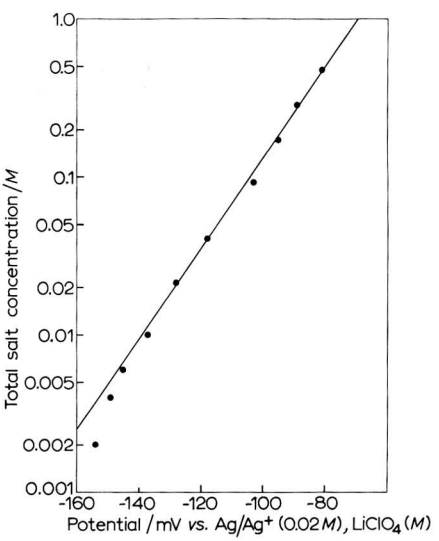

Fig. 5. Variation of potential of the Ag/Ag^+ (2 mM) couple with total salt concn. ($LiClO_4 + AgClO_4$).

(Fig. 5). From the Nernst equation, one has at constant concentration of supporting electrolyte ($LiClO_4$):

$$\left(\frac{\partial E}{\partial \log c_{Ag^+}}\right)_{c_{Li^+}} = \frac{2.3\,RT}{F}\left[1 + \left(\frac{\partial \log \gamma_{Ag^+}}{\partial \log c_{total}}\right)\left(\frac{\partial \log c_{total}}{\partial \log c_{Ag^+}}\right)\right] \quad (1)$$

and at constant concentration of silver ions:

$$\left(\frac{\partial E}{\partial \log c_{total}}\right)_{c_{Ag^+}} = \frac{2.3\,RT}{F}\left(\frac{\partial \log \gamma_{Ag^+}}{\partial \log c_{total}}\right) \quad (2)$$

where $c_{total} = c_{Ag^+} + c_{Li^+}$.

The experimental value of $(\partial E/\partial \log c_{total})_{c_{Ag^+}}$ is 35 mV (*cf.* Fig. 5). In the absence of supporting electrolyte ($\partial \log c_{total}/\partial \log c_{Ag^+} = 1$) and hence from eqn. (1) one obtains $(\partial E/\partial \log c_{Ag^+}) = 94$ mV, compared to a value of 110 mV found experimentally. In 0.2 *M* and 1.0 *M* concentration of supporting electrolyte, the observed slopes (*cf.* Fig. 2) were 67 mV and 65 mV, for a range of concentration of Ag^+ from 2 to 0.2 m*M*. The calculated slope from eqns. (1) and (2) are 64 and 61 mV, respectively.

Experiments were also performed with $(C_2H_5)_4NClO_4$ (1.0 *M*) as supporting electrolyte. A somewhat higher Nernst slope was observed (73 mV) and the electrode responded rather sluggishly.

It is noted that the activity coefficient γ_{Ag^+} increases with increasing ionic strength in the concentration range measured. Since activity coefficient data for Ag^+ in PC are not available, one assumes that the small discrepancy between the above results is due to specific ion effects. Although quantitative agreement cannot be expected here, the qualitatively correct trends are observed.

In conclusion, the $Ag/AgClO_4$ electrode was found to be a suitable reference electrode in pure propylene carbonate. A convenient construction for this reference electrode is shown in Fig. 1. The concentration of Ag^+ inside the reference electrode compartment can be varied in the range of *ca.* 2–200 m*M*. An intermediate value of 20 m*M* was found to be a good compromise between the requirements of high exchange current density and low liquid junction potential. The electrode can be used without a supporting electrolyte, but the liquid junction potential is minimized when an excess of supporting electrolyte (*e.g.* 0.2–1.0 *M* $LiClO_4$) is added. Tetraethyl ammonium perchlorate can be used as supporting electrolyte, but is less convenient because of the sluggish response of the electrode. High purity of the solvent is essential.

The electrode is easy to prepare and is stable for a period of several weeks. Equilibrium potential is reached rapidly (within seconds) and is reproducible to better than 0.5 mV.

SUMMARY

A Ag/Ag^+ reference electrode in propylene carbonate (PC) was developed. Simple preparation, fast response, good stability and high reproducibility characterize it. Nernst slopes for this electrode were determined at different concentrations of supporting electrolyte. Positive deviations from the expected slope of 2.3 RT/F were found. The activity coefficient γ_{Ag^+} increases with increasing concentration of supporting electrolyte, at constant silver ion concentration, in qualitative agreement with the positive deviations from the theoretical Nernst slopes. The exchange current den-

sity of Ag/Ag^+ (20 mM) is 2×10^{-5} A cm^{-2}. The effect of the addition of small amounts of water to the solvent was found to be of minor importance.

REFERENCES

1 R. F. NELSON AND R. N. ADAMS, *J. Electroanal. Chem.*, 13 (1967) 184.
2 R. JASINSKI, *High Energy Batteries*, Plenum Publishing Co., New York, 1967.
3 B. BURROWS AND R. JASINSKI, *J. Electrochem. Soc.*, 115 (1968) 365.
4 S. G. MEIBUHR, 135th National Meeting, 1969, The Electrochemical Society, Extended Abstracts, Vol. 5, p. 516.
5 F. G. K. BAUCKE AND C. W. TOBIAS, *J. Electrochem. Soc.*, 116 (1969) 34.
6 J. C. SYNOTT AND J. N. BUTLER, 135th National Meeting, 1969, The Electrochemical Society, Extended Abstracts, Vol. 4, p. 393.
7 J. N. BUTLER, D. R. COGLEY AND W. ZUROSKY, *J. Electrochem. Soc.*, 115 (1968) 445.
8 T. BIEGLER AND R. PARSONS, *J. Electroanal. Chem.*, 21 (1969) App. 4–6.
9 R. JASINSKI AND S. KIRKLAND, *Anal. Chem.*, 39 (1967) 1663.

ELECTROANALYTICAL CHEMISTRY AND INTERFACIAL ELECTROCHEMISTRY
Elsevier Sequoia S.A., Lausanne – Printed in The Netherlands

POUVOIR THERMOÉLECTRIQUE DU SÉLÉNIURE DE CUIVRE

RENÉ ROUTIÉ, MICHEL SUDRES ET JEAN MAHENC

Institut du Génie Chimique et Laboratoire d'Electrochimie de la Faculté des Sciences de Toulouse, 31-Toulouse-04 (France)

(Reçu le 13 octobre, 1969)

INTRODUCTION

Le séléniure de cuivre monovalent présente deux phases allotropiques, à structure à faces centrées[1,2], la température de transformation étant susceptible de varier suivant la composition du séléniure[3]. En effet, ce produit existe normalement sous une forme non stoechiométrique, due à un déficit en métal, ce qui explique la formule $Cu_{2-\delta}Se$, proposée par Lorenz et Wagner[4] et Mole et Hocart[5], et qui lui confère une conduction de type *p*, caractéristique d'un élément semi-conducteur.

Utilisant une pile de chaîne symbolique $Cu|CuBr|Cu_{2-\delta}Se|$graphite, Wagner[4] a pu déterminer l'activité du cuivre dans le séléniure cuivreux comme une fonction de la composition: opérant ainsi à 400°C, à l'aide de titrages coulométriques, il a relié l'indice stoechiométrique $(2-\delta)$ à la force électromotrice U de la pile, atteignant une valeur limite pour δ égale à 0.138. Le rapport (cuivre/sélénium) peut donc varier largement et influencer les propriétés semi-conductrices du composé.

Le présent travail est une étude de la variation du pouvoir thermoélectrique de ce corps avec la température et la stoechiométrie. Dans une première partie, l'influence de la température est envisagée pour des stoechiométries extrêmes, fixées par voies chimiques. Dans une deuxième étape, à température constante (400°C), le pouvoir thermoélectrique est mesuré en fonction de la concentration en trous positifs, qui est déterminée ici par voie électrochimique au moyen de la pile $Cu|CuI|Cu_{2-\delta}Se|$graphite. Une étude théorique faisant appel à la statistique de Fermi–Dirac permet enfin de confronter les valeurs théoriques aux résultats expérimentaux.

1. ÉTUDE À INDICE STOECHIOMÉTRIQUE IMPOSÉ PAR VOIES CHIMIQUES

(1°) *Préparation du séléniure cuivreux et principe de la mesure*

Le séléniure cuivreux est obtenu directement sous forme de pastilles cylindriques, de 10 mm de diamètre pour une hauteur sensiblement équivalente, par compression unilatérale (à 170°C durant une heure) de poudres très pures de cuivre et de sélénium, intimement mélangées dans les proportions atomiques de 1.8 Cu pour 1 Se.

Cet échantillon, soumis à un gradient thermique $\Delta\theta$ d'une dizaine de degrés au maximum, donne naissance à une force thermoélectrique E_θ. Le gradient thermique est obtenu en refroidissant la base inférieure du séléniure de cuivre (circulation d'un fluide thermorégularisé) et est mesuré à l'aide de deux thermocouples différentiels. La force thermoélectrique est repérée grâce à deux électrodes de platine, logées le plus

pres possible des thermocouples. L'ensemble est placé dans un four électrique sous atmosphère d'argon. Le montage expérimental est représenté par la Fig. 1.

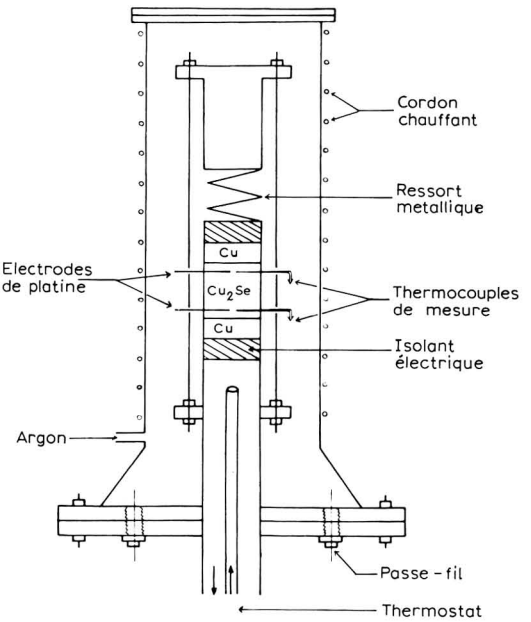

Fig. 1. Dispositif expérimental de mesure du pouvoir thermoélectrique de Cu_2Se en présence de cuivre.

(2°) *Influence de la température sur le pouvoir thermoélectrique*

Ce travail comporte deux parties distinctes, en ce sens qu'il est effectué pour deux stoechiométries fixes mais différentes : on étudie tout d'abord le cas du séléniure stoechiométrique Cu_2Se (type berzélianite) et ensuite du séléniure non stoechiométrique, d'indice le plus faible possible.

(*A*) *Séléniure stoechiométrique.* Les pastilles obtenues de la façon citée ci-dessus sont non stoechiométriques (examen aux rayons X[1] ou force électromotrice de la pile $Cu|CuBr|Cu_{2-\delta}S|C$ voisine de 300 mV, ce qui correspond à un indice stoechiométrique égal à environ 1.86[4]. On peut donner à ce séléniure l'indice stoechiométrique idéal par chauffage sous vide, en enlevant l'excédent en métalloïde[6] ou bien encore en insérant le séléniure entre deux pastilles de cuivre pur. Un ressort métallique maintient alors de bons contacts macroscopiques (Fig. 1).

Entre deux valeurs limites de température (35°–300° C), des mesures du pouvoir thermoélectrique sont effectuées par intervalles d'une dizaine de degrés environ. Les résultats sont portés sur la Fig. (2).

L'analyse de la courbe ainsi obtenue montre que le pouvoir thermoélectrique croît légèrement jusqu'à 100° C. Son ascension devient ensuite plus importante atteignant 220 μV deg^{-1} vers 133° C, température aux alentours de laquelle une chute brusque de 55 μV deg^{-1} est observée. Enfin, pour des températures supérieures à 133° C, le pouvoir thermoélectrique augmente de façon continue.

La variation très sensible du pouvoir thermoélectrique à 133° C correspond au

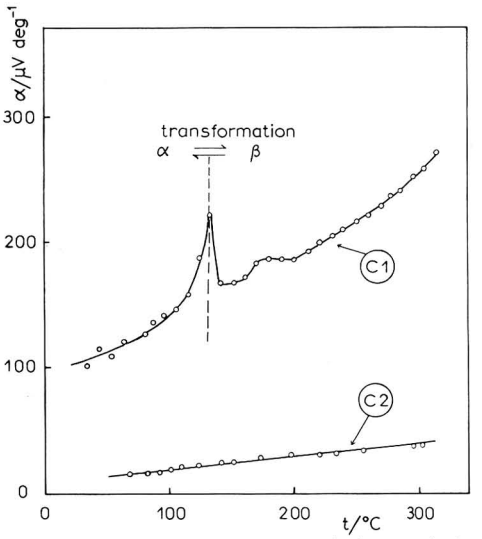

Fig. 2. Influence de la température: (C_1) Pouvoir thermoélectrique de Cu_2Se en présence de cuivre, (C_2) pouvoir thermoélectrique de $Cu_{2-\delta}Se$ en présence de sélénium.

changement de phase ($\beta \rightleftharpoons \alpha$) entre les deux variétés allotropiques. Divers auteurs notent pareillement un tel phénomène: Junod[3] signale une discontinuité vers 130°C pour le pouvoir thermoélectrique déterminé avec l'aluminium comme métal de référence; Celuska et Ogorelec[7] ont observé une petite irrégularité à 112°C concernant le pouvoir thermoélectrique intégral de $Cu_{1.96}Se$; enfin Abdullaev et coll.[8] constate un bond du pouvoir thermoélectrique, expérimentant sur des monocristaux de Cu_2Se. Notre valeur serait en bon accord avec celle de 131°C que donne Heyding[9] pour la température de transformation ($\beta \rightleftharpoons \alpha$), lors du calcul des enthalpies de transformation dans le système (cuivre/sélénium).

(*B*) *Séléniure de stoechiométrie minimale.* Celle-ci est atteinte, en disposant, à l'intérieur d'un tube de Téflon thermo-rétractable (Fig. 3), au-dessus du séléniure cuivreux, une pastille de sélénium, obtenue sous une pression de 4000 bars environ. Soumis à cette nouvelle atmosphère, l'indice stoechiométrique varie, tendant à devenir minimal. L'expérience elle-même est conduite comme précédemment et les résultats sont groupés sur la Fig. 2.

Le pouvoir thermoélectrique de l'ordre de 20 μV/°C, croît légèrement et linéai-

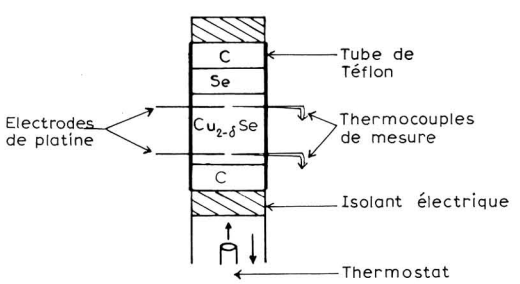

Fig. 3. Dispositif expérimental de mesure du pouvoir thermoélectrique de $Cu_{2-\delta}Se$ en présence de sélénium.

rement avec la température, sans présenter de discontinuités, entre 70° et 300°C. Dans ce cas, l'observation du changement de phase n'a point lieu. Il faut noter cependant que la température de transformation est modifiable suivant la stoechiométrie[3]. Le diagramme des phases de Heyding montre qu'elle est sensiblement voisine de 0°C pour un pourcentage atomique de 35% en sélénium, soit $Cu_{1.86}Se$, ce qui correspond à la valeur d'indice minimal ($\delta = 0.138$) rencontrée par Wagner.

2. POUVOIR THERMOÉLECTRIQUE DU SÉLÉNIURE CUIVREUX À INDICE STOECHIOMÉTRIQUE IMPOSÉ PAR VOIE ÉLECTROCHIMIQUE

(1°) *Principe*

Pour des valeurs de l'indice stoechiométrique, comprises entre 2.00 et 1.86 il est possible, grâce à l'emploi d'une pile solide $Cu|CuI|Cu_{2-\delta}Se|C$ de repérer la composition $(2-\delta)$ du séléniure de cuivre (à l'aide de la force électromotrice) ainsi que de faire varier commodément cette composition (à l'aide d'un titrage coulométrique). Cette méthode a déjà été décrite pour les sulfures[10,11].

L'iodure de cuivre possédant entre 380° et 450°C une conduction purement cathionique[12] (ions Cu^+), l'adjonction dans le circuit extérieur de pile d'un générateur électrique auxiliaire, monté en série ou en opposition, permet alors de transférer une certaine de quantité de cuivre de l'anode (cuivre métallique) à la cathode (séléniure), ou inversement de la cathode à l'anode (montage du générateur électrique auxiliaire en opposition).

La force électromotrice d'une telle pile est donnée par la relation :

$$-UF = \mu_{Cu(Cu_{2-\delta}Se)} - \mu^0_{Cu} \tag{1}$$

où $\mu_{Cu(Cu_{2-\delta}Se)}$ est le potentiel chimique du cuivre dans son séléniure d'indice stoechiométrique $(2-\delta)$; μ^0_{Cu} le potentiel chimique du cuivre à l'état standard ; F le nombre de Faraday.

Dans le but de satisfaire à la condition d'électroneutralité, le déficit de cuivre du séléniure est compensé par la formation de trous positifs (d'où son appelation de semi-conducteur p). Ainsi,

$$\mu_{Cu(Cu_{2-\delta}Se)} = \mu_{Cu^+} + \mu_{e^-} = \mu_{Cu^+} - \mu_{\oplus} \tag{2}$$

où μ_{Cu^+} est le potentiel chimique des ions cuivreux ; $\mu_{\oplus}$ potentiel chimique des trous positifs.

Comme les ions Cu^+ sont distribués statistiquement par rapport au grand nombre de sites existants, le potentiel chimique des ions Cu^+ peut être considéré comme constant. Il résulte alors des relations (1) et (2) que :

$$F \cdot dU = d\mu_{\oplus} \tag{3}$$

La force électromotrice de la pile apparaît donc comme une fonction du potentiel chimique des trous positifs, c'est-à-dire, de leur concentration. Ainsi, en chargeant ou en déchargeant la pile, on fixe la force électromotrice de cette dernière à une certaine valeur à laquelle correspond une concentration déterminée de trous. La variation de cette concentration entraîne une variation des propriétés électriques du séléniure de cuivre dont le pouvoir thermoélectrique qui fait l'objet de la présente étude.

(2°) *Montage expérimental*

Le montage expérimental est représenté par la Fig. (4). La charge ou la décharge de la pile s'effectue au moyen de disques de graphite, situés en bout de chaîne: graphite|Cu|CuI|$Cu_{2-\delta}Se$|graphite.

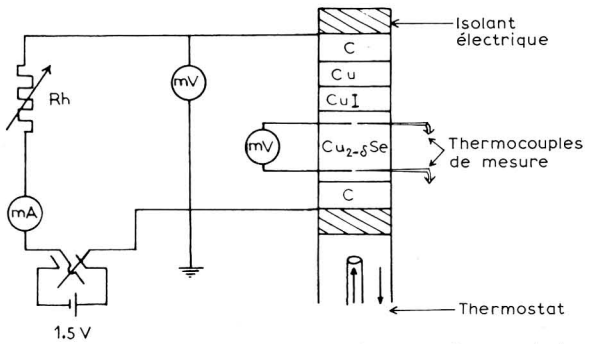

Fig. 4. Montage potentiométrique pour la mesure du pouvoir thermoélectrique du séléniure de cuivre en fonction du dosage du composé.

Une fois la force électromotrice stabilisée, le pouvoir thermoélectrique est recherché, comme dans la première partie, par les mesures du gradient thermique et de la force thermoélectrique correspondante. Les résultats expérimentaux sont transposés sur la Fig. (5) et peuvent être comparés aux valeurs théoriques.

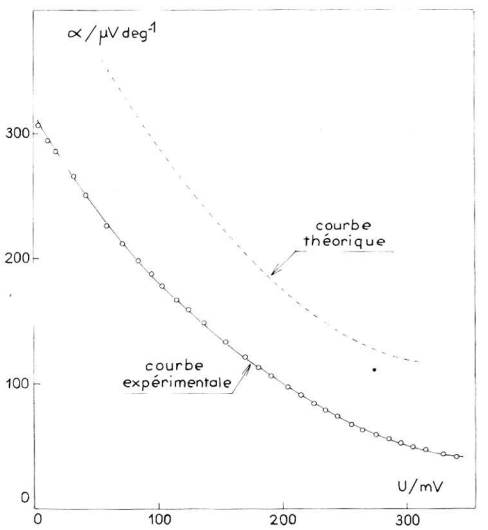

Fig. 5. Pouvoir thermoélectrique du séléniure de cuivre en fonction de la force électromotrice de la pile Cu|CuI|$Cu_{2-\delta}Se$|C.

(3°) *Discussion*

L'application de la statistique de Fermi–Dirac conduit à la formule la plus

générale du pouvoir thermoélectrique donnée par Ioffe[13] :

$$\alpha = -\frac{k}{e}\left[\frac{r+2}{r+1}\cdot\frac{F_{r+1}(\mu_\oplus/RT)}{F_r(\mu_\oplus/RT)} - \frac{\mu_\oplus}{RT}\right] \tag{4}$$

où F_r est la fonction de Fermi–Dirac, k la constante de Boltzman, e la charge de l'électron, $\mu_\oplus/RT$ le potentiel chimique réduit des trous et r indiquant le caractère des forces de liaison est estimé à 1/2 dans le cas des réseaux ioniques, ce qui implique :

$$\alpha = -\frac{k}{e}\left[\frac{5}{3}\cdot\frac{F_{3/2}(\mu_\oplus/RT)}{F_{1/2}(\mu_\oplus/RT)} - \frac{\mu_\oplus}{RT}\right] \tag{5}$$

La connaissance indispensable des différents facteurs entrant dans l'éqn. (5) ne peut être envisagée que si la densité des trous électroniques est connue :

$$n_\oplus = 4\pi\,\frac{(2m^*_\oplus kT)^{3/2}}{h^3}\cdot F_{1/2}(\mu_\oplus/RT) \tag{6}$$

où h est la constante de Planck et $m^*_\oplus$ la masse effective des trous et telle[4] que $m^*_\oplus/m = 4$ avec m = masse de l'électron.

Or, cette concentration est donnée par la formule

$$n_\oplus = \delta\cdot\frac{N_0}{V_m} \tag{7}$$

où N_0 est le nombre d'Avogadro et V_m le volume molaire du séléniure de cuivre = 31.4 cm^3.

L'égalité des relations (6) et (7) permet de calculer la fonction de Fermi–Dirac $F_{1/2}(\mu_\oplus/RT)$. Cette fonction donne la probabilité de trouver un électron, ou un trou positif, à un niveau d'energie W donné ; le potentiel chimique des trous et la fonction $F_{3/2}(\mu_\oplus/RT)$ sont déduits des tables de J. MacDougall et Stoner[14].

Le pouvoir thermoélectrique théorique est alors calculé à l'aide de la relation (5). La Fig. 5 représente la variation de ce pouvoir thermoélectrique théorique (en pointillé) en fonction de la force électromotrice de la pile.

La confrontation des courbes théorique et expérimentale du pouvoir thermoélectrique révèle un écart qui peut être dû au fait que les valeurs théoriques sont déjà déduites des valeurs elles-mêmes expérimentales de la courbe $U = f(\delta)$, trouvée par Wagner[4]. Il faut remarquer également, après examen du Tableau 1, que le potentiel chimique des trous positifs, dans le domaine étudié de composition du séléniure, est compris entre -4 et $+3$, ce qui correspond en fait, au passage de l'état de semiconducteur à l'état métallique : les propriétés électriques n'obéissent généralement pas, dans cette étape intermédiaire, à des lois aussi rigoureuses que celles que l'on rencontre dans les états extrêmes.

CONCLUSION

Le pouvoir thermoélectrique du séléniure de cuivre, semiconducteur de type p, à conduction par trous positifs, dépend considérablement de la composition de ce corps, définie par l'indice stoechiométrique. Cette composition dépend de l'atmosphère au contact de laquelle se trouve le séléniure.

En présence de cuivre métallique pur (indice stoechiométrique maximal), le

TABLEAU 1

U/mV	δ^a	$n^{\oplus} \cdot 10^{20}/cm^{-3}$	$F_{\frac{1}{2}}(\mu_{\oplus}/RT)$	$\mu_{\oplus}/RT$	$\frac{2}{3}F_{\frac{3}{2}}(\mu_{\oplus}/RT)$	$\alpha/\mu V\ K^{-1}$
300	0.133	25.51	3.383	+2.61	5.48	122.6
290	0.126	24.17	3.205	2.49	5.09	125.9
280	0.119	22.82	3.027	2.36	4.68	128.8
270	0.112	21.48	2.849	2.25	4.36	134.0
260	0.104	20.04	2.658	2.11	3.98	139.5
250	0.097	18.70	2.480	2.00	3.69	146.6
240	0.090	17.36	2.302	1.84	3.31	150.3
230	0.083	15.92	2.111	1.68	2.95	154.7
220	0.076	14.67	1.946	1.54	2.66	160.6
210	0.069	13.23	1.755	1.36	2.33	168.1
200	0.062	11.99	1.590	1.21	2.09	178.1
190	0.055	10.64	1.412	1.02	1.80	185.6
180	0.049	9.54	1.265	0.84	1.57	193.3
170	0.044	8.49	1.126	0.67	1.37	202.7
160	0.039	7.48	0.992	0.49	1.17	210.2
150	0.034	6.47	0.858	0.30	1.00	224.3
140	0.029	5.56	0.737	0.12	0.85	237.8
130	0.024	4.70	0.623	−0.06	0.73	255.5
120	0.021	3.98	0.528	−0.23	0.63	275.9
110	0.018	3.36	0.445	−0.42	0.52	288.7
100	0.015	2.83	0.375	−0.71	0.40	290.3
90	0.012	2.30	0.305	−0.93	0.33	312.3
80	0.010	1.92	0.254	−1.14	0.27	326.5
70	0.008	1.53	0.203	−1.39	0.21	341.8
60	0.0065	1.25	0.165	−1.62	0.17	360.8
50	0.005	0.96	0.127	−1.90	0.13	383.6
40	0.0037	0.72	0.095	−2.19	0.10	414.7
30	0.0025	0.48	0.064	−2.60	0.06	425.4
20	0.0015	0.29	0.038	−3.13	0.04	495.8
10	0.0007	0.14	0.019	−3.83	0.02	556.2

[a] Les valeurs de δ en fonction de U sont issues du travail de Wagner[4]. Nous avons de notre côté retrouvé ces mêmes valeurs.

pouvoir thermoélectrique du séléniure augmente régulièrement avec la température entre 35° et 300°C. Cependant, le changement de phase allotropique à 133°C est marqué ici par une anomalie dans la croissance de ce pouvoir thermoélectrique. En présence de sélénium (indice stoechiométrique minimal), le pouvoir thermoélectrique reste faible, de l'ordre de 20 μV deg^{-1}, ce qui dénote le caractère métallique de l'état du gaz électronique contenu dans le séléniure.

Entre ces deux cas extrêmes de composition, l'emploi d'une pile solide Cu|CuI|$Cu_{2-\delta}S$|C est extrêmement commode pour repérer et doser convenablement le séléniure. A chacune de ces concentrations, le pouvoir thermoélectrique a été mesuré et les résultats expérimentaux sont en bonne concordance avec les valeurs théoriques déduites de la statistique de Fermi–Dirac.

SOMMAIRE

Le pouvoir thermoélectrique du séléniure cuivreux, semi-conducteur de type p, dépend de la composition de ce corps, définie par son indice stoechiométrique. Le

pouvoir thermoélectrique est mesuré tout d'abord, lorsque le séléniure est en contact avec le cuivre métallique (indice stoechiométrique maximal) puis avec le sélénium (indice stoechiométrique minimal). Entre ces deux compositions extrêmes, l'emploi d'une pile Cu | CuI | $Cu_{2-\delta}Se$ | C permet de fixer et de faire varier la concentration en trous positifs du séléniure. Le pouvoir thermoélectrique est mesuré pour chacune de ces concentrations et les résultats expérimentaux sont comparés aux valeurs théoriques déduites de la statistique de Fermi–Dirac.

SUMMARY

The thermal electromotive force coefficient of cuprous selenide, an electron-hole semi-conductor, is related to the stoichiometric index of this compound. The thermal electromotive force coefficient is considered first when the selenide is in contact whith metallic copper (maximum stoichiometric index) and then when it is in contact with selenium (minimum stoichiometric index). Between these two extreme compositions, the hole concentration of the selenide is assured by a cell Cu|CuI| $Cu_{2-\delta}Se$|C. For each concentration, the thermal electromotive force coefficient is measured and the experimental results are compared with the theoretical results provided by the Fermi–Dirac statistical theory.

BIBLIOGRAPHIE

1 P. RAHLFS, *Z. Physik. Chem.*, B31 (1935) 157.
2 A. BOETTCHER, *Z. Angew. Phys.*, 7 (1955) 478.
3 P. JUNOD, *Helv. Phys. Acta*, 32 (1959) 567.
4 G. LORENZ ET C. WAGNER, *J. Chem. Phys.*, 26 (1957) 1607.
5 R. MOLE ET R. HOCART, *Bull. Soc. Chim. France*, (1954) 7.
6 J. J. ADOU ET J. BAUDET, *J. Chim. Phys.*, 64 (1967) 10, 1540.
7 B. CELUSKA ET Z. OGORELEC, *J. Phys. Chem. Solids*, 27 (1966) 615.
8 G. B. ABDULLAEV, Z. A. ALIYAROVA ET G. A. ASADOV, *Phys. Status Solidi*, 21 (1967) 461.
9 R. D. HEYDING, *Can. J. Chem.*, 44 (1966) 1233.
10 R. ROUTIÉ ET J. MAHENC, *J. Chim. Phys.*, 66 (1969) 6, 1103.
11 R. ROUTIÉ ET J. MAHENC, *J. Chim. Phys.*, 66 (1969) 5, 834.
12 J. B. WAGNER ET C. WAGNER, *J. Chem. Phys.*, 26 (1957) 1957.
13 A. F. IOFFE, *Semiconductor Thermoelements*, Infosearch, Ltd., London, 1957.
14 J. MACDOUGALL ET F. C. STONER, *Trans. Roy. Soc. London*, 64 (1967) 10, 1540.

ELECTROANALYTICAL CHEMISTRY AND INTERFACIAL ELECTROCHEMISTRY
Elsevier Sequoia S.A., Lausanne – Printed in The Netherlands

ELECTROSTATIC CHARGING IN THE LAMINAR FLOW IN PIPES OF VARYING LENGTH

J. C. GIBBINGS
Fluid Mechanics Division, University of Liverpool (Great Britain)
(Received November 26th, 1969)

NOTATION

C_f Coefficient of friction
d Pipe diameter
i_s Streaming current
i_{s_0} Streaming current from entry region
i_∞ Streaming current for $L=\infty$
I_s Non-dimensional streaming current, $\equiv \dfrac{i_s^2}{\lambda d^3 \rho \bar{u}^3}$
I_∞ Non-dimensional streaming current for $L=\infty$
j_w Wall current density
J_L Non-dimensional pipe length, $\equiv \dfrac{\lambda L}{\varepsilon \bar{u}}$
J_{L_0} Non-dimensional entry length
L Pipe length
L_e Length of entry charging region
L_0 Entry length correction
Re Reynolds number
$\bar{u}$ Mean pipe flow velocity
ε Dielectric coefficient
λ_0 Zero-charge conductivity
μ Liquid viscosity
ν Liquid kinematic viscosity $\equiv \mu/\rho$
ρ Liquid density
τ Relaxation time

1. INTRODUCTION

A previous paper[1] has reported an investigation into the electrostatic streaming current generation in the flow of a liquid along a pipe and the way in which it depended upon the length of that pipe. This was done for the flow in the turbulent regime and the result was that the streaming current i_s was found to obey the relation

$$i_s = i_\infty [1 - \exp - (J_L - J_{L_0})] \tag{1}$$

where i_∞ is the current corresponding to a pipe length L, of infinity and where the non-dimensional group J_L is defined by

$$J_L \equiv \lambda_0 L/\varepsilon\bar{u} \tag{2}$$

A physical interpretation of J_L has been given[2].

A significant feature of that investigation was the observation of the effect of the flow in the entry region to the pipe. This effect could be accounted for by the use of an entry length correction, L_0, with a corresponding non-dimensional group of J_{L_0}.

In the present paper a similar investigation for the laminar flow regime is reported.

2. APPARATUS

The pipe flow apparatus is that described in ref. 3 except that the receiver for the liquid after exit from the pipe rested upon PTFE blocks. The method used to measure the conductivity was as described in ref. 4* and the apparatus used for measuring the streaming current was an E.I.L. Vibron 33c electrometer with an E.I.L. converter unit B33c-2.

A single pipe of stainless steel was used with an internal surface roughness of the type and degree described as of Group I in ref. 3; that is it was of the class of smoother tubes. It had an internal diameter of 3.480×10^{-3} m. The same precautions in cutting it to a range of lengths were taken as was described in ref. 1. The lengths used were 1.5, 1.0, 0.75 and 0.5 m. The liquid used was a quantity of kerosene with a conductivity at zero charge density of about 10^{-11} mho m^{-1}. It was kindly donated by Messrs. Shell Research Ltd.

3. EXPERIMENTAL METHOD

The experiments were performed as described in refs. 1 and 3. The agreement of the measured frictional characteristics in the laminar flow regime with the analytical values was again confirmed. It was found to be particularly important to allow several hours before each run for all the charges in the upstream vessel to relax to the wall.

4. EFFECT OF ENTRY REGION CHARGING

The measured values of the streaming current plotted against the Reynolds number, Re, are shown in Fig. 1. Corresponding values of the non-dimensional current group, I_s, (ref. 3) are shown plotted in Fig. 2, where

$$I_s \equiv \frac{i_s^2}{\lambda_0 \rho \bar{u}^3 d^3} = \frac{\rho^2}{\lambda_0 \mu^3} \frac{i_s^2}{Re^3} \tag{1}$$

The purpose of the present experiments was to isolate the effect of varying the length of the pipe, L. Thus it is required that, along with other quantities, the zero-charge conductivity of the liquid, λ_0 be held constant. Values for the four experimental

* The cell constant for the conductivity cell described in ref. 4 has since been carefully determined. This and other measurements concerning the true zero-charge conductivity are to be the subject of another manuscript.

	$\lambda_s 10^{11}$.mho. m^{-1}	L.m^{-1}	L/d
•	1·04	0·5	144
⊡	1·095	0·75	216
▲	0·92	1·0	288
+	1·02	1·5	432

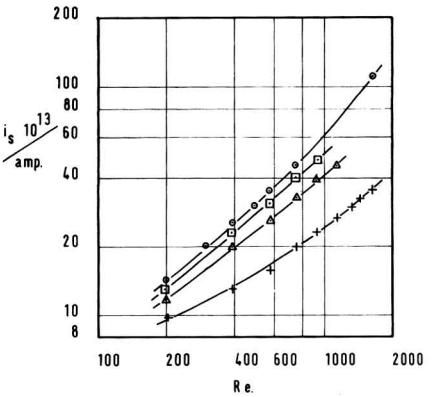

Fig. 1. Variation of streaming current with Reynolds number in the four pipe lengths.

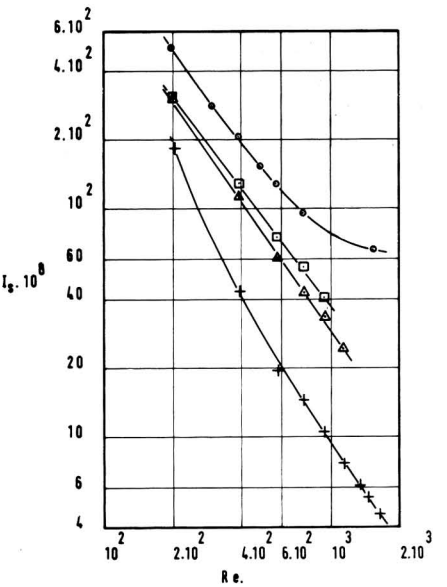

Fig. 2. Variation of the non-dimensional streaming current with Reynolds number. Symbol code of Fig. 1.

runs at the four pipe lengths are appended in Fig. 1 which shows that there was a slight variation in this conductivity. This occurred despite careful handling of the liquid between the runs and could not be avoided: it was considered to have only a secondary effect.

Unlike previous results for laminar and turbulent flow, the present results

show that there is not a simple power relationship between i_s and Re and hence between I_s and Re. The results in Figs. 1 and 2 show shallow curves.

Figure 1 shows a marked contrast for the laminar flow with the previous results[1] for turbulent flow. For the latter, at any fixed Reynolds number the streaming current increased with pipe length; here for laminar flow it decreases. An explanation for this difference is now sought.

The variation of current with length in the turbulent flow is represented by eqn. (1) and this is shown sketched as the line ABC in Fig. 3 giving a steady rise of

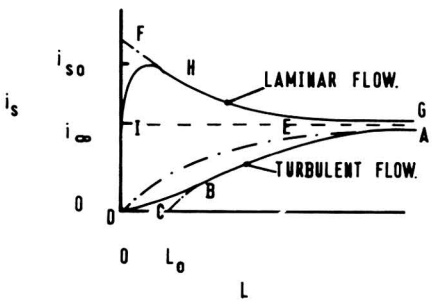

Fig. 3. Diagram of the variation of streaming current with pipe length.

current with length. Equation (1) relates to the development of the streaming current within that flow region that is fully developed downstream of the pipe entry and in which the velocity profile across the pipe is unchanged with distance along the pipe. Thus point C corresponds to a fictitious condition at a station where the flow has this velocity profile but the charge density is zero across the pipe.

If along the pipe, the wall current density is j_w, then from continuity of charge,

$$i_s = \int j_w \pi d \, dx$$

which differentiates to give

$$\frac{di_s}{dx} = j_w \pi d \tag{2}$$

Differentiating eqn. (1) and substituting eqn. (2) gives

$$j_w \pi d = i_\infty \left[\exp -(J_L - J_{L_0})\right] \frac{\lambda}{\varepsilon \bar{u}}$$

Putting $L = L_0$ gives

$$j_w = i_\infty \lambda / \pi d \varepsilon \bar{u} \tag{3}$$

As this corresponds to point C this value of j_w will be a pure charging current as, the fictitious charge density being zero, there will be neither a conduction nor a diffusion current in a radial direction.

The results of ref. 3 showed that

$$I_\infty = A\left(\frac{\varepsilon v}{\lambda d^2}\right)^{2.75} Re^{2.5}$$

so that

$$i_\infty = A^{\frac{1}{2}} \mu^{\frac{1}{8}} \lambda^{-\frac{7}{8}} \varepsilon^{11/8} \rho^{\frac{3}{8}} \bar{u}^{11/4} \tag{4}$$

Also for this turbulent pipe flow, the friction coefficient is given by

$$\begin{aligned} C_f &= B Re^{-\frac{1}{4}} \\ &= \frac{\tau}{\frac{1}{2}\rho \bar{u}^2} \\ &= \frac{2\mu(\mathrm{d}u/\mathrm{d}y)}{\rho \bar{u}^2} \end{aligned}$$

so that the velocity gradient at the wall is given by

$$\frac{\mathrm{d}u}{\mathrm{d}y} = \tfrac{1}{2} B \frac{\mu}{\rho d^2} Re^{7/4} \tag{5}$$

Substitution of eqns. (4) and (5) into eqn. (3) gives

$$j_w = \frac{2\sqrt{A}}{\pi B} \left(\frac{\lambda d^2}{\varepsilon \nu} \right)^{\frac{1}{8}} \frac{\varepsilon^{\frac{1}{2}} \rho^{\frac{1}{2}} \nu}{d} \frac{\mathrm{d}u}{\mathrm{d}y} \tag{6}$$

so that the initial charging current is directly proportional to $\mathrm{d}u/\mathrm{d}y$.

In the entry region to the pipe the flow will initially form a short separation bubble downstream of the sharp edge at the entrance to be followed by a laminar boundary layer. Here the shear stress, τ, and hence the velocity gradient $\mathrm{d}u/\mathrm{d}y$ will be lower than in the fully developed turbulent flow and so, if eqn. (6) is also valid in the entry region, the initial charging will be at a reduced rate there. Thus the charging would follow the curve DB in Fig. 3 and not the initial portion of DE which is given by eqn. (1) with L_0 put equal to zero.

In contrast, the entry flow conditions remain the same when the fully developed pipe flow is laminar but now the velocity gradient at the wall in the thin boundary layer will be higher than in the downstream laminar pipe flow and so if eqn. (6) remains valid then an enhanced charging would take place in the entry region gradually to die away downstream. Such a distribution is sketched as curve GHI in Fig. 3.

In the previously described flow pattern in the entrance region, the initial thickness of the boundary layer will develop slowly. The velocity outside the boundary layer will also remain closely constant at the mean velocity in the pipe and so the wall velocity gradient $\mathrm{d}u/\mathrm{d}y$ will also remain closely constant. If, in this initial region of length L_e, there is only a negligible degree of relaxation of the charge back to the wall* then the initial streaming current as indicated by i_{s_0} in Fig. 3, will be given by,

$$i_{s_0} = \int_0^{L_e} \pi d j_w \mathrm{d}x$$

For L_e fixed, though undetermined,

$$\left.\begin{aligned} i_{s_0} &\propto j_w \\ &\propto \mathrm{d}u/\mathrm{d}y \\ &\propto \bar{u} \\ &\propto Re, \end{aligned}\right\} \tag{7}$$

* An assumption that will receive some justification later.

where Re is the flow Reynolds number.

Figure 4 shows the result of cross plotting from Fig. 1. The straight line extrapolations shown give values of i_{s_0} for $L=0$. These values are shown plotted in Fig. 5 where the linear relationship predicted by eqn. (7) is confirmed by the experiments.

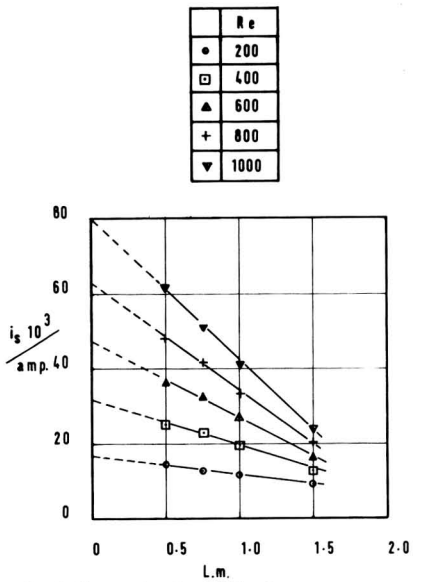

Fig. 4. Cross plot from Fig. 1.

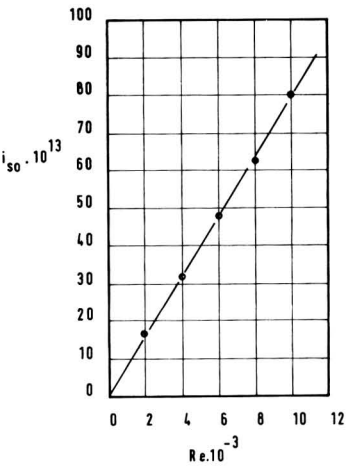

Fig. 5. Extrapolation from Fig. 4 of i_{s_0} as a function of the Reynolds number.

5. EFFECT OF PIPE LENGTH

Values of the streaming current, i_s, cross-plotted from Fig. 1, for a range of values of Re, are plotted against e^{-J_L} in Fig. 6. This suggests that over a limited range of e^{-J_L} a relation of the form

$$i_s = A + B\, e^{-J_L} \tag{8}$$

fits the experiments.

Over this range the slope, B is independent of the Reynolds number having the value 87.5×10^{-13} A. The constant A is shown plotted in Fig. 7. The experimental scatter is now large for this small term but it approximately fits the line shown drawn which is represented by,

$$A = 180 \times 10^{-13}\, Re^{-\frac{1}{2}} \tag{9}$$

The results shown in Fig. 6 suggest that they do not satisfy eqn. (8) when $L \leqq 0.5$ m or $L/d \leqq 144$. Indeed this equation cannot be valid for $L=0$ when $i_s = i_{s_0}$, for eqns. (8) and (9) would give $i_{s_0} \propto Re^{-\frac{1}{2}}$ whereas the results already presented show that $i_{s_0} \propto Re$ as given by eqn. (7).

Putting $L=\infty$ in eqn. (8) gives the corresponding value of the streaming current as equal to A. If eqn. (8) was valid up to $L=\infty$ then this current would be that

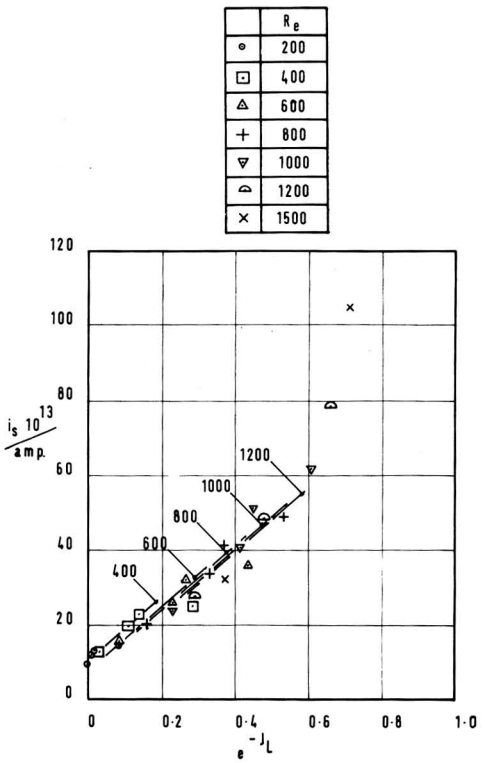

Fig. 6. Streaming current plotted *vs.* e^{-J_L} for values of the Reynolds number appended to the lines drawn.

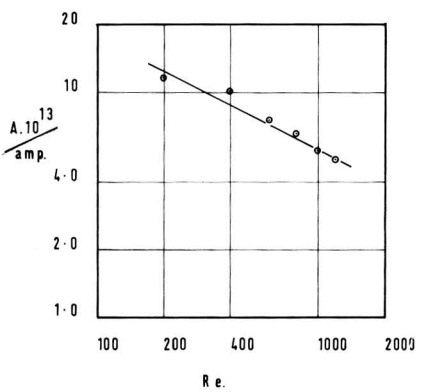

Fig. 7. Intercept of Fig. 6 for $L=\infty$, as a function of Reynolds number.

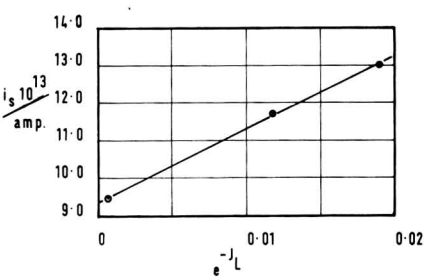

Fig. 8. Extended plot of Fig. 6 for $Re=200$.

in a pipe of infinite length, i_∞. There is some doubt as to whether eqn. (8) is valid to this limit. Figure 8 shows a plot of the experimental points for the three lowest values of e^{-J_L} which were obtained at $Re=200$. They fit the relation

$$i_s = 9.35\times10^{-13} + 195\times10^{-13}\, e^{-J_L} \tag{10}$$

in which the slope is twice that of eqn. (8) and the constant is approximately three-quarters of that given by eqn. (9).

Figure 6 also shows that i_{s_0} is about one order greater than i_∞ and thus indicates the importance of the charging in the entry region in laminar flow. Also Fig. 6 suggests that for the streaming current to be within 1% of i_∞ then e^{-J_L} should be of the order of 5×10^{-4} or $J_L = 7.6$. The significance of this is indicated by the physical significance of J_L which was shown in ref. 2 to be the ratio of the conduction current to the convection current. Also, as λ/ε is a measure of the relaxation time and as $\bar{u}/L$ is a measure of the residence time in the tube, then J_L is also a measure of the ratio of those two quantities.

The fall of the streaming current to a value of i_∞ indicated by the value of $J_L = 7.6$ is slower than the rise to i_∞ for the turbulent flow in a pipe. In the latter case an approach to 1% of i_∞ is obtained from eqn. (1) and ref. 1 as being given by $e^{-J_L} = 0.01$ $e^{-J_{L0}}$ or $e^{-J_L} = 9 \times 10^{-3}$ with correspondingly $J_L = 4.7$. The slowness of this fall justifies the assumption, used in deriving eqn. (7), of negligible relaxation of charge in the entry region.

6. CONCLUSIONS

The variation of streaming current with distance along a pipe is quite different in nature for laminar flow from that previously reported for turbulent flow.

The initial charging that takes place in the entrance region is of an order higher than that in a very long pipe and the drop to the asymptotic value for a pipe of infinite length is at a slow rate compared with the rise that takes place in turbulent flow.

ACKNOWLEDGEMENT

The author is grateful to D. R. Siswick and D. G. M. Hinds for assistance with the experimental work leading to the results described.

SUMMARY

The effect of the length of a pipe containing a laminar flow upon the streaming current developed was investigated experimentally to show a high charge being developed in the entrance region and a slow fall to the asymptotic value corresponding to a pipe of infinite length. An explanation is given for the different type of behaviour compared with the previously reported case of turbulent flow.

REFERENCES

1 E. T. HIGNETT AND J. C. GIBBINGS, *J. Electroanal. Chem.*, 9 (1965) 260.
2 J. C. GIBBINGS AND E. T. HIGNETT, *Electrochim. Acta*, 11 (1966) 815.
3 E. T. HIGNETT AND J. C. GIBBINGS, *J. Electroanal. Chem.*, 16 (1968) 239.
4 J. C. GIBBINGS AND R. W. VERYARD, *J. Electroanal. Chem.*, 14 (1967) 155.

ELECTROANALYTICAL CHEMISTRY AND INTERFACIAL ELECTROCHEMISTRY
Elsevier Sequoia S.A., Lausanne – Printed in The Netherlands

A POLAROGRAPHIC STUDY OF Sc(III) AND Y(III) IN WATER, ETHANOL–WATER MIXTURES, ABSOLUTE ETHANOL AND ACETONITRILE

J. SANCHO*, A. ALDAZ* AND A. PUJANTE
Department of Physical Chemistry, Faculty of Science, University Murcia, (Spain)
(Received May 22nd, 1969; in revised form December 1st, 1969)

INTRODUCTION

Polarographic studies of scandium and yttrium are not extensive; this paper describes the reduction at the dropping mercury electrode of these elements in the solvents: water, ethanol–water mixtures, ethanol and acetonitrile. Several authors have studied this problem in different conditions[1]. Purushottam and Raghava[2] found only one step in aqueous scandium solutions. The formation of scandium complexes has been studied by some investigators[3], and also the behavior of Y(III) in different solvents[4]. The study of these elements in ethanol–water mixtures has been carried out bearing in mind the investigations of Sancho *et al.*[5] in addition to the work of other authors[6]. The effect of variation of ethanol concentration on the stability of halide complexes with these elements has been carried out by Tur'yan[7] and others[8]. Problems related to the use of reference electrodes in acetonitrile have been studied by Coetzee and McGuire[9] and others[10].

EXPERIMENTAL

Instrumentation

The instruments used in this work are: a direct-recording model PO4 Radiometer polarograph, a Philips 7776 electronic current stabilizer and pH meter model GM 4494, and a Colora thermostat, NB model, with ± 0.01°C stability.

Reagents

YCl_3, LiCl, $LiClO_4$, $Y(ClO_4)_3$ and $Sc(ClO_4)_3$ have been used with ethyl alcohol and acetonitrile as solvents; with water and aqueous alcoholic mixtures, the salts were used in the form of chlorides. Scandium and yttrium chlorides and perchlorates were prepared from the oxides and were vacuum desiccated at 60°C for several hours. Lithium perchlorate was prepared from lithium carbonate p.a. and vacuum desiccated at about 60°C. Ethanol p.a. came from Probus and was vacuum desiccated for us. Merck and Riedel de Haen supplied acetonitrile which was later desiccated. Gelatin and Triton X-100 were used as maximum suppressors.

* Present address: Department of Chemistry, Faculty of Science, Autonomous University of Madrid (Spain).

RESULTS AND DISCUSSION

Scandium

One well-defined step appears in every case except with acetonitrile, where two steps are observed in ordinary and in derivative polarography. The study was carried out in water and in 25% and 50% (v/v) ethanol–water mixtures, with 0.1 *M* LiCl and 0.1 *M* $N(CH_3)_4Cl$; in absolute ethanol and acetonitrile with 0.1 *M* LiCl and 0.1 *M* $LiClO_4$, respectively; $ScCl_3$ was used in all cases, except in absolute ethanol and acetonitrile, where $Sc(ClO_4)_3$ was used. Substitution of LiCl for $N(CH_3)_4Cl$ was shown to produce no difference in the observed wave.

Solvents used—water, ethanol–water mixtures. Sc(III) was studied in these solvents in the pH* range 2.0–5.0. The limiting current remains constant at a minimum value in the range 3.1–3.7 when LiCl or $(CH_3)_4$ NCl was used as supporting electrolyte, except in water for the latter electrolyte where the stability interval is from 3.0 to 3.3. The Sc(III) concentration was 0.5–3 mmole l^{-1}.

In all cases the process is governed by diffusion, and the diffusion current is always directly proportional to the Sc(III) concentration. Table 1 shows the results

TABLE 1

Solvent	*Supporting electrolyte/ 0.1 M*	*pH*	*Tomes's slope/V*	$E_{\frac{1}{2}}/V$	E_p/V	$i_d/\mu A$	$i_p/\mu A$	*I*
H_2O		3.26	0.0358	−1.801	−1.817	5.96	2.31	2.151
H_2O–EtOH 25%	LiCl	3.11	0.0301	−1.802	−1.812	4.08	1.67	1.470
H_2O–EtOH 50%		3.06	0.0299	−1.818	−1.844	3.66	1.22	1.300
H_2O		3.11	0.0270	−1.840	−1.801	6.12	2.35	2.196
H_2O–EtOH 25%	$(CH_3)_4NCl$	2.86	0.0319	−1.852	−1.885	4.89	1.78	1.770
H_2O–EtOH 50%		3.27	0.0273	−1.734	−1.815	3.43	1.21	1.273
EtOH abs.	LiCl	—	0.1022	−1.681*	−1.752*	3.34	0.54	1.015
acetonitrile 1st wave	$LiClO_4$	—	0.1672	−1.825*	−1.965*	7.90	1.20	1.000
acetonitrile 2nd wave		—	0.0790	−2.299*	−2.336*	30.58	10.86	3.892

* *Versus* MPE. The concentration of Sc^{3+} for all the Table is 1.5 mmol l^- except for acetonitrile when it is 4.5 mmol l^{-1}. (MPE: mercury pool electrode.)

for 1.5 mmol l^{-1} Sc(III) concentration in the solvents studied (the Sc(III) concentration is 4.5 mmol l^{-1} in acetonitrile).

In all cases, the reduction process is irreversible and is due to the direct reduction of the scandium aquo-complex to metal scandium, since the steps obtained cannot be considered as due to the reduction of the probable H_3O^+ ion from the scandium weak acid aquo-complex, because the slopes of the $E_{\frac{1}{2}}$ *vs.* log $i_d/2$ diagram are very far from the value of −89 mV to be expected for H_3O^+.

* Since in aqueous alcoholic mixtures we want only to know the relative H_3O^+ concentration and to obtain reproducible results, we report pH as measured with a pH-meter using an aqueous reference electrode.

Data obtained by derivative polarography indicate that the peak current value may be used for analytical purposes since it is directly proportional to Sc(III) concentration.

Table 2 shows the results of analytical interest.

TABLE 2

Solvent	*Supporting electrolyte/ 0.1 M*	*pH*	*Tomes's slope/V*	$E_{\frac{1}{2}}/V$	E_p/V	*I*
H_2O		3.36	0.0242	−1.800	−1.822	2.244±0.295
H_2O–EtOH 25%	LiCl	3.41	0.0276	−1.763	−1.776	1.532±0.032
H_2O–EtOH 50%		3.38	0.0259	−1.777	−1.793	1.305±0.050
H_2O		3.25	0.0251	−1.820	−1.845	2.324±0.076
H_2O–EtOH 25%	$(CH_3)_4NCl$	3.08	0.0244	−1.816	−1.837	1.724±0.052
H_2O–EtOH 50%		3.35	0.0223	−1.796	−1.822	1.244±0.041
EtOH abs.	LiCl	—	0.1085	−1.711*	−1.778*	1.005±0.023
acetonitrile 1st wave	$LiClO_4$	—	0.1723	−1.822*	−1.946*	1.030±0.070
acetonitrile 2nd wave		—	0.0715	−2.253*	−2.289*	3.731±0.370

* *Versus* MPE. The concentration of Sc^{3+} in water and water–ethanol mixture is 1.5 mmol l^{-1}; in absolute ethanol it is 2 mmol l^{-1} and in acetonitrile 3 mmol l^{-1}.

Absolute ethanol solvent. The concentration range studied is from 1–3 mmol l^{-1}. One well-defined step is obtained, which splits with rise in temperature, but since the second step is very poorly defined its study has not been possible. The first step is due to a diffusion process and is irreversible. Diffusion and peak currents vary linearly with Sc(III) concentration (in the range studied), so that they may be used for quantitative determination of this element. The step observed with increase in temperature is of kinetic nature, since it varies greatly with temperature, but its characteristics have prevented the contribution of further data. There is no interaction between the OH group and Sc(III).

Anhydrous acetonitrile solvent. The concentration range is from 3–5.5 mmol l^{-1}. Two steps have been observed in every case, the half-wave potentials being very near to each other, and they are governed by the laws of diffusion. Both steps are irreversible. The diffusion currents are proportional to concentration and may therefore be used for the analytical determination of this element, though it is advisable to use the second step, since it presents a greater sensitivity to Sc(III) concentration. There is no interaction between Sc(III) ion and the C≡N group.

Yttrium

In acetonitrile one step is observed, while in water, 50% ethanol–water and absolute ethanol two steps appear; in 25% and 75% ethanol–water there are three, since the first one which was observed in water and 50 ethanol–water splits into two. A careful study of Y(III) has been carried out by derivative polarography, although in many cases the characteristics of the steps did not allow the values of i_p and E_p to be calculated. Table 3 shows the results obtained in 0.1 *M* LiCl for 3 mmol l^{-1} of

TABLE 3

Wave	*Solvent + supporting electrolyte / 0.1 M*	*pH*	*Tomes's slope/V*	$E_{\frac{1}{2}}/V$	E_p/V	*I*
1st	H_2O + LiCl	3.76	0.0293	−1.924	−1.928	3.874 ± 0.430
2nd		3.76	0.0691	−2.164	—	4.145 ± 0.411
1st		2.78	0.0260	−1.856	−1.898	0.752 ± 0.001
2nd	H_2O–EtOH 25% + LiCl	2.78	0.0188	−1.932	−1.950	1.830 ± 0.025
3rd		2.78	0.0767	−2.093	—	1.707 ± 0.081
1st	H_2O–EtOH 50% + LiCl	5.11	0.0650	−1.773	−1.789	2.320 ± 0.119
2nd		5.11	0.0421	−2.018	—	0.562 ± 0.001
1st		2.81	0.0334	−1.884	−1.898	1.078 ± 0.037
2nd	H_2O–EtOH 75% + LiCl	2.81	0.0352	−1.990	−1.962	1.206 ± 0.039
complete wave		4.76	0.0517	−1.757	−1.760	2.010 ± 0.250
1st	absolute EtOH + LiCl	—	0.0533	−1.496*	−1.566*	0.642 ± 0.196
2nd		—	0.0894	−1.825*	−1.727*	1.316 ± 0.060
single wave	acetonitrile + $LiClO_4$	—	0.0402	−1.709*	−1.778*	—

* *Versus* MPE. The concentration of Y^{3+} is 3 mmol l^{-1}.

Y(III); in acetonitrile and ethanol 0.1 *M* $LiClO_4$ was used as supporting electrolyte, the Y(III) concentration being 3 mmol l^{-1}.

A detailed investigation of each solvent is described, since it is practically impossible to summarise.

Y(III) in water, 0.1 M LiCl. Two steps were obtained and studied over the pH range 2.32–5.64. The first step is governed by the laws of diffusion and it is irreversible. Misumi and Ide[4] conclude that the reducible species is the H_3O^+ ion, proceeding from the dissociation of the yttrium aquo-complex, but the values of the slope of the graph $E_{\frac{1}{2}}$ *vs.* log $i_d/2$, calculated from their data, are very far from the theoretical value (−89 mV) for this type of process, so that it may be inferred that the reduction step is not due to deposition of these ions; this statement is borne out by the fact that, in this study, no such value has been obtained, for this slope; it may therefore be concluded, that the reduction is due to the depolarising action of the Y(III) aquo-complex.

The second step is irregular and presents at the end large anomalies due to electrode processes on the mercury drop which cause interruptions in the polarographic circuit. The values of the limiting current are higher than those of the first step, but in no case are they double that value, as might be expected if it were a reduction in which double the number of electrons were interfering, in accordance with the processes:

$$Y^{3+} + 1e^- \longleftrightarrow Y^{2+}; \quad Y^{2+} + 2\,e^- \longleftrightarrow Y^0$$

On the other hand, with increased alcohol concentration, the step decreases until it disappears completely (75% EtOH). This shows, contrary to the assumption

put forward by Purushottam and Raghava[2], that this step is not due to a direct Y^{2+} reduction, but to one of the following processes

$$Y(Hg)+3\,H_2O \leftarrow\!\!-\!\!\rightarrow Y(OH)_3+\tfrac{3}{2}H_2 \quad (1)$$

this reaction being possible because of the redox potential of yttrium (−2.37 V),

$$Y^{2+}+H_2O \leftarrow\!\!-\!\!\rightarrow Y^{3+}+OH^-+\tfrac{1}{2}H_2 \quad (2)$$

which is also possible on account of the unstable character of the probable Y^{2+} ion (in agreement with Almagro[5] the instantaneous formation of Y^{2+} is admitted). This process would be in agreement with the electrode circuit interruption caused by the $Y(OH)_3$ deposit on the drop or by H_2 occlusion within the capillary.

The limiting current of the second step seems to be governed by the laws of diffusion, although it is difficult to assign to it this character on account of its abnormal behaviour. It is irreversible. The diffusion and limiting currents of the two steps are directly proportional to the Y^{3+} concentration, so that they may used in analytical determinations of this ion, though in view of the character presented by the second step, it is preferable to use the first in these determinations.

Y(III) in 25% EtOH, 0.1 M LiCl. A splitting of the first step over the pH range 2.65–2.90 is observed, disappearing at higher pH values. The third step (which is the second in pure aqueous solutions) continues with the same characteristics. The splitting may be considered to be due to the presence of two complex species originated by the addition of ethanol to the medium, these species being in equilibrium; the one that deposits at a lower potential is unstable with temperature, the reaction shifting towards the formation of the second step complex species. This suggestion is borne out by the fact that the sum of the diffusion constants of the two steps is constant over the Y(III) concentration range studied. In the pH range 3.08–4.85, one step is observed, with a diffusion constant slightly lower than the sum of the former constants of the two steps. Both steps are irreversible.

The limiting current of the third step varies abnormally with the height of the mercury column, so that it is probably not governed by the laws of diffusion. It is irreversible.

Y(III) in 50% EtOH, 0.1 M LiCl. The splitting has not been obtained with the necessary clarity to warrant an accurate investigation; the study of this step was therefore carried out at pH value at which the splitting was not appreciable. The whole step is governed by the laws of diffusion. The reduction process is irreversible. The diffusion and peak currents are directly proportional to concentration.

The second step is studied over a pH range of 3.27–5.93 and seems to be governed by the laws of diffusion. Its nature is irreversible and its diffusion current is approximately proportional to Y(III) concentration.

Y(III) in 75% EtOH, 0.1 M LiCl. The splitting of the first step is clearly visible in the pH range 2.40–3.07. Both steps are governed by the laws of diffusion, and they are irreversible. The character of the second one is more definite than the first, as can be seen by the greater variation of the half-wave potential with drop time, temperature (2 mV and 2.5 mV per °C) and concentration.

The existence of these two steps may be interpreted in the same way as applied to 25% EtOH solvent; two complex species are present which were originated by

the addition of EtOH to the medium. As happened with 25% EtOH, the sum of the diffusion constants of the two steps remains constant over the concentration range studied.

The third step (which is the second in 25% EtOH) has completely disappeared.

Above pH 3.28, only one step is obtained, the value of constant I being equal to 2.307, which is slightly lower, than the sum of the constant I values for split steps. At these pH values the process is governed by the laws of diffusion, and the step is irreversible. The diffusion and peak currents are directly proportional to Y(III) concentration, and may be used for analytical determinations of this element.

Y(III) in absolute EtOH, 0.1 *M LiCl*. In this medium, two steps have been obtained for concentrations above 10^{-3} *M* in the reducible species, and only one at lower values. The steps are poorly defined, but are obtained more clearly in derivative polarography. The process seems to be governed by the laws of diffusion and is irreversible. The diffusion currents are directly proportional to Y(III) concentration.

Y(III) in acetonitrile, 0.1 *M* $LiClO_4$. One step is observed, which is governed by the laws of diffusion. The reduction process is irreversible. The diffusion and peak currents are not directly proportional to concentration over the range studied.

All values of analytical interest for each one of the solvents used, are to be found in Table 3.

In the spectrophotometric studies, no interaction has been observed between Sc(III) and Y(III) ions and the molecules of the different solvents used (ethanol–water mixtures, ethanol and acetonitrile), so that the steps obtained in all cases seem to be due to direct reduction of the ion on the dropping mercury electrode.

ACKNOWLEDGEMENT

We are indebted to Dr. Morcillo of Consejo Superior de Investigaciones Científicas, Madrid, for spectrophotometric studies carried out in his laboratories.

SUMMARY

Sc(III) and Y(III) have been studied polarographically in the solvents: water, ethanol–water (in different proportions), absolute ethanol and acetonitrile. The supporting electrolytes used were: 0.1 *M* LiCl, 0.1 *M* $LiClO_4$ and 0.1 *M* $N(CH_3)_4Cl$.

For Sc(III) one step has been obtained in all solvents used except acetonitrile, where two steps were observed. On the other hand, one step was obtained for Y(III) in acetonitrile, whilst in water, 50% ethanol–water and absolute ethanol, two steps appeared; in 25% and 75% ethanol–water, three steps were observed.

Data of analytical interest are presented, both in direct and derivative polarography. A brief spectrophotometric study of possible interactions between scandium and yttrium ions and the different solvents is appended.

REFERENCES

1 R. H. LEACH AND H. TERREY, *Trans. Faraday Soc.*, 33 (1937) 480; W. HOLLECK AND W. NODDACK, *Angew. Chem.*, 50 (1937) 819; W. NODDACK AND A. BRUCKL, *Angew. Chem.*, 50 (1937) 362.
2 A. PURUSHOTTAM AND BH. S. V. RAGHAVA RAO, *Anal. Chim. Acta*, 12 (1955) 589.
3 A. D. PAUL, *Phys. Chem.*, 66 (1962) 1248; G. L. REED, K. J. LUTTON AND D. F. MORRIS, *J. Inorg.*

Nucl. Chem., 26 (1964) 1227; A. P. SAMODELOV, *Radiokhimiya*, 6 (1964) 568; F. PETRU AND F. KŮTEK, *Collection Czech. Chem. Commun.*, 25 (1960) 1143.

4 H. NAMAGAUCHI, J. HASHIMOTO AND Y. NASUSAWA, *Nippon Kagaku Zasshi*, 80 (1959) 43; S. MISUMI AND Y. IDE, *Bull. Chem. Soc. Japan*, 33 (1960) 836; I. M. KOLTOFF AND J. COETZEE, *J. Am. Chem. Soc.*, 79 (1957) 1852; G. BIEDERMAN AND L. CLAVATTA, *Arkiv. Kemi*, 22 (1964) 253; G. CHOPPIN AND P. UNREIN, *J. Inorg. Chem.*, 60 (1938) 1770.

5 J. SANCHO AND V. ALMAGRO, *Anales Real Soc. Espan. Fís. Quím. Madrid*, LVI-B, (1960) 115; J. ALMAGRO, Doctor Thesis Pub. Murcia, 1962; A. PUJANTE, Doctor Thesis Pub. Murcia, 1967.

6 E. TEJERA, Doctor Thesis Pub. Univ. La Laguna, 1968; A. VIVO, Doctor Thesis Pub. Univ. La Laguna, 1968.

7 YA. TUR'YAN AND G. H. SEROVA, *Zh. Neorgan. Khim.*, 2 (1957) 336; YA. TUR'YAN AND N. I. SONDARENKO, *ibid.*, 4 (1959) 808, 1070.

8 O. KHOTSYANOVSKII AND O. KUDRA, *Izv. Vysshykh. Uchebn. Zavedenii Khim. i Khim. Tekhnol.*, 1 (1958) 43; 2 (1958) 36; O. KHOTSYANOVSKII, *J. Inorg. Chem. USSR*, 7 (1962) 198; P. MIGAL AND N. GRINBERG, *Uch. Zap. Kishinevsk. Gos. Univ.*, 56 (1960) 179; *J. Inorg. Chem. USSR*, 7 (1962) 675; P. MIGAL AND G. SEROVA, *J. Inorg. Chem. USSR*, 7 (1962) 827.

9 J. COETZEE AND D. MCGUIRE, *J. Phys. Chem.*, 67 (1963) 1810.

10 A. POPOV AND D. GESKE, *J. Am. Chem. Soc.*, 79 (1957) 2047; S. WAWZONECK AND N. RUNNER, *J. Electrochem. Soc.*, 99 (1952) 457; C. LARSON AND R. IWAMOTO, *J. Am. Chem. Soc.*, 82 (1960) 3239; 82 (1960) 3226.

Elsevier Sequoia S.A., Lausanne – Printed in The Netherlands

SHORT COMMUNICATION

Studies on the mixed ligand complexes of copper(I)
Part II. Potentiometric studies on the reaction of heterocyclic amines on tristhiourea copper(I) chloride and iodides

The complexes of copper(I) with heterocyclic amines are well known[1-3]; usually there is formation of 1 : 1 or 1 : 2 species. This is due to the weak π-bonding capacities of heterocyclic amines and because of this property it may not be possible for copper(I) ion to coordinate with more heterocyclic molecules as this would result in excessive charge accumulation around the copper(I) ion[4]. Considering the possibility of the interaction of heterocyclic amines with thiourea (Tu) complexes, in these complexes a $d\pi$–$d\pi$ bond is formed owing to the availability of vacant *d*-orbitals in sulphur which may also act as acceptor *d*-orbitals by taking excessive charge from the metal. The reaction of heterocyclic amines with tris Tu copper (I) iodide has recently been reported[5]. Mixed complexes such as $[CuTu_3Py]I$, $[CuTu_3$3-Pic$]I$ and $[CuTu_2Dipy]I$ are formed. In the formation of these complexes there is a tendency for copper(I) ion to attain its maximum coordination number of four. The present study is an extension of the work on the mixed ligand complexes of copper(I) iodide with sulphur and nitrogen-containing ligands. The composition and stability of the complex species are reported on the basis of potentiometric studies, and in a few cases spectrophotometric methods have also been employed. These studies are mainly concerned with the formation of mixed ligand complexes formed by the interaction of pyridine and dipyridyl with tris Tu copper(I) iodide and chlorides.

Experimental

Pyridine and 2,2-dipyridyl (analytical grade reagents) were used. Copper(I) chloride and copper(I) iodide were prepared as described earlier[1,2]

Potentiometric measurements were carried out with a Kaycee potentiometer type MG3 with a lamp and scale arrangement. Platinum and calomel were employed as indicator and reference electrodes, respectively.

Preparation of the complex tristhiourea copper(I) iodide. This complex was prepared by the method described earlier[5]. The purity of the sample was authenticated by C, H, N and S analyses.

Preparation of the complex tristhiourea copper(I) chloride. A concentrated solution of copper(I) chloride (2 g) was prepared in concentrated KCl solution. The cuprous solution was mixed with an aqueous solution containing about 4 g of thiourea. The resulting solution was warmed slightly with constant stirring and was then filtered. The filtrate was evaporated to dryness over a water bath. The product so obtained was washed several times with small aliquots of distilled water and was then dissolved in absolute alcohol. The insoluble portion was filtered out. The resulting solution was concentrated and then allowed to stand for about one hour when colourless crystals appeared. The crystals were separated and dried in a vacuum

desiccator. Found: Cu 19.3 (19.4), Cl 10.9 (10.85), N 25.4 (25.7), S 29.1 (29.3)%. Calculated values for $C_3H_{12}N_6S_3CuCl$ in brackets.

Standard 1×10^{-1} *M* nitric acid solution was used as a titrant in potentiometric titrations. A constant ionic strength was maintained in the solution by the addition of potassium chloride.

Spectrophotometric studies were carried out with a Bausch and Lomb spectronic-20 colorimeter using a 1 cm diameter cuvette. The wavelengths selected were chosen by the Vosburgh and Cooper method[8], and the composition was determined by Job's method of continuous variation[9].

Results and discussion

Potentiometric titrations were carried out with a view to investigating the composition and stability of the complexes formed on interacting heterocyclic amines and copper(I) thiourea complex. The composition and the calculated values of the stability constants of the complexes are given in Table 1.

TABLE 1

Curve No.	*Ionic strength*	$\bar{n}$	*Complex formed*	*Stability constant* $K/l\ mol^{-1}$
V	0.44	2	$Cu(Py)_2Cl$	—
VI	0.44	3	$Cu(Tu)_3Cl$	—
VII	0.62	1	Cu(Dipy)Cl	3.02×10^2
VIII	0.25	3(Tu),	$Cu(Tu)_3Cl+$	—
		2(Py)	$Cu(Py)_2Cl$	—
IX	2.0	—	—	—
X	0.44	1	$Cu(Tu)_3Py\ Cl$	—
XI	0.62	1	$Cu(Tu)_3Dipy\ Cl$	—
XIII	0.44	1	Cu(Py)I	—
XIV	0.44	3	$Cu(Tu)_3I$	—
XV	0.62	1	Cu(Dipy)I	1.82×10^{-2}
XVI	0.25	3(Tu)	$Cu(Tu)_3I$	—
		1(Py)	Cu(Py)I	—
XVIII	0.44	1	$[Cu(Tu)_3Py]I$	1.92×10^{-2}
XIX	0.62	1	$[Cu(Tu)_3Dipy]I$	

On the basis of potentiometric titrations, there is evidence for the formation of 1:1 species such as $[CuTu_3Py]Cl$, $[CuTu_3Dipy]Cl$, $[CuTu_3Py]I$ and $[CuTu_3Dipy]I$. $\bar{n}$ is the average number of ligands attached to one central group.

The mechanism of the reaction of pyridine with the thiourea complex is a simple one; a pyridine molecule is coordinated to the central atom with the result that copper attains its maximum coordination number of four. The copper atom in the central group $[Cu(Tu)_3]^+$ is capable of accepting at least one pyridine molecule as the resulting excessive charge accumulation on Cu^+ will be minimised by transferring it to the vacant $d\pi$ level of the ligand. In order of nucleophilicity the pK_a values for thiourea and pyridine are 0.4 and 5.3, respectively[7]. The higher pK_a value for pyridine is an indication of the greater tendency of the ligand to attach with the central metal

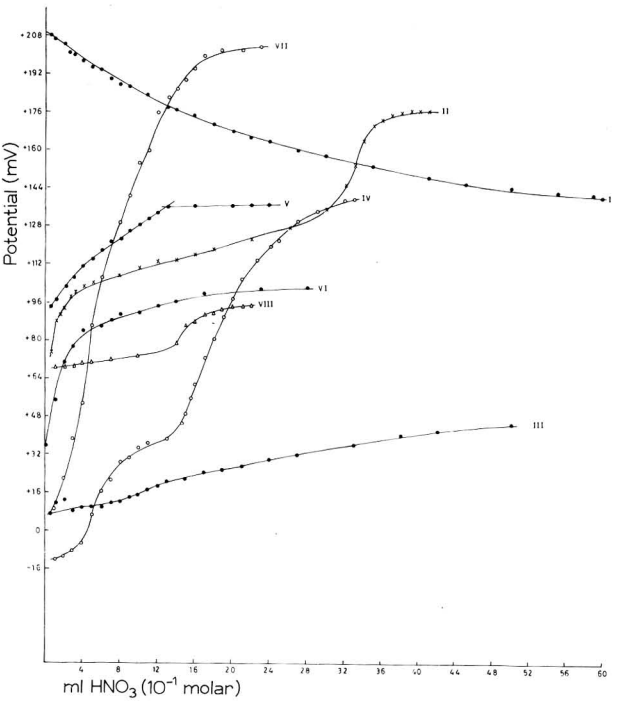

Fig. 1. Potentiometric titration curves using 1×10^{-1} *M* HNO_3 as titrant. (I) 10 ml CuCl (9.75×10^{-2} *M*), (II) 35 ml pyridine (1×10^{-1} *M*), (III) 35 ml thiourea (1×10^{-1} *M*), (IV) 22 ml dipyridyl (1×10^{-1} *M*), (V) I + II, (VI) I + III, (VII) I + IV, (VIII) I + II + III.

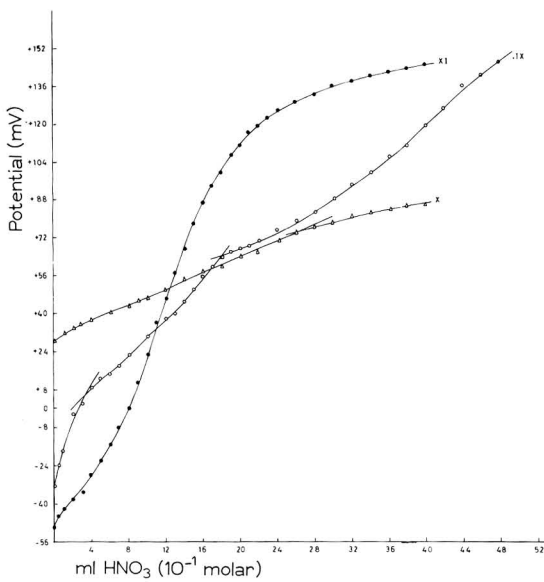

Fig. 2. Potentiometric titration curves using 1×10^{-1} *M* HNO_3 as titrant. (IX) 10 ml $Cu(Tu)_3Cl$ (1×10^{-1} *M*), (X) IX + 35 ml pyridine (1×10^{-1} *M*), (XI) IX + 22 ml dipyridyl (1×10^{-1} *M*).

ion. On the other hand, in the case of the 1 : 1 copper pyridine complex there is not much possibility of another pyridine molecule entering into the complex as it has weaker π-bonding ability and thereby an accumulation of excessive charge results on the copper(I) ion.

The reaction between $Cu(Tu)_3X$ (X = Cl, I) and dipyridyl is rather complex. Apparently the composition (on the basis of potentiometric studies) leads to the complexes (1 : 1) having a coordination number of five which is unusual for the d^{10} configuration. The mechanism

$$CuTu_3^+ + H_2O \xrightarrow{H_2O} [CuTu_3(H_2O)]^+ \xrightarrow{Dipy} [CuTu_2(Dipy)]^+ + Tu$$

would explain the formation of 1 : 1 ($CuTu_3X$: Dipy) complex as obtained from potentiometric titration curves. The mechanism suggested is substantiated by the isolation of the red crystalline mixed ligand complex $[CuTu_2Dipy]I$, which is fully characterised[4].

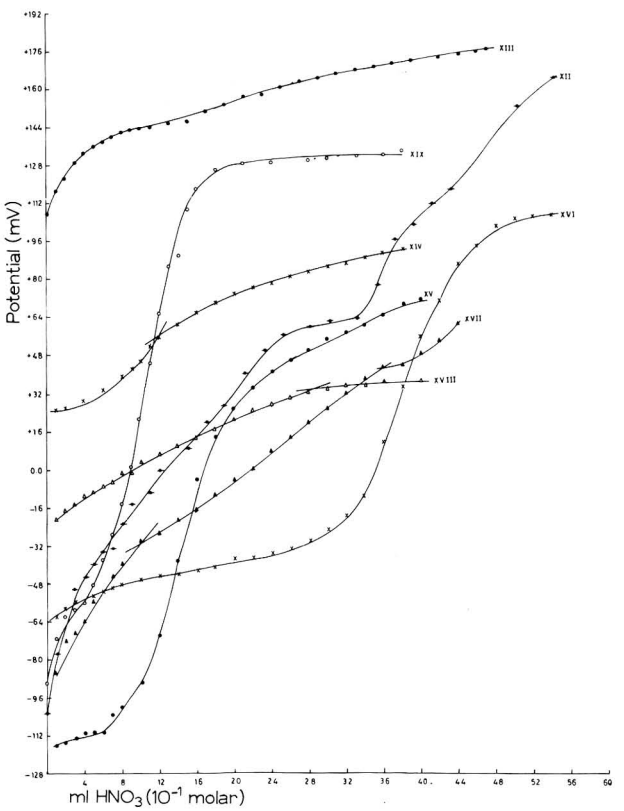

Fig. 3. Potentiometric titration curves using 1×10^{-1} *M* HNO_3 as titrant. (XII) 10 ml CuI (8.76×10^{-2} *M*), (XIII) XII + 35 ml pyridine (1×10^{-1} *M*), (XIV) XII + 35 ml thiourea (1×10^{-1} *M*), (XV) XII + 22 ml dipyridyl (1×10^{-1} *M*), (XVI) XIII + 35 ml thiourea (1×10^{-1} *M*), (XVII) 10 ml $Cu(Tu)_3I$ (1×10^{-1} *M*), (XVIII) XVII + 35 ml pyridine (1×10^{-1} *M*), (XIX) XVII + 22 ml dipyridyl (1×10^{-1} *M*).

An interesting aspect of the reaction between $CuTu_3X$ and dipyridyl is the result obtained on the basis of spectrophotometric studies. These studies showed that there is a combination of two dipyridyl molecules with one central group which may be explained by the mechanism:

$$[CuTu_3]^+ + H_2O \rightarrow [CuTu_3(H_2O)]^+ \xrightarrow[+\text{Dipy}]{-\text{Tu},\ -H_2O} [CuTu_2(\text{Dipy})]^+ + \text{Tu}$$

$$[Cu(\text{Dipy})_2]^+ \xleftarrow[+\text{Dipy}]{-Tu_2}$$

The above mechanism is not unlikely as the preliminary experiments showed that the absorbance of the complexes decreased rapidly with time and the concentration of dipyridyl is the rate-determining step in these reactions. The replacement of the remaining two thiourea molecules by a dipyridyl molecule with time is considered probable since the dipyridyl molecule is a better nucleophile and also a potential π-bonding ligand.

Further work on the mechanism of the above reaction is in progress.

Acknowledgement

The authors express their sincere thanks to Dr. S. M. F. Rahman Head, Department of Chemistry for providing facilities. One of the authors (M.M.K.) is also grateful to the University Grants Commission, New Delhi, for the award of a Senior Fellowship.

Department of Chemistry,
Aligarh Muslim University,
Aligarh (India)

M. Mahfooz Khan
A. U. Malik
S. A. A. Zaidi

Received November 6th, 1969

1 A. U. MALIK, *Z. Anorg. Allgem. Chem.*, 344 (1966) 107.
2 A. U. MALIK, *J. Inorg. Nucl. Chem.*, 29 (1967) 2106.
3 R. E. YINGST AND B. E. DOUGLAS, *Inorg. Chem.*, 3 (1964) 1177.
4 L. E. ORGEL, *An Introduction to Transition Metal Chemistry*, Methuen, London, 1963, Chap. IX.
5 A. U. MALIK, *Z. Anorg. Allgem. Chem.*, 363 (1968) 203.
6 J. BJERRUM, *Metal Amine Formation in Aqueous Solution*, P. Haase and Son, Copenhagen, 1941.
7 JOHN O. EDWARDS, *Inorganic Reaction Mechanisms*, W. A. Benjamin, Inc., New York, 1965, p. 54.
8 W. C. VOSBURGH AND R. C. COOPER, *J. Am. Chem. Soc.*, 63 (1941) 437.
9 P. JOB, *Compt. Rend.*, 180 (1925) 928.

Elsevier Sequoia S.A., Lausanne – Printed in The Netherlands

BOOK REVIEWS

Electrode Reactions of Organic Compounds, Discussions of the Faraday Society, No. 45, Butterworth and Co., London, 1968, 282 pages, £5.

This book records the Discussion of the Faraday Society which took place from 2nd to 4th April, 1968, in the School of Chemistry, University of Newcastle-upon-Tyne. It was the first discussion on electrode processes since 1947. The considerable progress of electrochemistry in general during the past 20 years is quite obvious from all papers presented, as well as from the discussion. The various contributions cover a wide scope of theoretical and methodical approaches to organic electrochemistry exemplified on a limited number of reaction types.

With the exception of the Moscow group, practically all important electrochemical research groups specialising in organic electrode processes were represented at the meeting. As one may expect, the work reported at the Discussion is mainly in the previous direction of interest of these groups and was, in part, published also elsewhere. This is, of course, no disadvantage since the reader may obtain, in this way, a very good picture of the present effort.

The topics dealt with in the Discussion include the theory of processes involving breaking the bond, electroluminescence, electrocatalysis (theoretical discussion of the influence of electrode material and search for the intermediate in methanol and CO oxidation), processes on organic insulator electrodes, investigation of intermediates using transparent electrodes, stereochemistry of electrode processes and investigations of mechanisms of various electrode processes, particularly various aspects of carbonyl bond reduction (altogether four papers including the introductory paper and the communication on the intermediate coupling with acrylonitrile), and of Kolbe reaction and other processes occurring at very positive potentials, and reduction of heterocyclic compounds, synthetic haemoprotein models and tetraalkylammonium ions. In fact, no completely new reaction was reported (perhaps in view of possible application?).

All interested in organic electrochemistry and in electrode processes in general should read this book.

J. Koryta, J. Heyrovský Institute of Polarography, Prague

Chemical Reactions in Solvents and Melts, by G. Charlot and B. Trémillon, Pergamon Press, Oxford, 1969, vii + 528 pages, £10/$27.00.

Chemical Reactions in Solvents and Melts is a translation of the French monograph of similar title published in 1963. No attempt has been made to update the material nor to correct errors in the original version. It is most disturbing to note that in a work concerned with a field expanding so rapidly as that of non-aqueous solvent chemistry, the literature coverage is *eight* years behind the publication date.

The book is divided into two parts: the first quarter deals with general properties of reactions in non-aqueous media while the remainder consists of data and references classified under particular solvents.

In Part I the reactions considered are divided into three main classes: acid–base reaction (in the Brønsted–Lowry sense), complex formation and oxidation–reduction. There is also a short chapter on solubility. The treatment is general and comprehensive: details, especially about the structure of solution species, are avoided. This approach necessarily suffers from a number of approximations. For instance a Bjerrum-type treatment for the dissociation of ion-pairs is used to predict variations of dissociation constant with dielectric constant, whereas it is known that there are severe limitations to this treatment especially where the electronic structures of the solvent molecules under consideration are dissimilar (*e.g.*, nitrobenzene and dimethylacetamide) or where such influences as hydrogen-bonding are present. Again, the authors consider the simple Born relation between solubility of salts and dielectric constant: this also has limited application where specific ion–solvent interactions can occur. Nevertheless this section is concerned to illustrate general trends and this is done most successfully. In particular, good use is made of what might be described as "free-energy level" diagrams or scales. These scales and their correlations are very useful: they are clearly explained and their limitations are noted.

Part II, the major section of the book, consists of a collection of data and literature references for individual solvents. In general, dielectric constant and melting or boiling point are given for each solvent together with information on polar nature, self-dissociation, etc. This is followed by a note of the reactions studied in the media and equilibrium constants if measured. The solvent index contains over three hundred titles, so that the field has been very extensively covered. There is however little information on lactones and lactams, only two sulphones are considered (briefly), and there is no reference to propylene carbonate.

There are a number of misprints and omissions in the text and equations but the majority of these are obvious. The Onsager equation on page 35 is incorrect. The translation by P. J. J. Harvey is an excellent one with very few confusing statements (an exception is on page 39 where "... the salts generally dissociate slightly differently" should perhaps be rendered as "... the difference in dissociation of the salts is generally slight"). The book is clearly printed and the presentation is of a high standard.

Most of the criticisms of this work are minor: the only serious defect is that, primarily a source book, it is eight years out of date. If the authors could be persuaded to bring out a revised edition it would make a valuable contribution to research in non-aqueous systems. For the moment it would be irresponsible to recommend the purchase of this volume to anyone interested in a contemporary view of the subject.

Colin A. Vincent, University of St. Andrews

JOURNAL OF ELECTROANALYTICAL CHEMISTRY AND INTERFACIAL ELECTROCHEMISTRY, VOLUME 25, 1970

AUTHOR INDEX

JOURNAL OF ELECTROANALYTICAL CHEMISTRY AND INTERFACIAL ELECTROCHEMISTRY, VOLUME 25, 1970

SUBJECT INDEX

Vol. 25 No. 3 JOURNAL OF ELECTROANALYTICAL CHEMISTRY AND INTERFACIAL ELECTROCHEMISTRY MAY 1970

CONTENTS

Reviews

Continued on page 4 of cover

Continued from inside page of cover